To my family

Contents

Introduction

In past decades, both energy demand and prices of fossil fuels grew up requiring the exploitation of new energy sources. Photovoltaic (PV) systems rapidly assume an important role among renewable energy sources since the primary source, i.e. the sun, has zero costs. Moreover, PV sytems can be easily embedded into existing building architectures and don't produce any noise, since the conversion of sunlight into electrical energy does not involve any moving part.

Despite technology improvements, the optimization of conversion of sunlight into electrical energy is an open issue. Optimization can be achieved at different levels: from technology of photovoltaic cells and efficient power devices to the use of high-capacity energy storage systems in order to minimize importing of energy from the external electrical grid.

Even if the efficiency of materials and power conversion increases, the shadow of a cloud passing on a photovoltaic field strongly reduces the generated power since the whole field is dominated by the behavior of less efficient photovoltaic units. Similarly, physical obstacles near the photovoltaic field, such as a chimney, could periodically shade some PV modules during the day.

For this reason, the generated power can be increased by properly disconnecting less efficient panels from the field or changing electrical connections among them in a way that increases the voltage and/or current of working point. In Literature, this kind of techniques is referred as *reconfiguration*.

Objective and Scientific Contribution of the Thesis

The first objective of this Thesis is the development of a Reconfiguration Algorithm for the Photovoltaic Systems. A Reconfiguration Algorithm changes the electrical connections among *photovoltaic units* in order to maximize the generated electrical power without violating given operating constraints of the system.
In Literature, the units of the photovoltaic field are tipically represented by modules, i.e. a series-connection of photovoltaic cells. Instead, the presented procedure considers as units of the photovoltaic field not only the modules, but also the panels, i.e. groups of series-connected modules each of them is protected by a bypass-diode in anti-parallel, since they are widely used as elements in large photovoltaic plants or in *Build Integrated Photovoltaic (BIPV)* plants.
Since a number, usually 2 or 3, of photovoltaic modules are constrained to remain series-connected in each PV panel, the complexity of the reconfiguration problem increases because of the reduced number of the degrees of freedom.
Some proposed reconfiguration techniques require the knowledge of each cell irradiance value [WLK+14] that is the most desired information to estimate the solar scenario over the photovoltaic field but it is expensive and difficult to achieve in large PV plants requiring the measurement of each cell current or an irradiance sensor for each cell.
The proposed algorithm only requires the acquisition of voltage-current characteristics of all panels at the reconfiguration instant. Moreover, respect to the present Literature (e.g., [VQGGPL+09] [NL08]), the proposed reconfiguration algorithm takes advantage of *all* panels of the photovoltaic field, i.e. it assumes that all panels can be series-connected to others and then, the obtained electrical rows, can be parallel-connected forming the desired PV field *configuration*.
More in general, the flexibility of whole photovoltaic system should be taken into account. Some proposed reconfiguration techniques

[CAN+10] [CDDSR07] have been developed for systems not achieving an high level of scalability. Instead, the proposed reconfiguration procedure can be applied to different structures of photovoltaic fields, having any possible number of modules or panels and any possible number of electrical rows.
For a *fixed structure* or *topology* of a PV field, the panels can be allocated into any position or being disconnected from the field through a *matrix of electrical switches*.

During the development of the reconfiguration algorithm, the *lowest execution time* of the reconfiguration algorithm has been considered the main goal to achieve in order to minimize the energy consumptions due to the reconfiguration process itself. During the reconfiguration process, the panels or a group of panels are disconnected from the field and they don't provide energy to the system. So, significant energy losses could occur. Since this algorithm is executed on Embedded Systems, i.e. on devices having minimal computational resources, both the reconfiguration algorithm and the techniques used for the reduction of execution time should exploit the minimum amount of computational resources.
In this Thesis, an *online* under-sampling technique to reduce the amount of analyzed data (voltage-current curves of photovoltaic panels) is illustrated. An additional aim of this under-sampling technique is the estimation of informations that can be used for diagnostic and prognostic purposes. In Literature, there is no algorithm that achieves the same results by analyzing voltage-current characteristics of *panels* and that, at the same time, minimizes the usage of computational resources.

The second goal of this Thesis is the analysis of environmental conditions suggesting the execution of the reconfiguration process. In particular, two methods for the optimized scheduling of the execution of the reconfiguration procedure are discussed. The former detects in real-time the presence of a shading phenomenon by measuring changes of the point of work, i.e. a variation of voltage and/or currents of the electrical rows of panels; the latter estimates

the motion of shadows covering the photovoltaic plant by processing informations retrieved by the under-sampling technique. This second method can also estimate the instant time when a shadow leaves the photovoltaic plant, suggesting to execute a new reconfiguration process or to reconnect all disconnected panels.

This Thesis attempts to reach the above-mentioned goals by means of an optimized Evolutionary Algorithm (EA). The Evolutionary Algorithm has been tested both on numerical and acquired voltage-current characteristics of panels. In particular, for each class of curves, the EA has been tested on the complete and the under-sampled voltage-current characteristics of panels.
In the EA, the representation of the solution as a structured data leads to achieve an high level of flexibility respect to the structure of the PV field. The complexity of the structured data only depends on the topology of the considered photovoltaic plant.
Moreover, the real operating constraints for commercial power inverters, properly sized for the simulated photovoltaic field, are considered.

In order to produce different solar radiance scenarios, a number of cases of shadows affecting a photovoltaic field having a Series-Parallel (SP) topology have been simulated and, for each cell, the solar radiance value has been calculated. Then, the numerical voltage-current characteristics of panels have been calculated, basing on the method proposed in [OGRSSRP14], by assuming the Bishop [BIS88] model for each photovoltaic cell.
The acquired voltage-current characteristics of panels have been provided by Bitron S.p.A. [Web14].

In order to produce different *dynamical* solar radiance scenarios, a shadow moving over a photovoltaic field has been simulated and, for each cell, at every considered instant time, the solar radiance value has been estimated depending on shading percentage. By applying the Bishop model [BIS88], each solar cell characteristic, and then the voltage-current characteristics of photo-

voltaic panels have been calculated by using the method shown in [OGRSSRP14] and under-sampled. For a given configuration of panels, the voltage-current and then the voltage-power curves of the photovoltaic field are then calculated.
A study on variations of the point of work respect to the movement of a shadow over a photovoltaic field has been performed. At the and, a list of decision rules has been obtained in order to decide when the reconfiguration process should be executed.
A further study on motion tracking of shadows passing over a photovoltaic field has been performed. The estimation of shadow position is obtained by processing current values of each photovoltaic module retrieved by the under-sampling procedure. The efficiency of the motion tracking method respect the properties of the shadow is discussed.

The main scientific contributions of this Thesis can be summerized as follows:

- An Evolutionary Reconfiguration Algorithm that takes advantage of all *panels* (i.e. series-connected modules protected by a bypass diode in anti-parallel) of a photovoltaic field

- An under-sampling algorithm to reduce the number of samples of voltage-current characteristics of *panels*

- A decision-rules based approach to detect events related to shading of photovoltaic field by measuring voltage and currents of electrical rows of panels

- A motion tracking method for shadows covering a photovoltaic field based on processing of current values of each photovoltaic module

The under-sampling algorithm and that suggesting the need of reconfiguring the photovoltaic field have been patented [usa13] [ada13] by Bitron S.p.A. [Web14].

Organization of the Thesis

This Thesis is organized as follows. The first Chapter introduces to the reader the background of photovoltaic systems subjected to mismatching phenomena. In particular, as regards the photovoltaic plant, the Bishop photovoltaic cell model and the reason of its usage are shortly presented. Then, the shading effects on the photovoltaic panels are illustrated, mentioning the effort of other authors to reduce them by testing different electrical connections among the photovoltaic modules (not *panels*). Then, power converters and their most typical topologies are briefly introduced. The shading effects on performance of *Maximum Power Point Tracking (MPPT)* procedure are illustrated. After the functional parts of a Photovoltaic Systems have been discussed, the motivations related to the development and to the execution of a reconfiguration procedure are introduced. The modified diagram block of a photovoltaic system acting the reconfiguration procedure is illustrated. At the end of this Chapter, the idea of developing an Evolutionary Algorithm, by comparing this choice respect to the other reconfiguration methods already presented in Literature, is discussed.

In the second Chapter, before analyzing the developed reconfiguration algorithm, the under-sampling procedure for voltage-current curves of photovoltaic panels is illustrated. The explanation of the procedure is divided into two main parts. In the first part the estimation of position absolute and relative maximum and minimum of voltage-power curve of the panel, also referred as *Maximum Power Points (MPP)* and *Inflection Points (IP)* respectively, with a very low computation effort. In the second part, the selection process of a minimum set of samples of the voltage-current curve of panels that minimize the difference between complete and under-sampled curve is discussed. At the end of this Chapter, the results of the under-sampling algorithm is shown for the most significant examples of voltage-current characteristics of panels and some limitations of the procedure are discussed.

The advantages of the under-sampling procedure are shown in the Chapter 3, where the Evolutionary Approach is introduced. In the first part of the Chapter, the genetic algorithm, the solutions encoding and the choice of the genetic operators are discussed. Furthermore, in order to speed up the genetic algorithm, the optimization of the objective function is illustrated. In the second part, different shading scenario are presented. For each scenario, the experimental results obtained with fully sampled and under-sampled voltage-current characteristics of PV panels are compared.

Chapter 4 introduces to the optimal reconfigurations scheduling. By starting from the periodical execution of the reconfiguration process, a first approach to shading detection is presented. Then, in order to further minimize energy loss, a procedure to predict the shadow's motion is discussed.

Finally, the conclusions of this Thesis are presented. In the end of the chapter some recommendations for further research work are presented.

Chapter 1

Background of the Thesis

This Chapter guides the reader into the area of interest of this Thesis.

In the first part, the causes and the effects of the *mismatching* among photovoltaic cells are discussed. Then, after a Literature review about some existent solutions, in the second part of the Chapter the *reconfiguration* of photovoltaic systems is introduced. Indeed, some technique proposed in Literature to detect shadowing phenomenon is discussed.

1.1 Photovoltaic Systems

A Photovoltaic (PV) System generates electrical power that can supply a generic load and/or be delivered into the grid in order to achieve some financial return.
Generally, a PV system is classified as *stand-alone* or *grid-connected* depending on its application. Stand-alone PV systems supply a load isolated by the electrical grid because this isn't accessible or, due to reduced energy consumption, the connection to the electrical grid isn't convenient. Instead, grid-connected PV systems supply both a local load and the electrical grid by selling a percentage of generated energy to the energy supplier. Thus the energy flux between the electrical grid and the PV system is bi-directional.

A PV system is composed by a photovoltaic generator, a DC-DC converter, the generic load and an energy storage system (battery).

In order to convert DC into AC, a further device is required: the inverter. This device works as a current source in phase with the grid voltage, injecting the available PV power into the grid (see Figure 1.1).

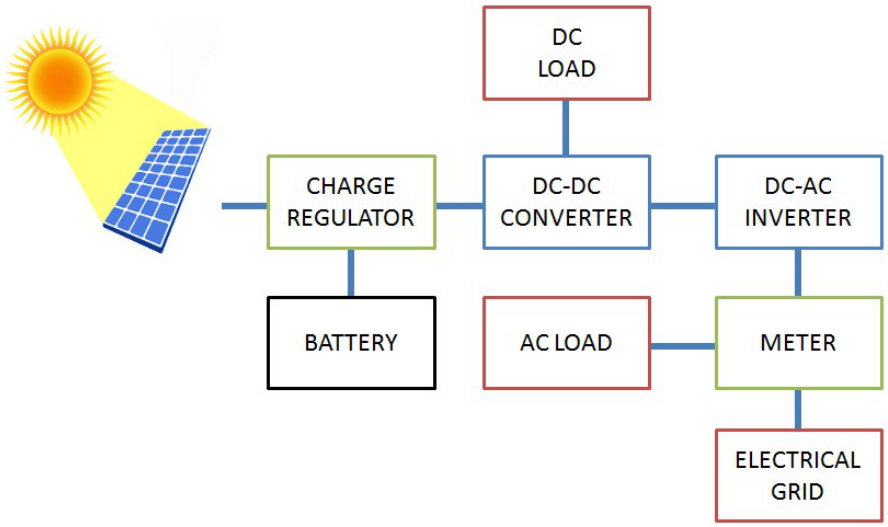

Figure 1.1: Block diagram of a photovoltaic system including all main components

1.1.1 The PV Generator

In a photovoltaic plant, solar cells convert sunlight into electrical energy. The voltage across a solar cell tipically assumes a value belonging to [0.5V–0.8V]. For this reason, solar cells are series-connected in order to increase the voltage across them. So, the number of series-connected solar cells depends on the required voltage.

The efficiency of a solar cell is defined as the ratio of output electrical power respect to incident optical power. This value depends

on many factors, related to the environment, such as the angle of incidence of solar radiance and the air temperature, or related to the physical device itself, such as the charge separation efficiency and the conductivity of electrical contacts. The maximum theoretically efficiency of most widely used solar cells is around 13% [NRE14].
Even if the PV cells are series-connected into *modules*, in order to boost performance, a partial shading affecting only one of the cells reduces the current by the whole module.
Since the same effect is obtained by series-connecting many modules, a bypass diode is connected in anti-parallel to each of them. A bypass diodes turns on when the PV module is shaded and its voltage assumes a negative value. By this way, the required current flows through the bypass diode and a lower power is dissipated.
The drawback is the presence of non-linearities in the voltage-power curve of the PV generator.

In Figure 1.2, both a panel and its electrical scheme are illustrated. In particular, the illustrated panel is *Axitec 250M/156-60S* that is used as reference model for calculus of numerical voltage-current characteristics in all this Thesis.

Before analyzing the effects of a partial shading phenomenon, the mathematical model of the PV cell are illustrated.

The PV Cell Models

In Literature, different photovoltaic cell models have been proposed. In particular, the single diode and the two-diodes models are widely used to describe the photovoltaic cell behavior when it acts as generator. Instead, the Bishop model is used to describe the PV cell behavior when it acts as a load and it is dissipating power.

The ideal equivalent circuit of a solar cell is a current source in parallel with a single-diode [ERC11], as the electrical scheme

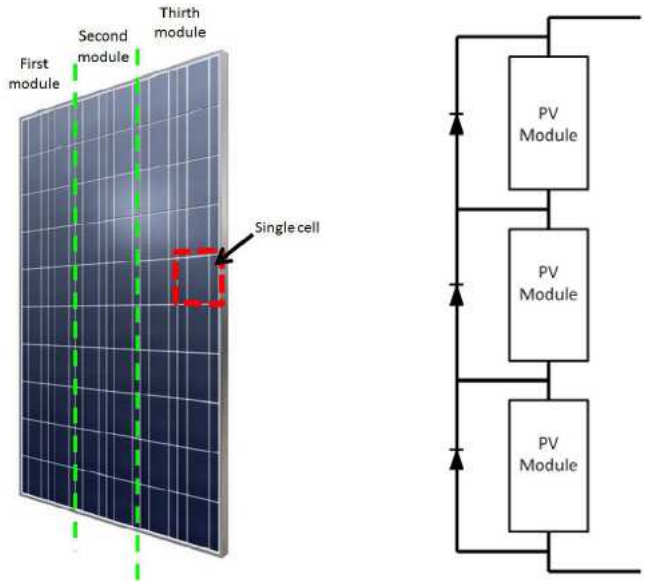

Figure 1.2: The Photovoltaic Panel Axitec AC-250M/156-60S [Sol14] and its electrical scheme

shown in Figure 1.3.

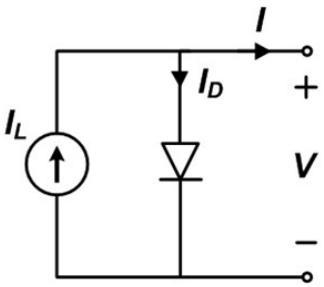

Figure 1.3: Ideal PV Cell Model

The photo-current source generates a current I_L that is proportional to the hitting light. In order to take into account the parasitic effects, two resistances are added to the model, obtaining the single diode model of photovoltaic cell. The equivalent

electrical scheme of the single diode model of photovoltaic cell is reported in Figure 1.4.

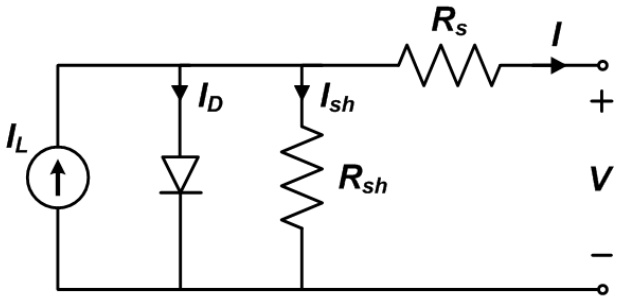

Figure 1.4: Single Diode Equivalent Circuit of PV cell

The equation of the output current by using the single diode model for the PV cell is:

$$I = I_L - I_{sat}\left[\exp\left(\frac{q\,(V + IR_s)}{nkT}\right) - 1\right] - \frac{V_j}{R_{sh}} \qquad (1.1)$$

where I_L is the photo-generated current, I_{sat} is the saturation current of diode that takes int account the effect of recombination of p-n junction of cell, q is the elementary electron charge, K is the Boltzmann constant = 1.38 $\times$ 10^{-23} J/K, T is the absolute temperature and R_s and R_{sh} are two parasitic resistances. These parasitics resistances reduce the power generated by cell. The series resistance value depends on contact resistance and on internal losses. The shunt resistance depends mainly on manufacturing defeats.

In Literature, a two diodes model is also used [Ibr11]. The two diodes model of photovoltaic model discerns the effects related to recombination occurring in two different regions of p-n junction: the quasi-neutral regions and the depletion region (ignored in the single diode model). The equivalent electrical scheme of the two diodes model of photovoltaic cell is reported in Figure 1.5.

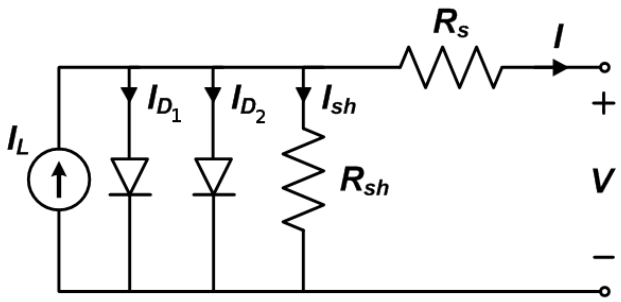

Figure 1.5: Two Diodes Model of Photovoltaic cell

The corresponding equation for the output current is:

$$I = I_L - I_{D1} - I_{D2} - \frac{V_j}{R_{sh}} \tag{1.2}$$

where:

$$I_{D1} = I_{sat1}\left[\exp\left(\frac{q\,(V + IR_{sh})}{kT}\right) - 1\right] \tag{1.3}$$

$$I_{D2} = I_{sat2}\left[\exp\left(\frac{q\,(V + IR_{sh})}{nkT}\right) - 1\right] \tag{1.4}$$

In these equations, I_{sat1} is the saturation current due to recombination in the quasi-neutral regions and I_{sat2} is the saturation current due to recombination in the depletion region.
The single and the two-diodes model describe the photovoltaic cell acting as generator.

The Bishop model [BIS88] is widely used to accurately describe the behavior of the photovoltaic cell in the breakdown region too.

In the Bishop model represented in Figure 1.6, a dependent voltage source $M(V_J)$ has been added to classic single diode model in order to describe the behavior of the photovoltaic cell in the breakdown region.

The equations related to the Bishop model are:

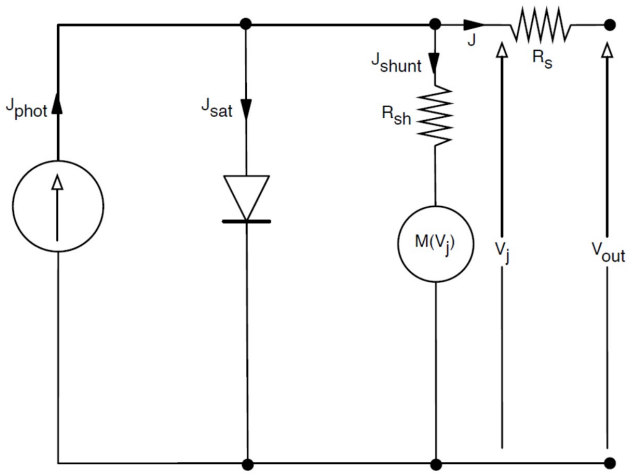

Figure 1.6: Bishop Model of Photovoltaic cell

$$J = J_{phot} - J_{sat}\left[\exp\left(\frac{q\left(V + JR_s\right)}{nkT}\right) - 1\right] - J_{shunt} \tag{1.5}$$

$$J_{shunt} = \frac{V_j}{R_{sh}}\left\{1 + a\left(1 - \frac{V_j}{V_{br}}\right)^{-m}\right\} \tag{1.6}$$

In the eq. (1.5) and (1.6) J_{phot} is the photo-induced current, J_{sat} is the saturation current, V_j is the voltage drop at the semiconductor junction, J is the cell current, R_s and R_{sh} are respectively the series and shunt resistances, n is the ideality factor, k is the Boltzmann constant, T is the reference temperature, V_{br} is the cell breakdown voltage, m is the avalanche breakdown exponent and a is the fraction of ohmic current involved into avalanche process.

Since the Bishop model well describes the solar cell behavior under shadowing conditions, it is used in this Thesis in order to retrieve the exact point of work of all panels for a given electrical configuration of the field and a given solar radiance scenario. The shading effects on PV cells are illustrated in the next part of this Section.

In particular, the voltage-current curves of solar cell, and so of the entire PV field, are obtained by using the method exposed in [OGRSSRP14]. The great advantage of this method is that no electrical simulator is required to model photovoltaic cell behavior and it can be implemented in any programming language.

The voltage-current characteristics of a cell belonging to the panel Axitec 250M/156-60S calculated by using the Bishop model and different irradiance values are illustrated in Figure 1.7.

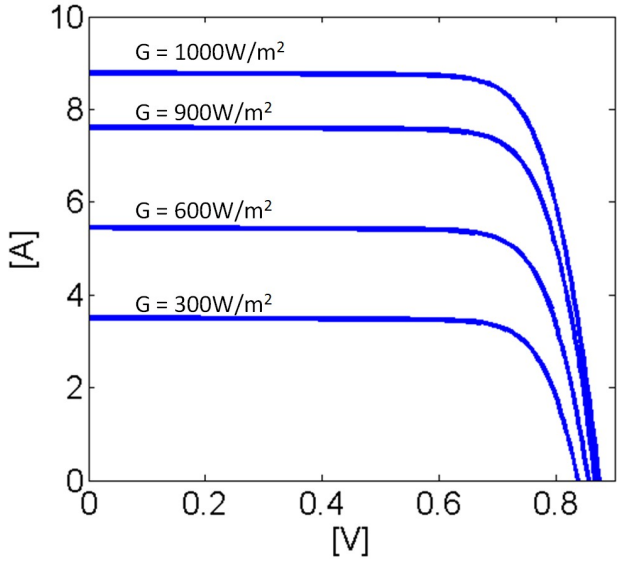

Figure 1.7: V-I curve of Photovoltaic cell for different irradiance values

In effect, the voltage across the solar cell can assume positive or negative values depending on required load current and the solar radiance hitting the cell.
As illustrated in Figure 1.8, when the PV cell assumes a negative value, the dependency of current respect to the voltage remains limited until a voltage threshold is achieved, known as *breakdown voltage*. In this case, the breakdown voltage is equal to -15V. Instead, when the cell voltage tends to this value, the current expo-

nentially increases and the PV cell is damaged. The achievement of this value is avoided by limiting the number of cells composing each PV module in a panel.

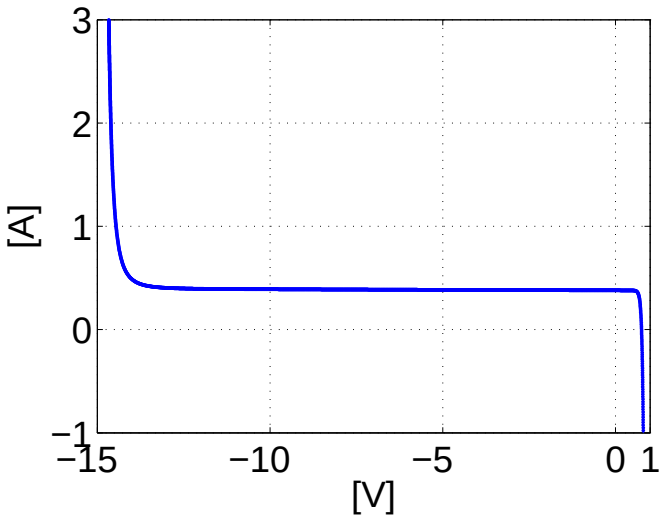

Figure 1.8: V-I curve of a shaded PV cell

The Bishop parameters of the cells of the panel Axitec 250M/156-60S are summarized in Table 1.1.

Bishop Parameter of PV Cell	Value
Short Circuit Current	8.8 A
Saturation Current	1.26 nA
Series Resistance	15 mOhm
Shunt Resistance	10 Ohm
η	1.5
Breakdown Voltage	-15V
a	0.002
m	3

Table 1.1: PV cells parameters

These parameters are used in all simulations of this Thesis and have been obtained through the procedure indicated in [NFV12].

The Shading Effects on the PV Cell

A single photovoltaic cell, under fully lighting conditions, acts as a generator, that is the desired behavior. Instead, if series-connected to other cells, under shading conditions, the solar cell could act as a load and dissipate power by heating.
Depending on required load current, the shaded cells can also reduce the voltage across the PV module.
In fact, if a row of cells supplies a load and a single cell is shaded, then the voltage across the shaded cell is reversed when the supplied load current is greater than short circuit current of the shaded cell [KK13]. In this case, the photovoltaic cell acts as a load (see Figure 1.9).

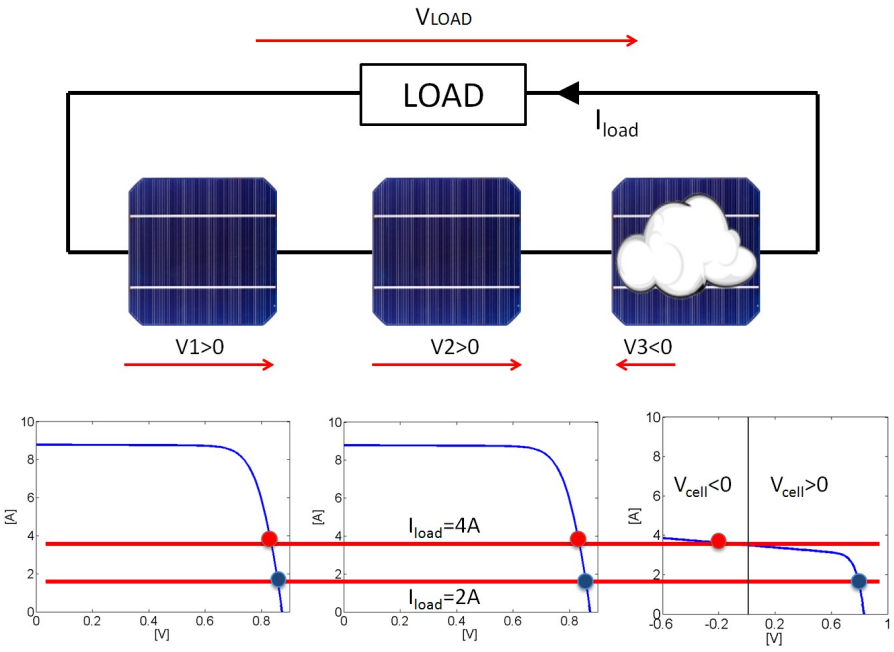

Figure 1.9: PV Cell - Shading Effects. Voltage across shaded cell reverses if a load current greater than its short circuit current is required.

In Figure 1.9, a series-connection of three PV cells is illustrated. One cell is partially shaded, so it can generate a current level lower than other two PV cells. In this example, if the load current is equal to 2A, then all three cells act as generator and the voltage is positive across all them. On the contrary, if a load current equal to 4A is required, the voltage across the shaded cell becomes negative in order to provide the same current value. So, the shaded cell acts as a load.

The behavior of photovoltaic cells depends strongly on temperature [ZMv11]. The lower is the environmental temperature, the greater is the efficiency of the PV cell. In Literature, it has been demonstrated that an increase of temperature leads to a narrowing of spectral response of cell [Mey12] and, for this reason, to a reduction of performances.

In this Thesis, the environmental temperature has been assumed constant and equal to 25°C (Standard Test Conditions, STC) in all analyzed cases. The temperature effects on voltage-current curves of cells hasn't been taken into account. By this way, the observed mismatching conditions among cells depend only on the solar radiance. In addition, all cells have the same parasitic parameters values. Despite this condition never occurs in real PV systems, it simplifies the analysis of the shading effects over a PV field since they don't depend on which cells are shaded.

In order to prevent negative effects of temperature, a bypass diode in anti-parallel to each cell should be used, but this is an expensive solution. So, this solution is considered only to protect many series-connected cells composing each photovoltaic module.

The Shading Effects on a PV Panel

In this Thesis, a series-connection of modules, each of them is protected by a bypass diode in anti-parallel, is referred as *photovoltaic panel*.

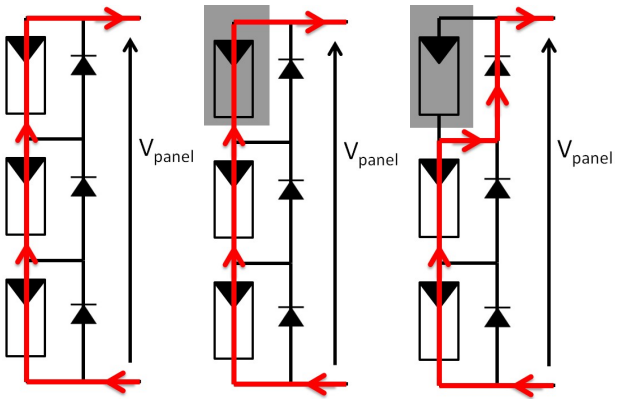

(a) No shading (b) Partial shadowing and low current load (c) Partial shadowing and high current load

Figure 1.10: Current flux (red line) under normal and shading conditions

Each module have its own short circuit current value depending on hitting solar radiance value.
If all modules receive the same solar radiance value, then they generate the same current and the voltage across them is positive. So their bypass diodes are all turned off (see Figure 1.10(a)).
If the load current is lower than the short circuit current of a shaded module, then the voltages across it is positive and, for this reason, its bypass diode remains turned off (see Figure 1.10(b)).
Instead, if the load current is higher than short circuit current of the shaded module, then the voltage across it tends to negative values enabling the switching on of the diode and allowing to the load current to flow into it (see Figure 1.10(c)). In effect, not all the load current flows through the bypass diode, but only that exceeding the current generated by the shaded module.

So, the voltage-current characteristic of a non-shaded panel has only one current level, like the red curve shown in Figure 1.11.
Instead, if one or more modules in panel are shaded, the voltage-current curve of the panel exhibits different current levels, as oc-

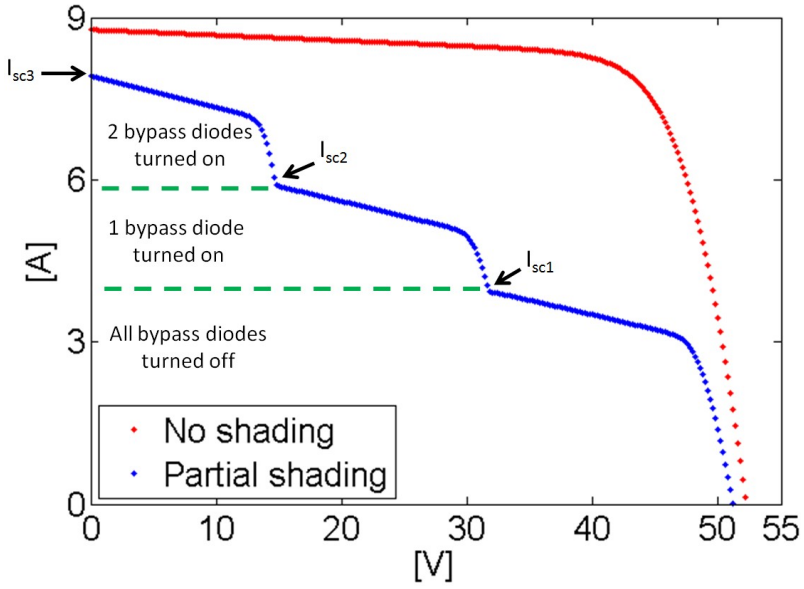

Figure 1.11: Voltage-current curve of a photovoltaic panel: non-shaded (red line) and partially shaded (blue line) case

curs for the blue colored curve in Figure 1.11.
For each module, its short circuit current I_{sc} and the number of turned on bypass diodes are indicated. In particular, I_{sc1} is the short circuit current of the most shaded module and I_{sc3} is the short circuit current of the module having the minimum shading and of the panel too.
The blue colored curve corresponds to a panel whose modules are all partial shaded and, for this reason, the short circuit currents of the red and blue colored curves have not the same value.

The number of photovoltaic units and the topology of PV plant are properly chosen in order to achieve the desired power production under nominal working conditions, i.e. when the photovoltaic units are completely radiated. In these conditions, the generated power is typically referred as the nominal power.

PV Plant Topologies

Photovoltaic panels can be connected into different topologies forming a PV field: Series-Parallel (SP), Total-Cross-Tied (TCT), Bridge-Link (BL) are the most commonly used.
These photovoltaic topologies are illustrated in the Figure 1.12.
In a Series-Parallel topology (see Figure 1.12(a)), panels are first series-connected into different rows in order to fit the voltage constraints of inverter and then these rows are parallel-connected in order to increase the generated current.
In a Total-Cross-Tied topology (see Figure 1.12(b)), on the contrary, the photovoltaic panels are first parallel-connected, and then the obtained parallel-connected panels are series-connected into a single row in order to fit the electrical constraints of inverter. The Bridge-Link topology (see Figure 1.12(c)) is obtained by removing half of parallel connection among panels of a TCT topology.

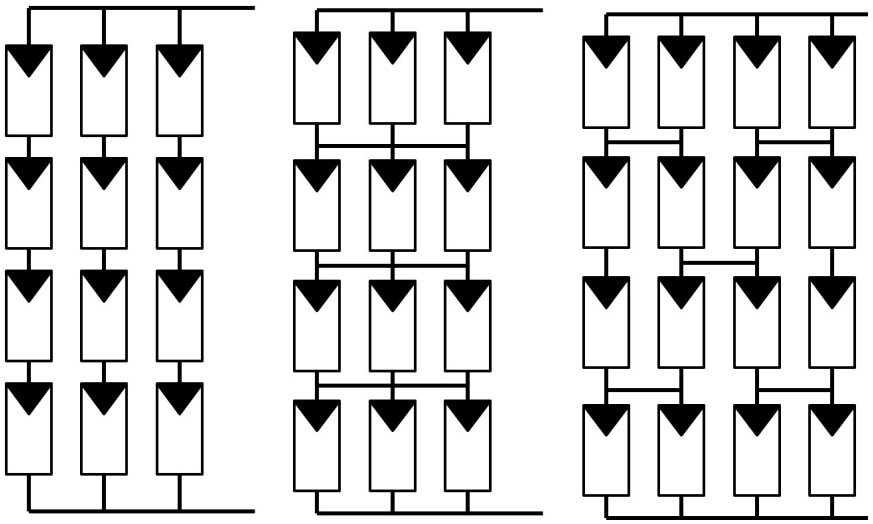

(a) Series-Parallel (b) Total-Cross-Tied (c) Bridge-Link

Figure 1.12: Three different PV plant topologies: Series-Parallel (SP), Total-Cross-Tied (TCT) and Bridge-Link (BL)

In Literature, the effects of a partial shading over these three

PV plants topologies has been analyzed showing that TCT topology achieves best performance when the photovoltaic plant is covered by a passing cloud [MJ14]. In general all the shadows properties, such as the shape, the size, the shadow strength, the sharpness, but also the direction of movement of shadow respect to modules orientation in the panels, affect differently the voltage-current characteristics of photovoltaic panels [KL13]. But, in general, a fixed PV field topology isn't an optimal solution since shadows properties are variable for each shading phenomenon and, above all, they are not predictable. At the end, there isn't *a priori* optimal topology of PV field.

1.1.2 Mismatch Losses Reduction

The photovoltaic panels could work under mismatched conditions because of many factors, related to internal behavior of physical devices or the environment where the panel has been installed. Manufacturer defeats, the corrosion of contacts or the aging of panels could increase parasitic effects. If not properly sized, bypass diodes can be broken due to the *thermal runaway* phenomenon. The thermal runaway is a self-feeding process occurring when the bypass diodes heat if an high current is flowing through them and their temperature exceeds a critical value [SSDG14]. This critical value, basing on [SSDG14], is equal to the junction temperature at which forward power dissipation in the diode equals reverse power dissipation for the given forward current and the given reverse voltage.
At the same time, the orientation of panels respect to the sun, the air temperature, the strength and orientation of wind change the conditions at which each panel and each cell in a panel work. In a partial-shaded panel, the difference among the temperature values of photovoltaic cells can normally exceed 20°C [HCW+14] while temperature can reach 150°C where an hotspot effect occurs [SM10].

Power converters maximize the generated power by searching for the maximum power point on the voltage-power curve of the PV field, independently of the chosen PV plant topology. This procedure, known as *Maximum Power Point Tracking (MPPT)*, analyzes locally the V-P curve of the field around a given reference point. This search process is generally based on a perturbative method, e.g. Perturb & Observe *(P&O)* or the incremental conductance *(IC)*, in order to detect any changes of the slope of the curve around the working point.

In Literature, a comparison of this methods is provided [HR00] [EC07]. In order to guarantee the minimum desired efficiency of power converters, the voltage of the MPP cannot assume all possible values but it should be restricted to a closed range of values. At the same time, the open circuit voltage of the PV field has to be limited because of security reasons.
The power converters have to be sized respect to the maximum power can be generated by the PV field. So, also the operating constraints depend on the chosen converter. An example of constraints for 6kW inverters are reported in Table 1.2.

Inverter Manufacturer	Operating Voltage Range	Maximum Open Circuit Voltage
Power One	180V – 530V	1000V
EnaSolar	120V – 450V	600V

Table 1.2: Typical inverter constraints for 6kW PV plant

In Figure 1.13, the constraints for the MPPT algorithm are overlapped to the voltage-power curve of a PV field. The operating voltage V_{mpp} can only assume a value belonging to the given range [180V–530V]. The open circuit voltage V_{oc} is much lower than its superior boundary (1000V).

A MPPT algorithm should find the best maximum power point independently of working conditions of the PV field.

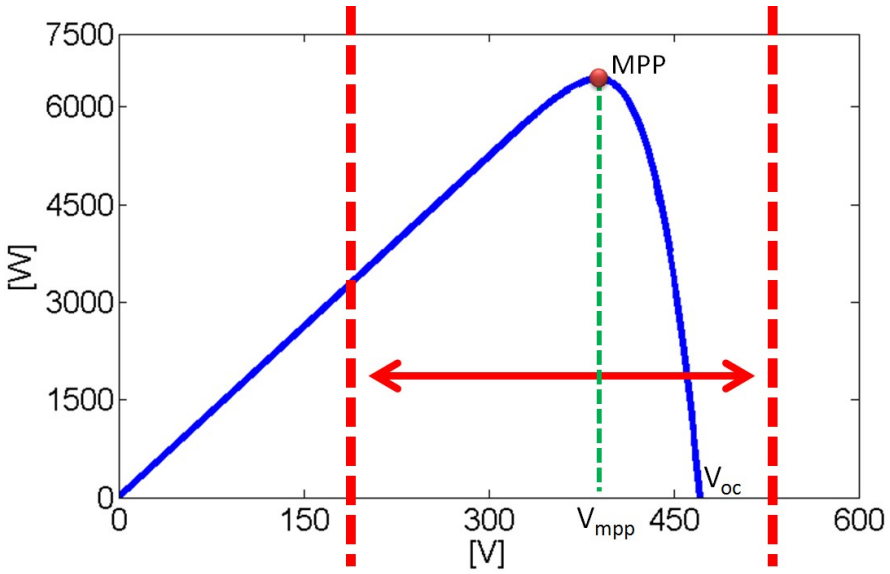

Figure 1.13: Range of acceptability of V_{mpp} voltage

Under partial shading of the PV field, since the V-I curve of each panel could exhibits different current levels, also different maximum power points (MPPs) occur in the voltage-power characteristic of the PV generator. In this case, the best MPP could be anywhere in the output curve of the PV field.

As shown in Figure 1.14, where the effects of a partial shading of the PV field are illustrated, the optimal MPP could be located anywhere on the voltage-power curve of the PV field. As shown, it could be located externally or near the allowed boundaries of voltage value of the PV generator. If the MPPT procedure finds a better MPP at a voltage in proximity of constraints values, the behavior of inverter is unpredictable [Hae05]. Some inverters power off if the MPP voltage is further reduced below the minimal allowed threshold. Since the start-up of inverter could require a significant amount of time, the is no advantage to choose a MPP belonging to the boundary regions.
Since the MPPT procedure is a local search algorithm, the achievement of the greatest power is not guaranteed.

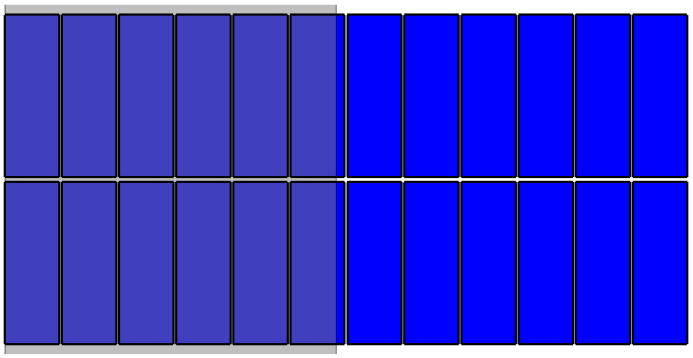

(a) Partially shaded PV generator

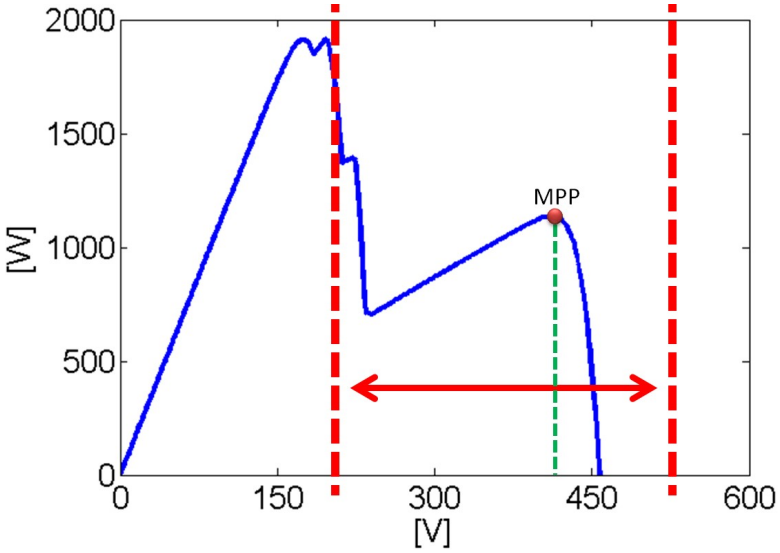

(b) Voltage-power curve of the PV generator

Figure 1.14: The voltage-power curve of a PV generator under shading exhibits different peaks reducing the MPPT efficiency

In Literature, the performances of the standard MPPT algorithms have been tested under shading conditions [CDDDN+13]

[MV14] showing that conventional methods are easy to implement but they suffer from oscillations at MPP and tracking speed is lower due to fixed perturb step [Say12]. In case of partial shading, the reduction in the overall efficiency of the system has reached about the 30% [GDdV13] because of MPPT failures.
Different MPPT algorithms have been proposed to track the global maximum under rapidly changing shading conditions [PA08] [JM14] [HNDM13] but they aren't commonly used into commercial inverters.

The mismatch losses reduction also depends on the chosen inverter topologies (see Figure 1.15).

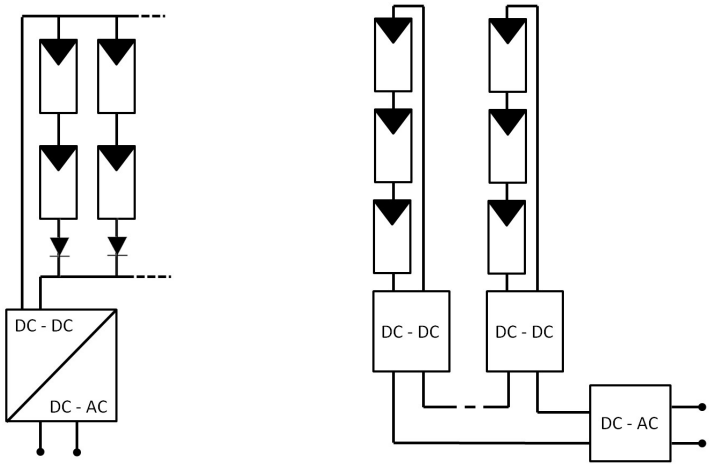

(a) (b)

The centralized and the multi-string inverter topologies, shown in Figures 1.15(a) and 1.15(b), are the most used, especially in large PV plants. In the former case, both the MPPT algorithm and the DC-AC conversion is provided by a unique power converter. In the latter case, the MPPT algorithm is executed for each row of panels but only the centralized inverter provides the DC-AC conversion.

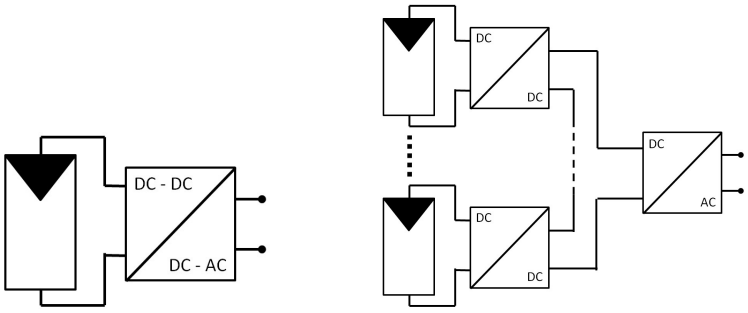

(c) (d)

Figure 1.15: Power converter topologies: (a) Centralized inverter, (b) multi-string inverter, (c) micro-inverter and (d) D-MPPT witch centralized inverter

In order to further reduce the mismatch losses, module-dedicated power converters topologies have been developed. So, instead of directly series-connecting all PV modules, without taking into account if they are working under mismatched conditions, a DC-DC converter is connected to each module and then the output of all module-dedicated power converters are series-connected in order to boost the string voltage.
Since the MPPT procedure is executed for each panel composing the PV field, this approach is named *Distributed MPPT (D-MPPT)*.

Thus, as regards the DC-AC conversion, two topologies are considered: in the former, each panel has its own DC-AC converter, and for this reason the power converter is also known as *micro-inverter*. In the latter, the DC-AC conversion is provided by the string or centralized inverter. These inverter topologies are shown in Figures 1.15(c) and 1.15(d).

The adoption of micro-inverters converting directly the extracted solar energy into AC power have different advantages. First, when shading phenomena occur, the generated energy is

maximized because a MPPT algorithm is executed on each panel. Even if it is correct, the continuous energy consumption due to the execution of the MPPT procedure itself has to be considered both when the PV field is working under mismatching conditions and in a full sunny day. In fact, when all the panels are working under the same conditions, the total efficiency of the system is reduced because a percentage of generated energy is uselessly consumed [FLP+08].
Nevertheless, because each panel is an independent PV generator unit, this inverter topology ensures an high modularity and robustness respect to the faults of single PV units.
Moreover, by using this architecture, simplified MPPT techniques as well as diagnostic procedures can be used.
Since it is executed on a smaller device, the MPPT procedure rapidly detects a shadowing phenomenon and change the voltage of the MPP in order to maximize the extracted power. In the worst case, even if the sweep of the whole voltage range of the panel characteristic should be executed, the time required to scanning the curve of the panel is much lower than that required to the same operation performed on the voltage-power curve of the field. During the voltage sweep operation, the total amount of generated energy isn't reduced because the other panels continue to working independently.
Obviously, since a dedicated inverter for each panel is used, the cost of the single photovoltaic unit increases. Instead, the direct production of AC power requires cabling having a lower cost as well as no blocking diodes installation. So, by using the micro-inverters, the fire risk is reduced since it limits the amount of DC current on a rooftop.

Instead, as regards the second topology, the adoption of DC-DC converters dedicated for each panel executing the MPPT procedure and of a centralized inverter requires an high voltage conversion ratio and efficiency to be affordable.

In effect, there isn't an optimal inverter topology. In [SWH14],

authors simulate the mentioned inverter topologies for four different PV installations (PV plant, rooftop, building facade, top of an electric vehicle) and estimate their performance for a time period of 30 years.
The performance of the inverter topologies change respect to the considered scenario. In particular, the multi-string inverter topology performs better in large PV plants and in high yield solar locations.
Instead, in the applications where complex shading scenarios occur, such as the building faced or the rooftop, the micro-inverters lead to boost energy production.
Also in [EAS+10], the authors demonstrate that the micro-inverters are the most suited inverter topology for small commercial and residential systems and that their performance, respect to centralized inverter, increases from 4% to 12%, depending also on the geographic location of the plant.

Moreover, even if the most suited inverter topology is used for a specific application and the MPPT tracking procedure has an efficiency of 100% (i.e., the optimal MPP is always found), during a shading phenomenon, the energy produced by all panels is not efficiently extracted by the PV field. In fact, the voltage and the current values of the optimal MPP depend on the characteristics of all panels belonging to the PV field but, due to the mismatching effects, the most shaded panels can reduce the MPP voltage and/or current.

In this case, a different electrical connection among panels or the disconnection of most shaded panels from the PV field can reduce the effects of the shadowing phenomenon and achieve different advantages.

1.2 The Reconfiguration of PV Plants

A dynamical reconfiguration of the PV field optimizes the utilization of all photovoltaic units leading to increase power production

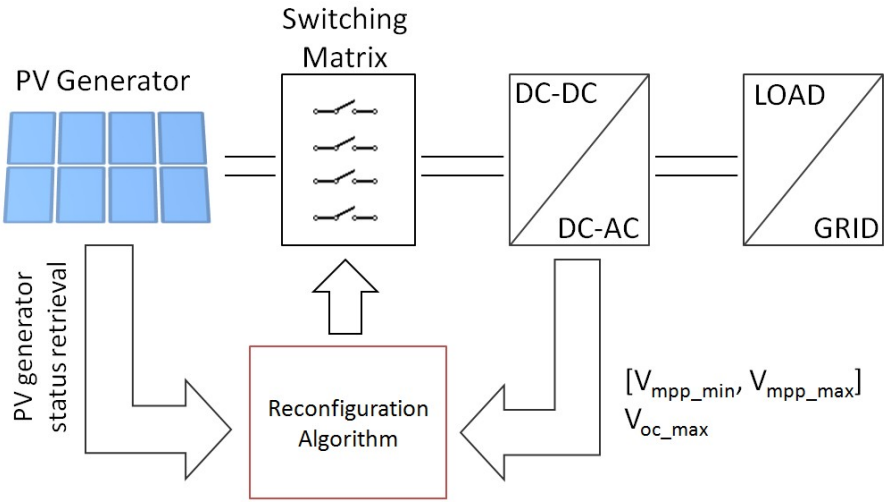

Figure 1.16: Block diagram of a Photovoltaic System Reconfiguration

in any environmental conditions without violating functional constraints of the power converter.

In Figure 1.16, a block diagram of a PV system including a generic reconfiguration process is shown. Respect to a standard PV System, the reconfiguration of PV plant requires at least two further functional elements: a) an intelligent unit processing some informations related to the PV system and providing the best electrical configuration for the panels and b) a *switching matrix* that modifies the electrical connections among panels.
In addition, the elements providing the informations related to the PV system should be considered.
From a general point of view, a reconfiguration algorithm requires the estimation of working conditions of all photovoltaic units as well as the knowledge of operating constraints of power converters. The informations describing the working conditions of PV modules/panels depend on the considered reconfiguration algorithm. The operating constraints of power converters are fixed for the chosen inverter.

If only shading effects on PV units are considered, then the solar radiance scenario over the PV generator should be sensed or estimated. In an ideal case, the solar radiance scenario should be achieved for each cell of the plant: this solution is unfeasible since a sensor for each cell is required, strongly increasing the photovoltaic system costs.
Conversely, the irradiance hitting each photovoltaic module could be sensed or estimated, but the solar radiance scenario is reconstructed by using a lower resolution.
In general, the PV systems performances could be improved taking into account all the phenomena negatively affecting them (e.g. permanent damages of photovoltaic units) and not only the solar radiance scenario at the reconfiguration instant.
For this reason, in this Thesis, the proposed reconfiguration algorithm doesn't consider the solar scenario at all, but takes directly into account the mismatching effects among panels and their operating status by processing their voltage-current curves.

Different electrical connections among panels increase the generated power and reduce the mismatch effects on voltage-power curve of the PV field.
In Figure 1.17, the solar radiance of a PV field is illustrated. In this solar scenario, the irradiance is symmetrically reduced on both rows. In particular, in each panels rows, five panels are totally shaded and only one is partially shaded.

The voltage-current curves of panels corresponding to this scenario are represented in Figure 1.18. The V-I curves of fully shaded panels have one current level only and a the lower short circuit current (blue colored line) while the partial shaded panels have multiple current levels (green colored line).

In Figures 1.19(a) and 1.19(b), panels having the same color are all series-connected in the same row. In particular, in Figure 1.19(a) the fixed standard configuration of panels is shown. Since the solar radiance is symmetrical on both rows, they have also the same voltage-current curve. The voltage-power of the field obtained by using standard configuration, represented by black

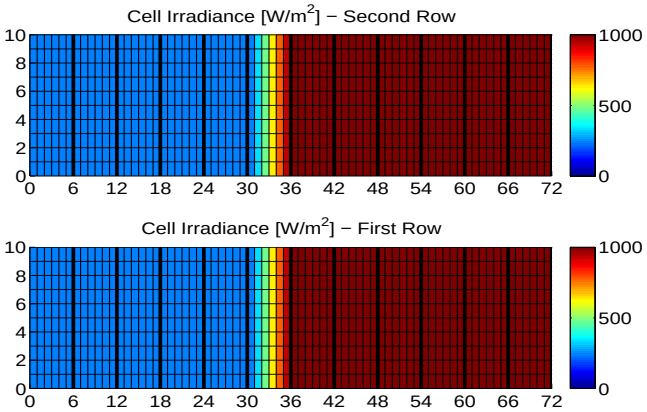

Figure 1.17: Solar radiance

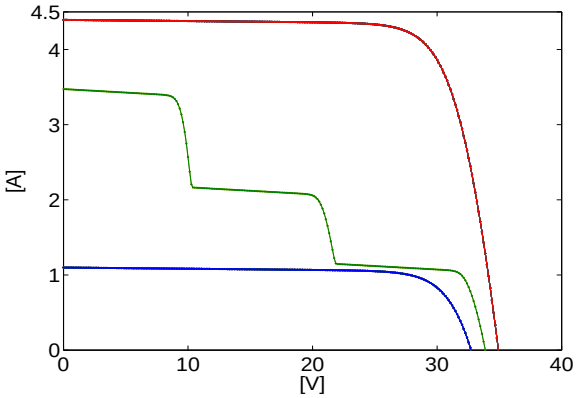

Figure 1.18: V-I curves of panels

colored line in Figure 1.19(c), has multiple MPPs.
In Figure 1.19(b), a possible result of a reconfiguration algorithm is shown. In this configuration, all fully and partially shaded panels are series-connected into the same string. In the voltage-power curve of the field corresponding to the modified configuration, the blue colored line shown in Figure 1.19(c), only two possible maximum power points having a power difference of around 20 Watts occur. Both the MPPs of the voltage-power curve of the recon-

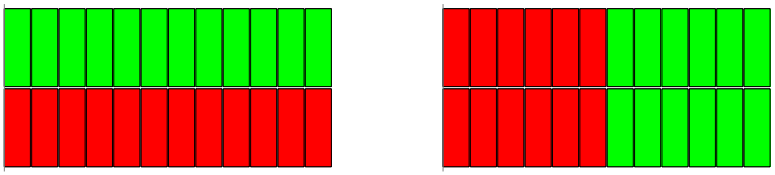

(a) Standard configuration (b) Modified configuration

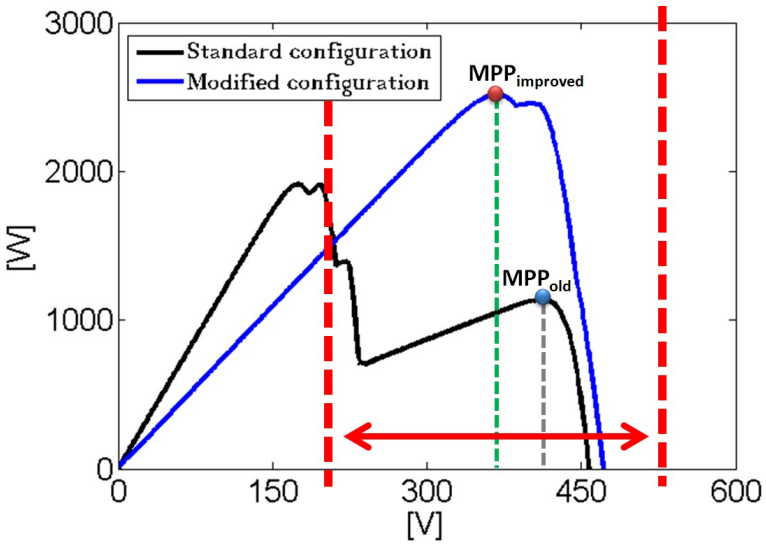

(c) Voltage-power curve of the PV field after electrical connections reconfiguration

Figure 1.19: The effect of PV reconfiguration

figured PV field are greater than all power peaks of the voltage-power curve obtained by using the standard configuration. So, if the MPPT algorithm chooses the lower peak as maximum power point, the mismatch losses are minimized anyway. For the example shown in Figure 1.19(c), respect to the standard configuration, the execution of reconfiguration procedure increases the generated power of 121%.

The reconfiguration procedure has different advantages. First, it maximizes the generated power of a PV field but also ensures

that power converters work always with their maximum efficiency. Moreover, safety conditions are easily respected, such as that on the open circuit voltage of the V-P curve of the field. In fact, in a PV system, all cables, switches, fuses, circuit breakers, and modules are rated for the maximum system voltage, that is 1000V, as established by the *National Electrical Code (NEC) 690-7*, in order to reduce the risk of fire.
Unlike D-MPPT, the reconfiguration algorithms require only the execution of single MPPT procedure and so only one centralized inverter is needed. At the same time, the PV panels don't require dedicated hardware. If a fault occurs, the reconfiguration procedure can detect which panels are working under abnormal conditions and it can disconnect them from the PV field. So, the reconfiguration procedure provides also monitoring and diagnostic functionalities.

The reconfiguration system strongly depends on the performance of the algorithm itself, both in terms of the required execution time and of the provided best electrical configuration of panels.
Depending on the algorithm, further sensors and a data acquisition system can be required. The hardware complexity is related to the needed information, that can be a voltage value measurement only or the acquisition of V-I curves of panels.
As regards the execution time of the whole reconfiguration procedure, it includes the time required to process data from sensors or to acquire the voltage-current curves of each panel, to execute the reconfiguration algorithm and to actuate the given configuration through the switching matrix.
This time as well as the energy consumptions strictly depend on the hardware technology.
A reconfiguration system, respect to a standard PV system, requires additional cabling in order to connect each panel to the switching matrix. The relays of switching matrix itself should be designed in order to reduce the risk of faults. In particular, semiconductor based relays have to be preferred to that electromechan-

ical, but they are more expensive.
The scalability of the reconfiguration systems depends not only on the algorithm, that has to consider the major number of both panels and strings, but above all on the number of relays of the switching matrix itself.
So, the reconfiguration procedure requires a dedicate hardware and software too, thus increasing the initial costs of the system.
Nevertheless, these costs can be much lower of the saved money if the reconfiguration procedure is well designed not only in order to achieve always the best configuration, but also to be executed when it is really necessary, i.e. during shading phenomena.

In general, the number of configuration to analyze to find the optimal solution depends on the number of panels, of electrical rows and on the chosen photovoltaic plant topology. Among all these configurations, only a subset respects required constraints of inverter. Moreover, the optimal or nearly optimal solution should be found in a very limited time, that is the hardest constraint to respect.

1.2.1 State of Art

In Literature, many approaches have been proposed for reconfiguring photovoltaic plants, such as based on deterministic and stochastic procedures as well as that based on statistical approaches. Deterministic procedures are developed to achieve a well-known desired goal that couldn't be only the maximization of power generation. In [SD90] and [APCO98], two reconfiguration procedures for a PV field supplying a motor have been illustrated. The chosen electrical configuration of modules depends mainly on operating conditions of the motor. So, these methods, even if they achieve the desired operating conditions of the motor load, cannot be applied in other situations where the maximization of the power extracted from the PV field is required. Moreover, they don't take into account the effective solar radiation hitting the modules but only maximize voltage or current injection into the motor to pro-

vide desired torque or speed.
These reconfiguration algorithms need a formalization and an *a priori* knowledge of the problem to be solved.
A further deterministic approach is based on irradiance equalization of rows of modules, as illustrated in [VQGGPL+09]. The basic principle is based on the reduction of the *bottle-necks* for current flux in a Total-Cross-Tied topology of modules by equalizing the current each row of modules provide. A similar approach has been used in [LPC10], where the *shading degree* for each row of modules in a Total-Cross-Tied PV plant topology is estimated basing on voltage and current measurements.
The shading level of modules is investigated also in the model based approach that has been developed in [NL08]. The estimation of the photo-generated current for each module is obtained by measuring only voltages across photovoltaic modules and by assuming a well known model for photovoltaic cells.
The measurement of the voltage and current generated by each module doesn't provide any information about the effective solar scenario over it. Instead, in these documents, it is assumed that the cells of the modules are always equally radiated at the estimated irradiance value. In many circumstances, PV modules are partially shaded and the generated current depends only on minimal irradiance hitting the cells of the module. The voltage, instead, depends also on the working conditions of the other modules connected in parallel if a TCT plant topology is used.
The efficiency of their procedure strongly depends on the assigned model of the PV module: the real behavior of a module, due to many reasons, such as mismatched working conditions of the PV cells, can differ from the numerical one.

In [VQGGPL+09], [LPC10] and [NL08], photovoltaic plants are divided into a static and a adaptive bank of modules. If modules belonging to the static bank work under mismatched conditions, then all these procedures ensure an improvement of performance by replacing modules of static bank generating the lower current with properly chosen module of the adaptive bank. Even if an improvement of performance has been demonstrated by using

these approaches, the distinction between a static and an adaptive bank of modules reduces the flexibility of the reconfiguration procedure respect to the many different shading scenarios. Moreover, in [EDKS13], the authors assume that the person using their system should have an a-priori knowledge of the shading scenario usually interesting his PV field and that he must select which modules should belong to the static part and which modules to the adaptive bank. That is the lower degree of flexibility. Moreover, since the reconfiguration procedure is a NP-hard problem, as also in [EDKS13] is assumed, then there is no deterministic procedure that could achieve an optimal solution in a time period that doesn't depend exponentially on the number of panels and the possible positions they can assume. The procedure proposed in [EDKS13] is based on the assumption that the reconfiguration is mixed integer quadratic programming (MIQP) problem. This kind of problem is usually solved by using a class of algorithms so-called branch and bound (BB) because they separate, if needed, the main problem into smaller ones by properly relaxing the constraints of each subproblem. The authors illustrate that they reconfigure a TCT topology of 6x4 modules by using different mathematical tools that are executed on a PC having an Intel Duo Processor, i.e. high computational resources, achieving for this reason an execution time of few tens of seconds. The same result is difficult to be achieved by the same procedure on a micro-controller, e.g. on devices having lower computational resources.

Stochastic procedures, such as that based on Ant Colony Optimization (ACO), Particle Swarm Optimization (PSO) and Evolutionary Algorithm (EA) are instead more flexible, as discussed in [PGBSA11]. In general, stochastic algorithms don't require any *a priori* knowledge about the problem to be solved but only the informations needed to estimate the reliability and the *fitness* of a proposed solution. The knowledge of the most suitable solution to the problem is acquired during the execution of the algorithm itself.
For example, a genetic algorithm learns by randomly exploring the solutions space. At each iteration, the provided solutions improve.

So, the analysis is focused only in the regions of solutions space containing the optimal solution. At the end of the procedure, the solution having the best fitness is provided.
Genetic algorithms, that are a subclass of the Evolutionary Algorithms, have been used mainly for the photovoltaic system design [KKPK06]. Instead, in [KMAP14], a genetic algorithm is used to reconfigure a photovoltaic plant that has been separated into a fixed and an adaptive bank of modules. The fixed part of the PV plant has a TCT topology. This algorithm, basing on the only short circuit currents of each panel, chooses which panels belonging to adaptive bank should be parallel-connected to each panels row belonging to the fixed PV field. The short circuit current of a panel is related to the solar radiance hitting it. As the authors assert, this choice is made in order to limit the execution time. Nevertheless, they don't consider that the maximum power point of the field doesn't depend on the short circuit current but on the whole voltage-current curves of the panels. For this reason, the maximization of the generated power is not guaranteed at all.
Instead, the genetic algorithm proposed in Chapter 3 chooses, in a reasonable time, the best solution basing on voltage-current curves of panels.

Reconfiguration algorithms can also be based on a statistical approach: in [BMV14], authors suggested to use the False Discovery Rate (FDR) to find a nearly optimal configuration. This statistical procedure lead to test only a subset of all possible configurations which is considerably smaller than the one needed by other methods. Nevertheless, statistical methods require at least a lot of memory usage and computational resources. So they aren't generally used in Embedded Systems.

1.2.2 Shading Detection and Forecast

The choice of time instant when the reconfiguration procedure should be executed plays a key role in the maximization of the

performance. In fact, if the energy losses, due to the repeated executions of the reconfiguration process, exceed the saved energy, then there is no advantage into applying it.
Some proposed reconfiguration algorithms [LPC10] [NL08] also attempts to detect partial shading phenomena by measuring voltage variations across one or multiple rows of modules.
Unfortunately, the major drawback of this technique is that the voltage change doesn't lead to distinguish a shading phenomenon from a global change of the solar radiance over the PV field, especially when the PV field is under low solar radiance levels (i.e. at the sunrise and sunset). Moreover, if the reconfiguration procedure allows the panels to be disconnected from the PV field, then any shadowing phenomenon occurring on disconnected panels is not sensed at all. Since no voltage change occurs when the shadow is moving over the disconnected panels, there's no way to understand if a shadow left the PV field.
In [CDDM$^+$14], authors show that voltage level can also be used to classify PV modules as fully lighted or shaded. In this case, the estimation of a proper (but not declared) threshold level for the voltage has been taken into account. So, these methods require a voltage sensor for each panel or row of panels leading to increase the system costs.
On the contrary, these methods don't measure changes of the currents provided by electrical rows. Furthermore, in [CDDM$^+$14] authors consider to install current sensors for each row but they don't use them in their algorithm, assuming that future detection algorithms can require these signals. In fact, a change in the currents of panels rows could indicate conditions for which the reconfiguration process shouldn't be executed even if a voltage change suggests it.
In order to solve this issue, it is necessary to acquire voltage and current values for each photovoltaic module (independently if it is disconnected or not) or to use a different approach.

In effect, an attempt to forecast shading scenario variations has been achieved by using different approaches.

Sophisticated algorithms have been proposed to estimate shadow motion over a PV plant basing on acquired sequential images near the PV plant itself [SKS12]. In the procedure illustrated in this document, no reconfiguration of PV plant has been considered, but only the prediction of the generated power trend. The great drawback of these methods is the need of installing a proper video capturing device. These procedures can be used to efficiently predict power generation and, in general, if a cloud has left a specific area. Despite they efficiently predict the cloud movement in the sky, it is very difficult to relate accurately the clouds position to that of its shadow over each panel of the PV field.

Chapter 2

The Undersampling Algorithm

In this Chapter, a technique to reduce the number of samples of voltage-current (V-I) characteristics of photovoltaic panels is illustrated.
This procedure is not specifically designed for the reconfiguration purposes, but it can also provide informations useful to the diagnosis of PV panels.

In the second part, the experimental results, obtained by applying the under-sampling algorithm to a set of acquired voltage-current curves of a real photovoltaic panels, are analyzed. In particular, the most problematic cases are discussed.

2.1 Introduction

The under-sampling technique proposed in this Chapter approximates the acquired V-I curves of panels by line segments.
In general, the samples belonging to piecewise linear V-I curves should be properly chosen to minimize the difference between the original and the under-sampled curves. This difference is referred as the *approximation* or *reconstruction error*.

The minimization of the approximation error is achieved by preserving the regions of the V-I curves having the greatest information level. For example, the comparison between the V-I curves of four series-connected panels and their own V-I curves in Figure 2.1 suggests to preserve all samples belonging to non-linear regions of V-I curves. In fact, the non-linear regions of V-I curves of single panels appear both in the V-I and V-P curves of series-connected panels.
So, the local maximum and minimum power points of the V-P curve belong to these regions.

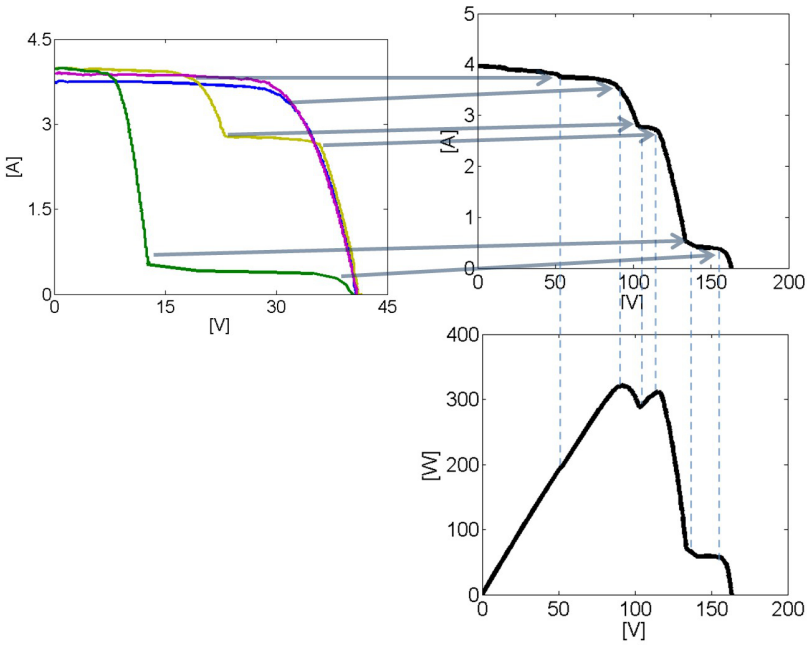

Figure 2.1: Voltage-current and voltage-power characteristics of a series-connection of four panels

The selection procedure of samples belonging to decimate V-I curves should be robust respect to non-idealities of V-I curves. In fact, the sampled data of V-I characteristics of panels could be

noisy, unordered, redundant or insufficient to well describe some parts of the curve itself.

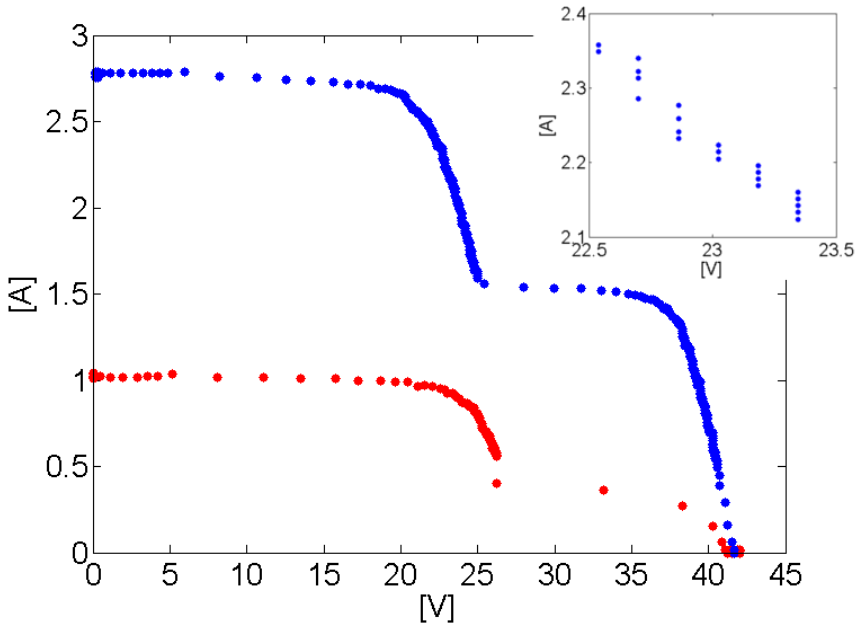

Figure 2.2: Two acquired voltage-current characteristics of a photovoltaic panel

In Figure 2.2, two acquired voltage-current characteristics of photovoltaic panels are illustrated. Both these characteristics exhibit an heterogeneous density of samples. In particular, in the current range [0.1A - 0.5A], the non-linear region of the red colored characteristic has only 3 samples. Duplicate data are present in different parts of the V-I characteristics due to the adopted sampling method and to the low sampling resolution of analog-to-digital converters (ADCs) for voltage and/or current measurements. Moreover, the samples aren't properly sorted by voltage or current values because of combined effect of measurement noise and low resolution of ADC.

This technique should also provides informations useful to the

diagnostic and prognostic of photovoltaic panels. A required information is, for example, the *degree* of mismatching working conditions of the PV panel that could be represented by the number of maximum power points of the voltage-power characteristic of the panel itself. So, the under-sampling technique should be able to find the maximum power points of the V-P curves.

The most critical constraint is the execution time of the procedure: the under-sampling technique should be executed in amount of time much lower of that required to acquire the V-I curve of a single panel (e.g., 60 milliseconds as required by the photovoltaic optimization system Endana [Web14]), so it can be considered a *real-time* procedure.

In Literature, there are different proposed methods to approximate a sampled curve by line segments [Yin06]. These approaches can be classified into three classes: sequential, split-and-merge and dominant point-detection.

The first class includes all methods that, after choosing a starting point, sequentially scan a curve in order to determine the longest possible line segment until the reconstruction error exceeds a fixed tolerance, then restarts the scan-along process at the next data point to find the remaining line segments. The quality of the approximation depends both on the starting point and on the chosen error threshold.

The second class includes methods that start with an initial random approximating polygon and then refine it by iteratively applying the two-phase split-and-merge process. At the splitting phase, the line segment is split into two segments at the data point which has the farthest distance from the original line segment if the reconstruction error exceeds a fixed error threshold. At the merging phase, two adjacent line segments are merged into a new one if the resulting approximation error maintains still below a fixed error threshold. The performance of the split-and-merge approaches depends on the initialization step and on the chosen thresholds. A well known algorithm belonging to this class is the

Ramer-Douglas-Peucker procedure [Ram72].

The methods belonging to the third class initially evaluate the curvature at every data point basing on its local property. Then the dominant points are detected by a non-maxima suppression process. The performance of most dominant point-detection methods depends on the strategy adopted for the curvature evaluation.

The approximation of V-I curves by using the introduced approaches is unfeasible for different reasons:

- these approaches are very general and they are not optimized for detecting the maximum power points on V-I curves of panels without multiplying voltage and current values for each sample of the curve. So, they are time-consuming since they don't guarantee the minimization of multiplication between voltage and current values.

- these approaches are susceptible to the noise and to the poor quality of data sampling process (e.g., unordered data).

- these methods require that the approximation error must be well defined, but, for the proposed goal, the error value should depend on both voltage and current (or voltage and power) values

Other approaches performing structural pattern analysis have been introduced basing on stochastic algorithms [Yin06][SSS03] or dynamic programming [TPM08] in order to decompose an analyzed curve into a set of lines and arcs.

The method proposed in [TPM08], that is based on the angular orientation analysis of the curve, needs the knowledge of the exact number of the arcs to be fitted on the analyzed curves. Even if some authors promise to find a procedure to estimate this number, it is a great limitation since in many scenarios, such as that analyzed, the number of non-linear regions is unknown.

In fact, the V-I curves of panels have a number of non-linear regions that depends on solar radiance conditions of each module

and on the number of modules itself.
Moreover, the non-linear regions of V-I curves are not well approximated by arcs but by *exponential* curves that are harder to fit.
At the end, each PV panel has its own properties that change during panels lifetime itself. So, a real-time procedure ensuring a good approximation of V-I and V-P curves of panels by using arcs and other more complex fitting functions cannot follow these approaches. In particular, if the local maximum and minimum power points of the V-P curves have to be correctly located.

Instead, the proposed procedure to approximate the V-I curves by line segments well fits the initially discussed constraints by only assuming the *monotonicity* of the analyzed curves. The monotonicity of curves is a feature not only of photovoltaic modules characteristics but also of other energy sources, such as the fuel cells.

2.2 The Under-sampling Method

Basing on the Section 2.1, the samples of the V-I characteristics of panels to choose for the minimization of approximation error belong to each non-linear region of the curves. In particular, among samples of these regions, both that having the maximum and minimum power values can be considered the fundamental points of the curves. The local maximums and minimums of voltage-power are also referred as *Maximum Power Points (MPP)* and *Inflection Points (IP)* of voltage-power characteristic of the panel.
Moreover, the starting and the final points of the V-I curve should be found too.

The desired final result of this procedure is overlapped to the complete numerical voltage-current curve in Figure 2.3. The samples at the open circuit voltage (i.e. having zero current) and that at the short circuit current (i.e. having zero voltage are indicated by filled green circles. The MPPs and the IPs are represented by

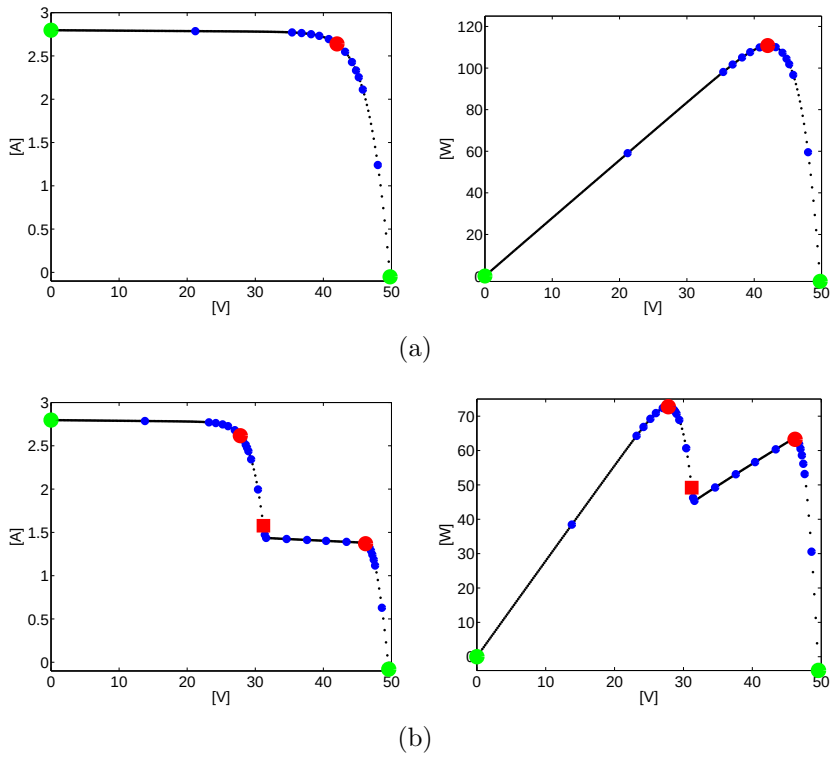

Figure 2.3: Result of the under-sampling procedure for a characteristic of a panel having only one MPP (a) and two MPPs (b)

red filled circles and squares respectively. The other selected samples are indicated by blue filled circles.
The non-linear regions corresponding to the peaks of voltage-power characteristic of the panels have a number of samples greater then inflection regions. In particular, these last regions have been represented by a single point because of net slope change around the inflection point. The net slope change is caused by switching on of the bypass diodes.

In a real PV system, where the voltage-current characteristics are acquired by means of a sampling process, the points of voltage-current curves couldn't have a constant current or voltage

difference, as illustrated in Figure 2.2, so the regions between each couple of MPPs and IPs containing very few samples are detected. Then, all samples belonging to these regions are selected.

The under-sampling procedure can be divided into two main parts: first, the localization of local maximum and minimum samples of voltage-power curve of the panel is achieved; then, basing on position of these fundamental points, a minimum set of samples of the voltage-current curve of panel is chosen in order to minimize the reconstruction error.

The proposed under-sampling technique reduces the computational costs by minimizing the usage of mathematical operations requiring a significant CPU time, such as multiplications and divisions. In fact, procedures like the search for local minimums and maximums of the V-P curves generally require the calculation of power values obtained by multiplying the only available voltage and current values. Instead, the proposed localization procedure of MPPs and IPs is based on comparisons, logical and mathematical operations having a lower computational cost, such as the addition and subtraction, that are executed on voltage and current data only.

2.3 Localization of MPPs and IPs

The first part of under-sampling procedure is composed by following steps:

- Evaluation of open circuit voltage V_{oc} and short circuit current I_{sc} values
- Histograms bins width estimation
- Density and Width Histograms Calculation
- Comparison between Normalized Values of Width Histograms

- Corrective Procedure for Maximum Power Points and Inflection Points Positions

2.3.1 Evaluation of V_{oc} and I_{sc} values

The under-sampling procedure is executed only on the samples of the curves of panels having both positive voltage and current values.

For this reason, the first step is the evaluation of open circuit voltage and short circuit current values, that are the end points of the V-I curve. By this way, the under-sampling algorithm analyzes only samples belonging to voltage range [0 - V_{oc}] and to current range [0 - I_{sc}].

The open circuit voltage is identified by the minimum voltage value of samples having a non-positive current or the highest voltage value if there aren't samples matching the requirements. Similarly, the short circuit current is identified by the minimum current value of samples having a non-positive voltage or the highest current value if there aren't samples matching the requirements.

The evaluation of V_{oc} and I_{sc} values also reduces the execution time of the under-sampling procedure by analyzing only a subset of the original data.

2.3.2 Histograms Bins Width Estimation

The position of MPPs and IPs is found by detecting regions of V-I curves having a significant slope change. The slope of different regions of V-I curves are described by an histogram for each axis. For each axis, an histogram bar measures the difference between the maximum and the minimum values of the quantity assumed by samples on the opposite axis. By this way, the interval widths covered by samples on the opposite axis are estimated.
If the estimated widths are divided by bins width, that are all equal for the same histogram, then also the incremental ratio is estimated. So, histograms can both measure widths of intervals that samples cover on the opposite axis and the slopes of regions

identified by histograms bins. In this Thesis, this kind of histograms are referred as *Width Histograms (WH)*.
For each histogram bin, the number of samples belonging to it is memorized too. So, a new histogram is obtained, referred as *Density Histogram (DH)*.
An example of both WHs and DHs for each axis are illustrated in the Figure 2.4 for a multi-modal V-I curve. For this curve, the WH and the DH calculated on voltage axis are very different since the samples are separated by a fixed voltage step independently of the local trend of the curve.

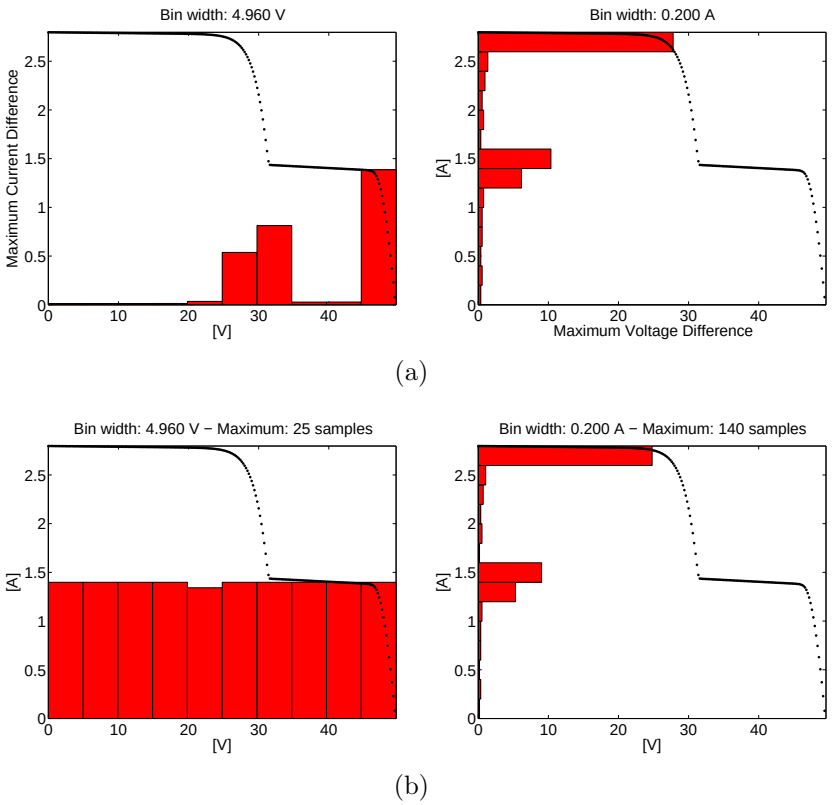

Figure 2.4: WHs (a) and DHs (b) calculated for a numerical V-I curve having two MPPs

The goal of using WHs is discerning *all* high-slope linear regions from that having a lower one.
The main drawback of using histograms is the choice of bins width that depends both on the slope of linear regions and on the local density of curves. In Figure 2.4, the width of histograms bins has been arbitrarily chosen.

In the voltage-current curves of panels, the slope of regions identified by the histograms bins depends on different parameters, such as the series and shunt resistances, the aging of panels or the switching on of by-pass diodes. Moreover, since solar radiance can hit differently each module in a photovoltaic panel, the voltage and current values at which slope change occurs are unpredictable. For these reasons, it is very difficult to estimate analytically the histograms bins width as well as the position of MPPs and IPs.

The bars height can be negatively influenced by the variable local density of V-I curves.
In Figure 2.5, three different bins widths of the histograms are used for the same voltage-current curve of a panel.
In the first case (see Figure 2.5(a) on the left), the histograms bins width is overrated (7.92V). So, the regions of V-I curve having different slopes are included into the same histogram bin and it is not possible to detect the two high slope regions in the range [25V – 40V] by only observing the histogram bars.
In the second case (see Figure 2.5(a) on the right), the histograms bins width is narrow (1.32V) and the bars heights are very susceptible to the local density of V-I curves. . Unfortunately, it is not possible to predict the density of V-I curves, so a wider bin should be accepted (3.96V, see Figure 2.5(b)). In this case, all high slope regions are included into its own bin and the susceptibility respect to the non-idealities of V-I curve (e.g., noise and data lacking) are reduced.

The methods already presented in Literature, such as the well known Friedman-Diaconis rule [FD81], aren't well suited to the

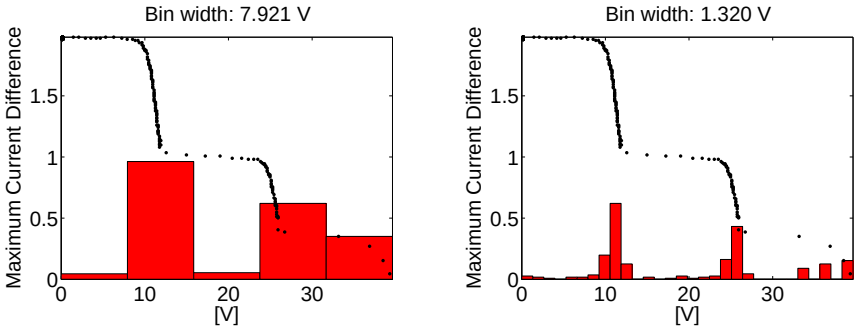

(a)

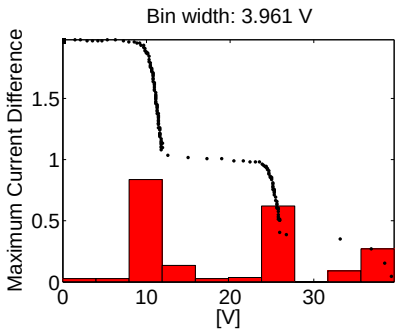

(b)

Figure 2.5: Bins width: overrated (a), underrated (b) and best (c)

histograms bins width estimation since they are based on the statistical analysis of the density of data. In the V-I curves of panels, instead, the points, depending on the sampling process, should have a fixed voltage or current difference among them (see Figure 2.4(b)). So, this estimation cannot be accurate for both histogram axis.

In a first attempt, bins width values have been calculated basing on typical values of series and shunt resistance of commercial panels. In particular, since bins width could be approximately by equations (2.1) and (2.2):

$$\Delta I = I_{sc} - I_{mpp} \tag{2.1}$$

$$\Delta V = V_{oc} - V_{mpp} \tag{2.2}$$

where I_{mpp} and V_{mpp} are respectively the current and the voltage of the MPP of a V-I curve of a module.

Basing on [NFV12], the following equation is obtained:

$$\frac{\Delta I}{V_{mpp}} = \frac{1}{R_{sh}} = \frac{I_{sc}}{R_{sh\_STC} I_{sh\_STC}} \tag{2.3}$$

that becomes:

$$\Delta I = \frac{V_{mpp} I_{sc}}{R_{sh\_STC} I_{sh\_STC}} = \frac{0.8 V_{oc} I_{sc}}{R_{sh\_STC} I_{sh\_STC}} \tag{2.4}$$

At the same time, the equation (2.2) becomes:

$$\Delta V = 0.2 V_{oc} \tag{2.5}$$

since, for a non-shaded photovoltaic panel, *statistically* the V_{mpp} value belongs to the interval $[0.8V_{oc}, V_{oc}]$.

Even the equations (2.4) and (2.5) are correct, the parasitics parameters change for each panel and they increase during panels lifetime. For these reasons, histograms bins width have been estimated through an iterative procedure.

The proposed procedure analyzes separately the distribution of samples respect to the voltage and current axis. For each axis, the histogram is calculated iteratively by setting an increasing number of bins until a maximum value has been reached. The maximum number of bins depends on the lowest density value among regions of the V-I curve in order to stop the procedure before reaching an under-optimal bins width value (see right Figure 2.5(a)). For the voltage (current) axis, this value is set by calculating two times the minimum positive current (voltage) difference between consecutive samples.

Initially, for each axis, the number of bins is set to one, i.e. equal to the full range on the considered axis.

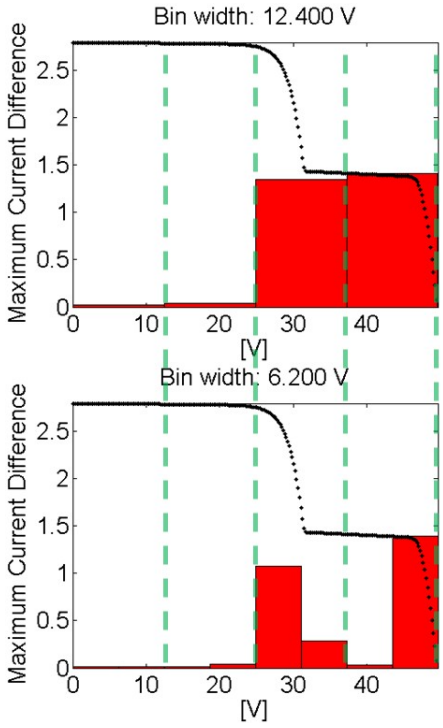

Figure 2.6: Doubling of histograms bins. The boundaries of histograms bins overlap when the number of bins is doubled.

Then, at each step of the procedure the number of bins is doubled so that a correspondence among bars position of two consecutive steps is maintained (see Figure 2.6). In particular, since at each step the number of bins is doubled, the boundaries of two consecutive bars at the j–th step overlap with boundaries of bars calculated at (j-1)–th step .
So, the heights of bars calculated at two consecutive steps of the procedure could be compared among them to discover significant differences between the histograms they belong to.
In particular, in order to detect a slope change at the j–th step, the difference of heights of two consecutive bars is compared respect to the height of the bar calculated at the (j-1)–th step that overlaps with them.

The greater is the number of bins, the more precise is the localization of the voltage or current values where a slope change occurs in the V-I curve. So, the points positions delimiting linear regions having an high slope can be estimated more precisely.

In particular, if an highest slope region has been detected by considering a lower number of bins, then two cases occur by iteratively increasing the number of bins: a) the same high slope linear region is always detected or b) the previously detected high slope linear region is split into two separated ones.

So, the initial number of bins is set to one. Then, this value is doubled until the estimated constraint is exceeded. For each given number of bins, the following steps are executed:

1. *Calculation of Width Histogram*
   For each histogram bin, the difference between the maximum and the minimum current values of samples belonging to that interval is calculated.

2. *High-slope Regions Detection*
   Each histogram bar value is compared respect to the nearest one. If a difference between the heights of the consecutive bars is significant, then a slope change occurs at voltage value where the bars are located.
   A slope change is detected when the heights difference exceeds 50% of bar height calculated at the previous step.
   Moreover, the *sign* of this difference defines the sign of the slope variation, as well as the presence of a MPP or an IP at that voltage value.
   At each step, for each region having an high slope respect to the voltage axis, a couple of voltage values at which slope changes are identified.
   The presence of an high-slope linear region is identified by an *ordered sequence* of its two boundaries: the former occurs at a voltage value corresponding to the non-linear re-

gion including the MPP, the latter occurs at a voltage value corresponding to the non-linear region including the IP. The difference between each couple of voltage values is the optimal voltage width for *that* high-slope region.

3. *Linear Regions Detection*
   If a detected region doesn't contain any further non-linear region, by increasing the number of histograms bins the difference height among bars belonging to it tends to lower and lower values. This ensures that an high-slope *linear* region has been definitively found.
   In particular, if the difference between the heights of two consecutive bars belonging to detected regions is lower than 50% of bar height calculated at the previous step and having the same voltage range, then a linear region has been found. Each time a linear region is definitively identified, it is marked to be considered during the final step of the estimation process.

At the end of the procedure, interval widths of different linear regions having the highest slope respect to the voltage axis have been identified. In a first attempt, the minimum voltage interval width of linear regions has been returned as optimal solution. Even if it can be correct, a very narrow histogram bin could not detect high slope regions having a very low density of samples (see right Figure 2.5(a)).For this reason, the average voltage width of linear regions is returned as optimal bins width value.
A procedure similar to that illustrated for voltage axis is applied on current axis.
At the end of this procedure, an optimal bins width for each axis has been obtained.

In Figures 2.7 and 2.8, the steps followed by the histograms bins width estimation procedure are illustrated for both a V-I curve having only one MPP and that having two MPPs.
In Figure 2.7, from the beginning of the procedure, a unique voltage interval (indicated by blue and green lines) is identified. This interval include two histograms bars having a difference greater

than 50% of the height of the bar calculated at the previous step (or of short circuit current value if it is the initial step). So, at each step the width of this interval is further narrowed until the minimum histogram width (estimated equal to 400mV) is reached. At the end, a voltage bins width equal to 12.45V is estimated.

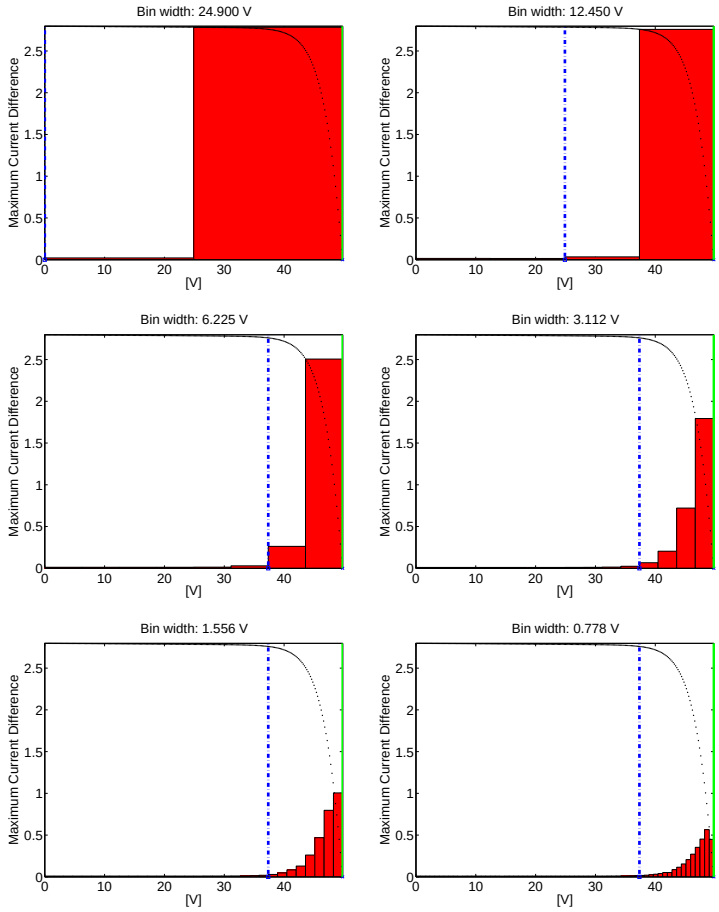

Figure 2.7: Bins width estimation procedure (one MPP)

In Figure 2.8, also in this case, at the beginning of the procedure, a unique voltage interval (indicated by blue and green lines) including two histograms bars having a difference greater than 50%

of short circuit current is identified. But, referring to the Figure 2.3.2 on the left, at this step this voltage interval is split into other three since three couples of bars having a great height difference are identified. Until the minimum bins width (estimated equal to 400mV) is reached, the width of these intervals is continuously refined at each step.
At the end, a voltage bins width equal to 7.086V is estimated.

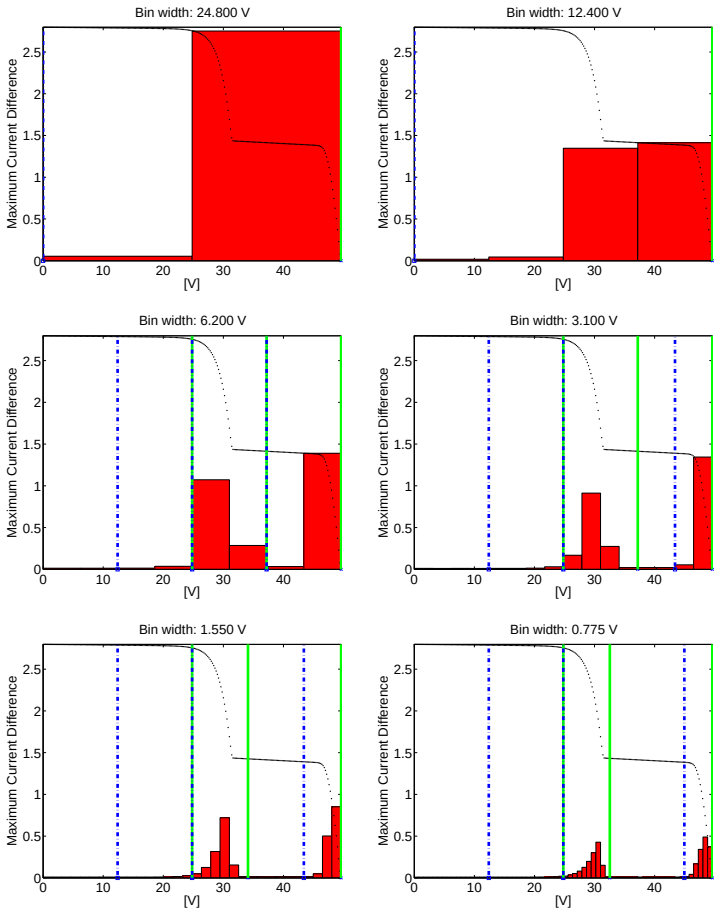

Figure 2.8: Bins width estimation procedure (2 MPPs)

2.3.3 Histograms Calculation

For each axis, two classes of histograms are calculated by assuming optimal bins width: a *Density* Histogram (DH) and a *Width* Histogram (WH). For each axis, the former represents the distribution of the samples of V-I curve of panel, the latter represents the interval width that samples cover on the other axis.

The procedure for the calculation of WH on voltage axis follows these steps:

- starting from the open circuit voltage, the range [0 - V_{oc}] on the voltage axis is divided into sub-intervals having equal width calculated by the related procedure.
- for each sub-interval, the maximum current values of samples belonging to each bin is looked for (see left Figures 2.9 and 2.10).
- for each sub-interval, starting from that at zero voltage, the index of nearest sub-intervals at lower voltage having at least one sample is found.
- for each sub-interval, starting from that at zero voltage, the difference between its maximum current value and that of the nearest non-empty bin previously found is calculated (see right-side Figures 2.9 and 2.10).

By excluding the empty bins from WHs calculation, the robustness of the procedure respect to data lacking is improved because the information about the trend of the curve is preserved.
A similar approach is applied on current axis, but considering the maximum current value I_{sc}.

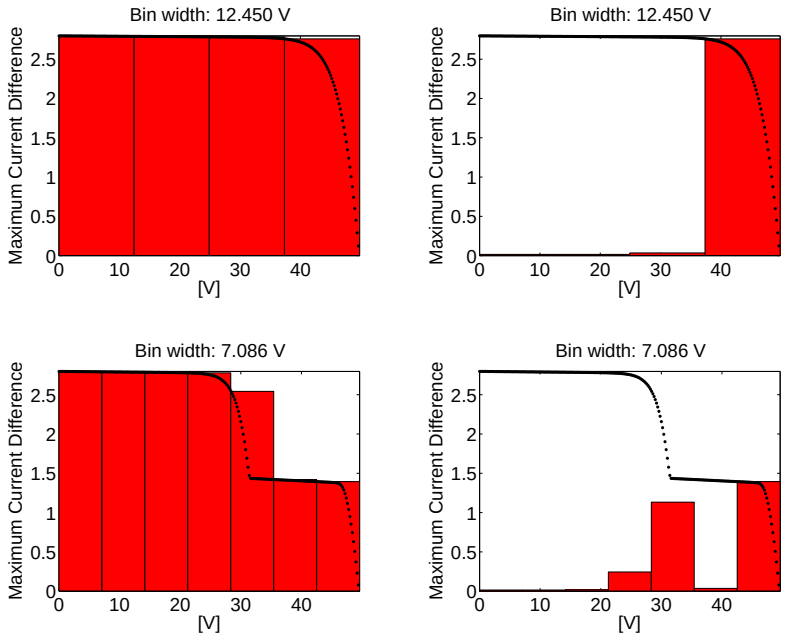

Figure 2.9: Calculation of Histograms on voltage axis: maximum detection (left) and the final result (right)

2.3.4 Comparison between Normalized Values of Width Histograms

Since Width Histograms are referred to different quantities (voltage and current), then they cannot be used for comparisons. For this reason, a normalization procedure should be executed: the values of each histogram are divided respect to their maximum value.

If the under-sampling procedure is executed on a 32-bit microcontroller having no float support, then the normalization procedure produces binary values (0 or 1) because of rounding operation to nearest integer.
Instead of applying a normalization procedure, histograms values are properly scaled in order to assume the same range. So, a scale factor should be calculated for each histogram. In order to

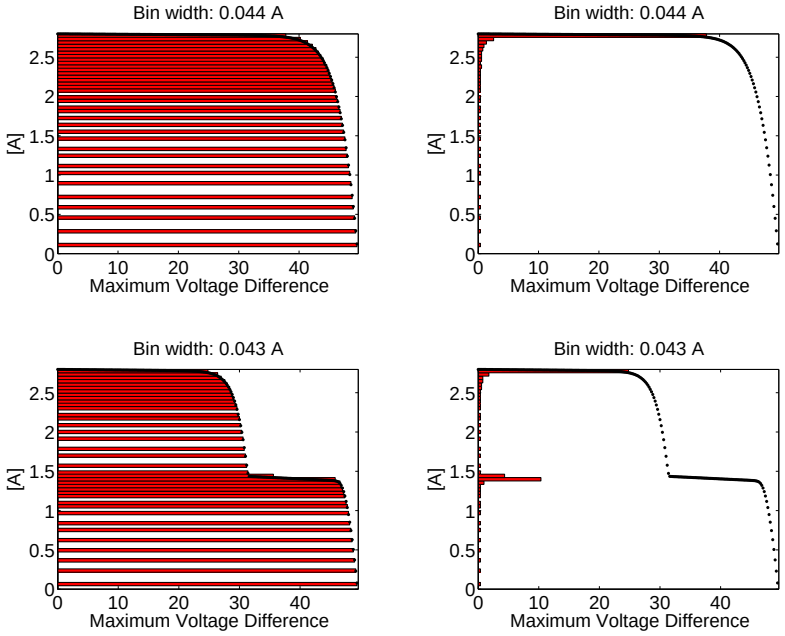

Figure 2.10: Calculation of Histograms on current axis: maximum detection (left) and the final result (right)

minimize the number of operations having an high computational cost, the ratio between the maximum value among bars of the two histograms and the maximum value of the considered histogram is chosen as scaling factor. Moreover, the normalization process can be applied only to the histogram having the lowest maximum value, that is generally that on the voltage axis, since the other one remains always unchanged.

For each sample of the voltage-current curve of the panel, the histograms bins on the voltage and on the current axis that contain it are identified and the corresponding *normalized* widths are compared.
The result of this comparison leads to guess the position of maximums and minimums of the voltage-power curve of the panel.

In the Figure 2.11, the result of the comparison among the normalized histograms bars for two numerical V-I curves is illustrated. In order to better visualize it, this comparison is illustrated as difference among the histogram bars values corresponding to each sample of the curves and by further scaling these values for a factor equal to $0.5 \cdot P_{max}$. So, a change of comparison value is detected by a sign change of the area plot and by their different color too. So, the cyan colored part of the graph correspond to that (blue colored) samples for which the normalized histograms bars on current axis are greater then those on voltage axis. Conversely, the magenta colored part of the graph correspond to that (red colored) samples for which the normalized histograms bars on voltage axis are greater then those on current axis.
The guessed positions of MPPs and IPs correspond to those of samples, indicated by black sign markers in Figure 2.11, for which a sign change occurs into the difference graph.

So, the guessed positions of MPPs and IPs are found without multiplying voltage and current values for each sample of the panels characteristics. Instead, the normalization step requires to execute a division for each histogram bar. Nevertheless, the total number of histograms bars is always lower than the total number of the samples of V-I curves.

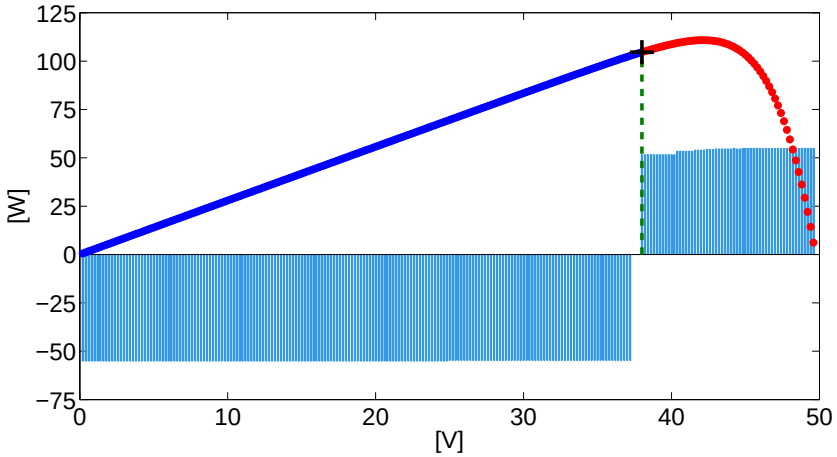

(a) Single MPP

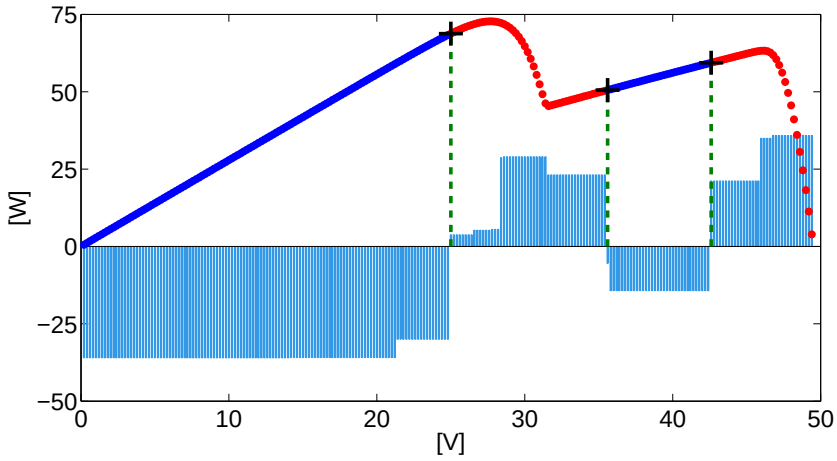

(b) Two MPPs

Figure 2.11: Normalized histrogram bars comparison for each sample of the V-I curves and guessing of MPPs and IPs positions

2.3.5 Iterative procedure for MPPs and IPs Positions Improvement

The guessed positions of MPPs (IPs) couldn't match real positions of maximum (minimums) in the voltage-power curve of the panel, as illustrated in Figure 2.11. The guessed positions of MPPs (IPs) can differ from the real ones mainly because they always correspond to the border position of the histogram bars but not necessarily to those of the highest bars. In fact, to detect the position of a MPP or IP only a change in comparison results is required, independently of the histograms bars values. In order to solve this problem, a further iterative procedure has been introduced.
This iterative procedure analyzes the regions around each guessed MPP or IP in the voltage-power curve of the panel verifying if a better MPP (i.e. a sample having an higher power value) or IP (i.e. a sample having a lower power value) can be found.
In particular, the analysis of voltage-power curve of the panel is performed by measuring the power and voltage change respect to a current step change.
By measuring the power variation, the procedure can estimate if a guessed MPP or IP have respectively the highest or the lowest power value respect to the samples around them.
By measuring the voltage variation, the procedure is more sensible to the presence of a further linear region having a different current level in proximity of the considered singular point.
So, by limiting voltage change respect to current change, also the *optimal* current step value can be properly calculated.

Initially, the current step value is assumed to be equal to the optimal bins width returned by procedure explained in Section 2.3.2. Every time the current perturbation leads to a the voltage change exceeding a threshold value, then the current step value is halved. The threshold value can be set equal to 10% of open circuit voltage of the V-I characteristic of the panel.
Once the optimal current step has been estimated, the current perturbation is performed in order to search for a better MPP or

IP on the voltage-power curve of the panel. If this happens, the current perturbation is iteratively performed until no better MPP or IP is found.

The result of this procedure is illustrated in the Figure 2.12.

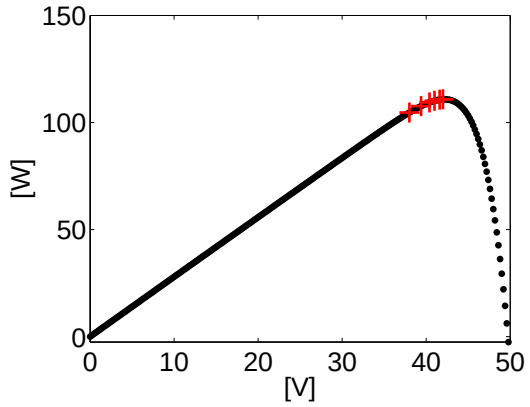

(a) Single MPP

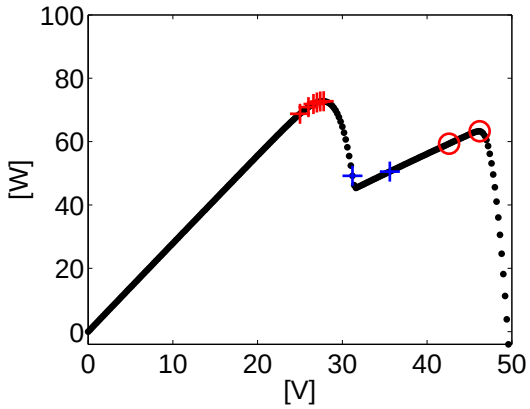

(b) Two MPPs

Figure 2.12: Iterative procedure to improve positioning of MPPs and IPs

2.4 Minimization of Reconstruction Error

Once the position of fundamental points of voltage-power curve of the panel has been correctly estimated, further samples of the V-I characteristic of the panel are selected in order to minimize the reconstruction error.

Until at this step, the under-sampled V-I curve of the panel is composed by the sample at the open circuit voltage, the sample at the short circuit current and by the samples corresponding to the MPPs and IPs.

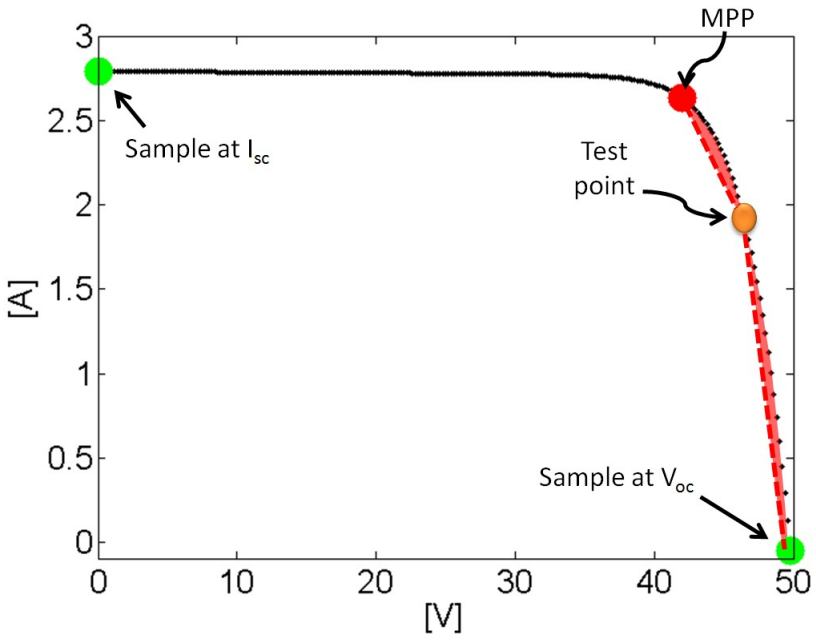

Figure 2.13: Error estimation: sum of the areas S1 and S2

The boundaries of non-linear regions that contain MPPs are found by minimizing the approximation error between the complete and the under-sampled voltage-current curves of the panel.

In Figure 2.13, the approximation error is point out by red colored areas. For the case represented in this Figure, the approximation error is calculated as average voltage difference for the set of samples between the MPP and the guessed position of an IP or between the MPP and the samples at the short or open circuit conditions. This last case occurs when only one MPP is present or if more than one MPP is present and the MPP is that nearest at one of these two samples.
Nevertheless, the number of the samples considered as test points must be limited in order to minimize the number of multiplications and divisions. In fact, in order to calculate the approximation error, the interpolated voltage values between the MPP and the considered test point and between the test point and the sample at the open-circuit voltage are required. Since the interpolation requires a division and a multiplication for each calculated voltage value, it cannot be executed for all the samples between two fundamental points.
For this reason, the calculation of the area is approximated by limiting its calculus to a maximum of 7 samples for each boundary of the MPP. In particular, these samples, that include that nearest to the considered fundamental points of the curve, are uniformly index spaced.
After this sum is calculated for all considered test points, then an error curve is achieved, as those shown in Figure 2.14 (right), where the best test point is indicated by a red cross.

Instead, the approximation error between the MPP and the sample at the short circuit condition is calculated as average current difference among the samples of the complete curve and those interpolated on the under-sampled curve. So, at the end, the error curve illustrated in Figure 2.14 (left) is obtained and the sample chosen as left boundary of the MPP is indicated by a red cross.

Since the samples of V-I curve are sorted by increasing current values, and so by decreasing voltage values, in the left pane of the Figure, the lower index represents that of the MPP, while in the

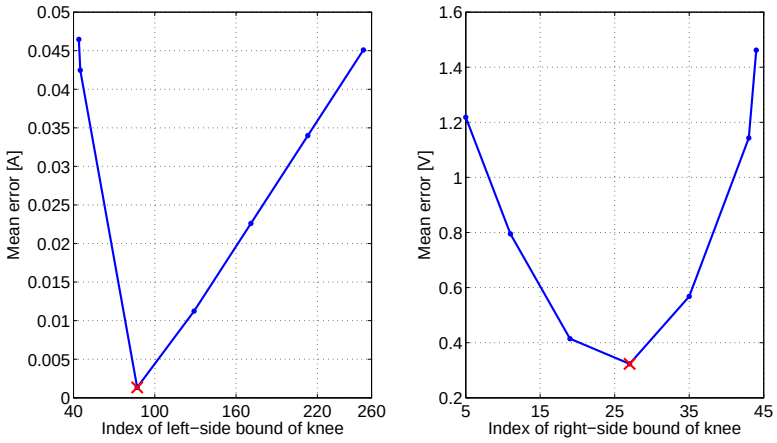

Figure 2.14: Minimization of the reconstruction error (V-I curve having only one MPP)

right pane the same point is found at the highest index.

In Figure 2.15, the approximation error is illustrated for the V-I curve having two MPPs.

Since the number of tested samples is reduced, also the error curve is approximated and, for this reason, a new cause of error is introduced.

In addition to the boundaries, up to ten samples inner to the non-linear regions are selected. Instead, as regards non-linear regions containing IPs, due to the net slope change around IPs, only one sample is selected.
Furthermore, for each linear region, only one further sample is selected. This sample is located at a current or voltage value, depending on the considered side of the MPP, equal to 60% of the range between the considered MPP and IP.
So, at the end, the under-sampled voltage-current characteristic of the panel is composed a set of samples that minimizes the reconstruction error.

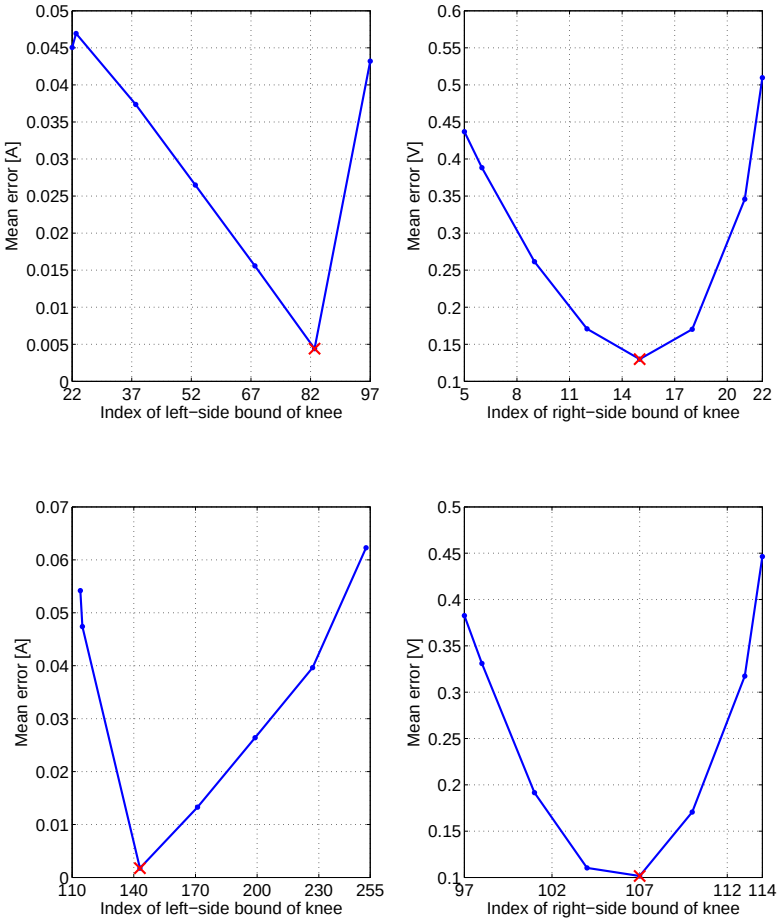

Figure 2.15: Minimization of the reconstruction error (V-I curve having two MPPs)

Generally, acquired voltage-current curves could have an heterogeneous density of samples. So, the under-sampling algorithm, at the end of the illustrated procedure, detects low-density regions when both voltage and current difference between each MPP and the nearest IPs is greater than proper thresholds. In fact, low-density regions cause failures of power peaks detection process and if a power peak hasn't been correctly detected both voltage

and current difference between MPPs and nearest IPs are significant.
The thresholds for the maximum voltage and current difference between a maximum power point and an inflection point are respectively equal to the 50% of the open-circuit voltage and to 30% of the short-circuit current.
So, if a power peak detection fails, then all samples inner to the detected voltage and current intervals and belonging to the bins of the Density Histograms (DHs) having a number of samples lower than the average value *on both axis* are selected.

At the end, for a generic curve of a PV panel having N_M MPPs, and so N_M - 1 IPs, the maximum expected number of samples selected by this procedure is:

$$N_{sel} = 13 \cdot N_M + (N_M - 1) + 2 + 2 = 14 \cdot N_M + 3 \tag{2.6}$$

since, for each non-linear region including MPPs, at maximum 13 samples are selected, while only one sample is used of IPs. To these samples, the ones selected on linear-regions and those at the open-circuit and short-circuit conditions have to be added.
The number of samples belonging to low-density regions should be excluded since it is not predictable and generally is zero if the data sampling process is designed to obtain a constant sampling step.

So, if the N_s is the number of samples of the original V-I curves of panels, then the compression ratio CR is:

$$CR = \frac{N_{sel}}{N_s} = \frac{14 \cdot N_M + 3}{N_s} \tag{2.7}$$

that is the ratio between the number of samples of under-sampled and original V-I curves.

2.5 Execution Time

A further flexibility of the proposed procedure is that it doesn't require the conversion of acquired data samples from quantized integers to the correspondent floating point values.
So, in order to further increase the execution speed and reduce the required memory allocation, the acquired data of V-I characteristics of panels are not subjected to any conversion when the under-sampling procedure is executed on Embedded Systems.
By this way, any library needed to floating points operations can be removed, further speeding up the under-sampling procedure.
The under-sampling algorithm has also implemented by Bitron S.p.A. on its own micro-controllers (Renesas V850ES/FJ3 [Ren14]) and an execution time of 220μs has been measured (see Figure 2.16).

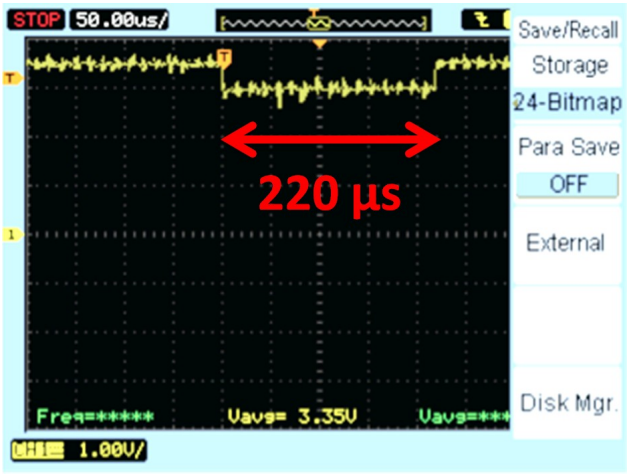

Figure 2.16: Execution time measured by Bitron S.p.A.

2.6 Test results

The under-sampling procedure has been tested on a set of 150 acquired voltage-current curves of panels (Sunowe SF125X125-72-M(L) mono-crystalline module) having all different short-circuit current values in the range [0.5A – 5A] and each of them is composed by 1000 samples.
In particular, in order to cover the majority of cases, the test set is divided into four groups basing on the number of non-linear regions: a first group of 48 V-I curves having only one MPP, a second group of 60 V-I curves having 2 MPPs, a third group of 32 V-I curves having 3 MPPs and a smallest group of 10 V-I curves whose number of non-linear regions is not so well definable.

The samples of V-I curves have been acquired with a resolution of 9mA and 161mV respectively for current and voltage measurements.

Due the sampling process, many duplicate data are present and in particular at zero or low negative voltage values. So, in a first attempt, the search for the samples at short circuit and open circuit conditions is a first measure of the useful amount of data respect to the original one.

In the Figure 2.17, the number of these samples (green colored line) and that of the under-sampled V-I curves of panels (red colored line) are compared. The number of samples of the original V-I curves is always 1 thousand, so it isn't reported in the Figure.

While the minimum number of useful data samples is 189, the number of samples is strongly reduced for all curves by the under-sampling procedure.
In particular, the minimum number samples is achieved, as expected, for the curves having only one MPP (see Figure 2.18). Then, in average the number of samples is proportional to the number of maximum power points (MPPs). Independently of the number of MPPs, the maximum number of samples is achieved

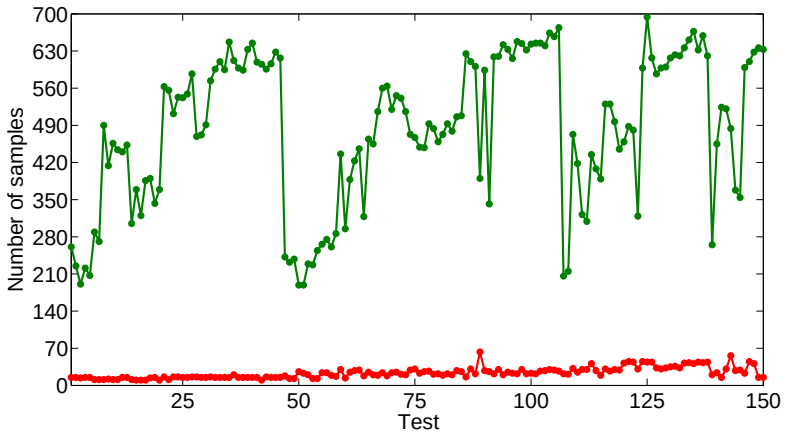

Figure 2.17: Comparison between the number of useful (green colored line) and under-sampled (red colored line) V-I curves of panels

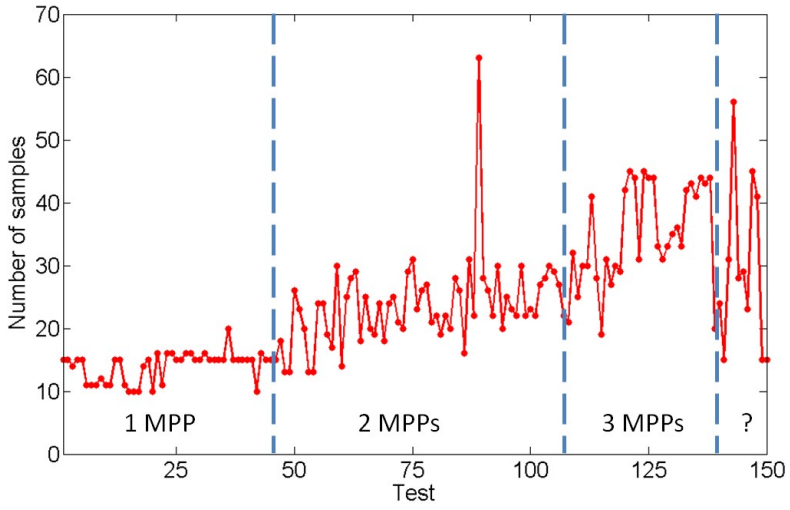

Figure 2.18: Number of the under-sampled V-I curves of panels

when a low-density region is detected and all samples belonging to these regions are selected for the under-sampled curves. This occurs for one under-sampled curve of the set having more than 60 samples. The under-sampled curve having the highest number

of samples is reported in Figure 2.19.

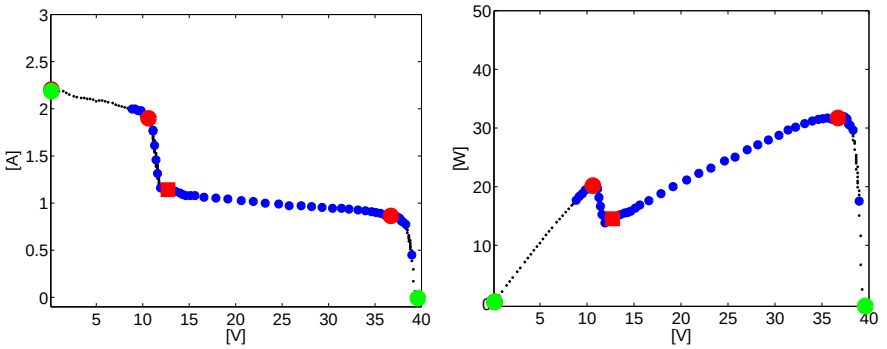

Figure 2.19: The under-sampled V-I and V-P curves having the greatest number of samples (63)

For this V-I curves, even if the maximum power points and the inflection points (indicated by red points) are well detected, due to a voltage difference greater than 20V between the inflection point and the MPP at lower current, the search for samples belonging to low density regions is triggered.

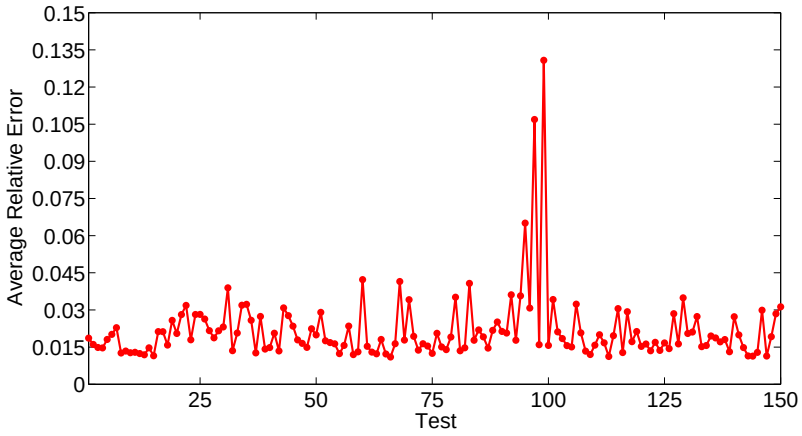

Figure 2.20: Average Relative Error

In Figure 2.20, the average approximation error is illustrated. On average, the approximation error, that is calculated as relative current difference between the each sample of the full and under-sample curves, maintains on about 2%.

Only three under-sampled curves verify an approximation error that exceeds the average value (3 spikes in Figure 2.20), since in each of them the position of the inflection points is different from the optimal one having the lower power value.

2.6.1 Case studies

Analysis of the curve having the maximum approximation error

The under-sampled V-I and V-P curves having the maximum reconstruction error are illustrated in Figure 2.21.

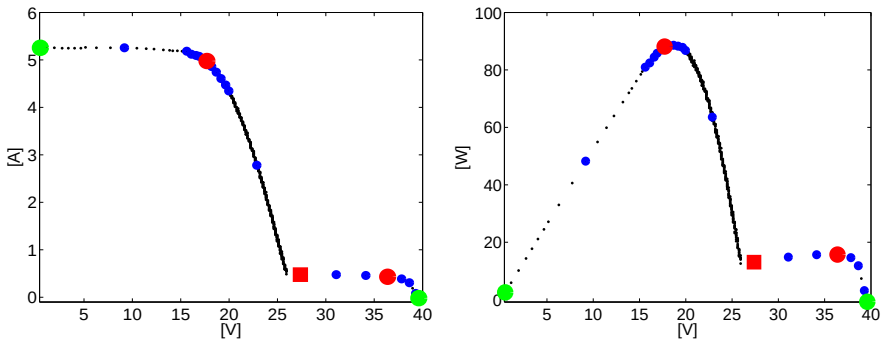

Figure 2.21: Under-sampled V-I and V-P curves

For the other two curves having the highest approximation error, the encountered problem is identical to that shown. For these curves, an high approximation error is achieved because the MPP and IP at the lower voltage are not correctly detected. For this reason, also the position of the right-side boundary of the MPP at the higher voltage isn't correctly estimated.

As shown in the Figure 2.22(a), the histograms are able to point out the presence of the current level even when a very low density of samples occurs. So, the high approximation error is achieved because of next steps.

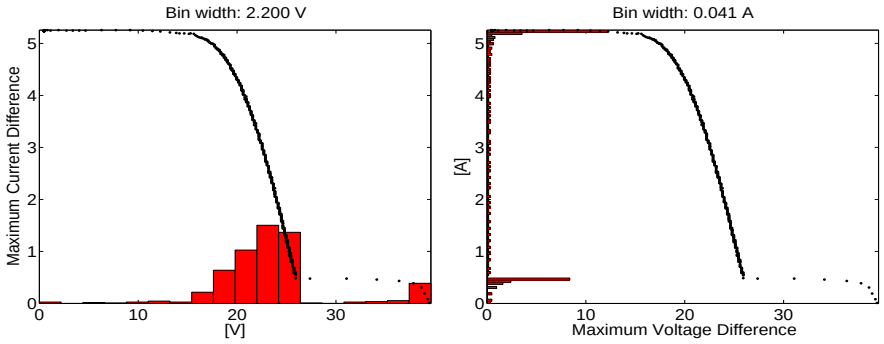

(a)

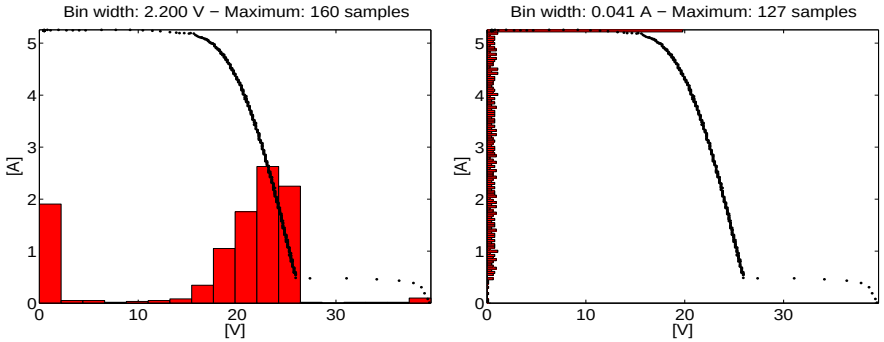

(b)

Figure 2.22: WHs (a) and DHs (b)

In fact, the IP is not optimally detected because of the lack of samples at current values lower than 500mA. So, the comparison among normalized histogram bars is not accurate (see left pane in the Figure 2.23).
Instead, the final position of the MPP doesn't correspond to the sample having the maximum power value because the iterative procedure is influenced by the noise and redundant data of the curve. So, a sub-optimal sample is chosen, as shown in the right

pane of the Figure 2.23.

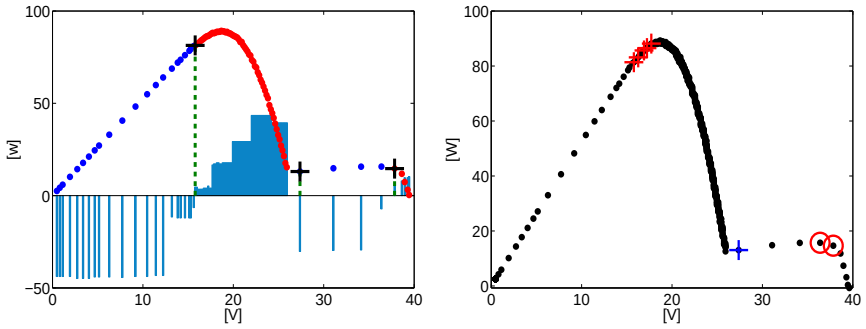

Figure 2.23: Normalized WHs comparison (left), positioning of MPPs and IPs (right)

Moreover, since the search for the sample minimizing the approximation error doesn't take into account the next addition of further samples to the non-linear region including the MPP, the estimated error is minimized by a sample that is very near to the MPP, as illustrated in the right pane of Figure 2.24(a). Instead, if the addition of further samples to the non-linear region is considered, then the procedure chooses a sample that is nearer to the IP. But, by considering the addition of furher samples at each calculation of the approximation error increases the execution time and so it is preferable to not include them, since only in a restricted number of cases ad that shown a great approximation error occurs. Moreover, the more efficient is the data sampling process, the lower is the approximation error achieved in the most problematic cases.

Thus, by adding up to 5 samples between the maximum power point and the right boundary of the non-linear region, the approximation error is further reduced but only between this two samples. The minimization of the error between a boundary of the non-linear region and the inflection point is guaranteed only by the placement of one sample in the linear region.
So, the incorrect detection of fundamental points and the conse-

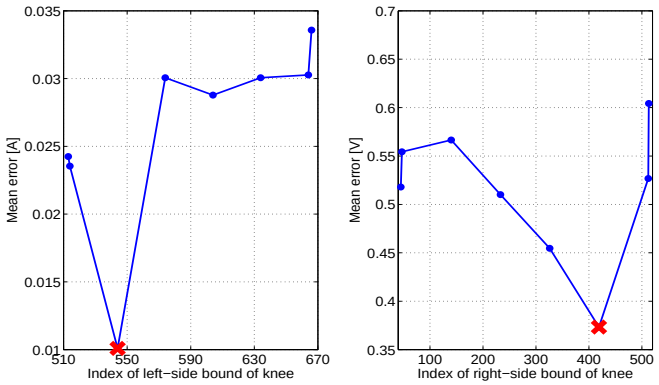

(a)

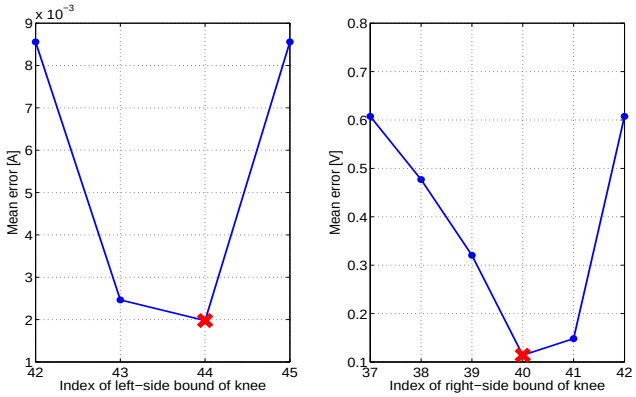

(b)

Figure 2.24: Minimization of approximation error of non-linear regions boundaries

quent incorrect placement of the other samples causes the approximation error in the voltage range [25V–28V] to exceed the 100%, as shown in Figure 2.25.

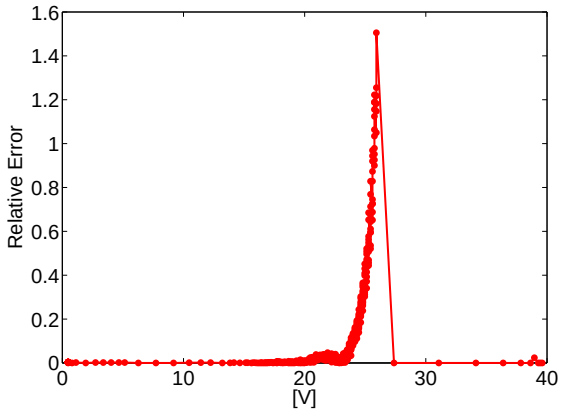

Figure 2.25: Curve of the approximation error

Multiple or not detected MPPs/IPs

The under-sampling procedure detects an erroneous number of MPPs only in the 8.7% of the analyzed voltage-current curves of panels. Nevertheless, each time this occurs, only one MPP is missed and, above all, the selection of samples belonging to the low-density regions, or sometimes the only sample selected between the boundary of a non-linear region and the next fundamental point, reduces the approximation error.

The low density of samples, as well as the noise, can lead to detect multiple MPPs for the same non-linear region or to not detect it at all, as occurs for the V-I curve in Figure 2.26.

Due to this very low density of samples, the histograms bins width on the voltage axis (2.227V) is underrated because it doesn't point out the high-slope linear region belonging to the low-density region. Instead, even if a greater histograms bins width could better point out the presence of the current level belonging to the low density region, an acceptable bins width on the current axis (96mA) is obtained (see Figure 2.27).

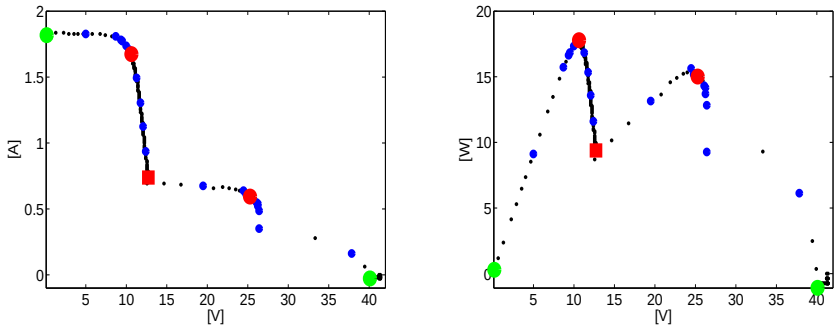

Figure 2.26: Missing MPP: V-I and V-P curves

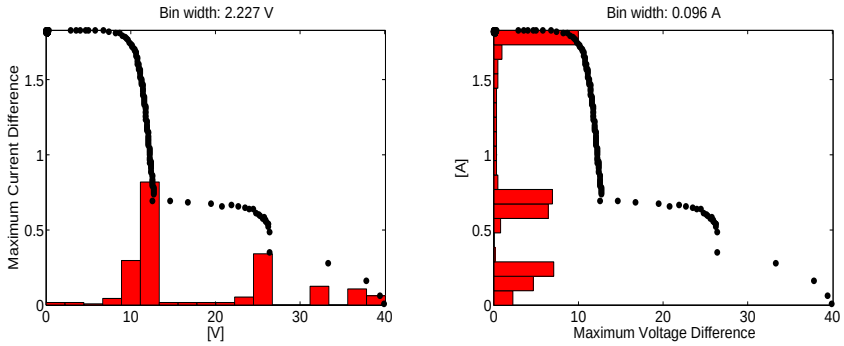

Figure 2.27: Missing MPP: WHs

For this reason, as shown in Figure 2.28, the comparison among histograms bars leads to detect multiple MPPs and IPs on the central non-linear region having a voltage difference of about 1V and to not detect any MPP on the non-linear region having the lower density of samples.

The detection of the multiple MPPs on the central non-linear region is mainly due to the noise (see Figure 2.29).

The missed detection of the MPP in the low-density region is due to the underrated bins width on the voltage axis. In fact, at high voltage, the comparison among the normalized histograms bar allows to detect an IP but not a MPP.

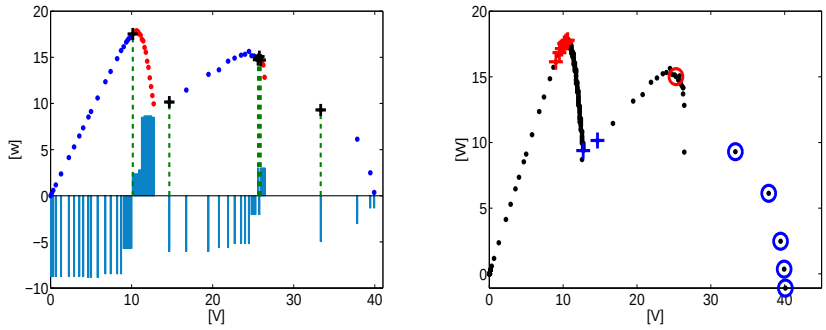

Figure 2.28: Missing MPP: (left pane) Normalized WHs comparison, (right pane) boundary positioning

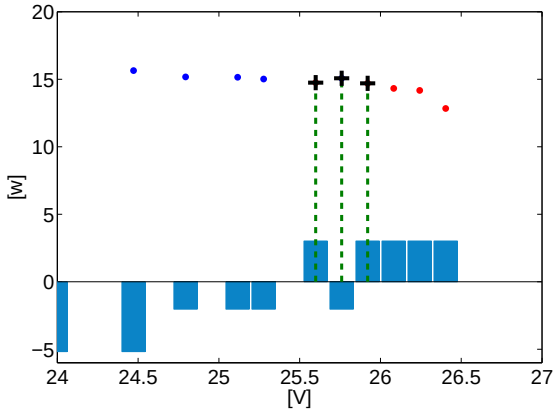

Figure 2.29: Missing MPP: Normalized WHs bars (detail)

After the iterative procedure has detected a better position for the MPP of the central non-linear region, the placement of the right-side boundary at the higher voltage value, and so at the lower index, minimizes the approximation error between this MPP and the guessed position of the inflection point. As shown in the right-side Figure 2.30(b), the boundary is placed next to the guessed position of the inflection point.

Then, when the iterative procedure searches for a better in-

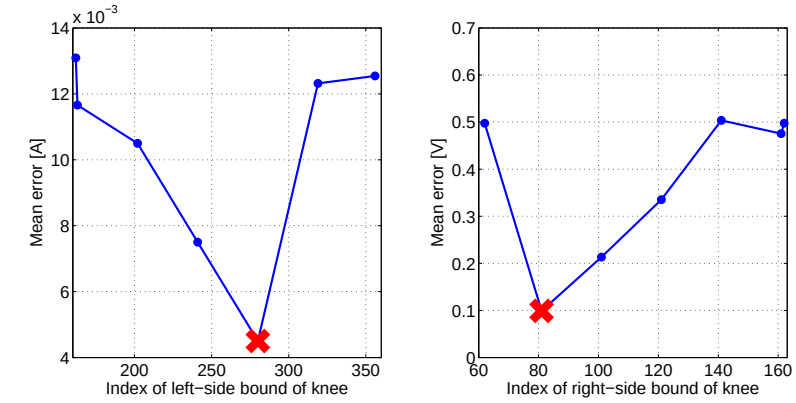

(a)

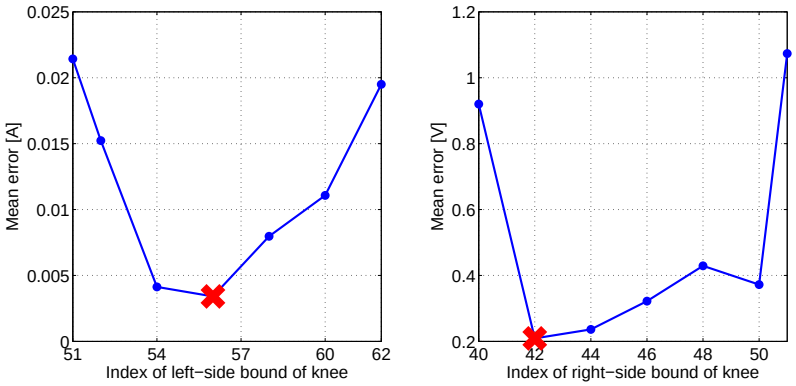

(b)

Figure 2.30: Missing MPP. Boundaries positioning: (a) MPP at low voltage, (b) central MPP

flection point at the voltage values near the open-circuit voltage, the guessed position is changed because the sample having a lower power value is found to be at the open-circuit voltage and so at zero current.
The under-sampling procedure removes successively multiple MPPs on the same non-linear region that have a voltage difference less than 3V, as well as all IPs that aren't between two MPPs are ignored.

For these reasons, at the end of the procedure, no fundamental points are in the low-density non-linear region of the V-I curve.
Nevertheless, since the under-sampled procedure selects a further sample between the right-side boundary of the non-linear region and the sample at the open-circuit voltage, then the reconstruction is improved.
Since a voltage difference between the open-circuit voltage and the voltage of the MPP on the central non-linear region is lower than $0.5 \cdot V_{oc}$, then the search for the samples belonging to the low-density regions isn't triggered.
So, the under-sampling procedure, despite these non-idealities, is able to prevent a further increase of the approximation error.

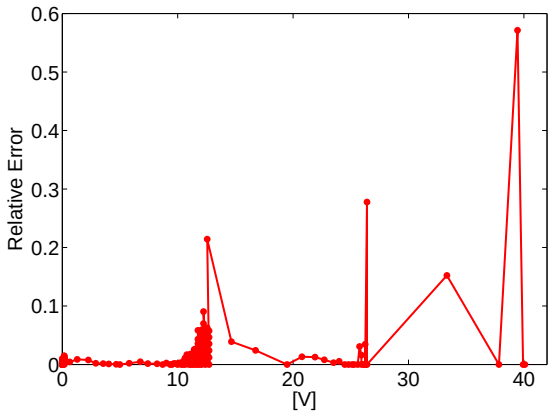

Figure 2.31: Missing MPP: approximation error curve

When the voltage difference between the open-circuit voltage (or the voltage of an IP) and the voltage of a MPP is greater than 50% of the open-circuit voltage, the search for the samples belonging to low-density regions is triggered. The same occurs when the current difference between an IP (or the short circuit current) and the MPP is greater then 30% of the short circuit current.

Detection of critical MPPs (first case)

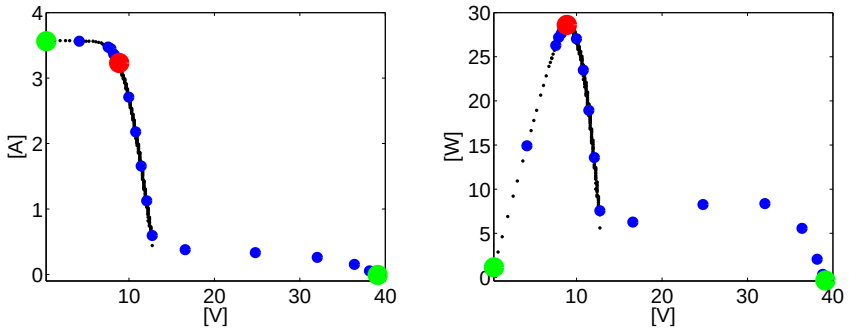

Figure 2.32: MPP not detected. (left) V-I curve, (right) V-P curve

For the V-I curve in Figure 2.32, the maximum power point at high voltage isn't detected due to the low density of samples in the voltage range [15V–40V].

Since all the samples belonging to this region have a low current value, it is difficult to find the histograms bins width that allow to point out the presence of an high-slope region in that voltage range.

Nevertheless, by using the estimated widths, the WHs point out the presence of a lower current level, as shown in the top right pane of Figure 2.33(a). On the contrary, the DHs aren't able to point out anything (see bottom panes in Figure 2.33(a)).

The comparison among the normalized histograms bars leads to detect only the MPP at 10V and the inflection point at 17V (see left pane in Figure 2.34).

In fact, the graph bar in the range [15V – 40V] is composed only by negative bars because the bars of the normalized WH on voltage axis aren't higher than those related to the same region on the current axis.

The iterative procedure is able to correctly locate only the MPP, while the inflection point remains at its guessed position. Instead, the nearest sample at lower voltage could be a better position.

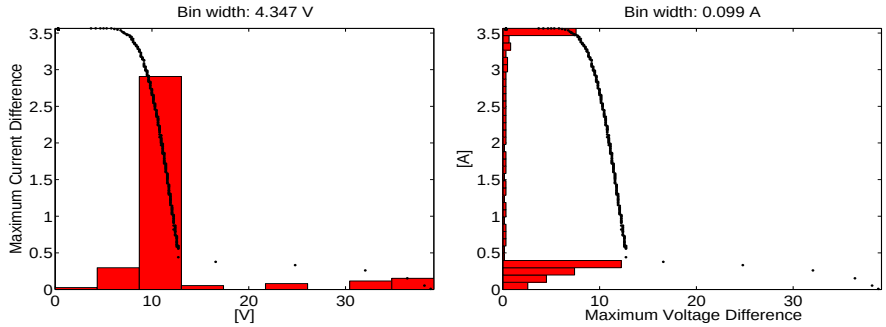

(a)

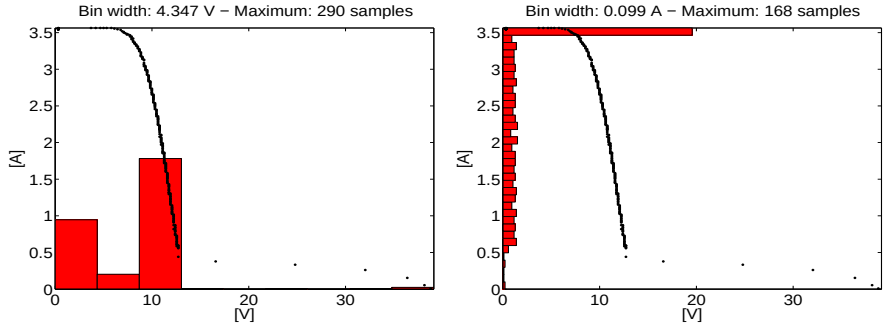

(b)

Figure 2.33: Missed MPP. WHs (top), DHs (bottom)

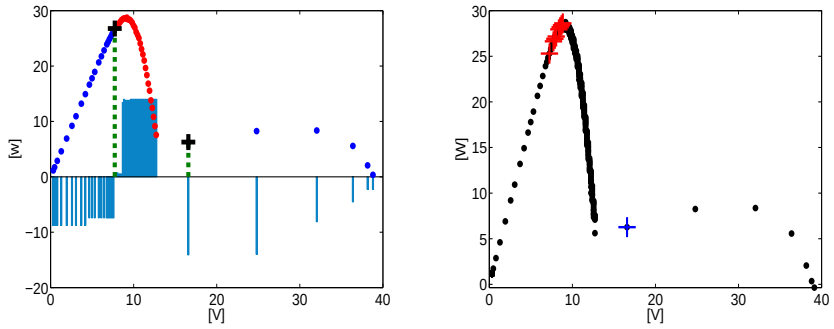

Figure 2.34: Missed MPP. Normalized WHs comparison (left), positioning of fundamental points (right)

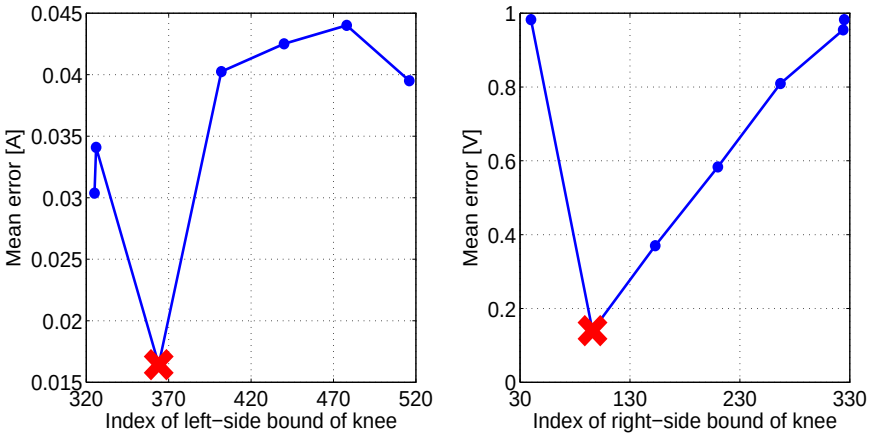

Figure 2.35: Missing MPP: positioning of boundaries

In this case, the minimization of the approximation error during the positioning of the boundaries belonging to the only detected non-linear region leads to choose a sample near to the inflection point (index value equal to 30), as shown in the right pane of Figure 2.35.

At the end, since a voltage difference greater than 50% of the open circuit voltage is achieved, all samples belonging to the detected low-density region are selected ensuring a low reconstruction error (see Figure 2.36).

The performance of the under-sampling procedure depend mainly on the estimated histograms bins width and, of course, on the sampled data too.
In all the analyzed cases, the noise effects are more evident when the voltage-current curve of the panel has an heterogeneous density of samples, since the amount of analyzed information is lower. Only when the histograms bar contain one or two sample at maximum the noise effect is more evident. Indeed, since the usage of the histograms allows to analyze how the samples are distributed

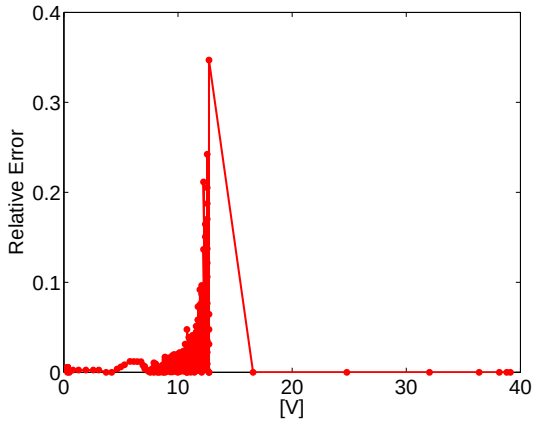

Figure 2.36: Missing MPP and selection of all samples belonging to the low-density region: approximation error curve.

on the V-I curve, the noise effects are not so evident because the histograms are calculated only by considering the samples having the maximum current or voltage values. For this reason, the under-sampling procedure is not susceptible to data missing or data redundancies.

In fact, by considering a V-I curve of panel really similar to that previously considered a very different result is obtained, as illustrated in Figure 2.37.

The under-sampling procedure is able to perfectly locate the maximum power points and the inflection point between them even if this is one of the hardest cases.
In fact, the density of samples is very heterogeneous and a consistent lack of data occurs in a wide voltage range, i.e. only 7 samples are present in the voltage range [15V–40V]. In addition, all samples belonging to this range have a current value lower than 500 mA.

But respect to the previous case, that is very similar, the MPP at 38V is detected because the samples at this voltage have an higher density, i.e. they are more close among them. So, this leads

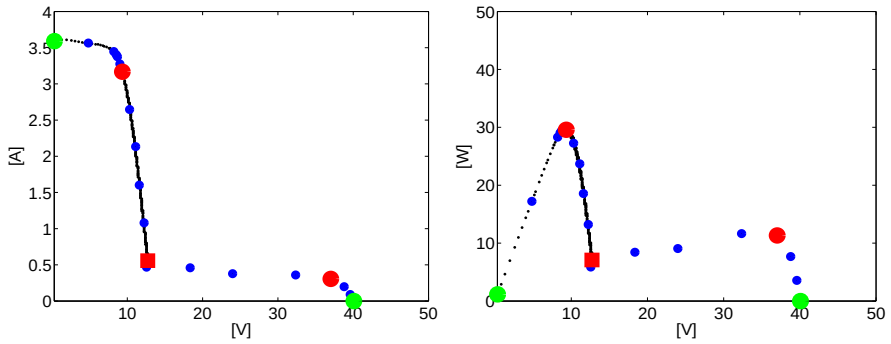

Figure 2.37: MPP detection on a low-density region: V-I and V-P curves

to point out better on voltage axis the high-slope linear region (see left pane in Figure 2.38(a)). The MPP detection at 38V is possible because, respect to the previous case, all the samples in the voltage range [15V–35V] have similar currents value and a low-slope linear region is obtained respect to the voltage axis. The presence of this subset of samples is pointed out by the histograms bars on current axis and, above all, a gap between two bars is present since no sample is present at 300mA (see right-side pane in Figure 2.38(a)).

This gap leads to detect a sample for which the comparison between its correspondent bars has different result respect to that of its closest samples and so to detect another MPP, as illustrated in the left pane of Figure 2.39.
In this case, the iterative procedure, shown in the right pane of the Figure 2.39, is able to place the MPPs and the IP in their best position, so to achieve a very low approximation error.

So, even if the average approximation error for this curve is estimated to 3.5%, then this high value occurs because of the spikes present in Figure 2.40. These spikes are caused by redundant data of the complete curves. In effect, the approximation error is lower than 3.5%.
In effect, even if the approximation error is minimized for more than 90% of the analyzed V-I curves. Moreover, these spikes de-

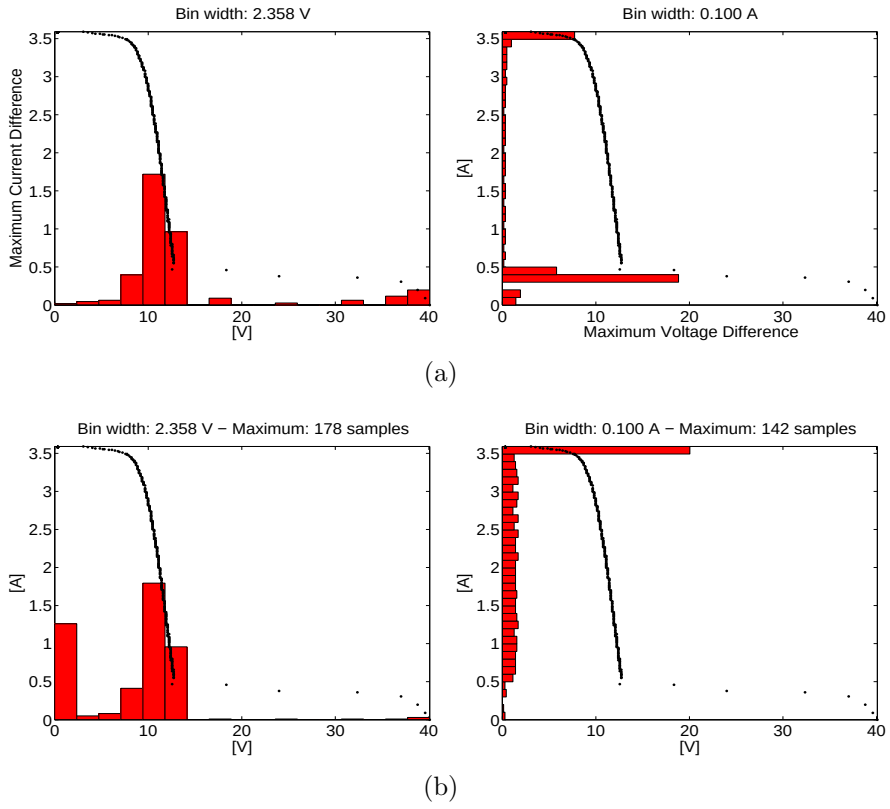

Figure 2.38: MPP detection on a low-density region: WHs (top), DHs (bottom)

pend also on current of samples. In fact, the lower is the current value of the original curve, the higher is the relative error peak.

Moreover, the average approximation error also depends on the density of samples. In fact, since the V-I curves haven't an homogeneous density of samples, the average error mainly depends on the error calculated for the highest density regions of the V-I curves. So, since in the analyzed cases, the regions of the curves having the higher error could have an higher density of samples too, then the average approximation error can be considered lower than that estimated.

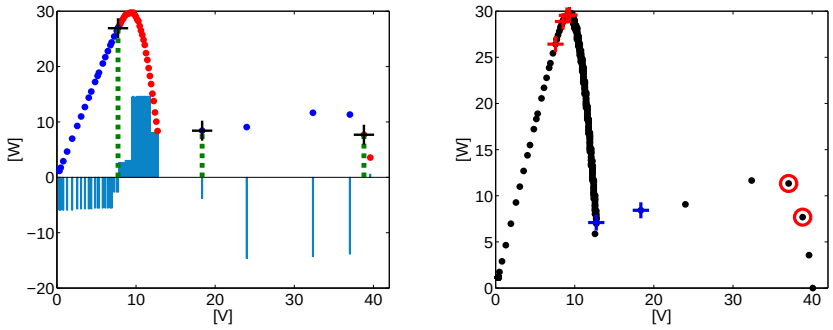

Figure 2.39: MPP detection on a low-density region: Normalized WHs comparison (left), positioning of the fundamental points (right)

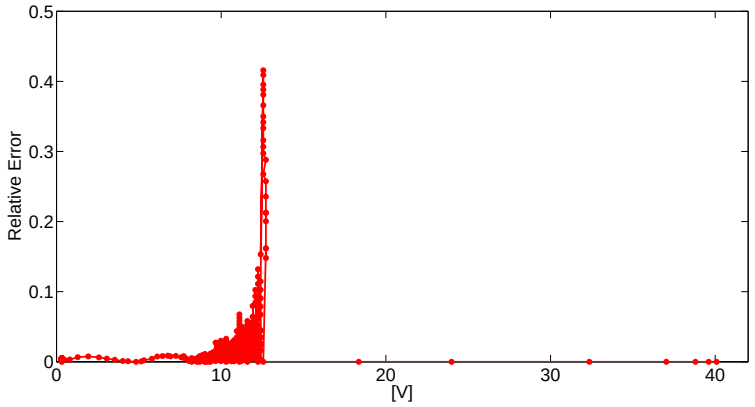

Figure 2.40: MPP detection on a low-density region: approximation error curve

Clearly, the performance of the under-sampling process mainly depends on that of the data sampling process.

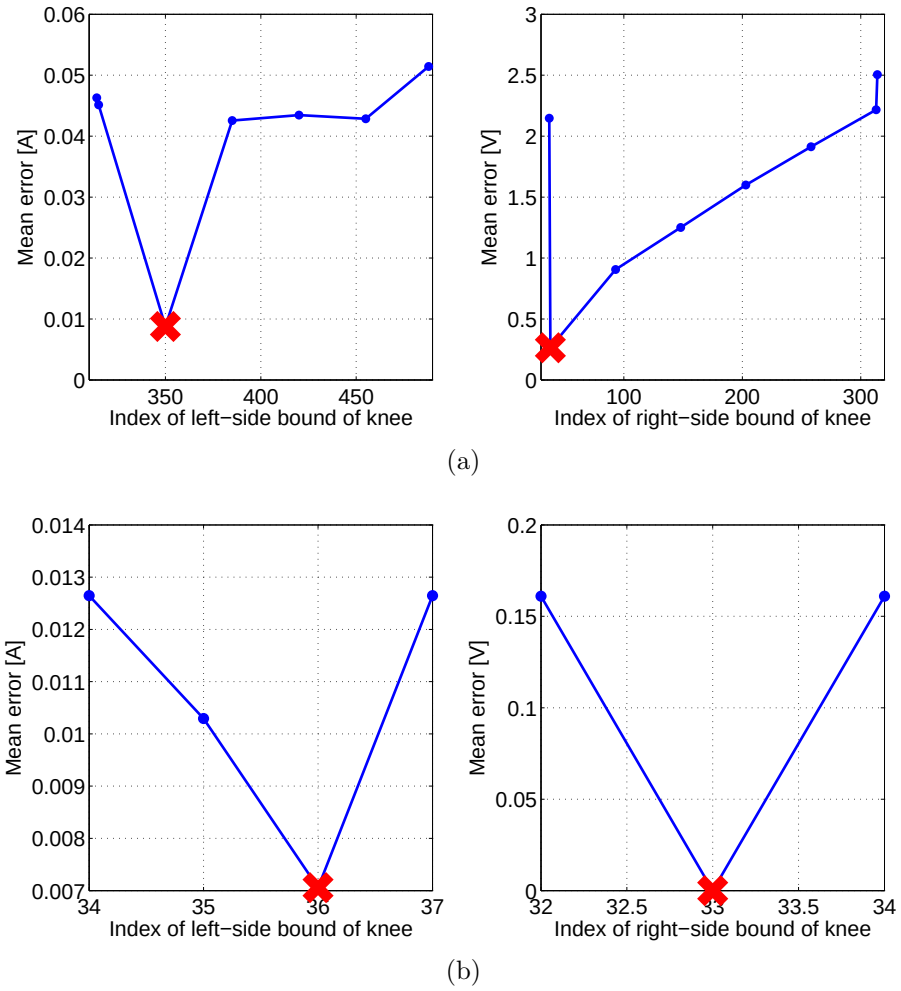

Figure 2.41: MPP detection on a low-density region. Error minimization: MPP at low voltage (a), MPP at high voltage (b)

Detection of critical MPPs (second case)

Another critical case, where again the histograms bars correspondent to the high-slope linear regions have a very different on voltage axis is the V-I curve shown in Figure 2.42.

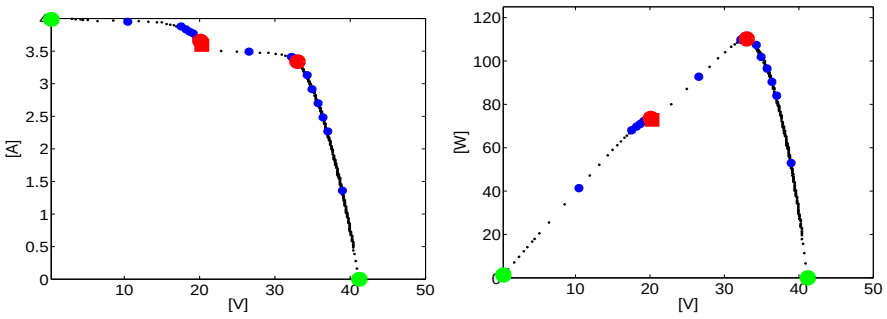

Figure 2.42: Critical position of a MPP: V-I and V-P curves

The linear region at 20 volt has a current width of only 450mA. So, respect to the linear region in the range [30V–40V] is more complicated to detect. Nevertheless, since the trend of the histograms bars in the range [3.5A–4A] on current axis points out the two different current levels, the comparison among histograms bars allows to detect both the MPP and the IP of the lowest non-linear region, as illustrated in the left pane of the Figure 2.44.
In fact, the regions of samples having almost the same current is well detected by only analyzing the histograms bars on the current axis. Moreover, the histogram bar on voltage axis corresponding to the same region has an height that the relationship among the normalized bars changes.

Then, as illustrated in the right pane of Figure 2.44, the iterative procedure fixes the position of the MPP and IP of this non-linear region to be very close.
Thus the positioning procedure for the boundaries of the non-linear region is applied. The redundant data of this V-I curve produce a noisy signal in the plots of Figure 2.45(b).

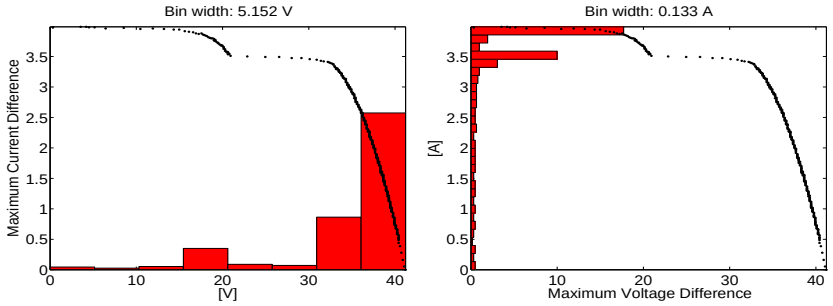

(a)

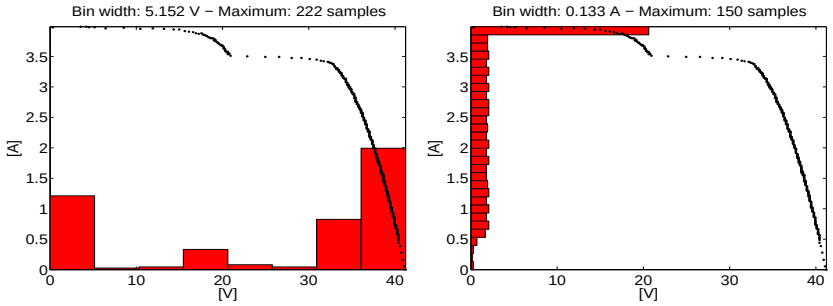

(b)

Figure 2.43: Critical position of a MPP: WHs (a), DHs (b)

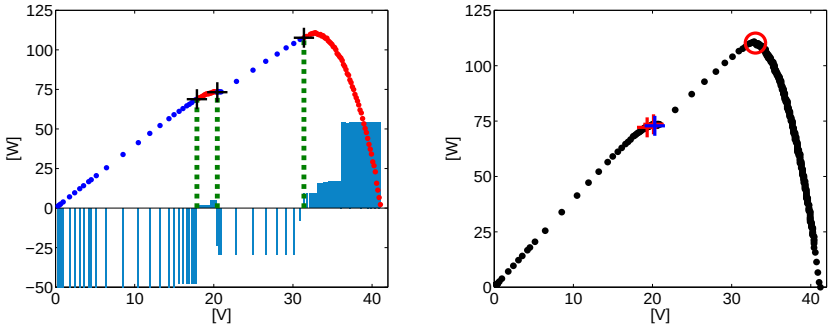

Figure 2.44: Critical position of a MPP. Normalized WHs comparison (left), positioning of fundamental points (right)

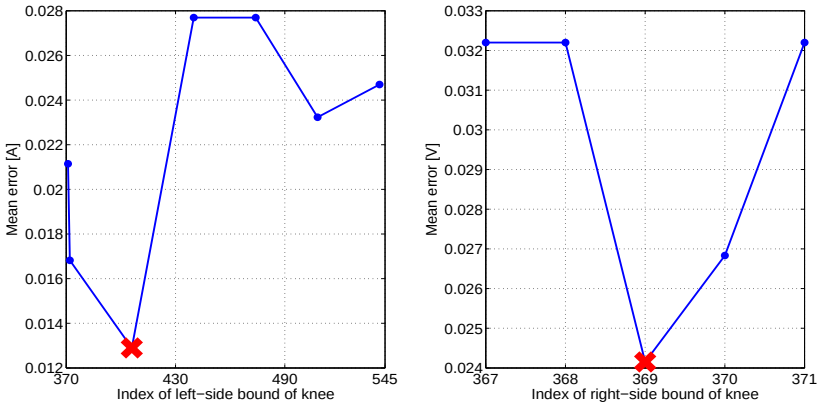

(a)

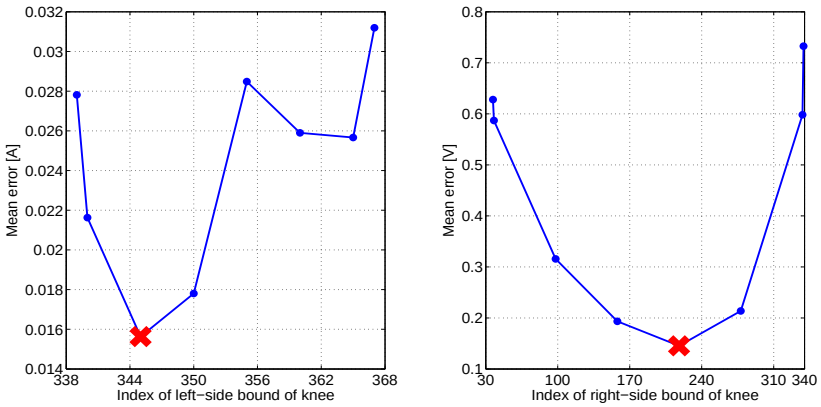

(b)

Figure 2.45: Critical position of a MPP. Positioning of boundaries: MPP at low voltage (a), MPP at high voltage (b)

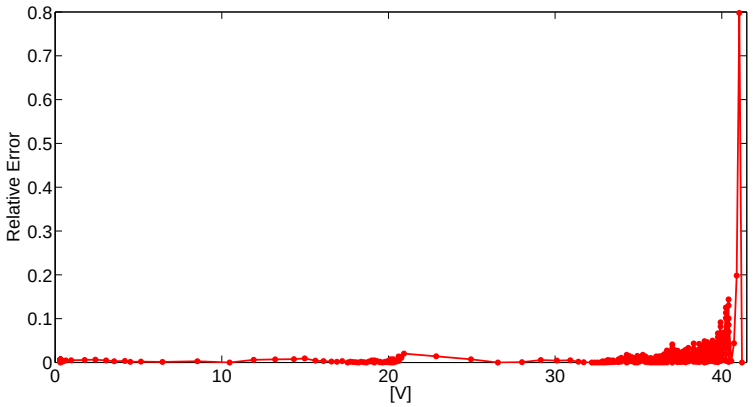

Figure 2.46: Critical position of a MPP. Curve of the approximation error.

Unpredictable number of MPPs

In some cases, it is difficult to decide the number of MPPs for a particular V-I curve of a panel.

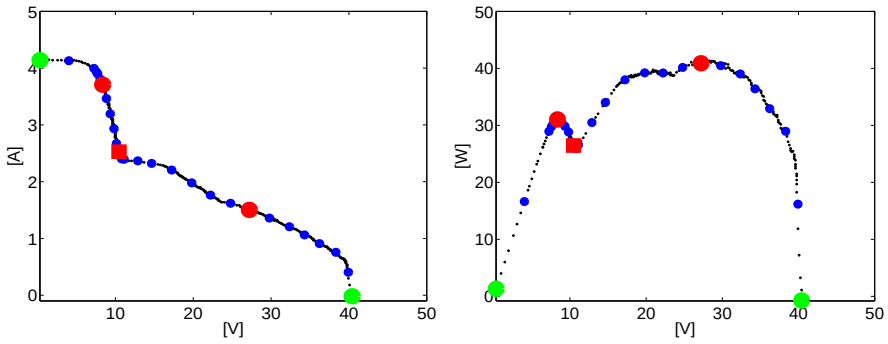

Figure 2.47: Unpredictable number of MPPs: V-I and V-P curves

For the curve in Figure 2.47, without looking at the V-P curve, it is not immediate to choose the right number of MPPs. This case could be critical, especially if a lower density occurs, because the choice made by the under-sampling procedure is unpredictable. In fact, the curve in the left pane of Figure 2.47, could have two

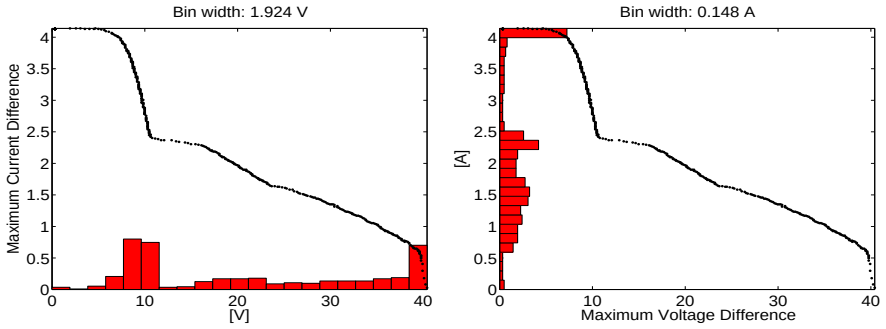

(a)

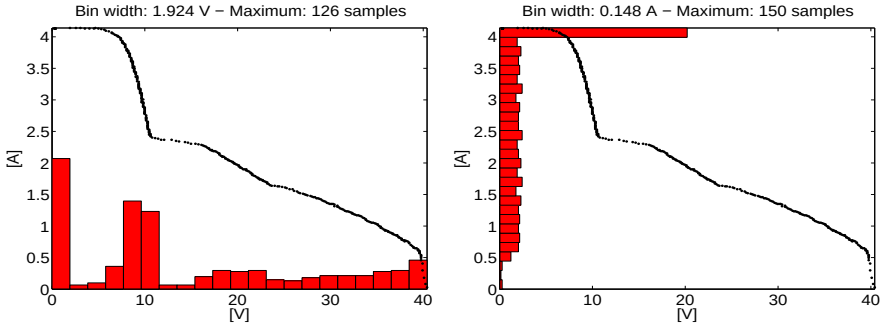

(b)

Figure 2.48: Unpredictable number of MPPs: WHs (a), DHs (b)

MPPs if the only non-linear region at the open-circuit voltage and at the short circuit current are detected, or three MPPs if the further slope change at 20V is detected.
By observing only the histograms bars both on voltage and on current axis corresponding to the linear region in the range [18V–40V], it is very difficult to detect a non-linear region in this voltage range because all bars have almost the same height and this means that a linear region is present.

The comparison among the normalized histograms bars, as illustrated in Figure 2.49, leads to detect only the two MPPs at the open-circuit voltage and at the short circuit current.
Instead, since the slope change at 20V isn't pointed out signifi-

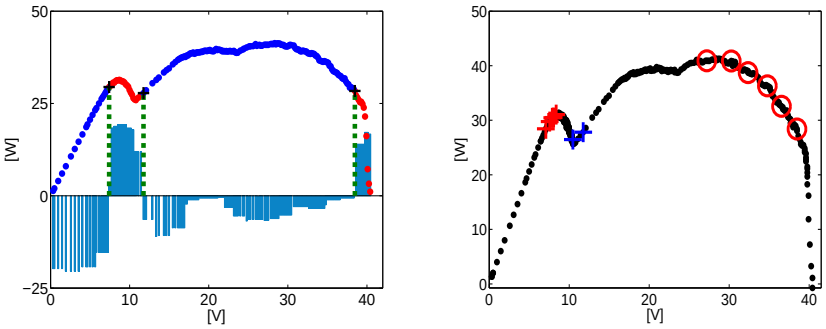

Figure 2.49: Unpredictable number of MPPs: normalized WHs comparison (left), positioning of fundamental points (right)

cantly and it involves only a limited part of the V-I curve, the bar graph in Figure 2.49 (left pane) doesn't have any positive bar at that voltage. Thus, when the iterative procedure is applied to find a better MPP or IP starting from the guessed position, then the initial MPP position at the open-circuit voltage is changed to a very different position at a lower voltage value as shown in Figure 2.49 (right pane). So, this procedure finds that the MPP doesn't correspond necessarily to an evident slope change of both V-I and V-P curves.

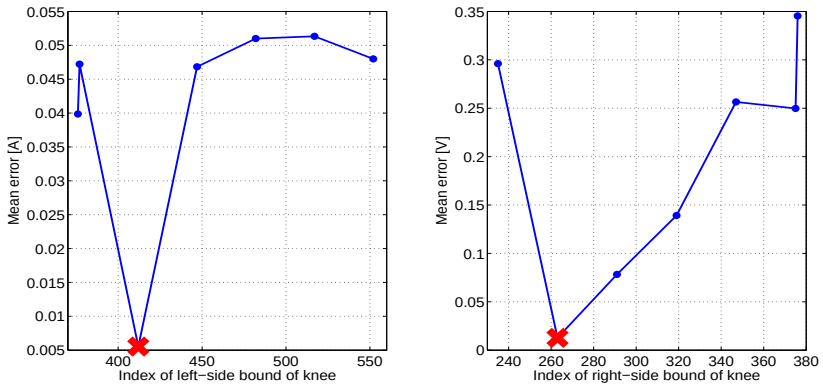

(a)

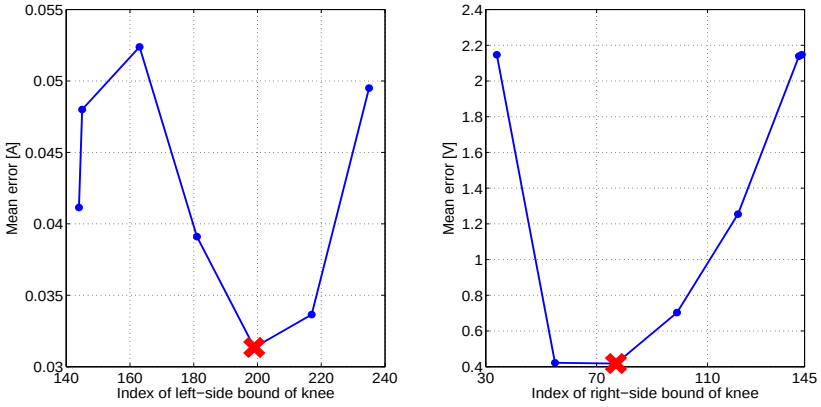

(b)

Figure 2.50: Unpredictable number of MPPs. Positioning of boundaries and minimization of the approximation error

A minimized approximation error is guaranteed by the proper positioning of the boundaries of the non-linear regions. Indeed, up to ten further samples are added to the under-sampled curve and maintain the error value under the 5% for almost the whole range of voltage values of the panel's curve (see Figure 2.51).

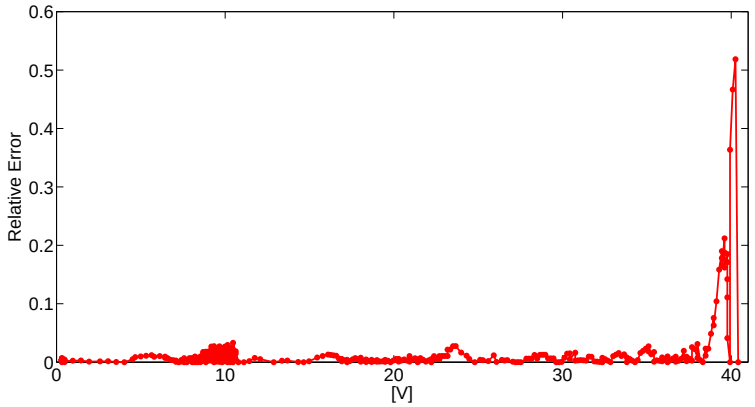

Figure 2.51: Unpredictable number of MPPs: curve of the approximation error

Chapter 3

An Evolutionary Approach

This Chapter introduces to the reader the Evolutionary Approach for the reconfiguration of Photovoltaic Systems. The Genetic Algorithms, that are a subclass of Evolutionary Algorithms, are used to calculate the optimal configuration of panels respecting given constraints.

In the second part of this Chapter, different shading scenarios are analyzed and, for each of them, the experimental results are discussed. In particular, the performances of the genetic algorithms using the original and under-sampled characteristics of panels, obtained by applying the procedure in Chapter 2, are compared, also respect to the standard configuration of the PV plant topology.

At the end, a statistical analysis is made in order to show how GAs performance are better than other optimization methods.

3.1 The Evolutionary Algorithm

In Literature, different optimization strategies have been illustrated [BMAM+11]. For many problems, the optimization is not only achieved by calculating the inputs that minimize/maximize a function, but also that inputs respecting given constraints. This

class of problems is the so-called NP-hard (Non-deterministic Polynomial time). In [EDKS13], the authors assert that the photovoltaic reconfiguration is a NP-hard problem. It is known that, for NP-Hard problems, there is no deterministic algorithms obtaining the best solution in a time having a polynomial trend respect to number of inputs, but in many cases the execution time diverges exponentially.
Independently of the class the reconfiguration problem belongs to, in effect the time constraint is the most critical since significant energy losses are associated to it. Moreover, a possible misalignment could occur between the shading scenario just before the start of the reconfiguration process and that after the new configuration has been actuated.

Meta-heuristic algorithms have been largely used to solve time-critical optimization problems by making only few assumptions about the underlying objective functions.
The two main categories of meta-heuristic algorithms are that trajectories-based and population-based. The former category includes all methods that are based on the improvement of a single solutions and iteratively improve it by using different strategies to escape from local optima (e.g. *Hill Climbing, Simulated Annealing, Tabu Search*). The latter category are based on a population of individual that evolves during a finite number of iterations (e.g. *Evolutionary Algorithms, Particle Swarm Optimization, Ant Colony Optimization*).
The definition of objective functions usually requires only few information about the structure of the problem space. As a consequence, the meta-heuristic algorithms perform consistently well in many different problem domains.

For these reasons, the developed reconfiguration procedure is based on Evolutionary Algorithms (EA) using standard operators.

All Evolutionary Algorithms proceed in principle according to the following scheme:

1. initially, a fixed-size population of individuals with a random

genome (the encoding that is adopted by each member of the population to solve a specific problem type) is created;

2. the values of the objective function are computed for each solution candidate in the current population. Depending on the problem at hand, this evaluation may incorporate complicated simulations and computations;

3. with the objective function, the utility of the different features of the solution candidates have been determined and a fitness value can now be assigned to each of them;

4. a subsequent selection process filters out the solution candidates with bad fitness and allows those with good fitness to enter the mating pool with a higher probability. Without loss of generality, if the fitness is subject to maximization, the higher the fitness values are, the higher is the (relative) utility of the individuals to whom they belong;

5. in the reproduction phase, offspring is created by varying or combining the genotypes of the selected individuals by means of genetic operators. These offspring are then subsequently integrated into the population;

6. finally, if a termination criterion is met, the evolution stops, otherwise, the algorithm continues at step 2.

EAs have been mainly used either to solve the MPPT problem under partial shading conditions for different PV fields fixed topologies [TSI+10, Ram, CCL13, MTF+11] or to design under static conditions large photovoltaic systems as well as hybrid energy systems [GLTGEE12, Kor10], including a number of renewable and classical energy sources, like wind or diesel.

Among all the EAs, Genetic algorithms (GAs) are well suited for facing the optimal arrangement of the panels among the photovoltaic string. The GAs are a subclass of EAs where the elements of the search space (genotypes) are binary strings or arrays of other elementary types. The genotypes are used in the reproduction operations, whereas the values of the objective functions are

computed on basis of the phenotypes in the problem space which are obtained via a genotype-phenotype mapping.
In order to find the electrical configuration among panels achieving the highest electrical power under a given solar irradiance condition, a crucial tasks are the choice of the encoding, of the genetic operators and of the fitness function to be used.

3.1.1 Solution Encoding

The GAs provide the maximum flexibility of the solution encoding respect to the electrical configuration it is mapping.
In fact, an array of integers is well suited for any considered PV plant topology: series-parallel (SP), total-cross-tied (TCT) and bridge-link (BL).

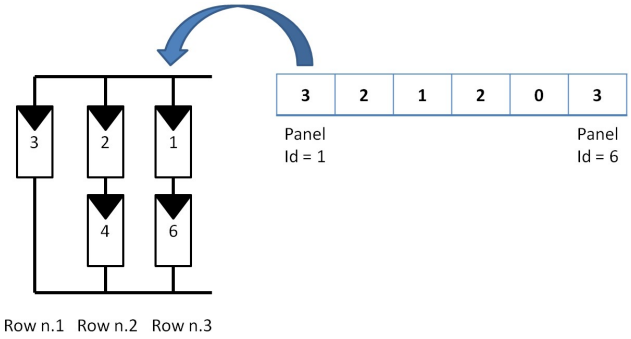

Figure 3.1: Solution encoding for a series-parallel PV plant topology

For the Series-Parallel (SP) plant topology, that has been used for simulations in this Thesis, the simplest representation of the individual is an array of N_p integers $\mathbf{g} = [g_1, \cdots, g_i, \cdots, g_{N_p}]$, where N_p is the total number of photovoltaic panels. The generic integer g_i belongs to the interval $A = [0, N_s]$, where N_s is equal to the number of PV strings under consideration and the value 0 means that the panel does not belong to any string, i.e., it is disconnected from the PV field (see Figure 3.1). In this case, the panel disconnection leads to short circuit its terminals.

Since each panel can be connected to only one string or at most it can be disconnected from the PV field, each symbol value can be set as follows:

$$g_i = \begin{cases} j \in [1, \cdots, N_s] & \text{if the } i\text{–th panel belongs to the } j\text{–th string} \\ 0, & \text{if the } i\text{–th panel is disconnected} \end{cases}$$

Since any possible combination of integers belonging to the set A is valid, the total number of solutions is equal to $(1 + N_s)^{N_p}$.

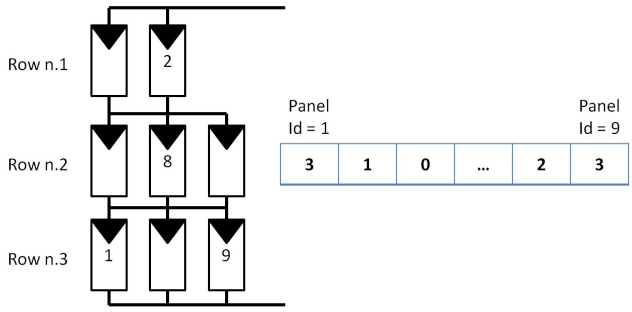

Figure 3.2: Solution encoding for a TCT PV plant topology

For a TCT topology, the array is composed of N_p integers $\mathbf{m} = [m_1, \cdots, m_i, \cdots, m_{N_p}]$, where N_p is the total number of photovoltaic panels.

In this case, the generic integer m_i belongs to the interval $B = [0, N_r]$, where N_r is equal to the maximum number of series-connected rows of TCT topology while the value 0 means that the panel does not belong to any row of TCT topology, i.e., it is disconnected from the PV field (see Figure 3.2). In this case, the disconnection of a panel leads to open its terminals.
Since each panel can be parallel-connected to only one row or at most it can be disconnected from the PV field, each symbol value can be set as follows:

$$m_i = \begin{cases} j \in [1, \cdots, N_r] & \text{if the } i\text{–th panel belongs to the } j\text{–th row} \\ 0, & \text{if the } i\text{–th panel is disconnected} \end{cases}$$

Since any possible combination of integers belonging to the set B is valid, the total number of solutions is equal to $(1 + N_r)^{N_p}$.

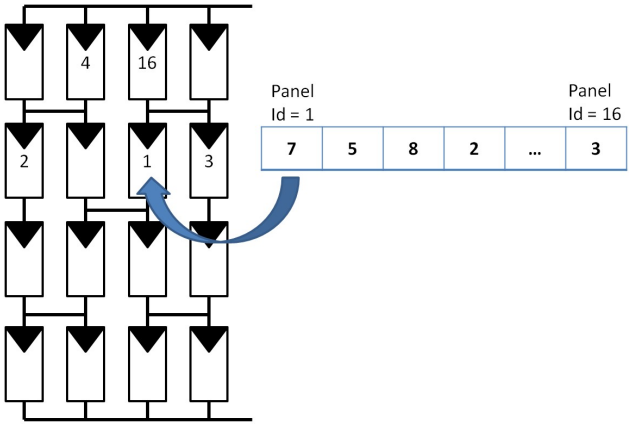

Figure 3.3: Solution encoding for a BL PV plant topology

Also, the simplest encoding can be considered for the BL topology is an array mapping each panel into a well-defined location of PV plant.
The array is composed of N_p integers $\mathbf{k} = [k_1, \cdots, k_i, \cdots, k_{N_p}]$, where N_p is the total number of photovoltaic panels.
In this case, the generic integer k_i belongs to the interval $C = [0, N_{pos}]$, where N_{pos} is equal to the number of all location of BL topology while the value 0 means that the panel is disconnected from the PV field and its terminals are open-connected. In fact, since it is assumed that each panel can be located anywhere or at most it can be disconnected from the PV field (see Figure 3.3), each symbol value can be set as follows:

$$k_i = \begin{cases} j \in [1, \cdots, N_{pos}] & \text{if the } i\text{–th panel is in the } j\text{–th location} \\ 0, & \text{if the } i\text{–th panel is disconnected} \end{cases}$$

Since any possible combination of integers belonging to the set C is valid, the total number of solutions is equal to $(1 + N_{pos})^{N_p}$.

3.1.2 Genetic Operators

During the development of this algorithm, different standard genetic operators have been tested. The choice of genetic operators affects the analysis of solutions space as well as the number of iterations required to achieve the optimal solution.
A GA has mainly three genetic operators: a selection operator, a crossover operator and a mutation operator.
Given a population of solutions, the selection operator chooses a set of solutions to cross in order to produce a new offspring of solutions. In order to preserve partial solutions schemes that increase power generation and pass them to the offspring, a selection operator having a *lower selective pressure* has been chosen, i.e. the *tournament selection*. According to it, T_s (tournament size) elements are picked from the population and compared with each other in a tournament. The winner of this competition will then enter mating pool. Although being a simple selection strategy, it is very powerful and therefore used in many practical applications, since couples of individuals having very different chromosomes are more likely to be chosen.
The choice of the crossover operator strongly affects the exploration of the solutions space, since it preserves or changes parts of the genotype of two selected solutions.
Two crossover operators have been tested: *one-point crossover* and *uniform crossover*: the former leads to a slow exploration of the solutions space and to an high number of iterations to achieve a nearly optimal solution; instead, the latter improves the learning process of algorithm, discarding quickly solutions schemes that

certainly don't lead to the maximum power generation and/or don't respect the given constraints.
Once a couple of individuals $(\mathbf{g}_i, \mathbf{g}_j)$ is selected, uniform crossover generates an offspring $\mathbf{o}$ as follows:

$$o_k = \begin{cases} g_k^i, \text{with probability } p_r \\ g_k^j, \text{with probability } (1 - p_r) \end{cases} \qquad k \in [1, \cdots, N_s]$$

Finally, a standard bit–flip mutation operator has been chosen, by assuming to change the selected *gene* always to a different one with a probability p_m.

3.1.3 Fitness Function

The fitness value is represented by the maximum electrical power that can be extracted by the PV field by using the configuration of panels mapped in a solution.
In order to compute the fitness of a solution $\mathbf{s}$, by assuming a series-parallel topology of the PV field, the proposed GA executes the following steps:

- mapping of the genotype of the solution into the correspondent electrical configuration of panels
- calculation of the voltage-current characteristics of each set of series-connecting panels
- calculation of the voltage-current and voltage-power characteristics of the photovoltaic field
- iterative search for maximum power value $\mathrm{P_{max}}$
- multiplication for a proper *penalty factor* if the voltage V_{mpp} corresponding to maximum power $\mathrm{P_{max}}$ doesn't respect given constraints

In fact, in order to obtain a feasible solution, the voltage V_{mpp} should be within a given range of values in order to guarantee a minimum inverter efficiency. In particular, the minimum voltage value is also that required to turn on the inverter, while the maximum one depends on safety standards too. Similarly, the open circuit voltage cannot exceed 1000V as established by the *National Electrical Code (NEC) 690-7*.
Although not explicitly stated by the NEC, its intent is that all cables, switches, fuses, circuit breakers, and modules in a PV system be rated for the maximum system voltage.
As a consequence, any electrical configuration for which inverter voltage constraints aren't respected is penalized by assuming a *penalty factor* that is proportional to the voltage difference from the nearest boundary.

Thus, the fitness function becomes:

$$\Phi(\mathbf{s}) = \begin{cases} P_{max} & \text{if } V_{mpp} \in [V_{Inv}^{min}, V_{Inv}^{max}] \\ P_{max} \cdot e^{V_{Inv}^{max} - V_{mpp}} & \text{if } V_{mpp} \in [V_{Inv}^{max}, V_{oc}^{max}] \\ P_{max} \cdot e^{V_{Inv}^{max} - V_{mpp}} \cdot e^{V_{oc}^{max} - V_{mpp}} & \text{if } V_{mpp} > V_{oc}^{max} \\ P_{max} \cdot e^{V_{mpp} - V_{Inv}^{min}} & \text{if } V_{mpp} < V_{Inv}^{min} \end{cases} \tag{3.1}$$

where $\mathbf{s}$ is a generic individual in the population.

3.1.4 The optimized procedure

In the developed GA, the major computational overhead is due to the fitness function.
Standard genetic operators, since they simply swap the values of genes or select individual basing on the pre-calculated fitnesses, don't require a huge amount of time to be executed.
On the contrary, the fitness function includes iterative search procedures, multiplication and division operations that can be executed a significant number of times.
For this reason, the developed genetic algorithm has been optimized in order to reduce, as possible, its execution time. In par-

ticular, all operations initially included in the fitness function that don't depend on the particular considered solution are executed at the beginning of the GA.
In fact, in order to quickly calculate the V-I characteristic of each panels row, all samples of the V-I characteristics of panels must be located exactly at the same current values. By this way, the V-I characteristic of a panel row is obtained by summing, for each current value, the corresponding voltages in the V-I characteristics of panels.
Unfortunately, there is no sampling process that can guarantee this condition. So, a proper procedure should be executed at the beginning of GA to pre-calculate missing data for each current value.
So, the original V-I curves of panels aren't used anymore.
At the same time, there is no conditions assuring the alignment of voltage values of all samples belonging to the V-I characteristics of panels rows since it depends on the considered solution. If so, the V-I curve of field could be obtained by simply summing the current values of the characteristics of the two panels rows.
For this reason, the missing data should be estimated during the fitness function execution. As might be expected, the greater is the number of samples of V-I characteristics of panels, and consequently of the PV field, the longer is the time of a single execution of the fitness function.
For this reason, the under-sampling procedure is applied to the characteristics of PV panels.

3.1.5 Problem complexity

According to both the enconding and the fitness function chosen, among all configurations, only a few number could be considered as good candidates for being the optimal one, since they achieve a high power and, at the same time, they respect the inverter voltage boundaries discussed above. Given a fixed number of panels, the chosen representation leads to increase the space of solutions

with the number of strings considered. Anyway, different solutions having the same voltage-power characteristic of the PV field, and so the maximum generated power value, might be obtained. These solutions can be defined as 'equivalent'. In particular, two different classes of equivalence exist:

1. in the first class of equivalence, a solution is equivalent to another one if all panels belonging to a couple of strings are mutually swapped.

2. in the second class of equivalence, solutions are equivalent if couples of panels assigned to different strings have the same I-V curve and are swapped among the strings they belong to.

While the number of equivalent solutions belonging to the first class depends only on number of panels rows, the number of equivalent solutions belonging to the second class depends on shape of V-I curves of PV panels and it cannot be estimated *a priori*. For this reason, the quantity:

$$\frac{(1+N_s)^{N_p}}{N_s}$$

represents an upper bound for the number of unique solutions, once the number of panels and strings have been assigned.

It should be stressed that this redundancy, while seems to be advantageous, can lead to a serious drawback in getting the optimal solution. In fact, the problem gets an additional twist if it is considered that, given a solution, either deactivating just one panel or assigning it to a different string can deeply influence the behaviour of other panels (epistasis [Dav90]) and, consequently, can lead to a fitness landscape unsteady or fluctuating (ruggedness [Kol97]), i. e., going up and down.

In biology, epistasis [Dav90] is defined as a form of interaction between different genes, while in optimization, it is the dependency of the contribution of one gene to the value of the objective function on the state of other genes.

Obviously, a problem is maximally epistatic when no proper subset of genes is independent of any other gene. Epistasis is mainly an aspect of the way in which the genome and the genotype-phenotype mapping are defined and has a strong influence on the search effectiveness. If one gene can turn off or affect the expression of other genes, a modification of this gene will lead to a large change in the features of the phenotype. Hence, the causality will be weakened and ruggedness ensues in the fitness landscape. As a consequence, it also becomes complex to define search operations with both good explorative and exploitive characters. In fact, optimization algorithms generally depend on some form of gradient in the fitness function. The landscape should be continuous and exhibit low total variation, so the optimizer can descend the gradient easily. When fitness functions are rugged, as in the case under study, it becomes complex for the optimization process to find the right directions to proceed to. The more rugged a function gets, the harder it becomes to optimize it.

Hence, although the problem of the rearrangement of photovoltaic panels seems at a first glance straightforward, from the above considerations it follows that it is very challenging in that dealing with both an epistatic genome and a rugged landscape.

3.2 Studied Cases

The Genetic Algorithm has been tested on eight shading scenarios obtained by simulations and on four scenarios properly built by collecting acquired voltage-current characteristics of real PV panels.
The simulated shading scenarios can be classified as *net, diagonal and gradual shading scenarios* depending on the trend of shadow strength and of orientation of shadows respect to modules. Moreover, a very critical scenario (spot shading) is considered.

Shadows having sharp contours: cases 1, 2 and 3

Buildings or the same PV panels could generate shadows having a sharp shape on some panels. Three different cases are considered: partial shading of one of the two PV panels rows, partial shading of all modules belonging to the same PV panel row and symmetrical partial shading of both the two PV panels rows.

In the first case, illustrated in Figure 3.4(a) (left), the sharp shadow covers all modules of the six left-side panels of the bottom row and partially one panel only.

In the second case, all panels belonging to the second row have a strongly reduced current since all modules are partially and equally covered by the same net shadow, as illustrated in Figure 3.4(b) (left).

In the third case, both panels rows have been symmetrically affected by a shadow. In particular, in both the rows, four panels are completely shaded, while one panel for each row is half-shaded, as shown in the solar irradiance chart Figure 3.4(c) (left).

Both in first and third scenarios, the V-I characteristics of panels can be grouped into three categories. The first class includes V-I characteristics having an high short circuit current and only one MPP, as occurs for the non-shadowed panels. The second class includes V-I characteristics having a low short circuit current and one MPP, as occurs for the totally shadowed panels. The third group includes the V-I characteristics having more than one MPP, as occurs for the partially shadowed panels. As regards the second scenario, instead, the V-I characteristics of panels only belong the first two classes.
For each case, the V-I characteristics are shown on the right in the Figures 3.4(a), 3.4(b), 3.4(c).

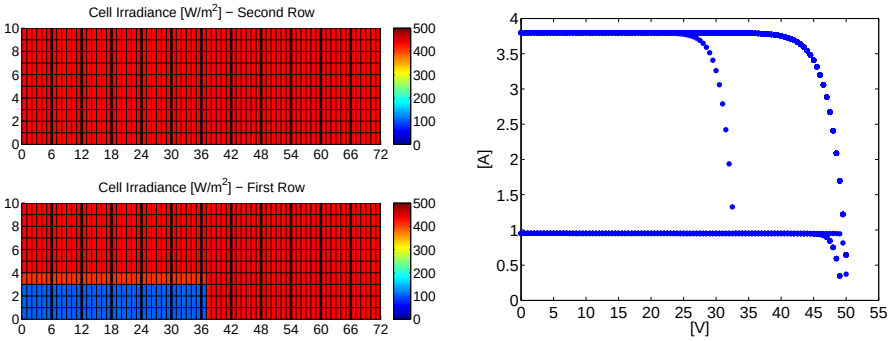

(a) Partial shading of a panels row

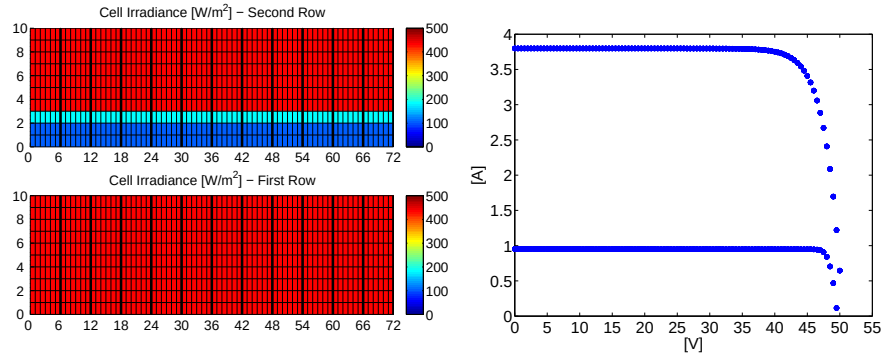

(b) The second panels row is shaded by the first one

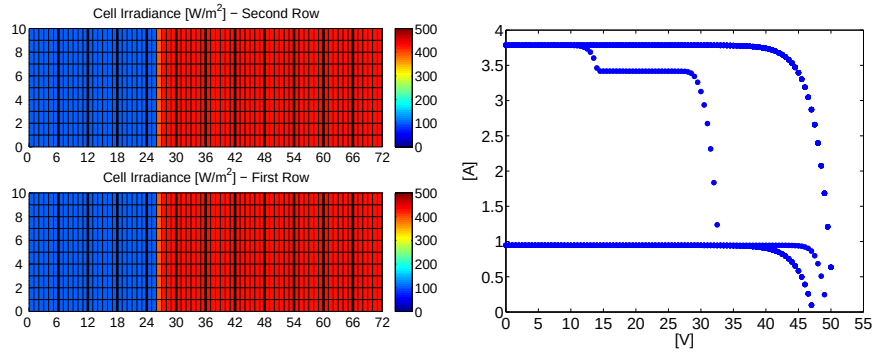

(c) Both panels rows are simmetrically shaded

Figure 3.4: Shadows having a sharp shape. Solar Irradiance (left) and voltage-current characteristics of PV panels (right). Top pane: first case. Middle pane: second case. Bottom pane: third case.

Diagonal shadowing: cases 4 and 5

The presence of light poles or cables generates, during some hours of the day, undesirable shadows which reduce the amount of the generated PV power.

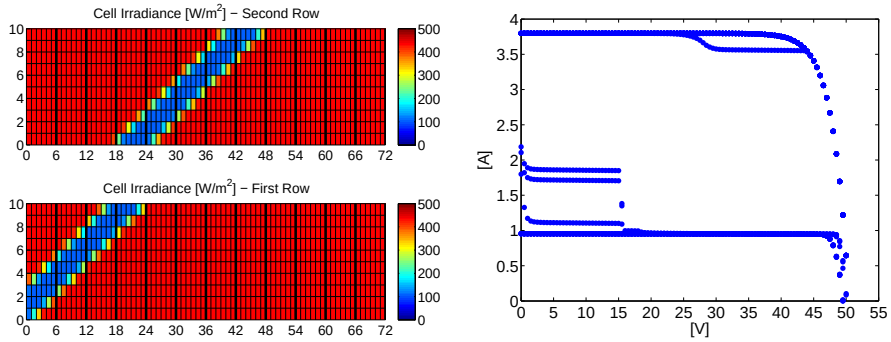

(a) Shadow of a pole

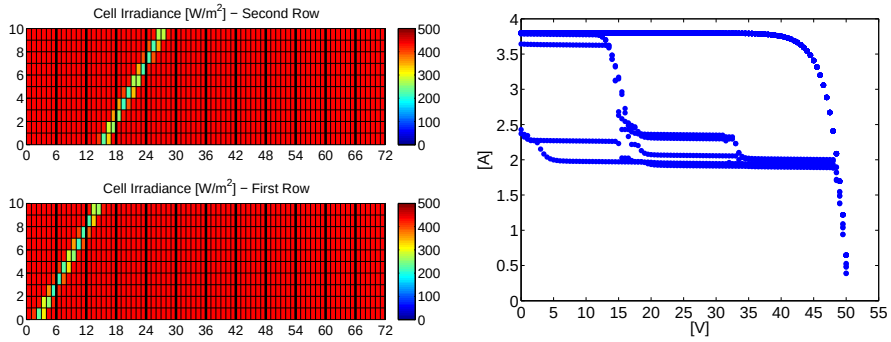

(b) Shadow of a cable

Figure 3.5: Diagonal shadowing. Solar Irradiance (left) and voltage-current characteristics of PV panels (right). Top pane: fourth case. Bottom pane: fifth case.

Also in this case, two different cases have been considered: shadow of a pole and shadow due to a cable. In the first one, a 3-4 cells wide shadow diagonally covers the simulated PV field, as shown in Figure 3.5(a). Even if this shadow could not be very wide, it covers all modules of partially shaded panels. For this

reason, all these panels generate a very low current independently of their voltage. The V-I characteristics of panels can be classified into three groups, exactly as occurred for sharp shading scenarios, depending on the number of shaded modules for each panel. The V-I characteristics of panels are shown in Figure 3.5(a) (right).

Another case is the shadow of a cable or any linear thin obstacle covering a PV field. The main difference with respect to the previous scenario is the lack of a sharp shading. In Figure 3.5(b) (left), the shaded cells have very different solar irradiance values, due to the absence of fully shaded cells. In fact, no cell has an irradiance equal to minimum value, since the shadow is always thinner than the cell width.

In this case, only two of six partially shaded panels, due to the vertical orientation of modules, lead to a V-I curve having a unique current level. Instead, the voltage-current curves of the other shaded panels have two or three different current levels (see Figure 3.5(b) right).

Gradual shadowing: cases 6 and 7

This scenario can occur in presence of transient clouds having a heterogeneous density or when the panels are mounted on bended surfaces. Two different cases have been considered: a longitudinal and an asymmetrical gradual shadow. According to a symmetrical gradual pattern of solar irradiance, each cell receives a different quantity of solar radiation but the irradiance pattern is quite similar for the two panel strings. In Figure 3.6(a) (left), the irradiance has a gradual variation along the longitudinal direction of the simulated PV field. For this reason, each right-sided module generates an higher current than left-sided ones. By this way, the PV panels show multi-peaks V-P curves, as can be deduced from the curves shown in Figure 3.6(a) (right).

When dealing with an asymmetrical gradual shadow, the effects of both different levels of solar irradiance and an heterogeneous density obstacle (such as a tree or a cloud) have been

considered.

In Figure 3.6(b) (left), in both panels rows, all left-sided panels have been affected by a homogeneous shadow, similarly to the second scenario discussed above. Moreover, an heterogeneous shadow has been added to the second panels row (blue colored cells). All the panels interested by an heterogeneous solar radiation exhibit more than one MPP (see Figure 3.6(b)).

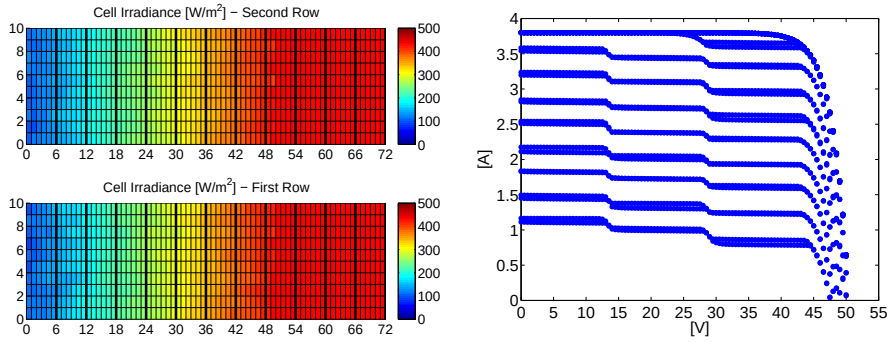

(a) Longitudinal Gradual Solar Irradiance

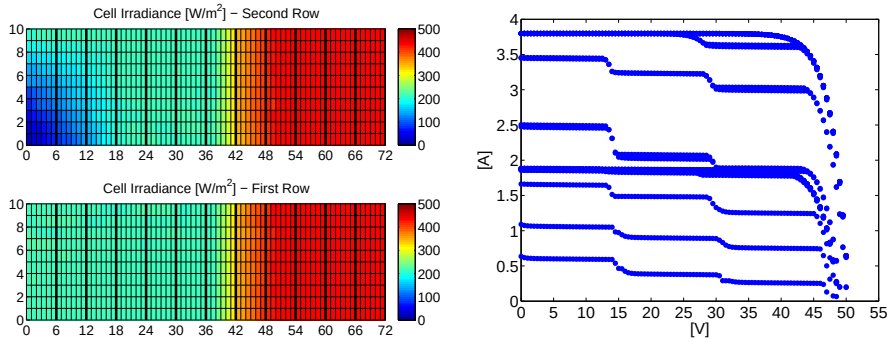

(b) Asymmetrical Gradual Solar Irradiance

Figure 3.6: Gradual shadowing. Solar Irradiance (left) and voltage-current characteristics of PV panels (right). Top pane: sixth case. Bottom pane: seventh case.

Spot shadowing: case 8

As final simulated case, the effects of dust, frost or birds dropping on PV panels has been analyzed. If an obstacle covers a cell, the current generated by the module containing that cell is inexorably reduced. For this reason, the size of shadow affects the V-I characteristics of each photo-voltaic panel.

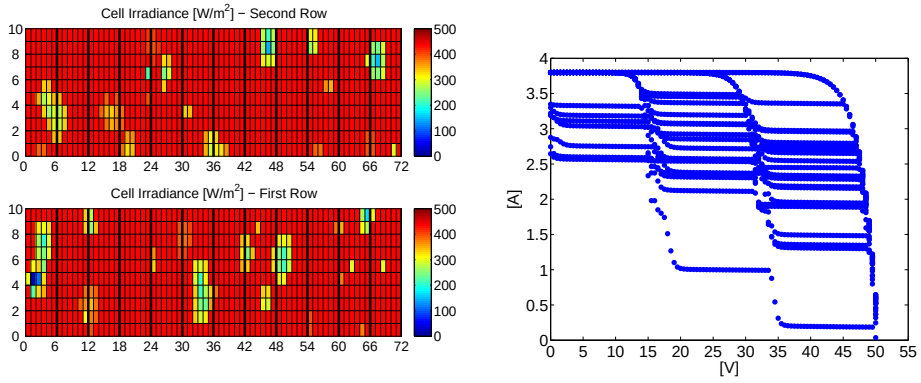

(a)

Figure 3.7: Spot shadowing: eight case. Solar Irradiance (left) and voltage-current characteristics of PV panels (right).

The solar irradiance chart in Figure 3.7 (left) exhibits many shadow spots of different opacity and size. Generally, these kinds of shadows happen very often, especially when the cleaning of panels is not performed on a regular basis. Even if the percentage of shading of each panel is low, a considerable mismatching of PV panel characteristics has been verified (see Figure 3.7 right).

Real V-I characteristics: case 9, 10, 11 and 12

In order to analyze GA performances under real working conditions, four sets of real acquired characteristics of PV panels have been considered.

The characteristics shown in this section have been obtained by measuring voltage and current values across the panel *Sunowe*

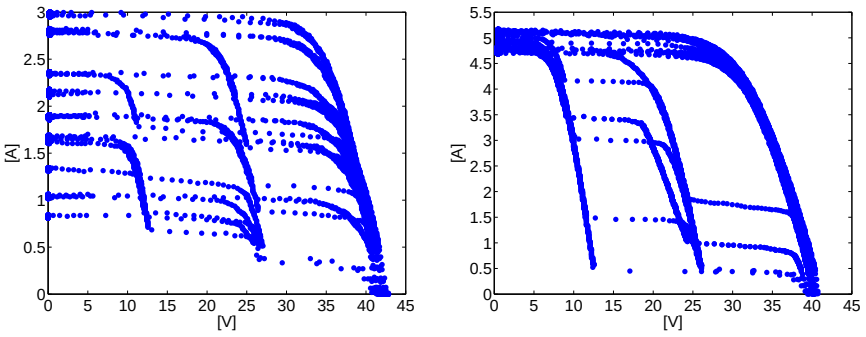

(a)

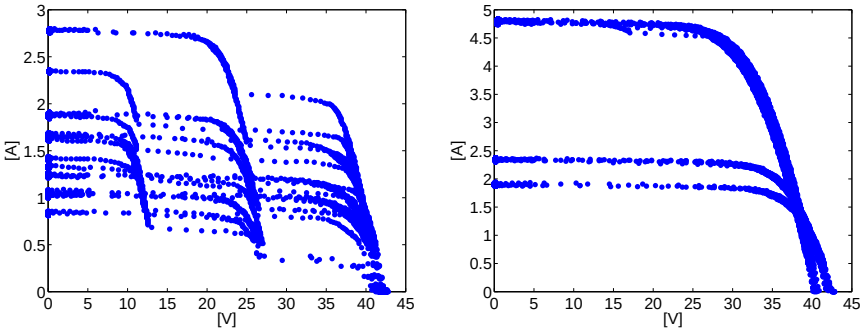

(b)

Figure 3.8: Acquired voltage-current characteristics of PV panels. Top left pane: ninth case. Top right pane: tenth case. Bottom left pane: eleventh case. Bottom right pane: twelfth case.

SF125X125-72-M(L).

In the case 9, the V-I characteristics of panels, illustrated in Figure 3.8(a) (left), have can be classified into different groups depending on short circuit current value and on the number of non-linear regions.

In the case 10, the V-I characteristics of the panels, illustrated in Figure 3.8(a) (right), have been acquired when a single row is partially shaded and the shadow doesn't have sharp edges. So, the

75% of these characteristics have a great short circuit current and only one maximum power point (MPP). The remaining percentage of characteristics are obtained from partially shaded panels and, for this reason, they have multiple MPP.

In the case 11, the V-I characteristics, illustrated in Figure 3.8(b) (left), have been acquired under worst solar conditions, during a very cloudy day, and so they all exhibit multiple current levels.

In the case 12, the V-I characteristics of panels, illustrated in Figure 3.8(b) (right), have been acquired in a scenario very similar to the case 2 (simulated) where all modules of a single row have been equally partially shaded.

3.3 Experimental Results

The under-sampling procedure presented in the Chapter 2 and the Genetic Algorithm (GA) have been tested both on a BeagleBoard XM [Bea14].
The GA has been executed by using the parameters shown in Table 3.1.

Population size	100
Number of generations	200
Tournament size	10%
Mutation rate	0.042
Recombination rate	0.9
Number of runs	20

Table 3.1: Parameters of the Genetic Algorithm

For each scenario, the following elements are provided:

- a table summarizing the best solutions achieved by GA with complete and under-sampling V-I curves of panels

- the under-sampled V-I characteristics of panels
- the graphical synopsis of each best solution, where the panels assume a different color according to the string they belong to (red means string 1, green string 2 and white means that a panel is disconnected
- the comparison between voltage-power characteristic of the field obtained with each best solution and that achieved by using the default configuration. The graphical synompsis of the default configuration is illustrated in Figure 3.9. If a solution has been found by using under-sampled V-I curves, then the full and under-sampled V-P curves of the field are compared too.
- the evolution of the best fitness for each generation averaged over all the 20 runs and its standard deviation

At the end of this Section, a table summarizing the average execution times of GA when full-sampled and under-sampled V-I characteristics are used is provided.

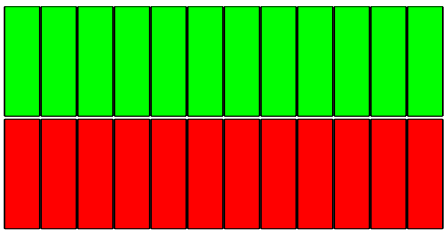

Figure 3.9: Graphical synopsis of the default configuration

Shadows having a sharp shape

Case 1 (see Figure 3.4(a)).

Id.	GA			GA (under-sampling)		
	$\mathbf{V}_{mpp}$[V]	$\mathbf{P}_{max}$[W]	Hits	$\mathbf{V}_{mpp}$[V]	$\mathbf{P}_{max}$[W]	Hits
S1	380.81	2748.53	20/20	380.71	2745.92	19/20
S2	-	-	-	714.14	2593.98	1/20

Table 3.2: Partial shading of 7 panels in single row. Comparison between solutions of GA using original and under-sampled V-I characteristics of panels.

The results of the Genetic Algorithm by using V-I characteristics of panels and their under-sampled version are compared in Table 3.2. The under-sampled characteristics of panels are illustrated in Figure 3.10.

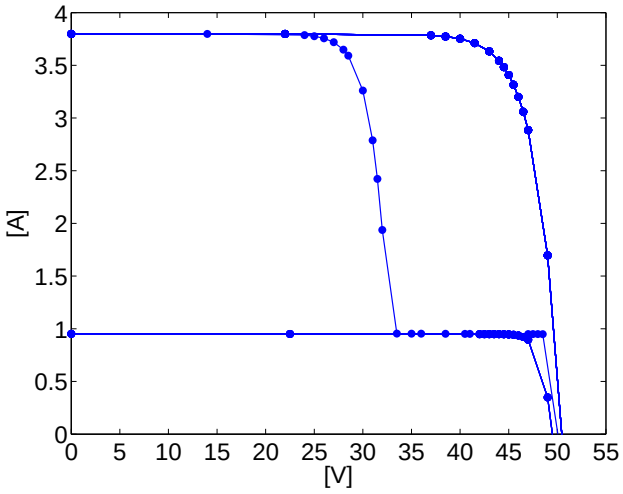

Figure 3.10: Partial shading of one of the two PV panels rows: under-sampled V-I characteristics of panels

For each solution, identified by a generic label S_n, the voltage, the maximum power and the number of occurrences are reported. The solutions are sorted by the MPP value in the descending order.

For this scenario, when the original V-I characteristics of panels are used, the Genetic Algorithm (GA) chooses always the same solution S1. Instead, by using the under-sampled characteristics, this solutions occurs in 19 over 20 runs.

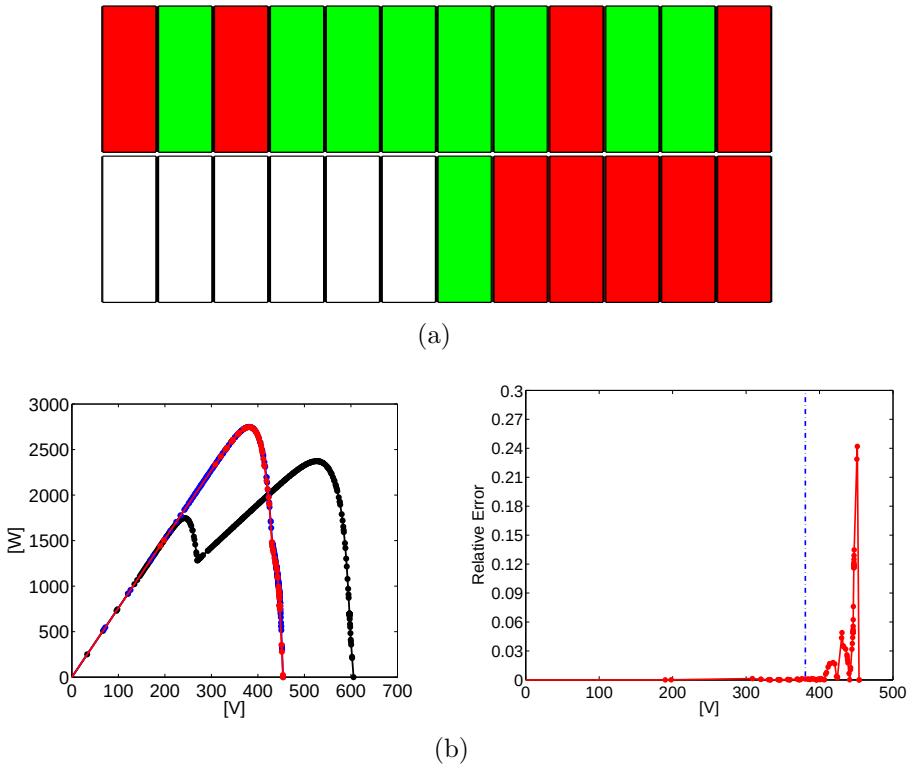

Figure 3.11: Partial shading of one panels row. Top pane (a): electrical configuration chosen by the GA. Top pane (b): Voltage-Power characteristics of the PV field. Best solution obtained by the GA (blue line), default configuration (black line).

A graphical representation of the solution S1 is shown in Figure 3.11(a). It is evident that the chosen configuration is obtained by disconnecting all the shadowed panels. The remaining panels are arranged into two identical strings. Since all the panels forming the optimal solution have exactly the same V-I curve, there

are many equivalent ways to arrange them in the two PV strings having the same identical V-P characteristic.
The V-P characteristics of the optimal configuration obtained with both original and under-sampled V-I characteristics of panels is illustrated in Figure 3.11(b) (left).
The V-P characteristic of the optimal configuration shows only one MPP corresponding to a power equal to 2748.53W at V_{mpp} 380.81V, that means an increase of +15.86% respect to the power generated by the default configuration (2372.24W at V_{mpp} 528V). Moreover, the V-P curve of the default configuration exhibits two different MPPs.
In effect the choice of the MPP of the default configuration depends both on two aspects: the strategy adopted by the MPPT algorithm and the dynamic of the shadow itself over the PV field. In fact, depending on one of these two factors, also the MPP at the voltage around 240V can be chosen. If so, not only the generated power is reduced, but also the voltage of the MPP could strongly be affected by shadow movement over the PV field. In particular, if the voltage of the MPP is lowered under the minimum voltage constraint, then the inverter could be turned off. The reconfiguration procedure helps to avoid this condition.
By using the under-sampled V-I characteristics of panels, the estimated MPP value is equal to 2745.92W at V_{mpp} 380.71V, that is a power difference of around 3W. Despite this difference, the approximation error between the original and the under-sampled V-P characteristic is minimized, as illustrated in Figure 3.11(b) (right), where the relative error is less than 0.2% at the V_{mpp} voltage indicated by a blue colored dashed line.

The second solution S2, whose graphical synopsis is illustrated in Figure 3.12(a), has been found only by using under-sampled V-I characteristics of panels. Unfortunately, this solution is unfeasible since the V_{mpp} voltage value is greater than maximum voltage constraint, even if their difference is only 14V. For this reason, it must be discarded.

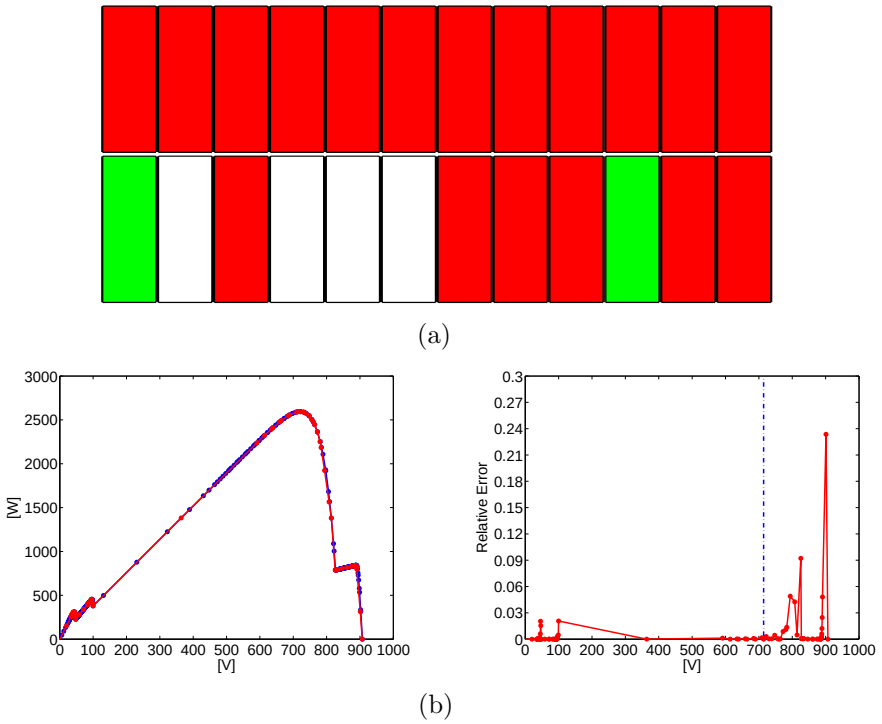

Figure 3.12: Partial shading of one panels row. Top pane (a): unfeasible electrical configuration. Bottom left pane (b): Voltage-Power characteristics of the PV field bu using original V-I characteristics (blue line) and under-sampled ones (blue line). Bottom right pane (b): relative error between the complete and under-sampled V-P characteristics (red line).

The solution S1 is obtained in a very few amount of generations. In Figures 3.3 and 3.3, for each generation, the best fitness (MPP) values averaged over the 20 runs (blue solid line) and its standard deviation (red dotted line) are plotted. The highest maximum power is obtained at the end of all the twenty runs in less than 20 generations. In fact, after the 20th generation, the standard deviation collapses to zero.
By comparing these two plots, the standard deviation in the Figure 3.3 exhibits a slower reduction due to different exploration of

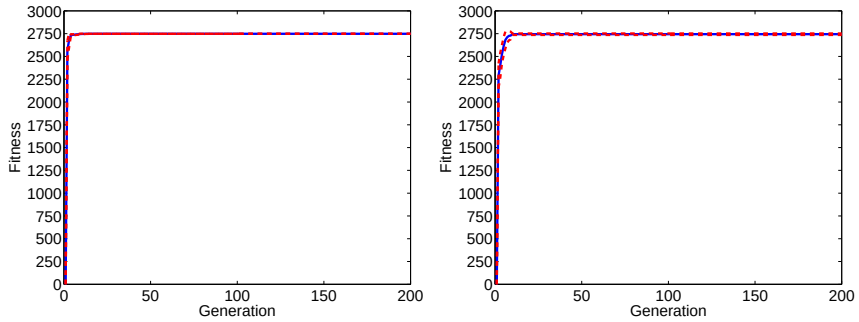

Figure 3.13: Partial shading of one panels row. Evolution of the best fitnesses averaged over 20 runs. Mean fitness (blue line) +/− standard deviation (red dotted line). Left pane: original V-I characteristics. Right pane: under-sampled V-I characteristics.

solutions space.

In fact, the under-sampled characteristics change the MPPs and the correspondent V_{mpp} voltage values for all individuals created by GA. This change affects the sorting of *some* individuals in the population, and so the results of genetic operators. This could lead to the same best solution in a lower or greater number of iterations respect to using the high-density V-I curves.
This effect should be properly minimized. In fact, if the variation of MPP values depends strongly on the considered solution, then all or the majority of individuals can be randomly sorted in the population not respecting their real ranking.
For all these reasons, by using V-I curves having a different density of sample, also different solutions could be obtained.

Case 2 (see Figure 3.4(b)).

Id.	**GA**			**GA (under-sampling)**		
	$\mathbf{V}_{mpp}$**[V]**	$\mathbf{P}_{max}$**[W]**	**Hits**	$\mathbf{V}_{mpp}$**[V]**	$\mathbf{P}_{max}$**[W]**	**Hits**
S1	528	2372.14 (*)	5/20	528	2371.86 (*)	20/20
S2	261	1875	15/20	-	-	-

Table 3.3: Partial shading of all modules belonging to a panels row. Comparison between solutions of GA using original and under-sampled V-I characteristics of panels.

In a real PV plant, when sun altitude decreases, one row of panels could shade that on the back. So, all shaded modules of a row generate the same current and no mismatching effects occur.

In these conditions, there is no other better configuration than default since effectively all panels are exploited with their maximum performances. If the full-sampled V-I characteristics of panels are used, the GA isn't able to achieve always the default configuration S1, indicated by an asterisk in Table 3.3.

Instead, by using under-sampled characteristics, illustrated in Figure 3.15, this is achieved in all 20 runs. This is an unexpected but really positive result due to the application of the under-sampling algorithm.
In fact, it demonstrates that also a minimal difference respect to the original V-I curves of panels could lead both to get worst or better results. As in the previous case, the error introduced in the fitness evaluation of all considered solutions is not constant and so their ranking sort and the GA's evolution are changed.
The different evolution of GAs is evident by comparing the best fitnesses trend in Figure 3.16. In the top pane of this Figure, the number of generations required to achieve the solutions S1 and S2 is lower than 30 but the standard deviation never collapse to zero. In the plot at the bottom, instead, the best fitnesses trend is very abrupt and the best solution is available after 20 generations.

The V-P characteristics of field obtained by both solutions by using the complete V-I curves of panels are compared in Figure

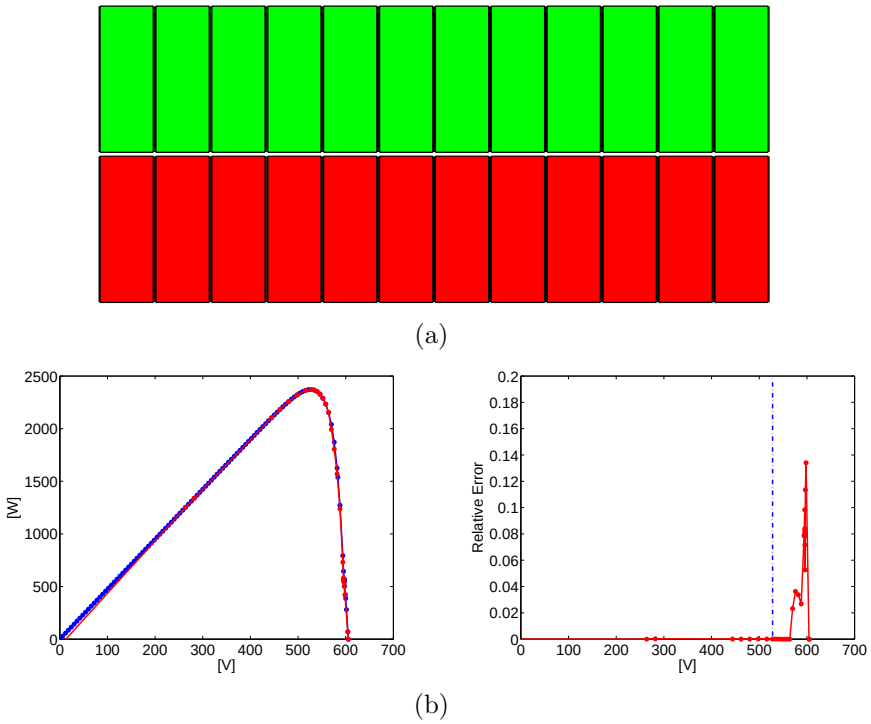

Figure 3.14: Partial shading of all modules belonging to a panels row. Top pane (a): optimal electrical configuration. Bottom left pane (b): Voltage-Power characteristics of the PV field by using original V-I characteristics (blue line) and under-sampled ones (blue line). Bottom right pane (b): relative error between the complete and under-sampled V-P characteristics (red line).

3.17 (right). The achieved MPP value is 1875 W at V_{mpp} 261V for the solution S2, so a reduction of 20.05% respect to power generated by the default configuration S1 (2372.14W at V_{mpp} 528V) is verified.

Also in this case, the V-P characteristics is well reconstructed by under-sampled V-I curves of panels, as illustrated in Figure 3.14(b).
The reconstruction error maintains under 1% for the whole voltage range, while, as expected, a bigger error occurs at lower current

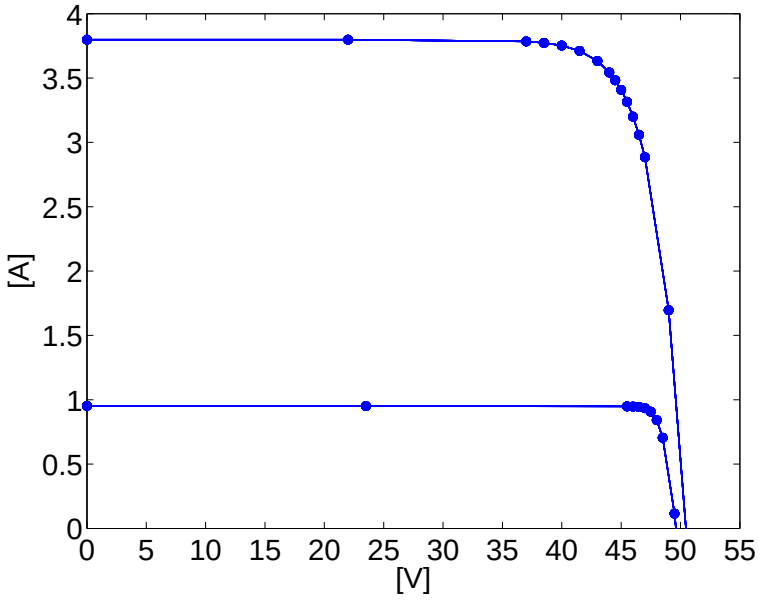

Figure 3.15: Partial shading of all modules belonging to a panels row: under-sampled V-I characteristics of panels

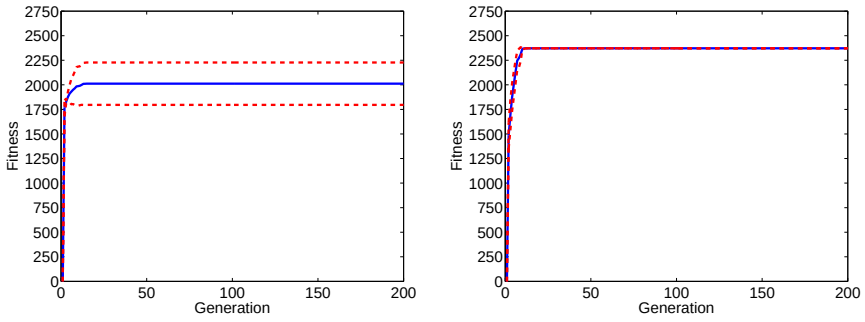

Figure 3.16: Partial shading of all modules belonging to a panels row. Evolution of the best fitnesses averaged over 20 runs. Mean fitness (blue line) +/− standard deviation (red dotted line). Left pane: original V-I characteristics. Right pane: under-sampled V-I characteristics.

values on high-slope linear regions.

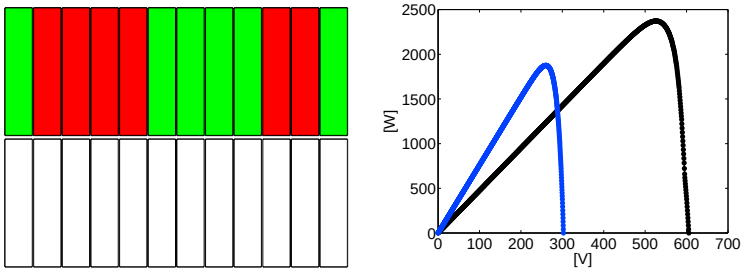

Figure 3.17: Partial shading of all modules belonging to a panels row. Top pane (a): electrical configuration chosen by the GA. Top pane (b): Voltage-Power characteristics of the PV field. Under-optimal solution obtained by the GA (blue line), default configuration (black line).

Case 3. (see Figure 3.4(c)).

Id.	**GA**			**GA (under-sampling)**		
	$\mathbf{V}_{mpp}$**[V]**	$\mathbf{P}_{max}$**[W]**	**Hits**	$\mathbf{V}_{mpp}$**[V]**	$\mathbf{P}_{max}$**[W]**	**Hits**
S1	342.45	2333.7	20/20	340	2323.29	8/20
S2	-	-	-	680.082	2323.29	12/20

Table 3.4: Symmetrical sharp shading of both panels rows. Comparison between solutions of GA using original and under-sampled V-I characteristics of panels.

Also in this case, the GA using the under-sampled V-I characteristics of panels shown in Figure 3.18 is able to better explore the solutions space. In fact, it not only returns the same solution S1 achieved by GA using the complete V-I curves, but also a set of *equivalent solutions* S2 having the same power values of S1 but a greater V_{mpp} voltage.

The GA using the complete V-I curves of the panels obtains always the same solution S1, shown in Figure 3.19(a) where the fully shaded panels are disconnected and the other panels have been arranged according to a symmetrical irradiance pattern of the two panels strings.

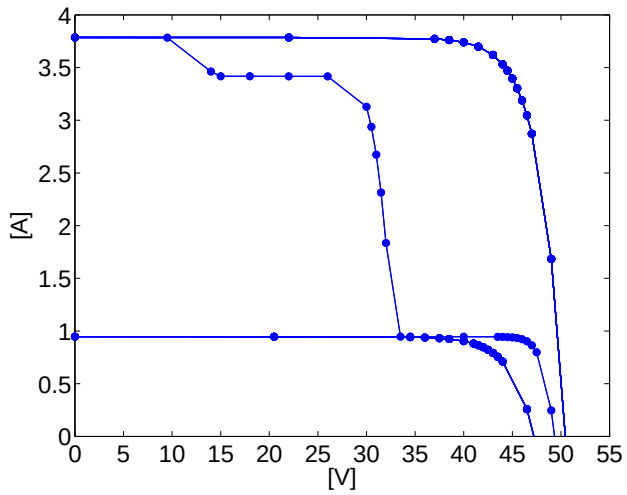

Figure 3.18: Sharp symmetrica shadow: under-sampled V-I characteristics of panels

Instead, the GA using the under-sampled V-I curves of panels achieves the solution S1 only in 40% of times while, in the remaining part of times, also a *set of equivalent solutions* S2 is obtained. In the whole set of solutions S2, whose graphical synopsis are represented in Figure 3.20, the unshaded panels are all series-connected into a unique row, while a variable percentage of the remaining panels are disconnected or series-connected into the other row. In 5 of the suboptimal solutions, a row of the field is composed by only three series-connected panels as shown in the first plot in the Figure 3.20.

The V-P curve of the configuration S1, shown in Figure 3.19(b) (left), exhibits three MPPs since partially shaded panels haven't been disconnected.
The two MPPs at lower voltage are the best ones, since their difference is only 60W. Instead, a lower MPP at 391V remains but, respect to the V-P curve of the default configuration, is nearer to the high-slope region of the higher MPP, so that a MPPT algorithm can more easily detect it.

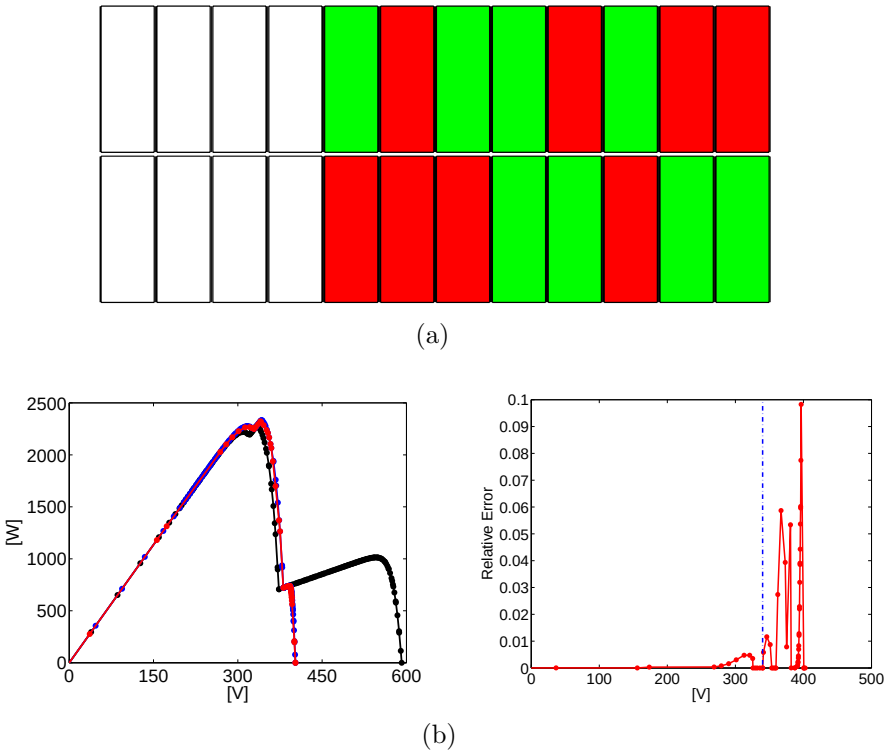

Figure 3.19: Sharp symmetrical shadow. Top pane (a): optimal electrical configuration chosen by GAs (S1 in Table 3.4). Bottom left pane (b): Voltage-Power characteristics of the PV field. Best solution obtained by the faster GA (red line), standard GA (blue line), default configuration (black line). Bottom right pane: relative error between original and under-sampled V-P curve.

The V-P curves of the set S2 are illustrated in each bottom left pane of Figure 3.20. The MPP value at the lower voltage depends on the number of the series-connected panels.
Even if this solution is feasible, the V_{mpp} voltage is very near to the maximum constraint, so that, due to an unpredictable change in solar scenario, the V_{mpp} voltage could exceed it. So, the choice of the solution S1 make the system more robust respect to changes of the shading scenario.

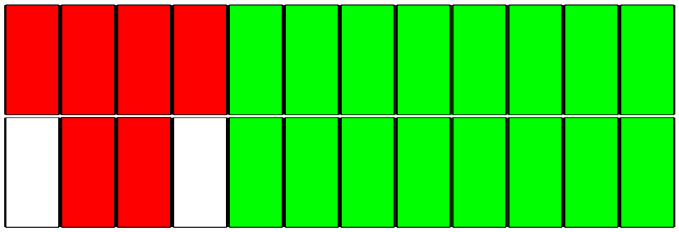

(a)

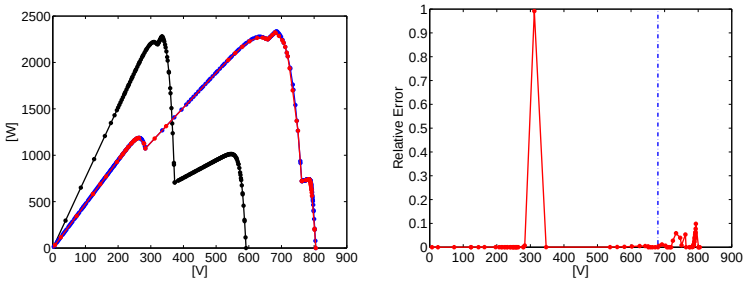

(b)

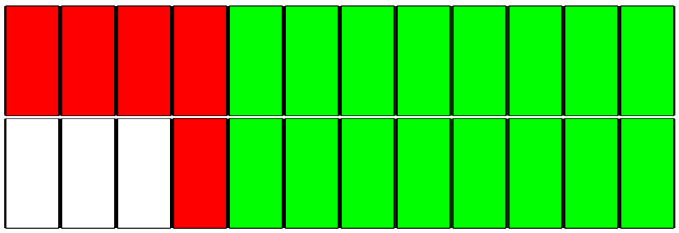

(c)

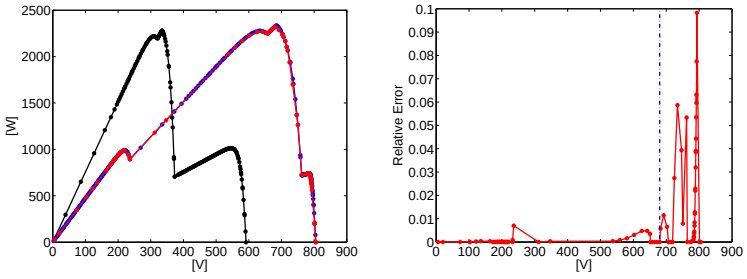

(d)

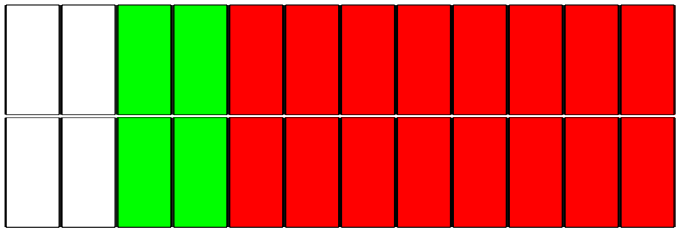

(e)

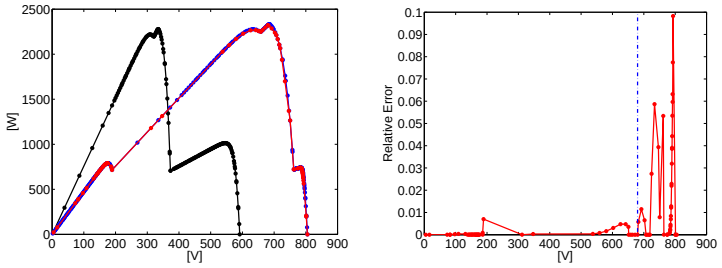

(f)

Respect to the default configuration, whose MPP value is 2279.18W at 334.46V, these solutions provide a power increase of +2.4%.

The comparison between the trends of the fitnesses evolution (see Figure 3.21) shows that in both cases the final solution is achieved in around 30 generations. In Figure 3.21, after the 20th generation, the standard deviation (red dotted) and average fitness (blue) lines overlap.

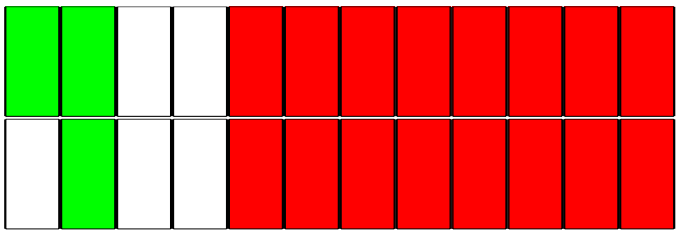

(g)

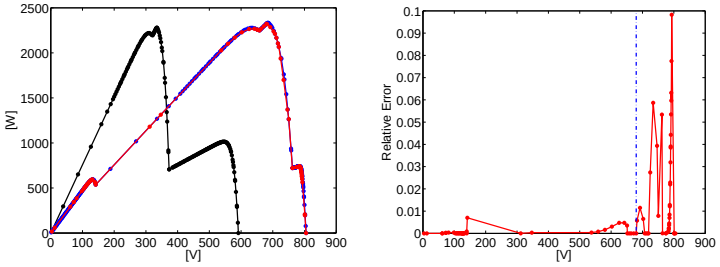

(h)

Figure 3.20: Sharp symmetrical shadow. Set of suboptimal solutions. Top pane: electrical configuration (S2 in Table 3.4). Bottom left pane: V-P curves of the field. Solution obtained by using under-sampled curves (red line), standard GA (blue line), default configuration (black line). Bottom right pane: the approximation error.

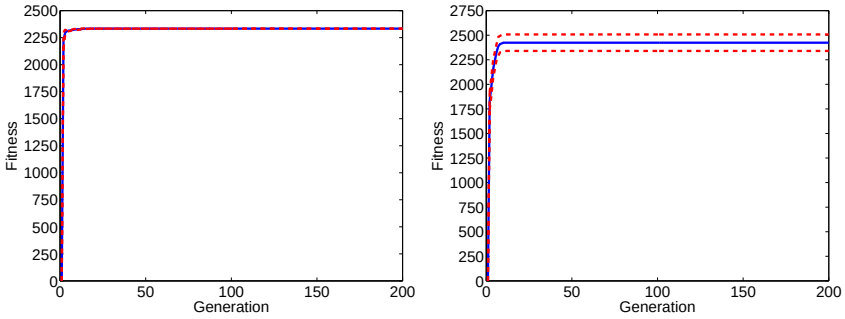

Figure 3.21: Symmetrical sharp shading of both panels rows. Evolution of the best fitnesses averaged over 20 runs. Mean fitness (blue line) +/− standard deviation (red dotted line). Left pane: original V-I characteristics. Right pane: under-sampled V-I characteristics.

Diagonal shadowing

Case 4. (see Figure 3.5(a)).

Id.	GA			GA (under-sampling)		
	$\mathbf{V}_{mpp}$[V]	$\mathbf{P}_{max}$[W]	Hits	$\mathbf{V}_{mpp}$[V]	$\mathbf{P}_{max}$[W]	Hits
S1	-	-	-	526.77	2455	10/20
S2	312	2258.59	20/20	318.4	2251	10/20

Table 3.5: Pole shadow. Comparison between solutions of GA using original and under-sampled V-I characteristics of panels.

Despite the considered shadow is very different from that previously considered, the two shading scenarios are very similar.
In fact, despite the shadow is not so wide to completely cover all interested modules, the pole shadow lead to two main set of V-I curves of panels having both one current levels but two different short circuit current values.
The under-sampled V-I curves of panels are shown in Figure 3.22.

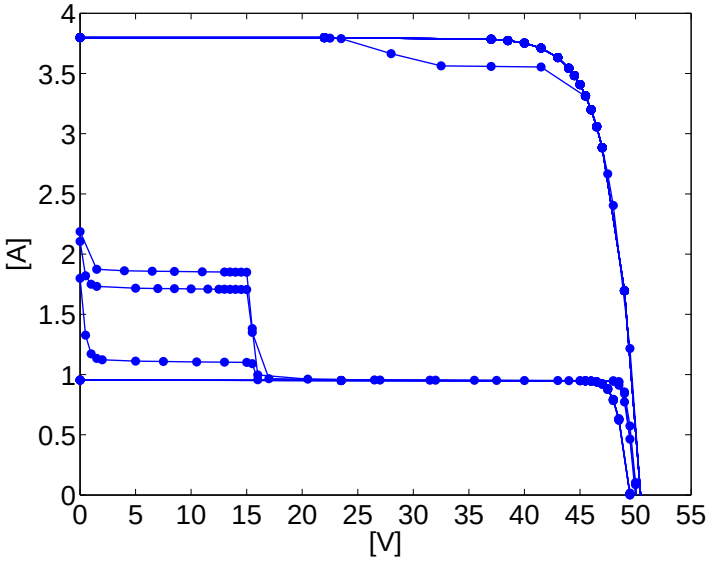

Figure 3.22: Pole shadow: under-sampled V-I characteristics of panels

As shown in the Table 3.5, the GA using full V-I curves of samples never achieves the best solution. In fact, since the nine shaded panels are disconnected, there isn't a full exploitation of the whole PV generator.
In this solution, the unshaded panels are re-distributed between the two photovoltaic strings in order to have the same solar radiance pattern (see Figure 3.23(a)).

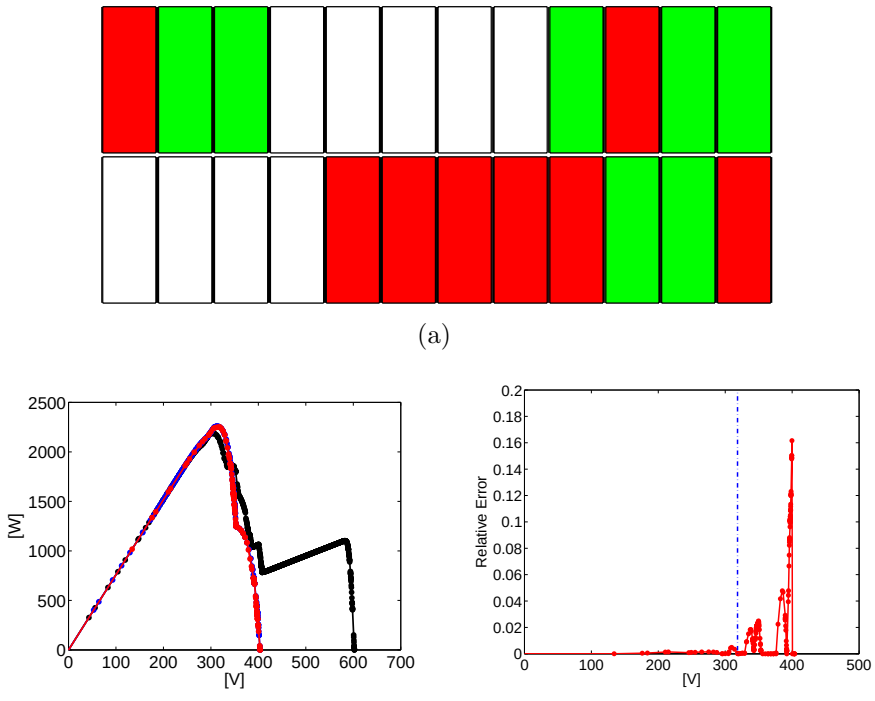

Figure 3.23: Pole shadow. Top pane (a): sub-optimal electrical configuration chosen by GAs (S2 in Table 3.5). Bottom left pane (b): Voltage-Power characteristics of the PV field. Best solution obtained by the faster GA (red line), standard GA (blue line), default configuration (black line). Bottom right pane: relative error between original and under-sampled V-P curve.

Respect to the MPP value provided by the default configura-

tion (2187.76W at 305.1V), the generated power of solution S2 provides an increase of +3.24%. The voltage-power curve of the photovoltaic field is shown in Figure 3.23(b). Despite the generated power increase, in effect the V_{mpp} voltage is very near to the lower boundary. Since a further shadow movement could lead to an unpredicted change of the V-P curve, also the V_{mpp} voltage could change in an unpredicted way and if the lower boundary is reached, then the inverter could be turned off. This doesn't occurs by considering the solution S1, whose graphical synopsis is shown in Figure 3.24(a).

In the solution S1, one string is composed of unshaded panels only, while in the other the shaded panels are series-connected to a small group of unshaded panels in order to achieve the same voltage value.
The V-P curve of the best solution S1 is shown in Figure 3.24(b). While the V-P curve of the field for the solution S2 has only one MPP, the V-P curve of the field of the solution S1 has multiple MPPs at high voltage. Nevertheless, respect to the solution S2, this one is more robust respect to further change of the shadow position since the V_{mpp} voltage is farther from its boundaries.

The V-P curves of both solutions are correctly reconstructed by the under-sampled V-I curves of panels, as shown in the reconstruction error curves in Figures 3.24(b) and 3.23(b), where the error is under 1% at the V_{mpp} voltage.

The fitness trend is very abrupt by using both complete and under-sampled V-I curves and the solutions are found in less than 20 generations, or equivalently in less then 2000 evaluations of the fitness function (see Figure 3.25).

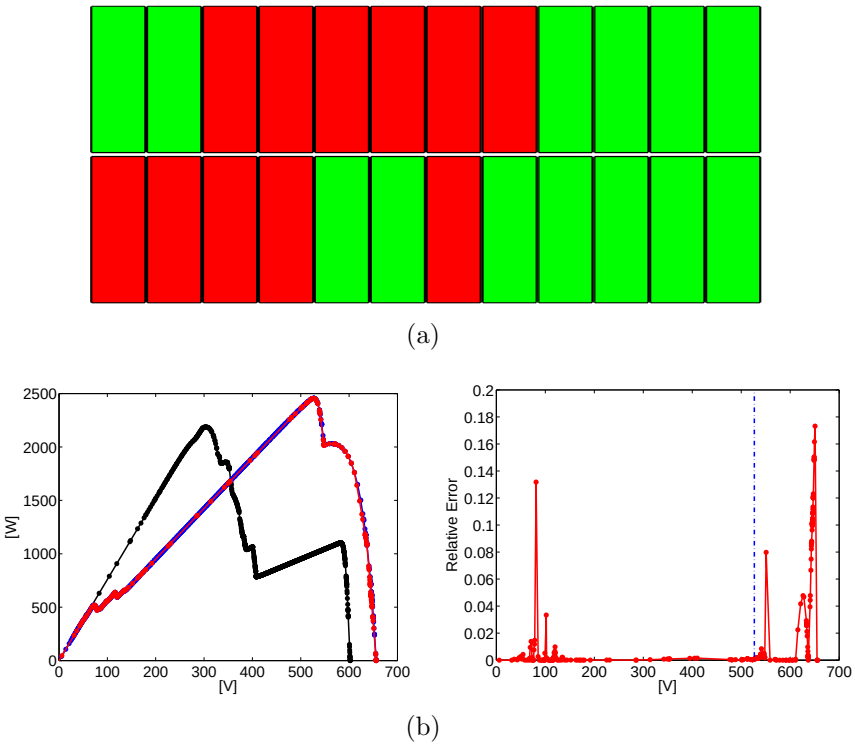

Figure 3.24: Pole shadow. Top pane (a): optimal electrical configuration chosen by GAs (S1 in Table 3.5). Bottom left pane (b): Voltage-Power characteristics of the PV field. Best solution obtained by the faster GA (red line), standard GA (blue line), default configuration (black line). Bottom right pane: relative error between original and under-sampled V-P curve.

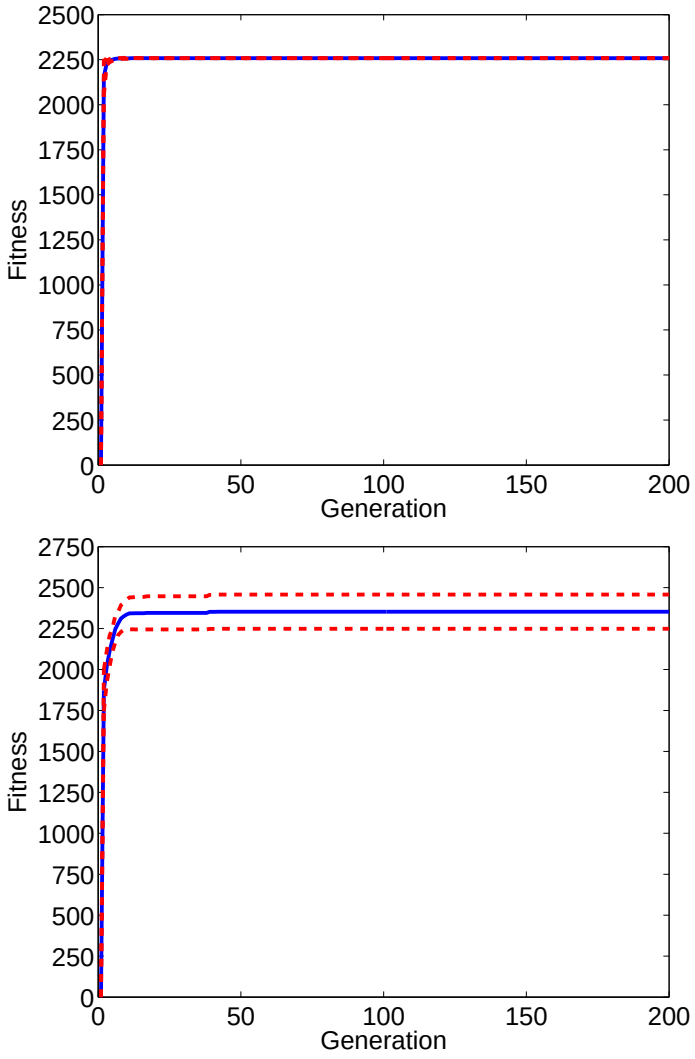

Figure 3.25: Pole shadow. Evolution of the best fitnesses averaged over 20 runs obtained by using complete (top pane) and under-sampled V-I curves of panels (bottom pane). Mean fitness (blue curve) +/- standard deviation (dotted red curve).

Case 5. (see Figure 3.5(b)).

Id.	**GA**			**GA (under-sampling)**		
	$\mathbf{V}_{mpp}$**[V]**	$\mathbf{P}_{max}$**[W]**	**Hits**	$\mathbf{V}_{mpp}$**[V]**	$\mathbf{P}_{max}$**[W]**	**Hits**
S1	418.54	3007.7	20/20	415.05	3004.58	20/20

Table 3.6: Cable shadow. Comparison between solutions of GA using original and under-sampled V-I characteristics of panels.

In this case, due to the vertical orientation of modules, only two of six partially shaded panels have only one current level in their V-I characteristics, while the remaining shaded panels have two or three different current levels.
The under-sampled curves of panels are illustrated in Figure 3.26.

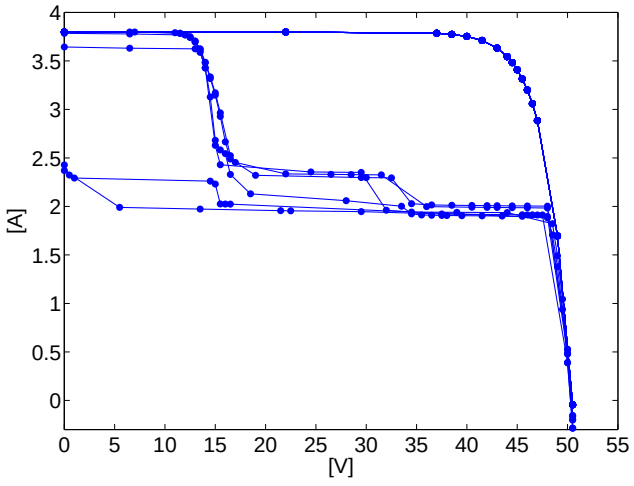

Figure 3.26: Cable shadow: under-sampled V-I characteristics of panels

The GA chooses, even if the under-sampled V-I curves are used, always the same solution where only the panels having all modules covered by the cable shadow, and so a unique lower current level in their V-I curves, are disconnected.
As in the previous scenario, in order to obtain a symmetrical solar radiance pattern and so similar V_{mpp} voltage for both rows,

the panels are arranged as shown in Figure 3.27(a). In particular, one string is composed on all unshaded panels, while the others is a series-connection of 8 unshaded panels and all partially shaded panels.

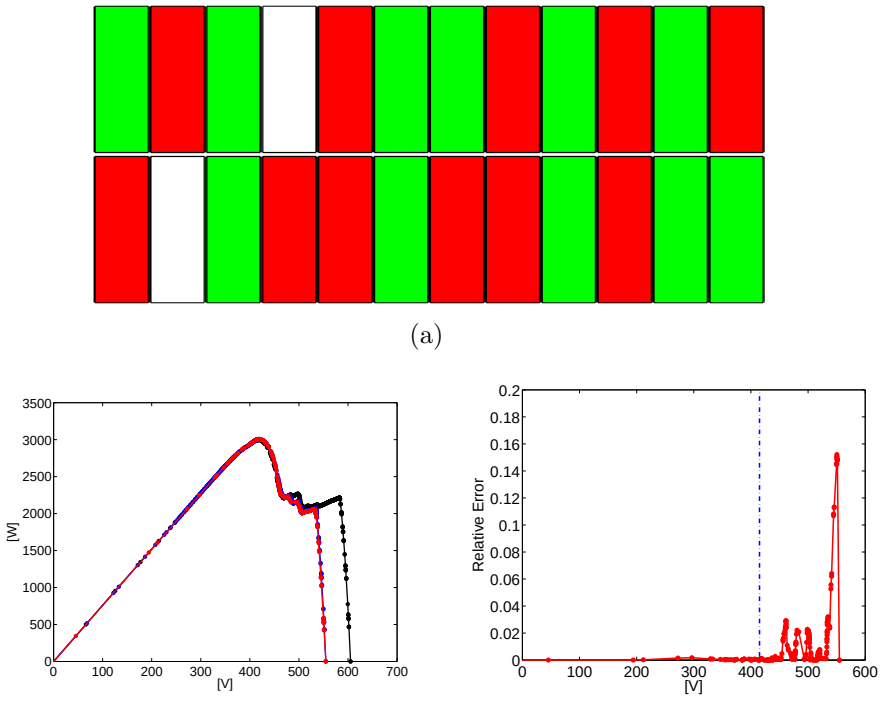

Figure 3.27: Cable shadow. Top pane (a): optimal electrical configuration chosen by GAs (S1 in Table 3.6). Bottom left pane (b): Voltage-Power characteristics of the PV field. Best solution obtained by the faster GA (red line), standard GA (blue line), default configuration (black line). Bottom right pane: relative error between original and under-sampled V-P curve.

The effect of partially shaded panels determines V-P curve of the field exhibiting many local MPPs (see Figure 3.27(b)). The global maximum power value is equal to 3007.69W at V_{mpp} 418.54V, while the standard configuration shows a MPP equal to

2993.32W V_{mpp} at 416.5V. So, the generated power increases of only +0.48%.

The disconnection of one panel for each string leads to an increase of the V_{mpp} voltage equal to around 2V, that is the main reason an increased power value is achieved. In fact, the turning on of one bypass diode cause the reduction of V_{mpp} voltage of around 0.6V. So, if all modules of the shaded panel generate a current lower than that of the MPP, then the voltage reduces of around 2V.

Only 20 generations are required to obtain the best solution, due to the high number of equivalent solutions, by using both complete V-I curves of panels and their under-sampled version, as shown in the fitness evolution graph (Figure 3.28). In these Figures, the standard deviation (red dotted line) and the trend of the best fitnesses (blue line) overlap in about 20 generations.

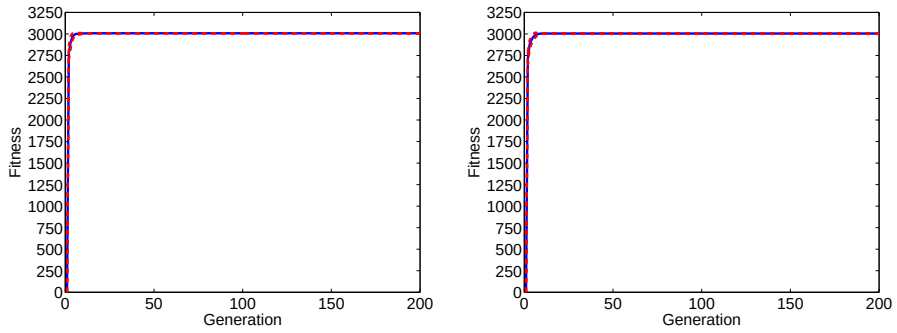

Figure 3.28: Cable shadow. Evolution of the best fitnesses averaged over 20 runs obtained by using complete (left pane) and under-sampled V-I curves of panels (right pane). Mean fitness (blue curve) +/- standard deviation (dotted red curve).

Gradual shadowing

Case 6. (see Figure 3.6(a)).

Id.	GA			GA (under-sampling)		
	$\mathbf{V}_{mpp}$[V]	$\mathbf{P}_{max}$[W]	Hits	$\mathbf{V}_{mpp}$[V]	$\mathbf{P}_{max}$[W]	Hits
S1	450.4	2212.06	15/20	451.7	2215	20/20
S2	406.4	2134.54	5/20	-	-	-

Table 3.7: Gradual symmetrical shading. Comparison between solutions of GA using original and under-sampled V-I characteristics of panels.

The GA using the complete V-I curves of panels, at the end of the 20 runs, generates two different solutions having a significant difference in terms of maximum power, as reported in the Table 3.7. This is mainly due to the different number of disconnected panels. Nevertheless, the electrical configuration provided by these two solutions are very similar, as shown by their graphical synopsis in Figure 3.29.

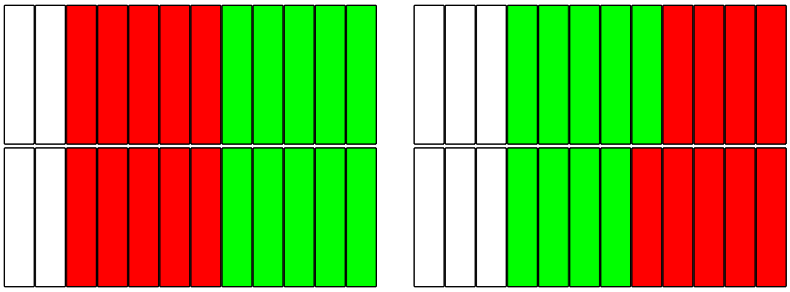

(a) (b)

Figure 3.29: Gradual symmetrical shading. Graphical synopsis: (a) S1 (b) S2

In the optimal solution S1, only the panels receiving the lowest irradiance ($G < 400W/m^2$) are disconnected, while the other panels are arranged in order to obtain two strings having the same

solar irradiance level. In the solution S2, all panels having cell solar irradiance G under 500 W/m^2 have been disconnected. The remaining panels are arranged in order to have two PV strings having the same irradiance level.

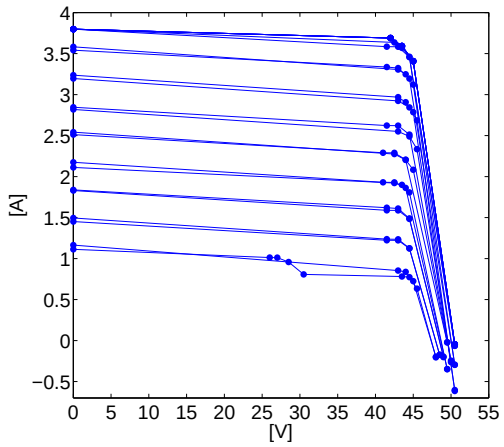

Figure 3.30: Gradual Symmetrical shadow: under-sampled V-I characteristics of panels

Instead, as occurred also in some previous cases, the GA using the under-sampled V-I curves, shown in Figure 3.30, chooses always the same optimal solution S1 that, respect to the MPP value of the default configuration (1677.93W at 367.6V), provides a power increase of +31.7%. The reconstruction error is under 1% as shown in the right pane of Figure 3.31, where higher error peaks are due to the samples having a current value lower than 1A.

In the V-P curve corresponding to the solution S2, as shown in Figure 3.32 (red line), the MPP value is equal to 2134.54W @ V_{mpp} 406.39V, so that a power increase of +27.2% respect to the MPP of the default configuration is achieved. Moreover, the relative difference between MPPs of the two solutions is only 3.63%.

In this scenario, by using the complete V-I curves of panels, the proposed GA takes 164 generations to reach the desired solution,

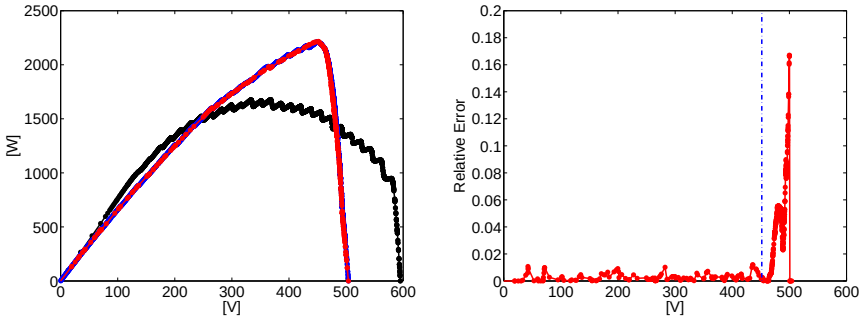

Figure 3.31: Gradual symmetrical shadow: solution S1. Left pane (b): Voltage-Power characteristics of the PV field. Best solution obtained by the faster GA (red line), standard GA (blue line), default configuration (black line). Right pane: approximation error of the V-P curve.

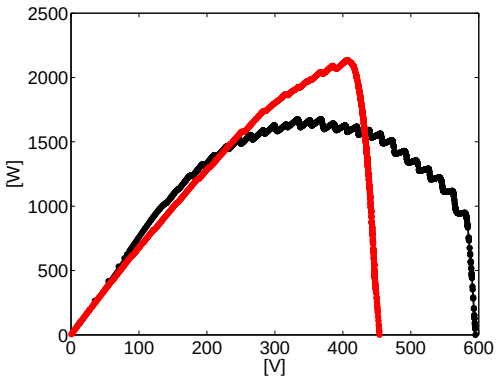

Figure 3.32: Gradual symmetrical shadow: solution S2. Voltage-Power characteristics of the PV field. Best solution obtained by the GA (red line), standard GA (blue line), default configuration (black line).

even if the average fitness (blue line) reaches a stable value just after 50 generations (see Figures 3.33(a) and 3.33(a)).
An higher number of generations is required when the difference of solar irradiance among panels or among group of panels is very negligible. In this case, the algorithm could take several generation to obtain the solution that gives rigorously the best phenotype.

From a practical point of view, the solution S2 discussed for this scenario, thus the suboptimal one, is interesting because it is achieved in a number of generations that is significantly smaller than the one requested by the absolute optimal solution. The optimal solution S1 has been obtained in the 60% of the GA runs, while in the remaining 40% the very close solution S2 is achieved. Instead, by using the under-sampled V-I curves of panels, the optimal solution S1 is always achieved. Moreover, the GA takes no more than 30 generations, that is the most interesting result.

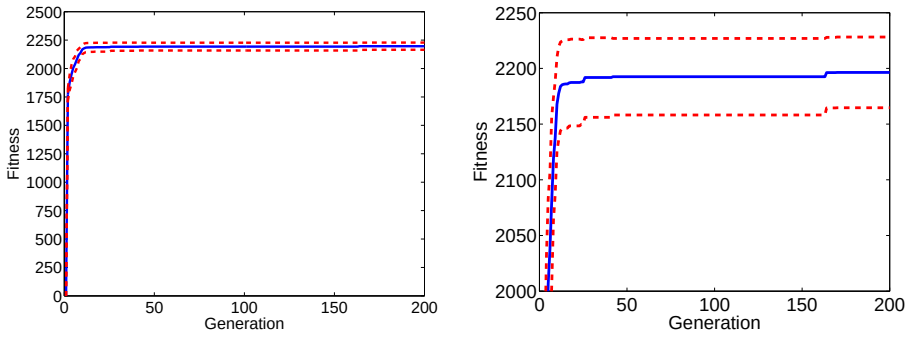

(a)

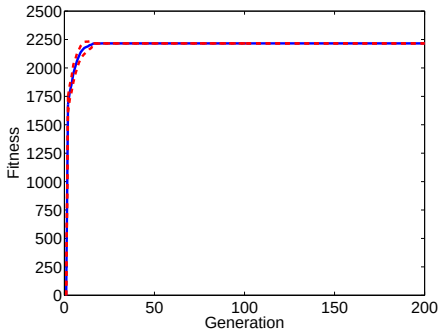

(b)

Figure 3.33: Gradual symmetrical shadow. Evolution of the best fitnesses averaged over 20 runs obtained by using complete (top panes) and under-sampled V-I curves of panels (bottom pane). Mean fitness (blue curve) +/- standard deviation (dotted red curve).

The use of the under-sampled V-I curves of panels changes the ranking order of found solutions in the population. Moreover, it could also amplify the difference among classes of the under-optimal and optimal solutions because of the introduced approximation error in the fitness calculation, so permitting to the optimal solution to be found in a reduced amount of generations.

Case 7. (see Figure 3.6(b)).

Id.	**GA**			**GA (under-sampling)**		
	$\mathbf{V}_{mpp}$**[V]**	$\mathbf{P}_{max}$**[W]**	**Hits**	$\mathbf{V}_{mpp}$**[V]**	$\mathbf{P}_{max}$**[W]**	**Hits**
S1	461.86	2199.98	20/20	456.16	2182.03	20/20

Table 3.8: Gradual asymmetrical shadow. Comparison between solutions of GA using original and under-sampled V-I characteristics of panels.

As summarized in Table 3.8, the GA always returns the same best solution both when the complete V-I curves of panels or their under-sampled version is used. The under-sampled curves of panels are shown in Figure 3.34.

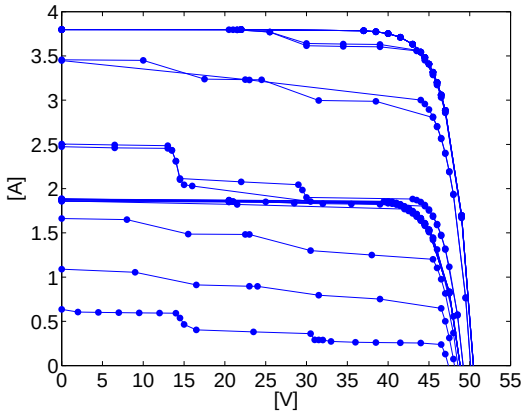

Figure 3.34: Gradual Asymmetrical shadow: under-sampled V-I characteristics of panels

Also in this case, the most shaded panels have been disconnected by the proposed GA (see Figure 3.35(a)). The optimal electrical configuration is, again, obtained by disposing the equal radiated panels in order to achieve the same pattern radiance for both panels rows.

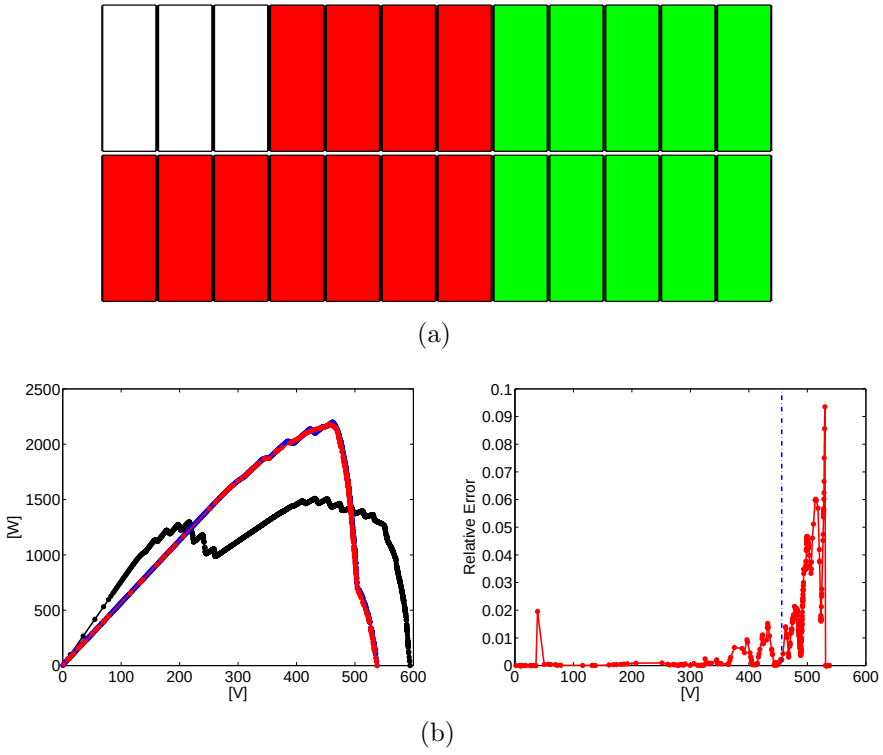

(a)

(b)

Figure 3.35: Gradual asymmetrical shadow. Top pane (a): optimal electrical configuration chosen by GAs (S1 in Table 3.8). Bottom left pane (b): Voltage-Power characteristics of the PV field. Best solution obtained by the faster GA (red line), standard GA (blue line), default configuration (black line). Bottom right pane: relative error between original and under-sampled V-P curve.

The default configuration is really inefficient when this kind of solar radiance scenario occurs. In fact, the V-P curve of the default configuration exhibits many different local MPPs and the

maximum power that can be extracted is equal to 1510W @ V_{mpp} 431.5V. Instead, the V-P curve of the best solution, illustrated in Figure 3.35(b), exhibits some unimportant lower MPP close to the global one having a power value equal to 2199.98W @ V_{mpp} 461.87V, that corresponds to an increase of +45.7%.

The optimal solution has been found in less of 20 generations by both using decimate and complete V-I curves of panels, but the comparison of the fitness evolution plots (see Figure 3.36) shows that the standard deviation has greater values when the under-sampled curves are used before collapsing to zero.

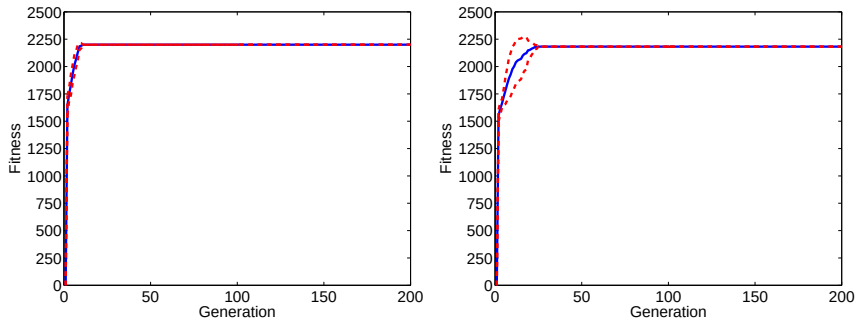

Figure 3.36: Gradual Asymmetrical shadow. Evolution of the best fitnesses averaged over 20 runs obtained by using complete (left pane) and under-sampled V-I curves of panels (right pane). Mean fitness (blue curve) +/- standard deviation (dotted red curve).

Spot shadowing

Case 8. (see Figure 3.7)

Since there is not a precise geometrical solar irradiance pattern, in this case it is very difficult to predict which electrical configuration could be the optimal one.
For this scenario, in all provided solutions, no panels have been disconnected, so achieving the maximum exploitation of all PV

Id.	GA			GA (under-sampling)		
	$\mathbf{V}_{mpp}$[V]	$\mathbf{P}_{max}$[W]	Hits	$\mathbf{V}_{mpp}$[V]	$\mathbf{P}_{max}$[W]	Hits
S1	505.3	2407.85	14/20	495.49	2379.6	12/20
S2	506.28	2365	5/20	-	-	-
S3	472.2	2362	1/20	-	-	-
S4	-	-	-	480.32	2357.55	2/20
S5	-	-	-	478.15	2342.49	1/20
S6	-	-	-	486.72	2340.68	1/20
S7	-	-	-	493.53	2340.07	1/20
S8	-	-	-	493.36	2338.78	1/20
S9	-	-	-	495.3	2336.17	1/20
S10	-	-	-	476.44	2289.39	1/20

Table 3.9: Spot. Comparison between solutions of GA using original and under-sampled V-I characteristics of panels.

panels.

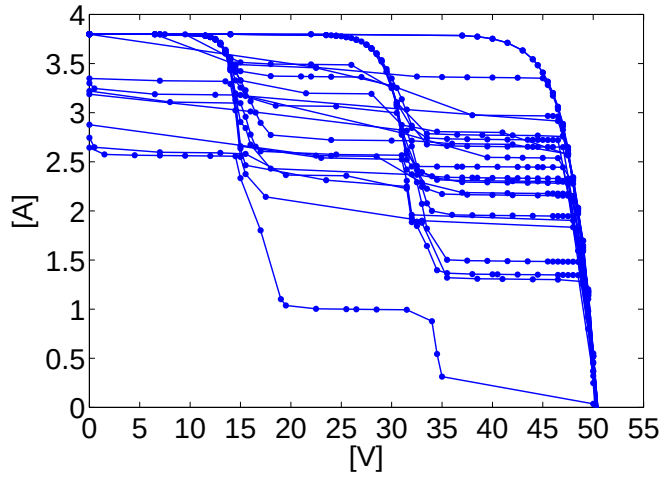

Figure 3.37: Spot shadow: under-sampled V-I characteristics of panels

Nevertheless, the GA using the complete V-I curves of panels achieves better performance than that using the under-sampled

version of curves, shown in Figure 3.37.

Three different solutions have been found by the GA using complete V-I curves of panels during the 20 runs (refer to Table 3.9).

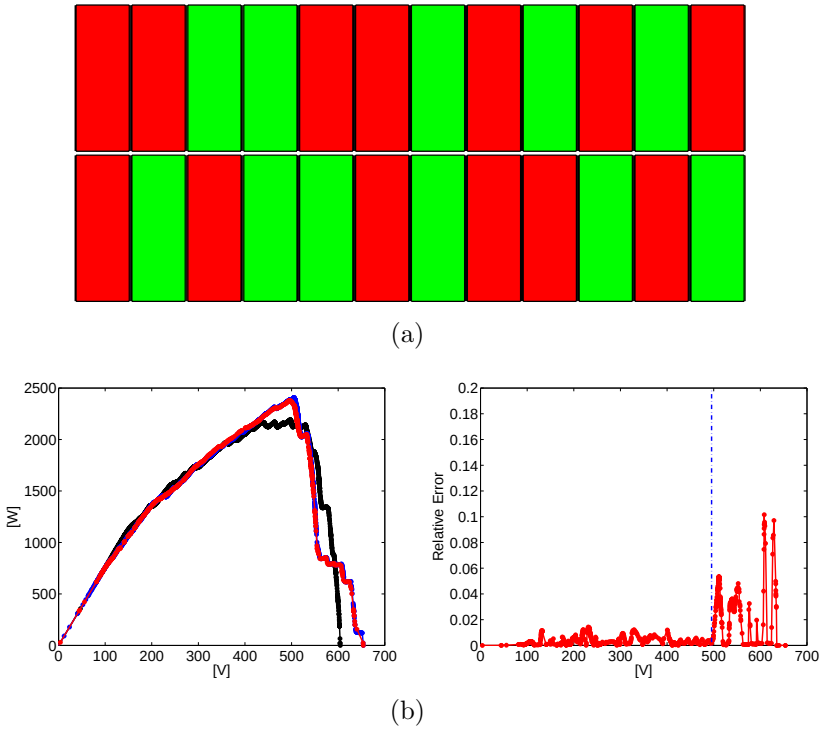

Figure 3.38: Spot shadow. Top pane (a): optimal electrical configuration (S1 in Table 3.9). Bottom left pane (b): V-P curves of the PV field. Under-sampled (red line), complete (blue line), default configuration (black line). Bottom right pane: relative error between original and under-sampled V-P curve.

The optimal solution S1 chosen by GA improves power generation by 9.75% respect to the default configuration, whose V-P characteristic exhibits multiple MPPs near to the highest MPP value equal to 2194.035W at 497.545 V (see Figure 3.38(b)). The solution S1 has been found by both using complete and decimate

V-I curves of panels.

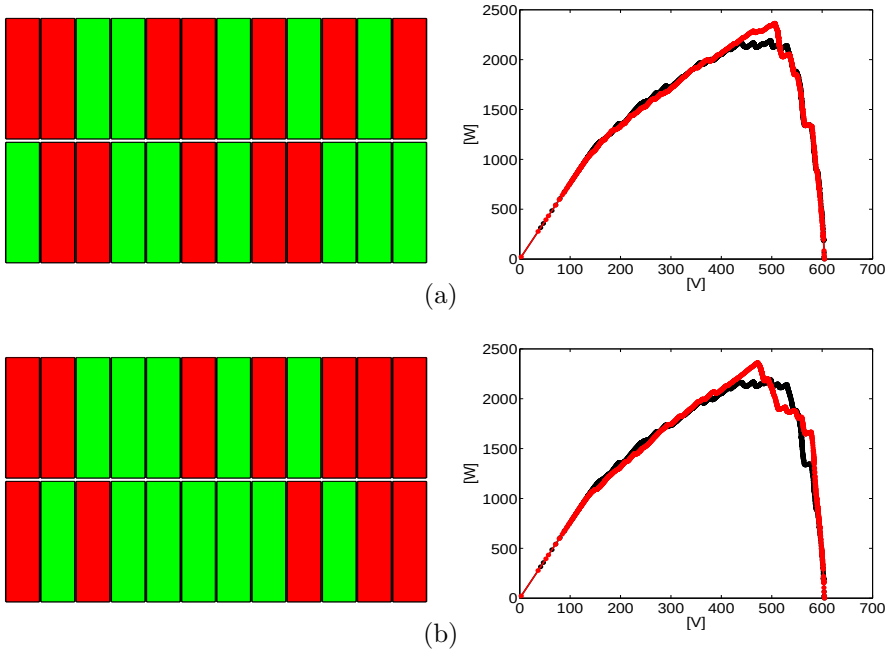

Figure 3.39: Spot shadow. Top and bottom left panes: electrical configuration chosen by GAs (S2 and S3 respectively in Table 3.9). Top and bottom left panes: Voltage-Power characteristics of the PV field. Best solution obtained by the faster GA (red line), standard GA (blue line), default configuration (black line).

The V-P curve of the field for the solution S2 (see Figure 3.39(a)) provides the minimal mismatching effects even if not the highest MPP value. In general, there isn't any solution providing only a unique MPP because of many different current levels.

Instead, the under-sampling of V-I curves of panels lead to achieve the majority of runs (12/20) the optimal solution S1 (see Figure 3.38(a)) and, during the remaining runs, a set of other 7 different solutions generating an electrical power varying between 2289.39 and 2357.55 Watts. These solutions have been reported in Figure 3.40.

The achievement of these multiple solutions is mainly due to the low efficiency of the under-sampling algorithm. In fact, some non-linear regions at current values less then 1A is not properly reconstructed by selected samples for the under-sampled V-I curves of panels. So, an high approximation error could be due both to an underrate or an overrate of the current values in some part of the voltage-current curves of panels. In fact, due to the lack of samples, the slope of some linear regions of the V-I curve can be higher than that real.
So, in this case, the use of the under-sampling algorithm leads to worst results as well as to a slower solutions improvement.

The reconstruction error of V-P curves for all solutions remains below 2%, as occurs for the V-P curve for the solution S1, and, especially at the V_{mpp} voltages, the high-density of samples leads to minimize the power difference between the decimate and full-sampled non-linear region.

The trend of fitness evolution appears very abrupt, as shown in Figure 3.41, but, for this scenario, the number of generations required to achieve the best configurations is much greater than other case studies. In particular, by using the complete V-I curves of panels, the average fitness (blue line) reaches a stable value in about 100 generations. On the contrary, by using the under-sampled V-I curves of panels, the average fitness trend doesn't stabilize at all during the assumed number of generations (200) but it continuous to grow up.

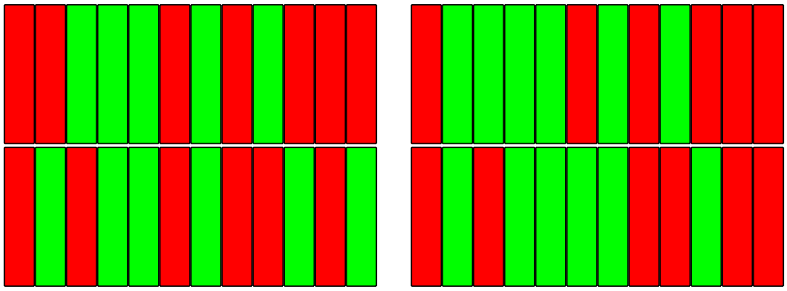

(a)

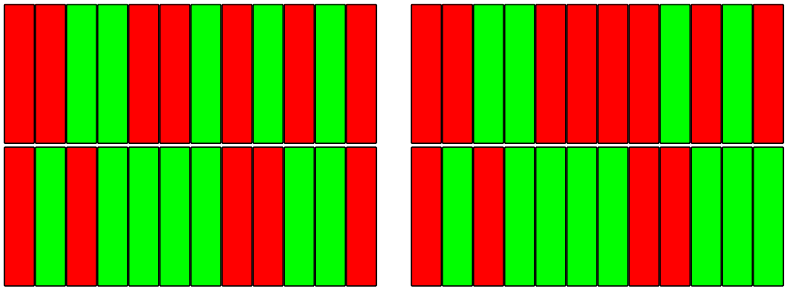

(b)

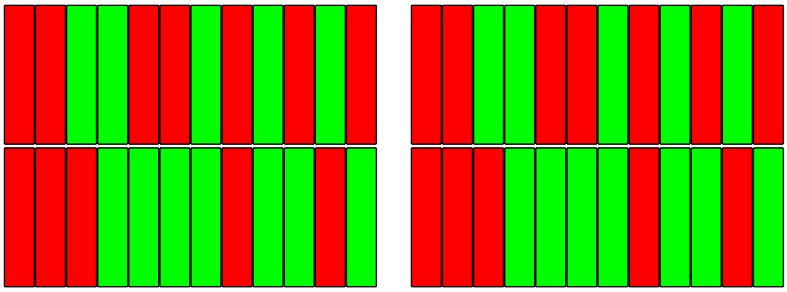

(c)

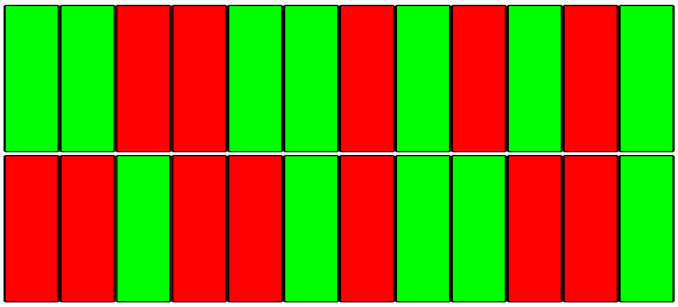

(d)

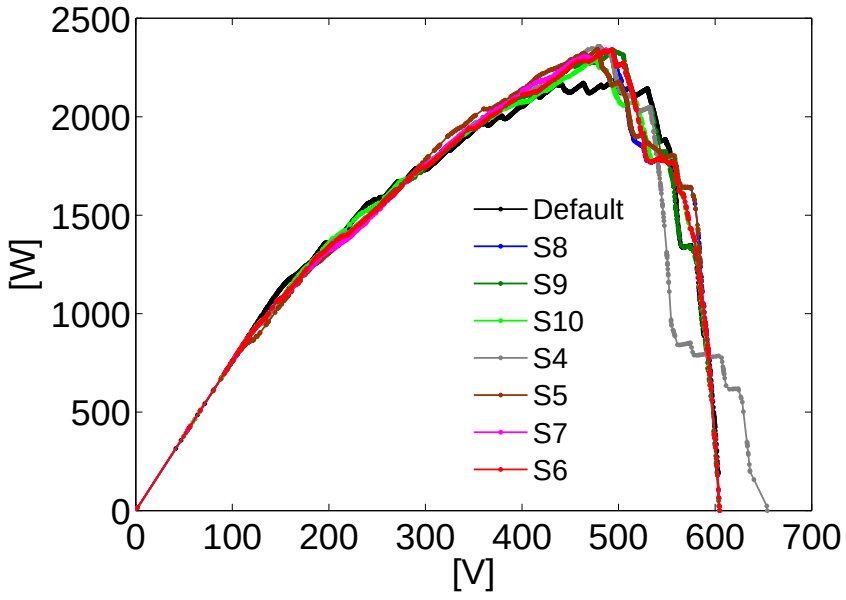

(e)

Figure 3.40: Spot shadowing. Synopsis and voltage-power curves of the solutions S4–S10 chosen by GA using decimate V-I curves of panels.

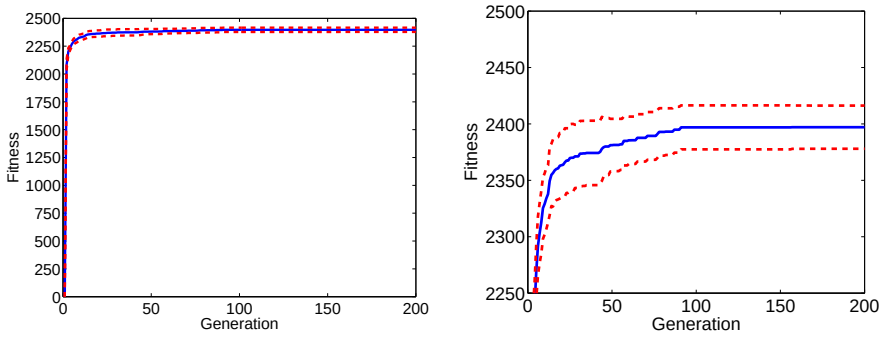

(a)

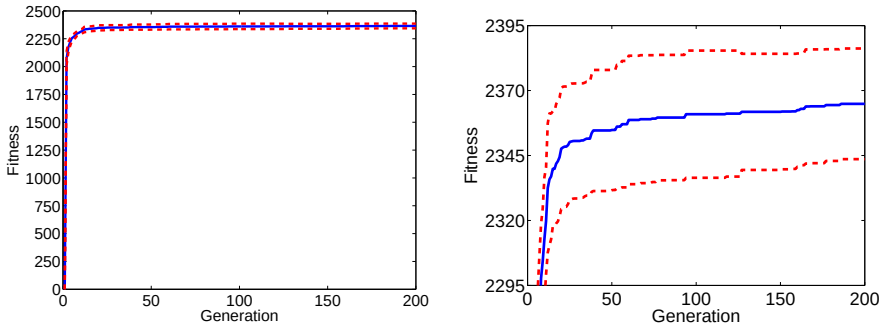

(b)

Figure 3.41: Spot Shadow. Evolution of the best fitnesses averaged over 20 runs obtained by using complete (top left pane) and undersampled V-I curves of panels (bottom left pane). Mean fitness (blue curve) +/- standard deviation (dotted red curve). Top and bottom right panes: details of the correspondent fitness evolution.

Real V-I characteristics of panels

Case 9. (see left Figure 3.8(a))

The two GAs achieve the same results but that using under-sampled V-I curves obtains one near-optimal result more, as reported in Table 3.10.

Id.	GA			GA (under-sampling)		
	$\mathbf{V}_{mpp}$[V]	$\mathbf{P}_{max}$[W]	Hits	$\mathbf{V}_{mpp}$[V]	$\mathbf{P}_{max}$[W]	Hits
S1	355.32	1066.26	3/20	355.59	1065.59	5/20
S2	374.64	1065.09	3/20	375.38	1063.32	8/20
S3	284.91	1050.14	14/20	287.07	1043.83	6/20
S4	-	-	-	286.97	1041.17	1/20

Table 3.10: Case 9. Comparison between solutions of GA using original and under-sampled V-I characteristics of panels.

The solutions S1 and S2, as well as S3 and S4, have similar fitness values since they differ only for the position of two and one panels respectively.

The under-sampled V-I characteristics of panels are illustrated in Figure 3.42. In two of these curves, the MPP at low current values haven't been detected, but, independently of that, GAs using both complete and under-sampled curves find the same group of solutions.

The optimal solution S1 is reported in Figure 3.43(a). A PV panel having the lowest short circuit current has been disconnected. Since the V-I characteristics of panels can be grouped into couples basing on their similarity, as occurs for the simulated gradual symmetrical shading scenario (case 6), then, in the optimal solution, the correspondent panels are separated into the two strings.

In Figure 3.43(b) (left), the under-sampled and the complete V-P curves of field overlap. In fact, the relative error in Figure 3.43(b) (right) is always below 10% and it is around 1% at the V_{mpp} voltage (indicated by a blue dashed line).

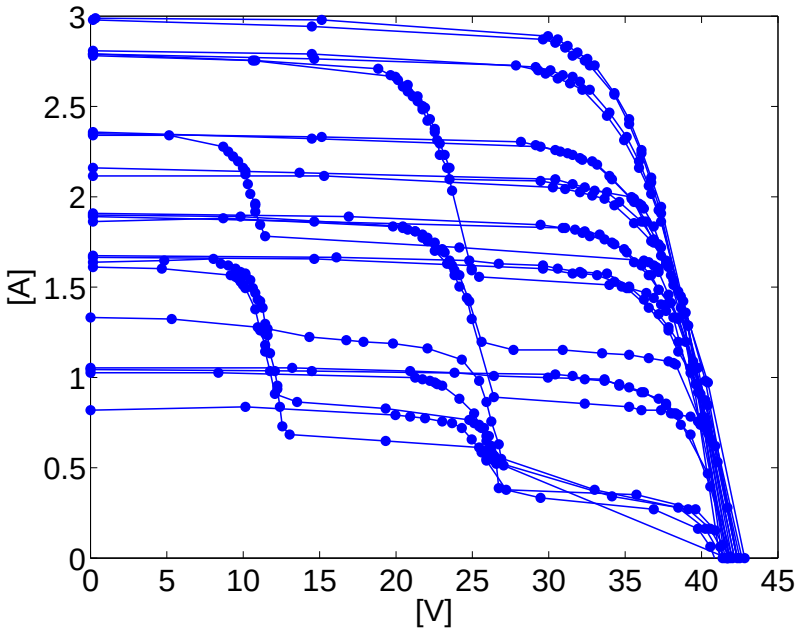

Figure 3.42: Case 9: under-sampled V-I characteristics of panels

Very high spikes in the reconstruction error curve, such as at 440V, are due to low sampling resolution of V-I curves, so they don't correspond effectively to an high error value.
The MPP value obtained by the default configuration is equal to 1051.42W at V_{mpp} 347.69V, so the solution S1 provides a +1.41% of power generation increase.

The first near-optimal solution S2 is illustrated in Figure 3.44(a). Also in this case, only the most shaded panel is disconnected. Moreover, some panels are swapped between the two strings due to their similar V-I curve. This also leads to a MPP value of the solutions S2 lower than only 0.1% of that of the optimal solution S1, so they could be considered 'equivalent'.

In the solution S3 (see Figure 3.45(a)), five panels have been disconnected and the V-P curve of the field is well different from

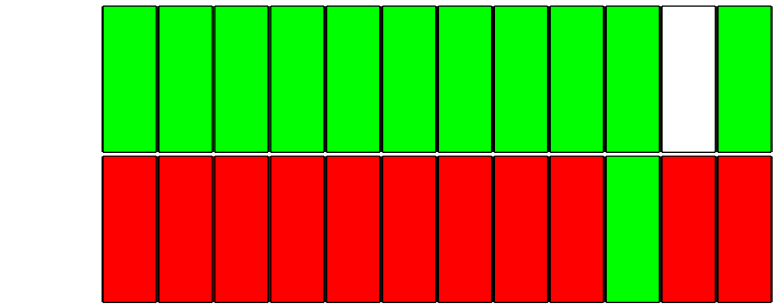

(a)

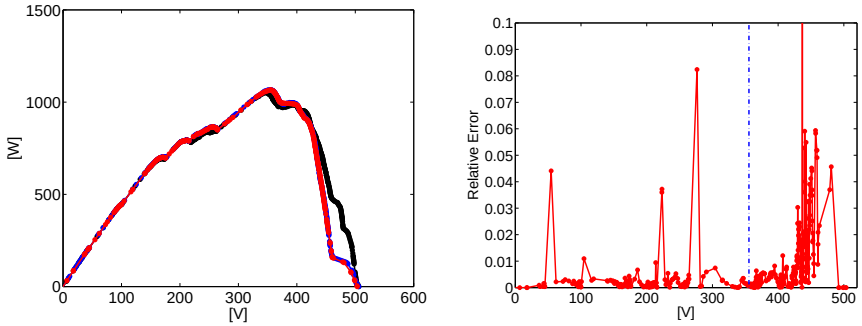

(b)

Figure 3.43: Case 9. Top pane (a): optimal electrical configuration chosen by GAs (S1 in Table 3.10). Bottom left pane (b): Voltage-Power characteristics of the PV field. Best solution obtained by the faster GA (red line), standard GA (blue line), default configuration (black line). Bottom right pane: relative error between original and under-sampled V-P curve.

that of the default solution, but they generate both the same power, even if the default configuration generate around 0.12% more, so, in this case it is preferable.

The solution S4 (see Figure 3.46(a)) is very similar to the previous one, since the same panels have been disconnected.

For V-P curves of both solutions S3 and S4, the reconstruction error (see Figures 3.45(b) and 3.46(b)) are below 5% in the voltage

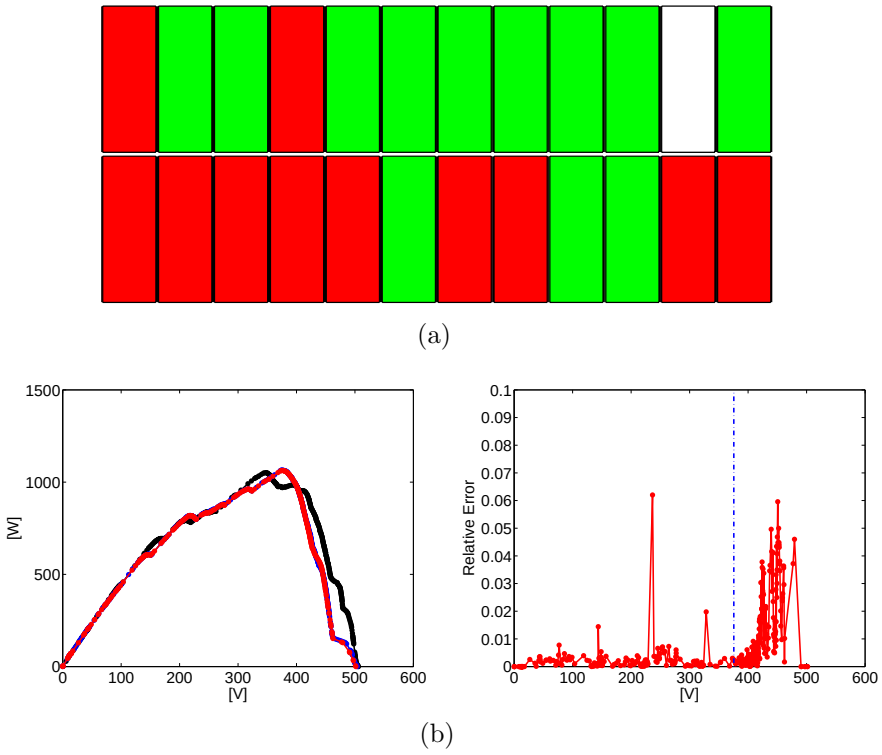

Figure 3.44: Case 9. Top pane (a): near-optimal electrical configuration chosen by GAs (S2 in Table 3.10). Bottom left pane (b): V-P characteristics of the PV field. Under-sampled (red line), complete (blue line), default configuration (black line). Bottom right pane: relative error between original and under-sampled V-P curve.

range [100V–350V].

The trend of the average values of the best fitness, illustrated in 3.47, is abrupt by using both complete and under-sampled V-I curves of panels but, in this latter case, the standard deviation doesn't collapse to zero. In both cases, the best solutions are achieved at around the 100th generation.

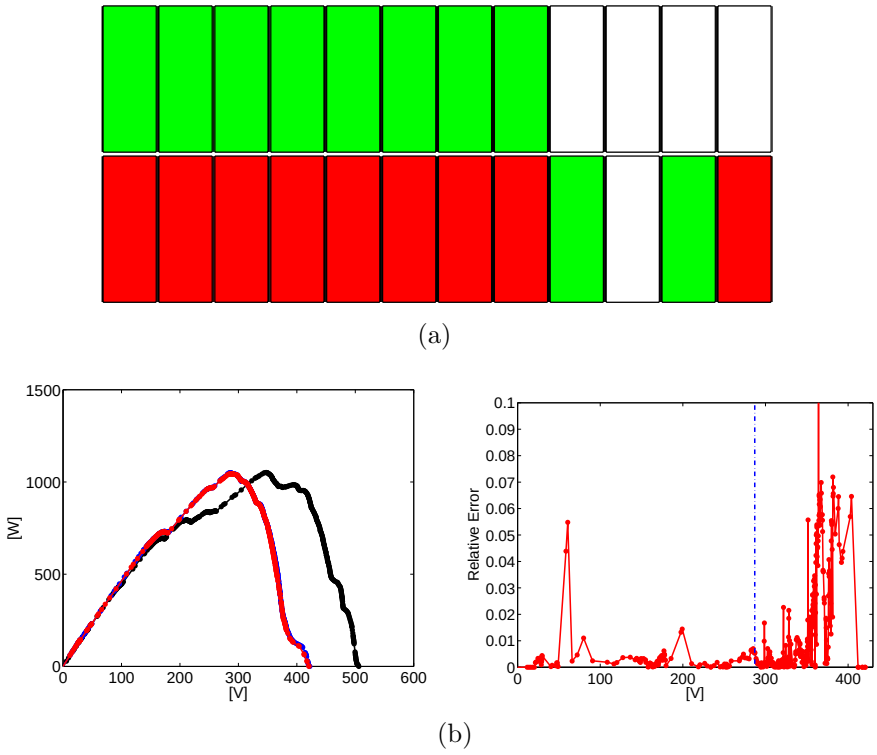

Figure 3.45: Case 9. Top pane (a): electrical configuration S3 in Table 3.10. Bottom left pane (b): V-P curve of the PV field. Undersampled (red line), complete (blue line), default configuration (black line). Bottom right pane: approximation error.

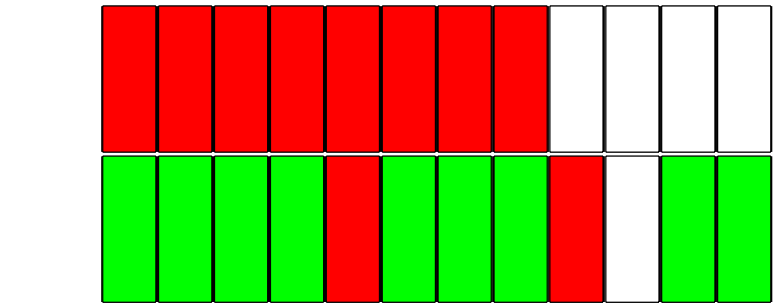

(a)

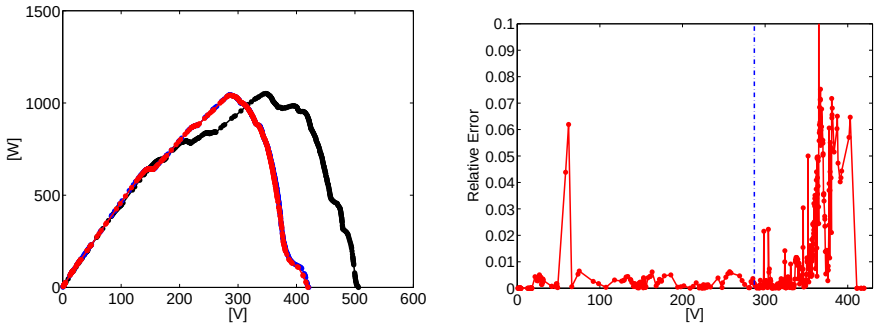

(b)

Figure 3.46: Case 9. Top pane (a): electrical configuration S4 in Table 3.10. Bottom left pane (b): V-P characteristics of the PV field. Undersampled (red line), complete curve (blue line), default configuration (black line). Bottom right pane: approximation error.

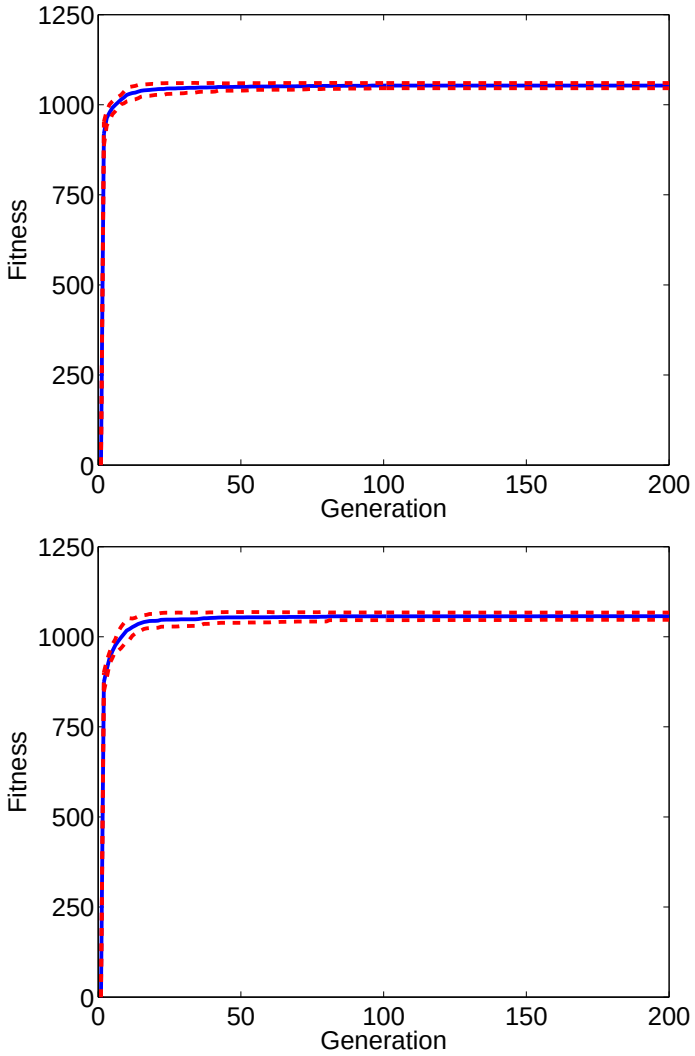

Figure 3.47: Case 9. Evolution of the best fitnesses averaged over 20 runs obtained by using complete (top pane) and under-sampled V-I curves of panels (bottom pane). Mean fitness (blue curve) +/- standard deviation (dotted red curve).

Case 10. (see right Figure 3.8(a))

Id.	**GA**			**GA (under-sampling)**		
	$\mathbf{V}_{mpp}$**[V]**	$\mathbf{P}_{max}$**[W]**	**Hits**	$\mathbf{V}_{mpp}$**[V]**	$\mathbf{P}_{max}$**[W]**	**Hits**
S1	296.16	2557.75	7/20	295	2554.81	3/20
S2	296.16	2555.98	1/20	-	-	-
S3	295.51	2550.59	1/20	-	-	-
S4	295.35	2550.02	9/20	295.36	2548.25	2/20
S5	295.03	2547.97	1/20	-	-	-
S6	295.35	2546.82	1/20	-	-	-
S7	-	-	-	295.06	2548.53	10/20
S8	-	-	-	292.14	2545.44	5/20

Table 3.11: Case 10. Comparison between solutions of GA using original and under-sampled V-I characteristics of panels.

The solutions obtained by GA have many different genotypes but their power values belong to the narrow range [2545W–2558W]. For this reason, they can be considered more or less equivalent since the maximum relative difference respect to the MPP of the best solution is around 0.5%.

In the Table 3.11, the solutions found by using the complete V-I curves of panels overlap only to a minimal subset of the solutions found by using their under-sampled version (shown in Figure 3.48). Moreover, the best solution S1 (see Figure 3.43(a)) is obtained with a frequency that is much lower than the GA using the complete V-I curves.

All these solutions provide an huge power increase respect to that provided by the default configuration. In fact, the MPP value of the default configuration is equal to 2380.2 W at V_{mpp} 315.77V. Respect to the default configuration, the solution S1 provides an increase of +7.46% of the generated power, while the solution S8, that is the less efficient, an increase of +6.94%.

Even if power is increased, the solution S1 and S2 (see right Figures 3.49(b) and 3.50) also increase the open circuit voltage

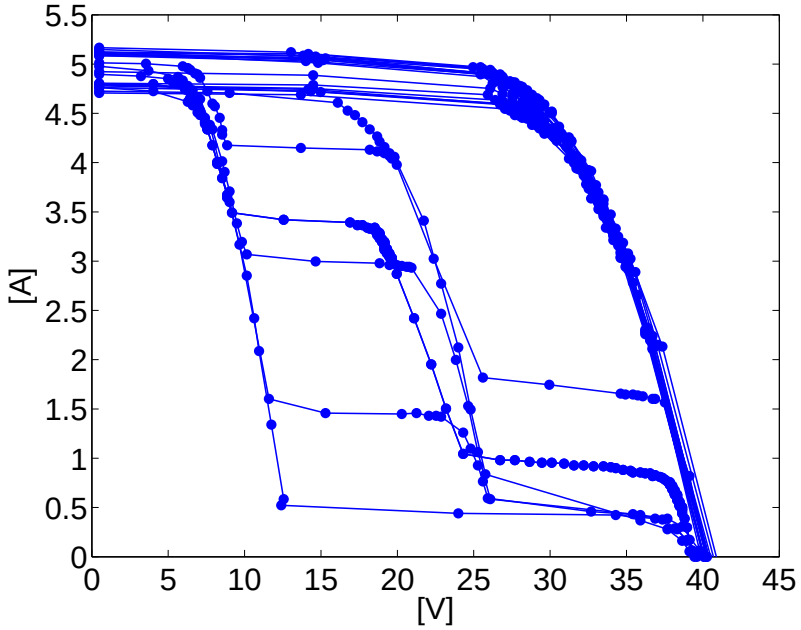

Figure 3.48: Case 10: under-sampled V-I characteristics of panels

and a lower MPP is located at 550V. This doesn't occur in all the remaining solutions (see Figures 3.3, 3.52(b), 3.3, 3.3, 3.55(b)) and 3.56(b), where the mismatching effects are reduced even if a lower power value is achieved by the unique MPP.

The trend of the best fitness values is the same by using both complete and under-sampled V-I characteristics of panels , as shown in Figure 3.3, and in this case the best solutions are achieved in a ten of generations.

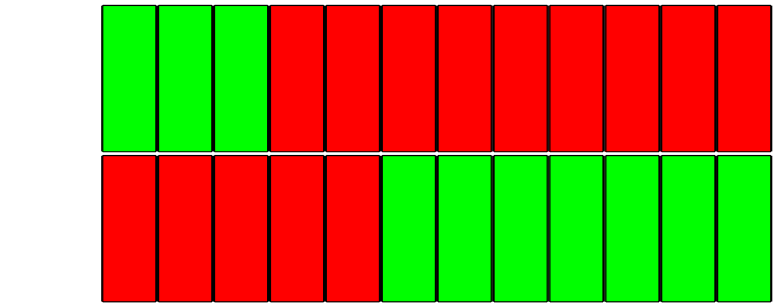

(a)

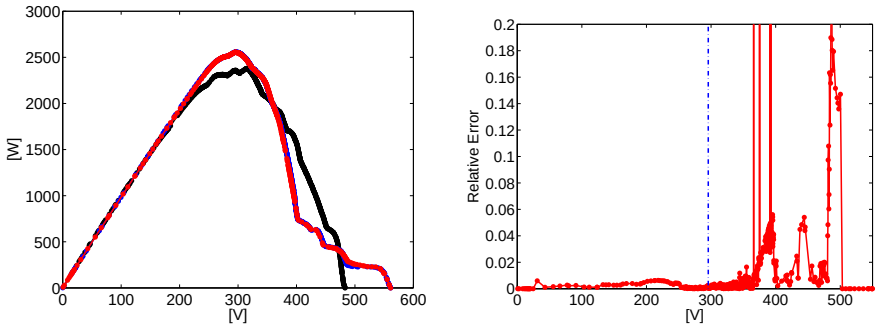

(b)

Figure 3.49: Case 10. Top pane (a): optimal electrical configuration chosen by GAs (S1 in Table 3.11). Bottom left pane (b): Voltage-Power characteristics of the PV field. Best solution obtained by the faster GA (red line), standard GA (blue line), default configuration (black line). Bottom right pane: relative error between original and under-sampled V-P curve.

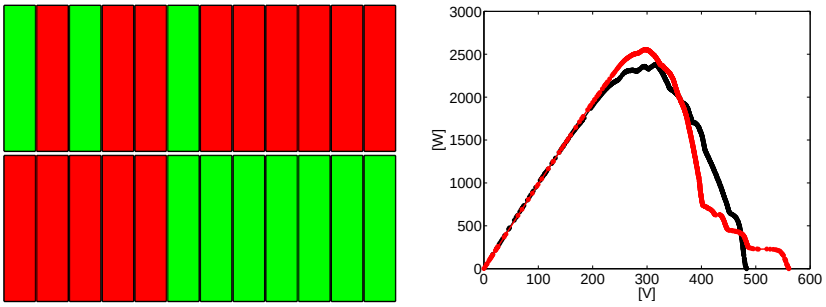

Figure 3.50: Case 10. Top pane (a): optimal electrical configuration chosen by GAs (S2 in Table 3.11). Bottom left pane (b): Voltage-Power characteristics of the PV field. Best solution obtained by the faster GA (red line), standard GA (blue line), default configuration (black line). Bottom right pane: relative error between original and under-sampled V-P curve.

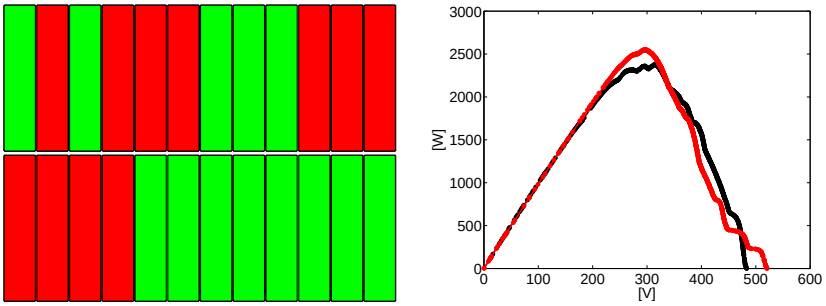

Figure 3.51: Case 10. Top pane (a): optimal electrical configuration chosen by GAs (S3 in Table 3.11). Bottom left pane (b): Voltage-Power characteristics of the PV field. Best solution obtained by the faster GA (red line), standard GA (blue line), default configuration (black line). Bottom right pane: relative error between original and under-sampled V-P curve.

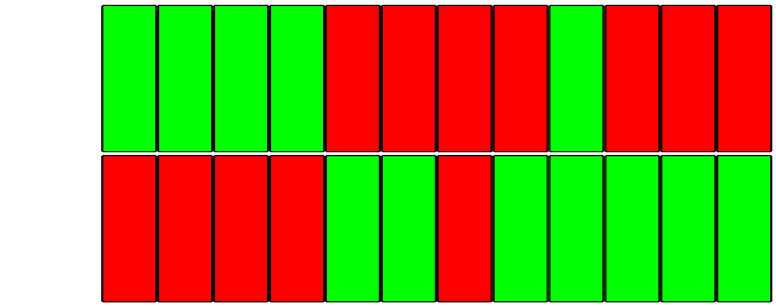

(a)

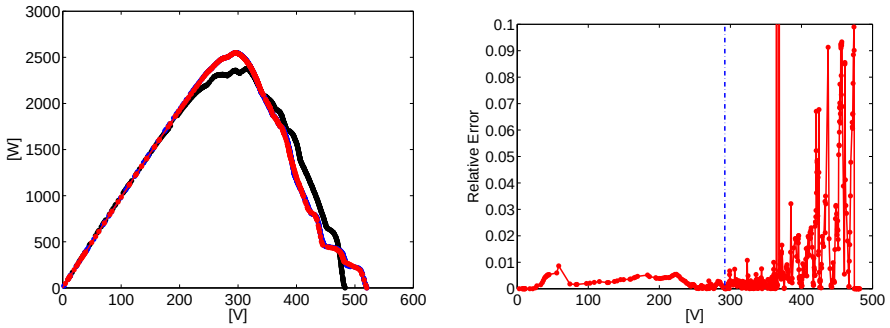

(b)

Figure 3.52: Case 10. Top pane (a): electrical configuration chosen by GA (S4 in Table 3.11). Bottom left pane (b): Voltage-Power characteristics of the PV field. Best solution obtained by the faster GA (red line), standard GA (blue line), default configuration (black line). Bottom right pane: relative error between original and under-sampled V-P curve.

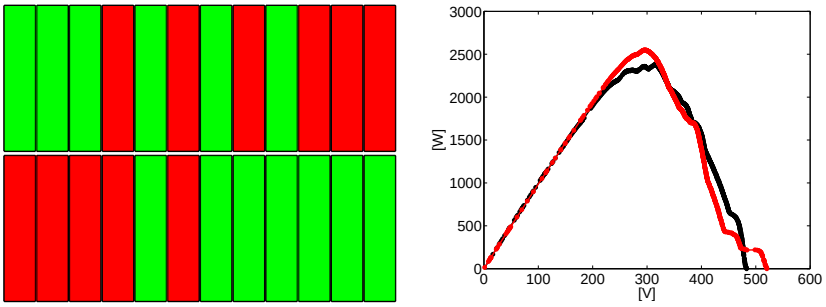

Figure 3.53: Case 10. Top pane (a): electrical configuration chosen by GA (S5 in Table 3.11). Bottom left pane (b): Voltage-Power characteristics of the PV field. Best solution obtained by the faster GA (red line), standard GA (blue line), default configuration (black line). Bottom right pane: relative error between original and under-sampled V-P curve.

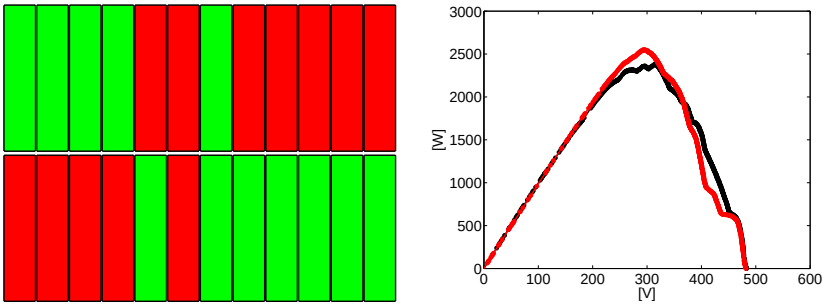

Figure 3.54: Case 10. Top pane (a): electrical configuration chosen by GA (S6 in Table 3.11). Bottom left pane (b): Voltage-Power characteristics of the PV field. Best solution obtained by the faster GA (red line), standard GA (blue line), default configuration (black line). Bottom right pane: relative error between original and under-sampled V-P curve.

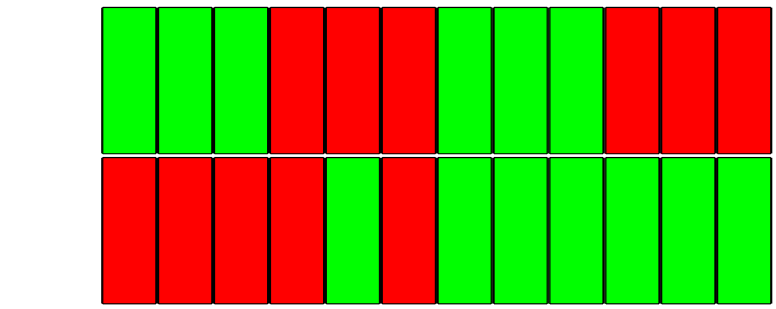

(a)

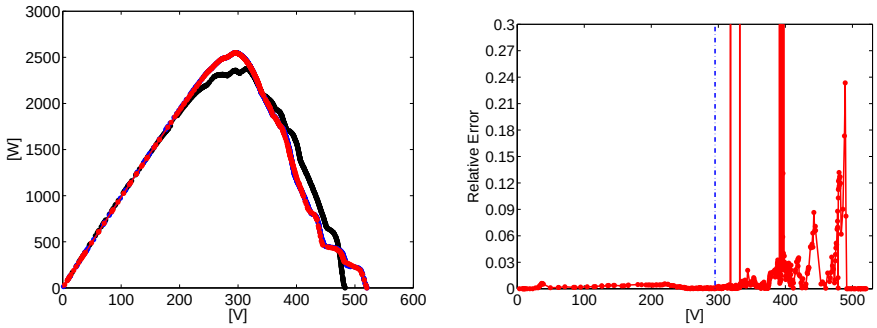

(b)

Figure 3.55: Case 10. Top pane (a): electrical configuration chosen by GA (S7 in Table 3.11). Bottom left pane (b): Voltage-Power characteristics of the PV field. Best solution obtained by the faster GA (red line), standard GA (blue line), default configuration (black line). Bottom right pane: relative error between original and under-sampled V-P curve.

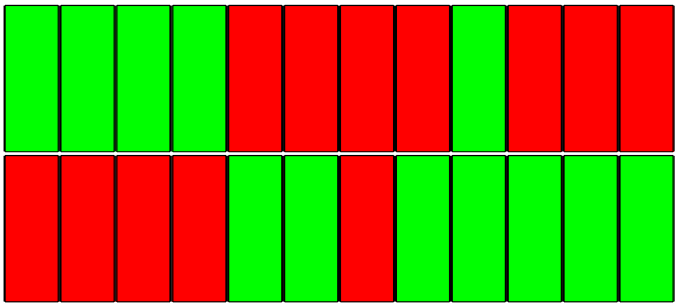

(a)

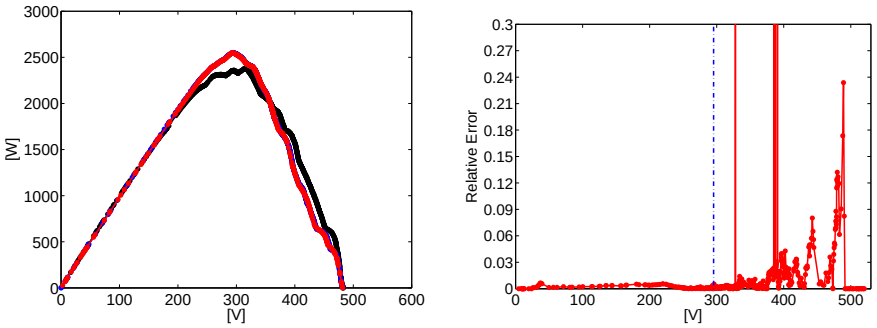

(b)

Figure 3.56: Case 10. Top pane (a): electrical configuration chosen by GA (S8 in Table 3.11). Bottom left pane (b): Voltage-Power characteristics of the PV field. Best solution obtained by the faster GA (red line), standard GA (blue line), default configuration (black line). Bottom right pane: relative error between original and under-sampled V-P curve.

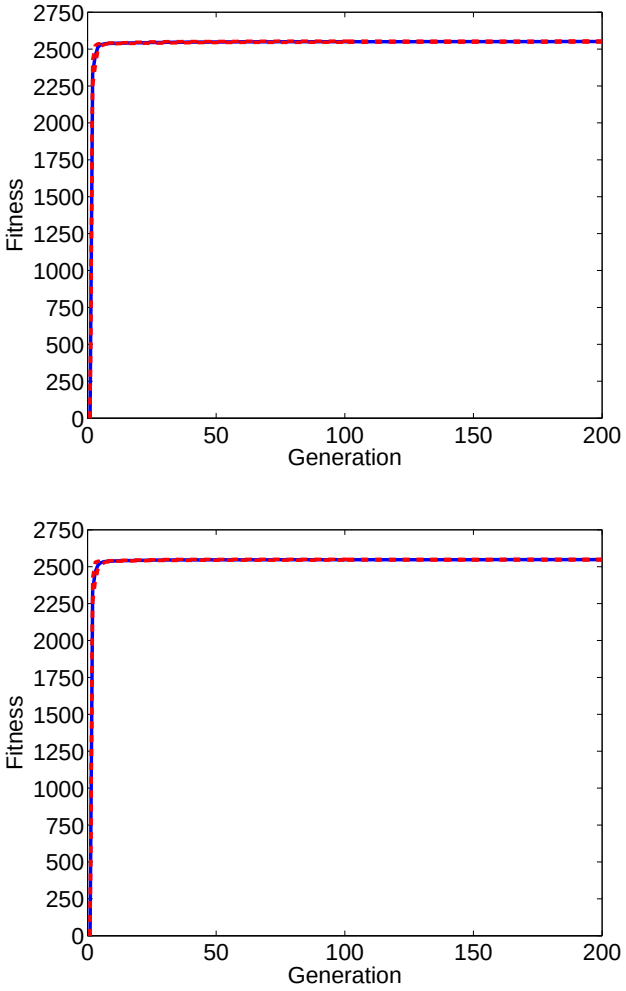

Figure 3.57: Case 10. Evolution of the best fitnesses averaged over 20 runs obtained by using complete (top pane) and under-sampled V-I curves of panels (bottom pane). Mean fitness (blue curve) +/- standard deviation (dotted red curve).

Case 11. (see left Figure 3.8(b))

Id.	GA			GA (under-sampling)		
	$\mathbf{V}_{mpp}$[V]	$\mathbf{P}_{max}$[W]	Hits	$\mathbf{V}_{mpp}$[V]	$\mathbf{P}_{max}$[W]	Hits
S1	398.63	768.56	20/20	399.4	767.8	19/20
S2	-	-	-	393.43	756.6	1/20

Table 3.12: Case 11. Comparison between solutions of GA using original and under-sampled V-I characteristics of panels.

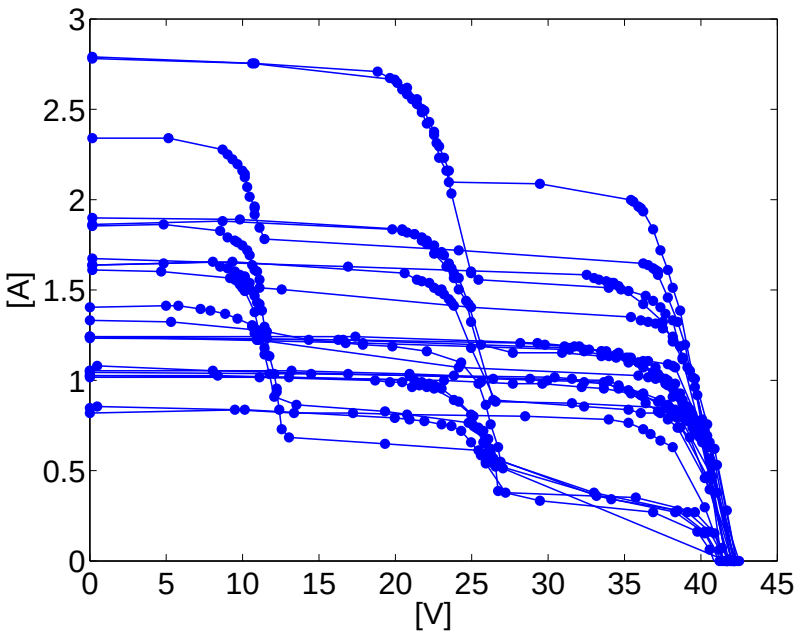

Figure 3.58: Case 11: under-sampled V-I characteristics of panels

For this scenario, the same optimal solution is obtained by using complete and under-sampled V-I curves, as reported in Table 3.12. The under-sampled V-I curves of panels are illustrated in Figure 3.58. By using these curves, a sub-optimal solution is achieved only in one of 20 runs. Also the MPP value of this solution is greater than that provided by the default configuration (675.7W at 373.38V).

In any case, both solutions reduce the number of MPP of the V-P curves of the field to only one, that is a great advantage for any MPPT algorithm.
The number of generations required to achieve these solution is around 100 generations by using the under-sampled curves, while additional 50 generations are required by using the complete V-I curves.

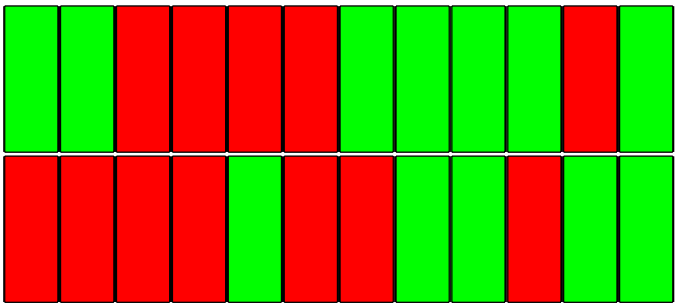

(a)

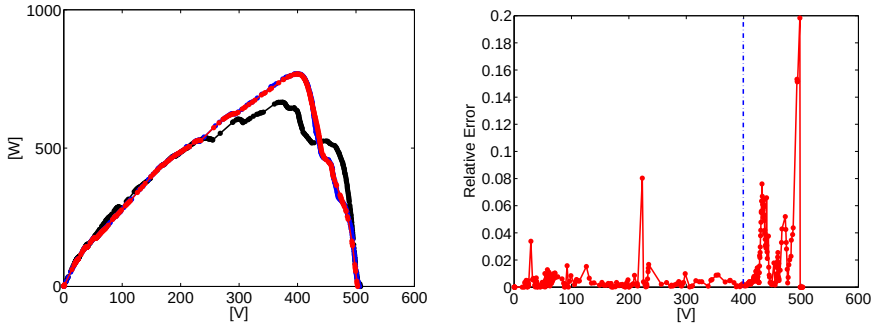

(b)

Figure 3.59: Case 11. Top pane (a): optimal electrical configuration chosen by GAs (S1 in Table 3.12). Bottom left pane (b): Voltage-Power characteristics of the PV field. Best solution obtained by the faster GA (red line), standard GA (blue line), default configuration (black line). Bottom right pane: relative error between original and under-sampled V-P curve.

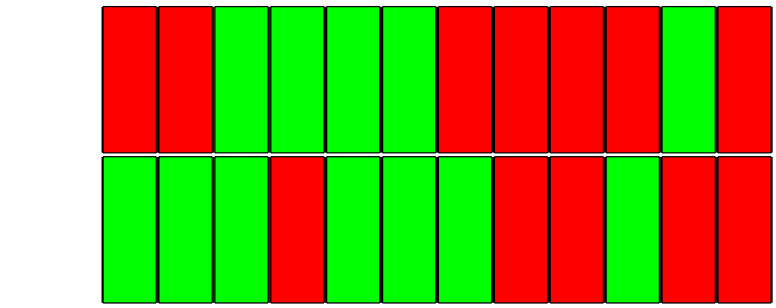

(a)

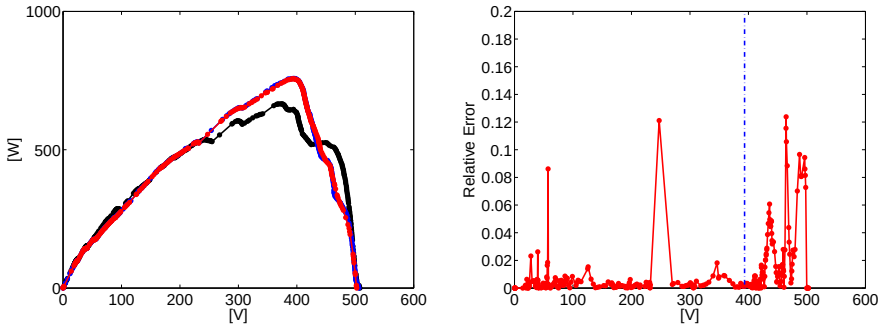

(b)

Figure 3.60: Case 11. Top pane (a): near-optimal electrical configuration chosen by faster GA (S2 in Table 3.12). Bottom left pane (b): Voltage-Power characteristics of the PV field. Best solution obtained by the faster GA (red line), standard GA (blue line), default configuration (black line). Bottom right pane: relative error between original and under-sampled V-P curve.

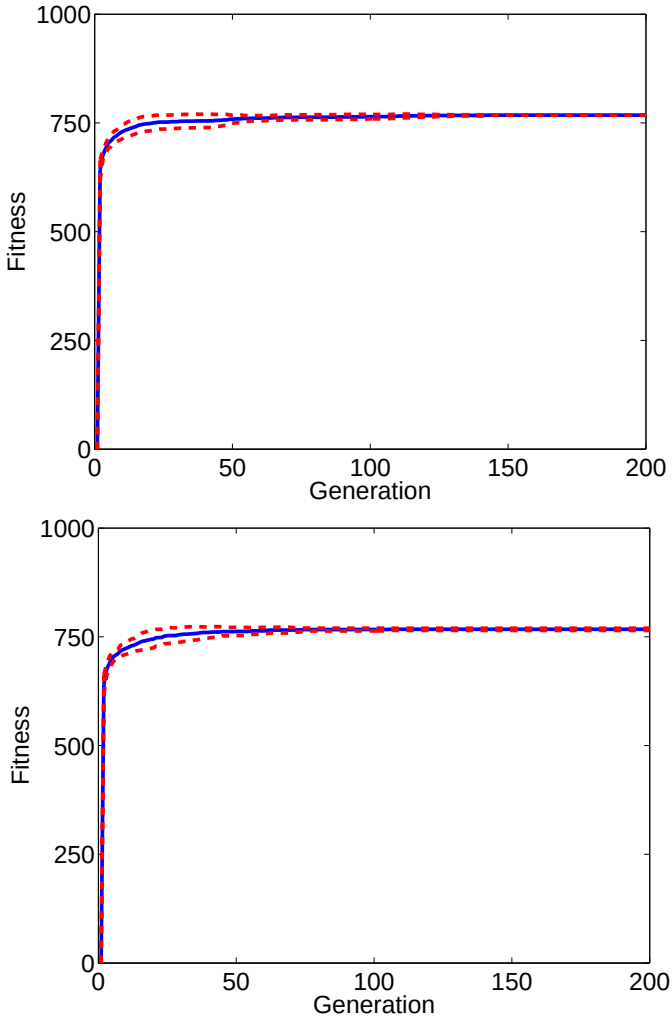

Figure 3.61: Case 11. Evolution of the best fitnesses averaged over 20 runs obtained by using complete (top pane) and under-sampled V-I curves of panels (bottom pane). Mean fitness (blue curve) +/- standard deviation (dotted red curve).

Case 12. (see right Figure 3.8(b))

Id.	GA			GA (under-sampling)		
	$\mathbf{V}_{mpp}$[V]	$\mathbf{P}_{max}$[W]	Hits	$\mathbf{V}_{mpp}$[V]	$\mathbf{P}_{max}$[W]	Hits
S1	369.98	2235.93 (*)	20/20	371.81	2228.93 (*)	20/20

Table 3.13: Case 12. Comparison between solutions of GA using original and under-sampled V-I characteristics of panels.

For this scenario, similar to the case 2, the maximum power generation is always achieved by using the default configuration (see Table 3.13), by using both the complete and decimated V-I curves.

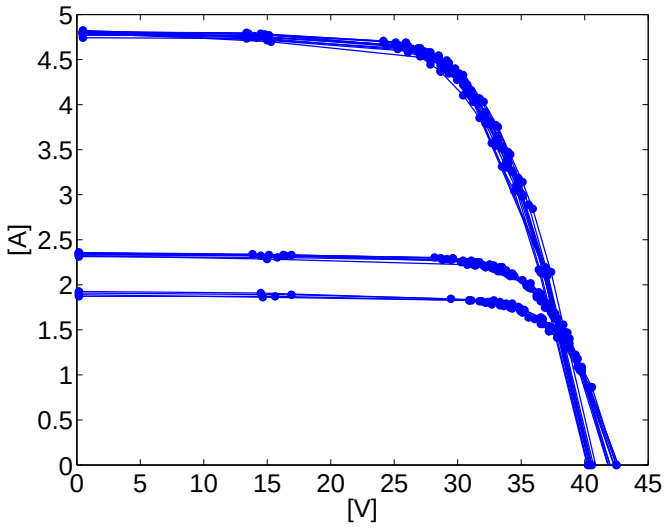

Figure 3.62: Case 12: under-sampled V-I characteristics of panels

The under-sampled curves are illustrated in Figure 3.62.
The reconstruction error is lower than 2% for all voltage range of the V-P curve of the field (see Figure 3.63(b)). The optimal performance are confirmed also by the abrupt trend of the best fitness values.

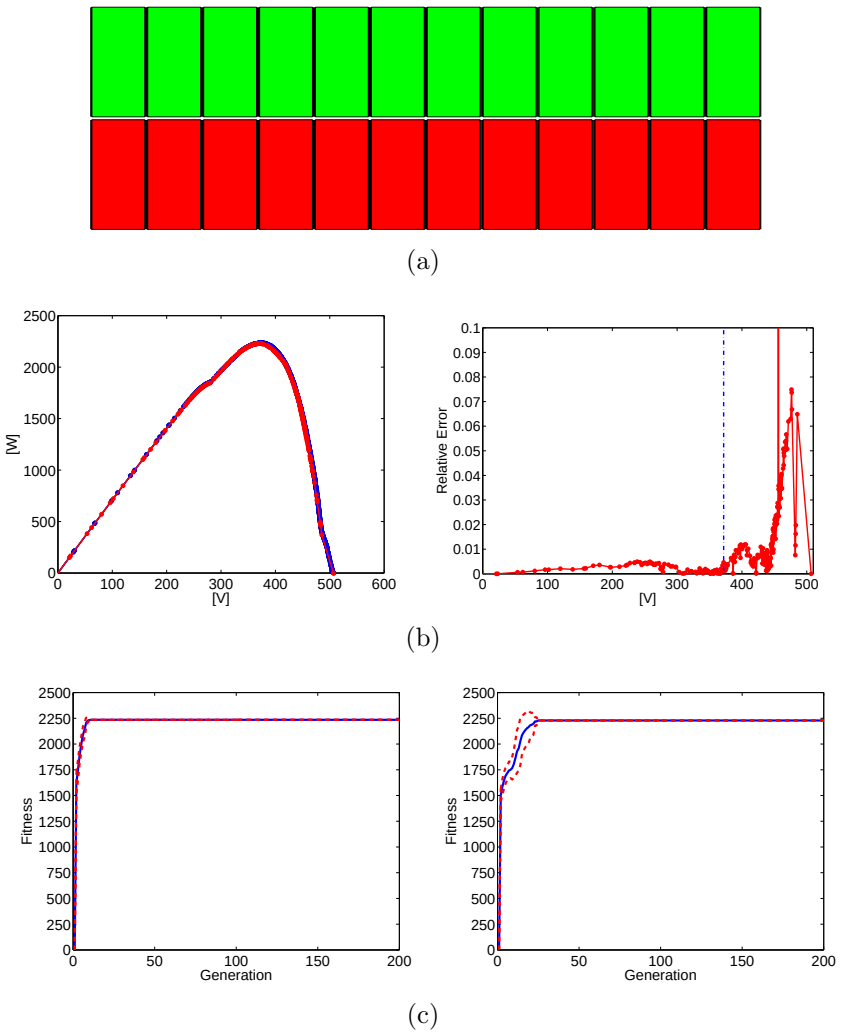

Figure 3.63: Case 12. Top pane (a): electrical configuration chosen by GAs. Middle left pane (b): Voltage-Power characteristics of the PV field. Best solution obtained by the faster GA (red line), standard GA (blue line), default configuration (black line). Middle right pane: relative error between original and under-sampled V-P curve. Bottom panes: evolution of the best fitnesses averaged over 20 runs obtained by using complete (left pane) and under-sampled V-I curves of panels (right pane). Mean fitness (blue curve) +/- standard deviation (dotted red curve).

The reduction of samples of V-I curves of panels lead to the desired effect, that is a significant reduction of the average execution time of the genetic algorithm. Nevertheless, even if the density of each V-I curve has been properly reduced, the genetic algorithm elaborates V-I curves having all the same density of samples, that are pre-calculated to speed up the calculation of V-I characteristics of each string of panels.
In the Table 3.14, for each case, the total amount of unique samples of V-I characteristics used by GA and the correspondent execution times are shown. Unfortunately, this density could be greater than the maximum density of V-I curves, since it depends of location of samples of all V-I curves. As expected, the execution time is strictly related to the number of unique samples. This value doesn't depend on the considered electrical configuration, but only on the location of samples belonging to all under-sampled V-I curves of panels.

Case	**Total n. of unique samples of V-I curves**			**GA - Average Execution Time [s]**		
	All	**Under sampled**	%	**All**	**Under sampled**	%
1	209	52	**-75%**	37.43	11.7	**-68.74%**
2	152	26	**-82%**	21.3	9.86	**-53.7%**
3	194	56	**-71.1%**	46.05	11.5	**-75.02%**
4	654	150	**-77%**	162.25	18.829	**-88.4%**
5	601	131	**-78.2%**	391.76	28.43	**-92.74%**
6	1716	256	**-85.67%**	2054.4	26.22	**-98.72%**
7	1410	261	**-81.49%**	985.135	51.261	**-94.8%**
9	321	236	**-26.48%**	253.9	58.2	**-77.07%**
10	558	295	**-47.13%**	794.27	59.28	**-92.5%**
11	293	203	**-30.7%**	190.6	54.076	**-71.63%**
12	528	195	**-63.07%**	465.9	30.891	**-93.37%**

Table 3.14: Comparison between average CPU times

The relationship between the execution time and the number of unique samples of all V-I curves is also shown in Figure 3.64.

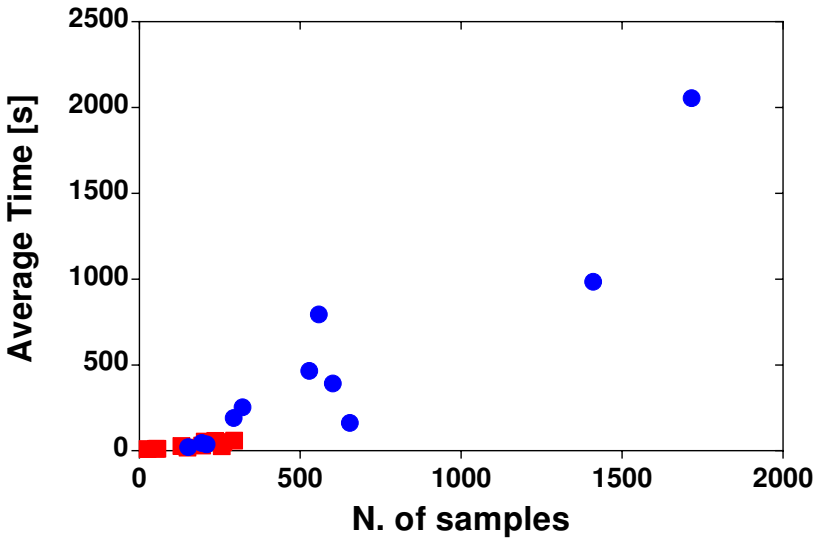

Figure 3.64: Comparison between average CPU times: high-density V-I curves (blue) and under-sampled V-I curves (red)

Furthermore, an unexpected effect has been observed: in some case, the use of decimation leads to a better result or to an higher number of occurrences of the best solution. It occurs because the fitness of all solutions change respect to the value that is obtained by using high density curves (this can be used as reference). So, under equal boundary conditions, the approximation of V-I curves changes the sorting of individuals in each population calculated by GA. The different sorting of individuals affects the results of the genetic operators and, at the end, the best solution of GA.

3.4 Statistical Analysis

A statistical analysis has been performed in order to assess if the genetic algorithm is the best one in terms of average fitness respect

to the RMHC.

	GA			RMHC		
Case	Φ_b	$\langle\Phi_b\rangle$	σ_Φ	Φ_b	$\langle\Phi_b\rangle$	σ_Φ
1	**2748.53**	**2748.53**	**0**	2734.09	2724.17	10.04
3	**2333.70**	**2333.70**	**0**	2308.71	2300.72	5.40
4	**2258.59**	**2258.59**	**0**	2253.66	2241.51	9.76
5	**3007.69**	**3007.69**	**0**	2992.53	2924.92	58.08
6	**2212.06**	**2196.41**	**31.74**	1888.21	1845.05	52.18
7	**2199.98**	**2199.98**	**0**	1781.14	1744.97	27.79
8	**2407.85**	**2397.08**	**19.16**	2241.99	2186.72	41.27

Table 3.15: Experimental findings.

A classical approach based on nonparametric statistical tests has been carried out in order to compare the GA and the RMHC performances, following [She07]. In particular, the Wilcoxon Signed Rank test is a non-parametric test used to determine whether two matched groups of data are different. The Wilcoxon Signed Rank test is robust in that it does not require the data to have a Gaussian distribution. As is common with hypothesis testing in general, it has been start out with a Null Hypothesis, which can be thought of as our default assumption. The Null Hypothesis for the Wilcoxon Signed Rank test is that the two groups of data belong to the same population. Based on the W statistic, which is calculated from the data, it is determined whether to accept or reject the Null Hypothesis.
In presence of a large enough number of samples (over 25), it is possible to use the calculated p-value to either accept or reject the Null Hypothesis. For a smaller sample size, it is read off the critical value of W from a table, and if the calculated W statistic is below the critical W value the Null Hypothesis is rejected. The p-value is the probability of obtaining either the observed difference or a more extreme value of the difference between the two groups, purely based on chance. If the p-value is below a threshold value,

the Null Hypothesis is rejected and the result is considered significant.
On the other hand, if the p-value is greater than the threshold value, the Null Hypothesis is accepted.

The statistic for Wilconxon p-value is 28.0 with 1 and 5 degrees of freedom. The p-value for Wilconxon is 0.015625. The W–value is 0, while the critical value of W for 7 at $p \leq 0.05$ is 2. Therefore, the result is significant at $p \leq 0.05$, i.e., the Null Hypothesis is rejected. In other words, the statistical analysis confirms that the proposed GA outperforms the RMHC.

Chapter 4

Adaptive Reconfiguration

In this Chapter, two different techniques to achieve an optimized execution planning of the reconfiguration algorithm are illustrated.

Despite the execution time of the reconfiguration algorithm has been reduced to tens of seconds, there is always an amount of the generated energy that is lost. In fact, at each execution of the reconfiguration process, all the PV panels must be disconnected, basing on an adopted strategy, in order to acquire each V-I curve of panels.
An estimation of the energy loss during this time period is very hard to be given. In fact, they depend on the sequence adopted for disconnecting the panels from the strings in order to measure their V-I curves, to the frequency of the reconfiguration process and to the time needed for setting up the new calculated configuration.
During the data acquisition procedure, all panels can be disconnected at the same time, but it is very unpractical because of the problems it should give to the inverter behavior. In fact, in this case, the risk is that the inverter turns off because of the null power sensed at its input for a long time interval.
So, a reasonable procedure would consider the disconnection of one panel at a time, in sequence, thus letting the remaining ones producing their own power, although they are not connected in the best electrical configuration.

Moreover, after every reconfiguration, the inverter MPPT needs time to reach the new MPP. For this reason, during start period, the generated power is always lower than maximum value.
So, a number of reconfigurations as low as possible would be preferable.

In the first section of this Chapter, the advantages of reconfiguring the PV field at a fixed frequency respect to using a fixed configuration are illustrated. Then, in order to detect partial shading phenomena, an *adaptive* reconfiguration system is introduced. In general, an adaptive reconfiguration system is able to detect a shading phenomenon occurring over the PV generator by processing some related feedback signals.
The proposed algorithm triggers the reconfiguration only if proper decision rules are verified. These rules have been deducted by inspecting system performances during shading phenomena.

This rules-based procedure cannot minimize the number of reconfigurations, since it cannot predict the shadow movement over a PV field.
For this reason, in the second part of this Chapter, a further procedure to improve the adaptivity of PV system reconfiguration is illustrated. This procedure, by processing informations provided by the under-sampling technique, can predict the motion path of shadows covering the PV field and so, by using this information, the time required by the shadow to leave the PV generator or move along a fixed distance.

Both techniques improve the adaptivity of the reconfiguration system. In fact, by using the rules-based procedure, it is possible to quickly detect partial shading phenomena occurring over the PV field and trigger the reconfiguration process. A minimum of two executions of reconfiguration process are required to predict the motion path of the shadow. So, the usage of the actuated configuration is maximized by predicting the time instant when a new reconfiguration should be executed or, due to the disappearing of

the shadow from the PV field, when the default configuration of the PV field should be actuated.

The prediction of shaded modules in a PV field helps to reduce the number of analyzed configurations during a reconfiguration process and so reduce its execution time too.

4.1 Synchronous Reconfiguration

In a PV system, the reconfiguration process can be executed at a constant frequency in order to optimize the system performances during the day.

The choice of the reconfiguration frequency plays a key role, since it affects the performances of the procedure but also the life-time of the system itself.

In fact, a low frequency value misaligns the reconfiguration with the fast moving shadows, but a too high frequency value requires continuous disconnections of the panels from the PV field for the analysis of their operating conditions, thus reducing the power production.
At same time, a too high frequency value negatively affects the life-time of switching devices actuating the desired configuration among panels. The robustness of these devices respect to the continuous stresses depends on their technology.
In fact, the switching matrix must be able to interrupt up to ten amperes and to ensure an high reliability of the hardware performing the reconfiguration of the modules connections. Nevertheless, the hardware lifetime can be improved by using suitable techniques employing electromechanical as well as semiconductor switching [BVF+11].

The reconfiguration process is executed at constant time intervals without taking into account if panels shadowing is occurring

or not. In general, the reconfiguration process could increase the generated power only if mismatching effects occur, otherwise it is inefficient.

In this Chapter, a PV field having a series-parallel topology and composed by 24 panels divided into two panels rows is considered (see Figure 4.1).

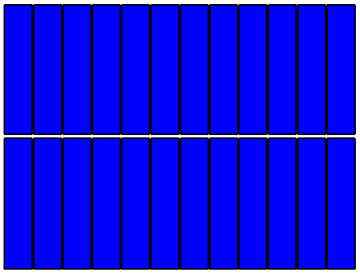

Figure 4.1: PV field - Series-parallel topology

For this PV field, the reconfiguration process illustrated in Chapter 3 is executed every 30 minutes during the day. The allowed V_{mpp} voltage for the inverter is assumed equal to [200V – 700V].
Moreover, a central inverter topology and a Perturbe&Observe (P&O) MPPT algorithm have been considered.
Basing on the photovoltaic optimizer Endana [Web14], it is assumed that the time required to acquire each curve of panels is equal to 60 milliseconds and that the reconfiguration process takes 30 seconds each time it is executed. The given execution time is an average value, since the execution time of the genetic algorithm illustrated in Chapter 3 depends on the shading scenario itself. The execution time of the reconfiguration process also include that required to actuate the new configuration itself.
Even if the panels couldn't all be disconnected from inverter in order to maintain it turned on, the maximum reconfiguration energy cost has been considered in order to be independent of any chosen data acquisition strategy.

So, when the reconfiguration process is executed at a generic time instant j the energy losses are equal to:

$$E_{loss} = P_{max}(j) \cdot (T_{reconf} + N_p \cdot T_{sampling}) \tag{4.1}$$

where P_{max} is the extracted power at the reconfiguration instant j, N_p is the number of panels, T_{reconf} and $T_{sampling}$ are respectively the reconfiguration and the sampling time.

So, if the synchronous reconfiguration procedure is executed during a full sunny day, then a reduction of the generated energy is always expected respect to the case no reconfiguration occurs.

In Figure 4.2, the trend of electrical power, inverter voltage and the string currents during a full sunny day are illustrated.

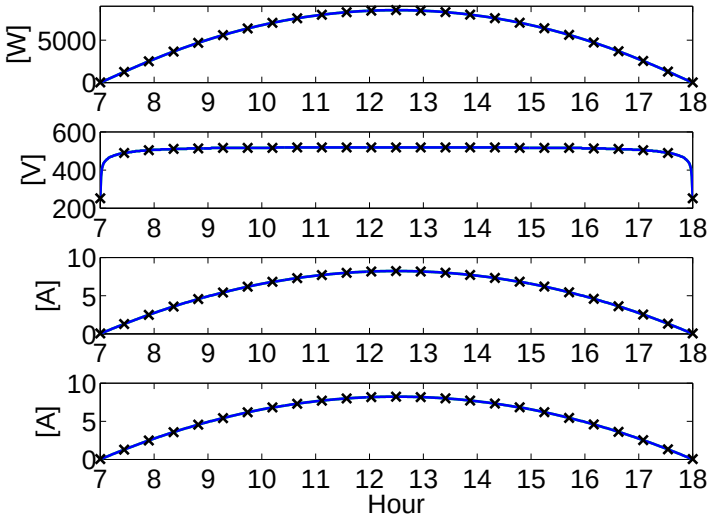

Figure 4.2: Trend of the generated power P_{max}, voltage V_{mpp} and string currents I_1 and I_2 during a full sunny day. No reconfiguration (green line), synchronous reconfiguration (blue line), reconfiguration instants (black crosses)

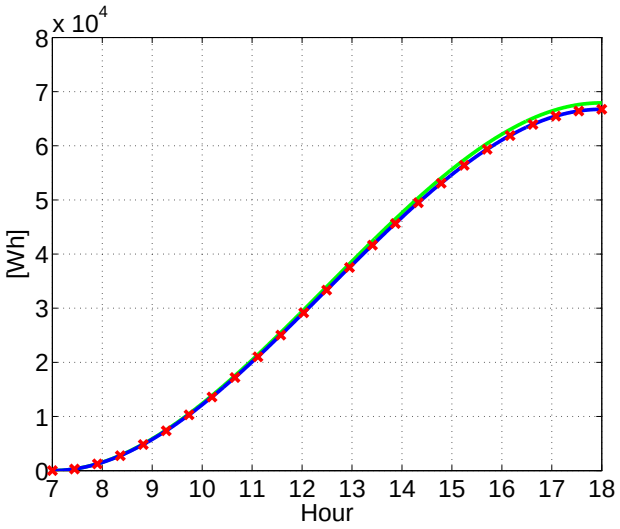

Figure 4.3: Generated energy trend. No reconfiguration (green line), synchronous reconfiguration (blue line), reconfiguration instants (red crosses)

The analysis of the energy curve for the synchronous reconfiguration (blue colored line in Figure 4.3), calculated from 7 AM to 18 PM, shows that a reduction of about 200Wh occurs respect to the case no reconfiguration at all is executed (green colored line).

In order to evaluate the performance of the periodical reconfiguration, in addition to the previously illustrated scenario, other five simulated shading scenarios are considered.
In the first scenario, a sharp shadow is covering symmetrically both panels rows by moving along the longitudinal axis of the PV field (see Figure 4.4).

In the second case, a sharp shadow is moving along the vertical direction by covering first all modules of the bottom row and then it covers the upper row of panels. At the end, the shadow leaves the PV generator (see Figure 4.5).

In the third scenario, a pole shadow is rotating over the PV field (see Figure 4.6). This kind of shadow is the most interesting

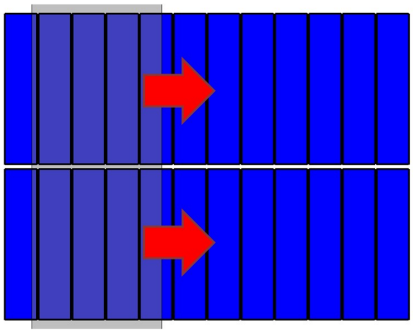

Figure 4.4: Sharp shadow moving longitudinally over the PV field

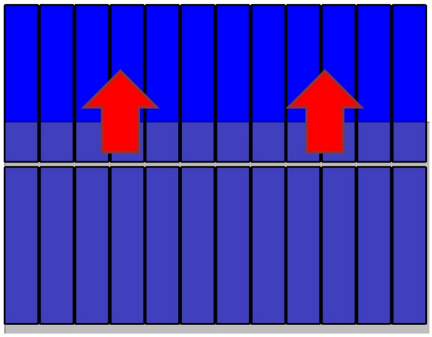

Figure 4.5: Sharp shadow moving over one row at a time

since it assumes all possible angular orientations over the PV field, covering both two panels rows at the beginning of the day and by covering only one panels row during the remaining hours of the day.

In the fourth and fifth scenarios two asymmetrical sharp shadows are considered, i.e. shadows covering only one panels row. In the former scenario, the shadow of a chimney is simulated (see Figure 4.7). This shadow appears only at the sunrise and at the sunset and it disappears during the central hours of the day.
Instead, in the latter scenario, a sharp shadows move longitudinally over a panel string covering one module at time (see Figure 4.8).

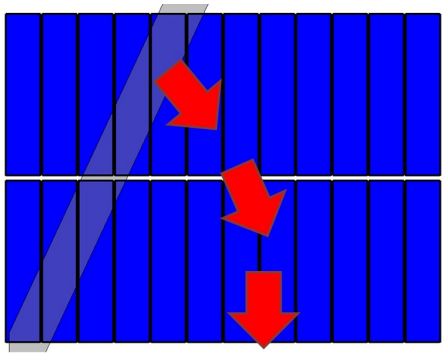

Figure 4.6: Pole shadow rotating over the PV field

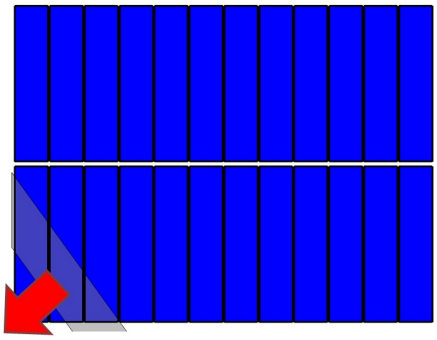

Figure 4.7: Shadow of a chimney

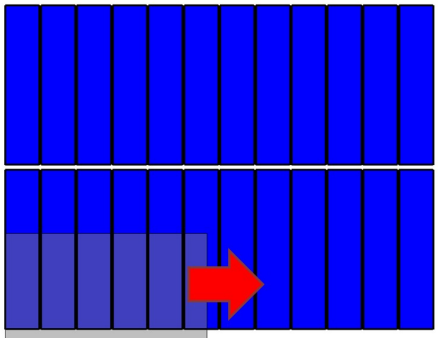

Figure 4.8: Sharp asymmetrical shadow (building)

For each case, the temporal analysis of voltage V_{mpp}, of the string currents I_1 and I_2 and of the generated power P are illustrated for two different values of the shadow strength. In particular, the shaded PV cells receive a solar radiance value that is 25% or 75% lower than unshaded cells.
The shadow strength value affects not only the generated daily energy but mainly the choice made by the reconfiguration algorithm.

The daily energy generated without reconfiguring and by executing the synchronous reconfiguration (25 reconfigurations from 7AM to 18PM) are compared in the Table 4.1.

	Energy [kWh]		**%**	
	No reconfiguration		**Synchronous**	
	Shadow strength			
Case name	**25%**	**75%**	**25%**	**75%**
No shadow	67.920		-1.74	
Horizontal moving	57.215	50.477	0.99	-3.29
Vertical moving	63.287	52.493	-1.73	-2.01
Pole	60.828	56.170	2.13	-2.38
Chimney	66.255	64.681	-1.73	-0.61
Building	63.155	49.834	-1.74	13.86

Table 4.1: Energy gain achieved by synchronous reconfiguration

In this Table, only in two scenarios the synchronous reconfiguration ensures a positive energy gain, and this occurs mainly because the execution of the reconfiguration process is executed also when no shading phenomenon is occurring.

Sharp symmetrical shadows

In the first shading scenario, both panels rows are symmetrical shaded so that, by using the default configuration, the same ef-

fects occur on both the string currents.
The arrival of the shadow reduces the generated power since the maximum power point (MPP) reduces its voltage or current value. For the lowest value of the shadow strength (25%), only in the initial phases of the shading phenomenon, the power generated by the default configuration is reduced. After this initial step, the MPP increases its voltage value and reduces both string currents by about 25%, by stabilizing its position at the highest voltage on the voltage-power curve of the field. In this position, the MPP is less sensitive to shadow effects because the shading percentage remains fixed due to the finite shadow width (4 meters) as well as the electrical connections among panels.

Instead, for the same reason, by using synchronous reconfiguration, the V_{mpp} voltage has some oscillations when new PV modules become shaded. In fact, even if the percentage of the shaded portion of the PV field is maintained fixed, the chosen configurations make the MPP to be more susceptible respect to the shadow movement over the PV field.
Moreover, the evident oscillations of the V_{mpp} voltage in the time interval [1 P.M. – 3 P.M.] are also due to the misalignment between the chosen reconfiguration frequency and the transit speed of the shadow. In this case, a greater frequency is required, but this sure increases the energy losses due to the reconfiguration itself.
So, it is evident how the actuated configuration influences the performances of the synchronous reconfiguration process since it affects the trend of electrical parameters.
The reconfiguration procedure never disconnects the shaded panels and it is able to increase the generated power respect to the case no reconfiguration at all is considered.

Instead, a greater shadow strength value (75%), the generated power trend is clearly different from previous ones since the MPP voltage reduces by an amount that depends on the number of the shaded modules, that are disconnected, in each string but the currents maintain an high value. In fact, the MPP is more sensi-

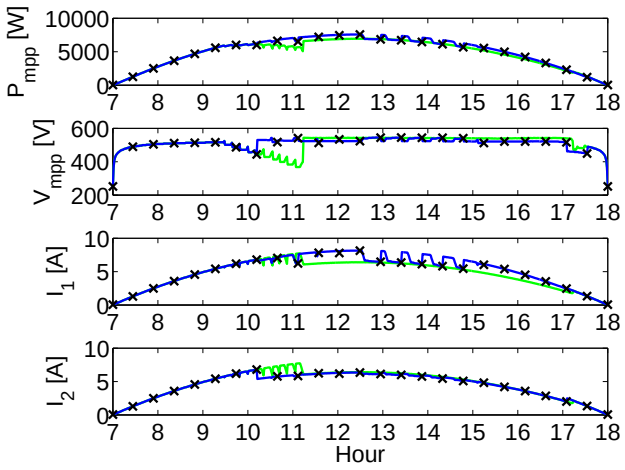

(a)

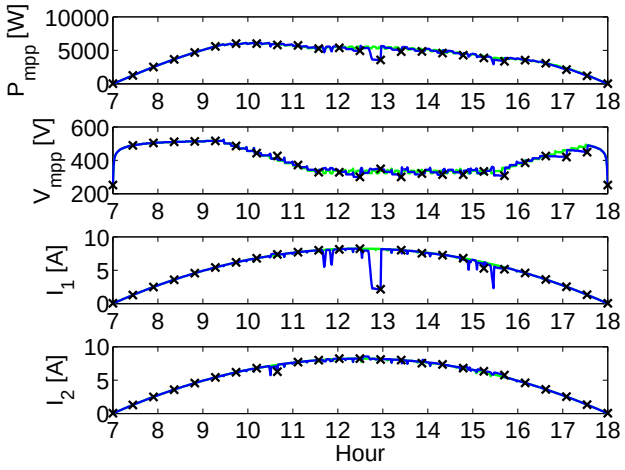

(b)

Figure 4.9: Sharp shadow moving longitudinally over the PV field. Trend of generated power, voltage V_{mpp} and string currents I_1 and I_2. Shadow strength = 25% (a) and 75% (b)

tive to the passage of the shadow since only unshaded panels are connected to the PV field and so, when they are covered by the shadow, the point of work change quickly its position.

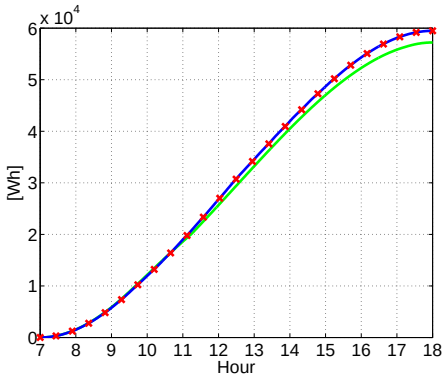

(a)

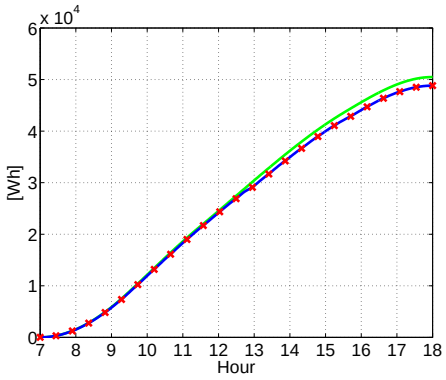

(b)

Figure 4.10: Sharp shadow moving longitudinally over the PV field . Daily Energy generated by no reconfiguring (green colored line) and by synchronously reconfiguring the PV field every 30 minutes (blue colored line). The reconfiguration instants are indicated by red crosses markers. Shadow strength = 25% (a) and 75% (b)

Moreover, in this case, the susceptibility of the MPP respect to the electrical configuration chosen by GA is evident at instant 1 P.M. when a strong current reduction of only one string occurs. In fact, previously the reconfiguration process has chosen a new configuration where the panels that are located at the border of the shadow are both series-connected to the first string. So, when

the shadow moves over them, a strong reduction of the current of the first string occurs, while the V_{mpp} voltage remains fixed by the other string that is generating an higher current value.

So, in this scenario, the reconfiguration process increases effectively the generated energy only when the shadow strength assumes a low value (see Figure 4.10). If not, in order to improve the performance, it is necessary to better align the frequency reconfiguration to the shadow speed on both panels rows.
By this way, the energy reduction reported in Table 4.1 is avoided.

Sharp shadow covering equally all modules of a string

In this scenario, no reconfiguration at all is needed. In fact, if all modules of a string are equally shaded, then their current is equally reduced but the whole PV field behaves as it is composed by two parallel-connected strings having a different electrical performance.
These considerations are independently of the shadow strength value.
In fact, as illustrated in Figure 4.11, the reconfiguration process can only worsen the performance of the PV system. In this case, not only the energy losses due to the reconfiguration procedure are not reducibly, but the choice of the reconfiguration procedure itself and the misalignment respect to the shadow movement affect the generated power.

For this reason, the daily energy trend of default configuration is always expected to be better in this scenario (see Figure 4.12).

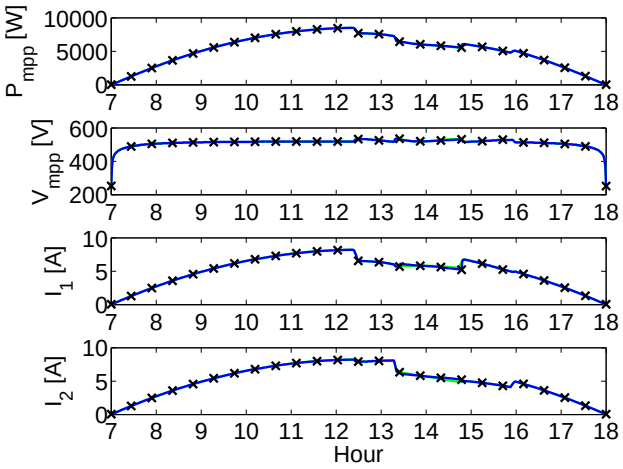

(a)

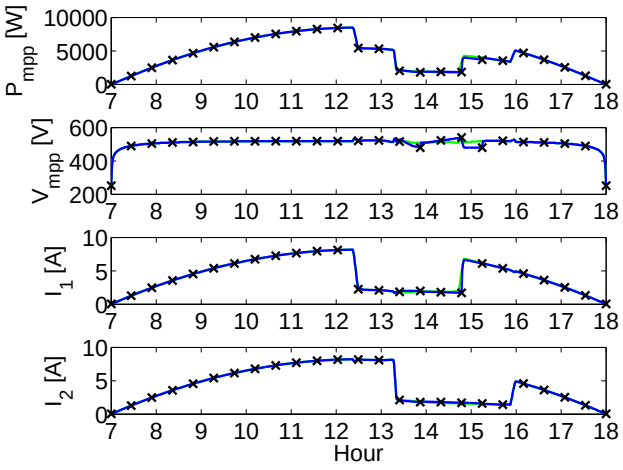

(b)

Figure 4.11: Sharp shadow moving over the PV field on row at a time. Trend of generated power, voltage V_{mpp} and string currents I_1 and I_2. Shadow strength = 25% (a) and 75% (b)

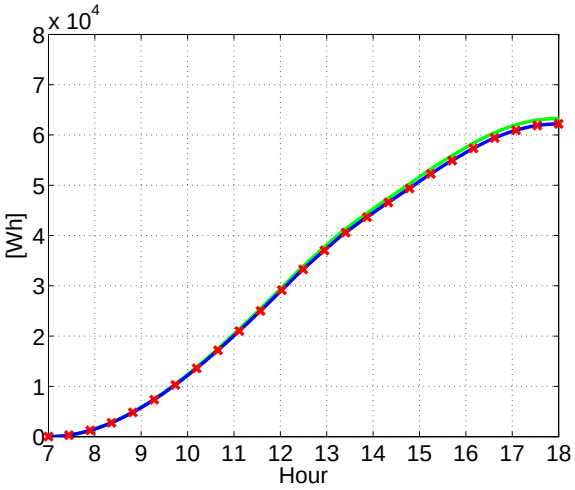

(a)

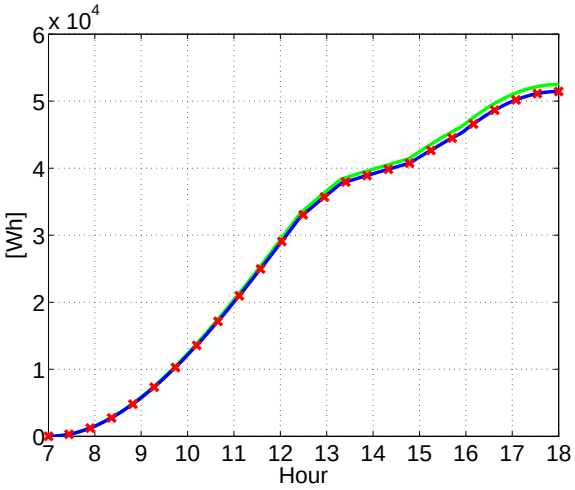

(b)

Figure 4.12: Sharp shadow moving over the PV field on row at a time. Daily Energy generated by no reconfiguring (green colored line) and by synchronously reconfiguring the PV field every 30 minutes (blue colored line). The reconfiguration instants are indicated by red crosses markers. Shadow strength = 25% (a) and 75% (b)

Pole shadow rotating over the PV field

The pole shading scenario is one of the most interesting because the shadow assumes different angular positions during the day.
This shadows covers for a long time interval both panels rows (from 10:30 AM to about 2 PM) and, until it leaves the PV field at 3PM, only the first panels row.

In this case, the synchronous reconfiguration increases the generated power but the performance are worst when a great shadow strength value is considered.
In fact, when the shadow strength value is equal to 75%, the performance of the procedure are worst in the time interval [2 PM – 3PM] when the shadow is leaving the PV field (see Figure 4.13).
Also in this case, the misalignment between the execution of the reconfiguration process and the transient speed of the shadow reduces the amount of the power could be generated.
Nevertheless, it should be stressed that the reconfiguration of the PV field at about 2 PM allows to the V_{mpp} voltage to not further reduce under the minimal constraint of inverter (200V) avoiding the turning off of the inverter.
In this case, the reduction of the V_{mpp} voltage under the minimum value occurs just before the shadow leaves the PV field and it is covering the great percentage of a single row of panels.

The misalignment between the shadow and the reconfiguration frequency, especially during the final phases of the shadowing phenomenon, leads to have a daily energy trend always lower than using the standard configuration of the PV field (see Figure 4.14), but to avoid the turning off of inverter.

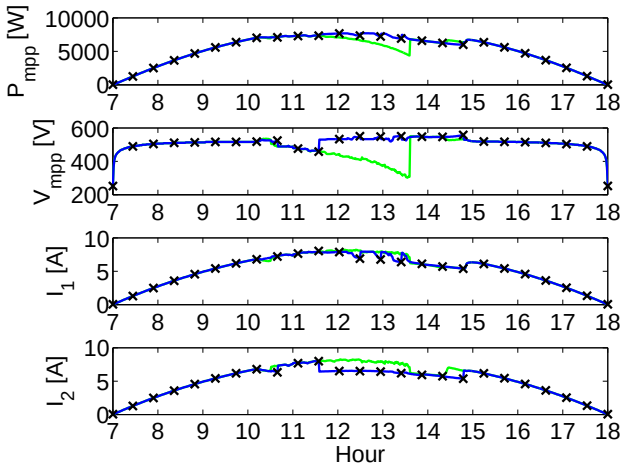

(a)

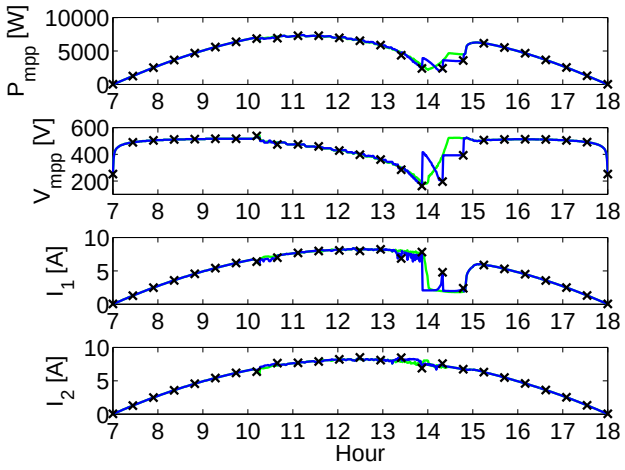

(b)

Figure 4.13: Pole shadow rotating over the PV field. Trend of generated power, voltage V_{mpp} and string currents I_1 and I_2. Shadow strength = 25% (a) and 75% (b)

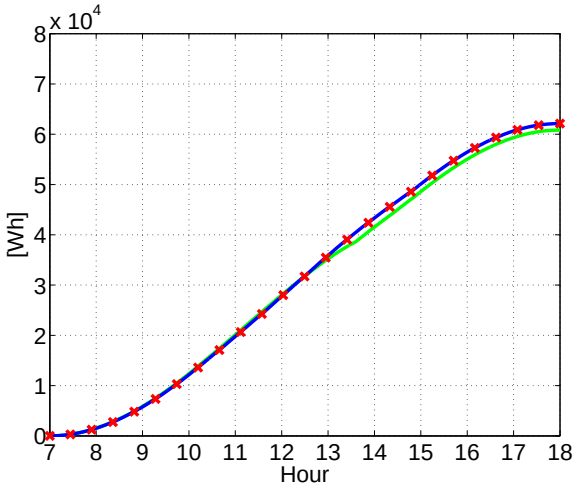

(a)

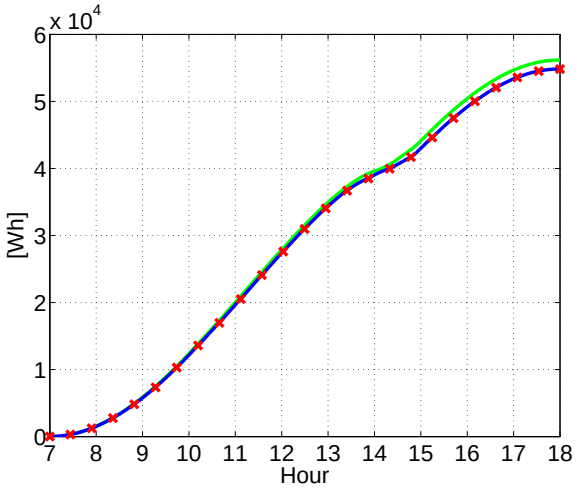

(b)

Figure 4.14: Pole shadow rotating over the PV field. Daily Energy generated by no reconfiguring (green colored line) and by synchronously reconfiguring the PV field every 30 minutes (blue colored line). The reconfiguration instants are indicated by red crosses markers. Shadow strength = 25% (a) and 75% (b)

Shadow of a chimney

The reconfiguration procedure, executed every 30 minutes, chooses always the electrical configuration increasing the generated power (see Figure 4.15). Nevertheless, the gained energy at the sunrise and at the sunset is inexorably lost because of repeated reconfigurations during the central part of the day when no shadows are covering the PV field.
For this reason, the synchronous reconfiguration is very inefficient (see Figure 4.16).
The presence of this shadow, having a strength of 25%, leads to sequentially disconnect one and two panels of the PV field until the shadow leaves the PV field.
Instead, by considering a shadow strength equal to 75%, then more panels are disconnected and, when this occurs, the PV generator could become less efficient when the shadows moves.

In fact, if the shadow moves, the generated power could be reduced by further shading different PV modules or, that is the most interesting case, when the shadow moves away from the PV field and the disconnected panels are fully radiated again, no energy increase can be measured.
A synchronous reconfiguration system reconnects the unshaded panels only at given fixed time instants. So, in the worst case, the shadow leaves the PV field just after the new configuration is actuated and it must be maintained for all time period until a new reconfiguration process is triggered.
If the maximum sensitivity respect to shading conditions is required, clearly no panels have to be disconnected but this reduces the generated power and or increase the number of local MPPs of the voltage-power curves of the field.

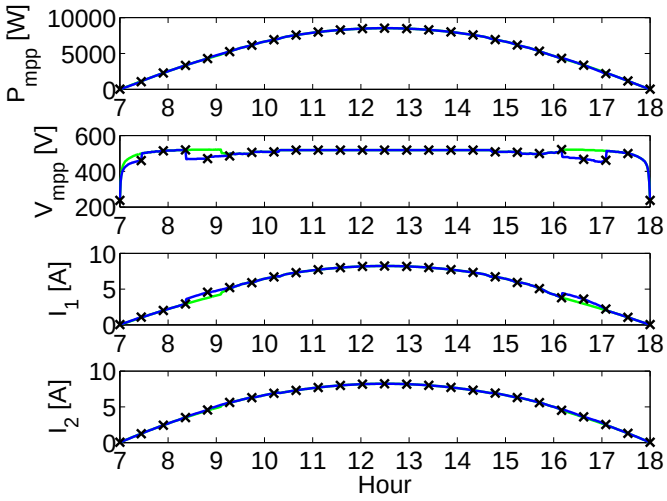

(a)

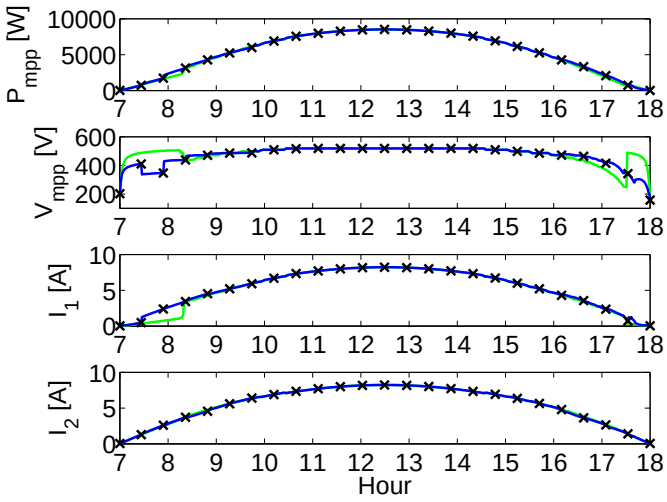

(b)

Figure 4.15: Shadow of a chimney appearing at sunrise and at the sunset. Trend of generated power, voltage V_{mpp} and string currents I_1 and I_2. Shadow strength = 25% (a) and 75% (b)

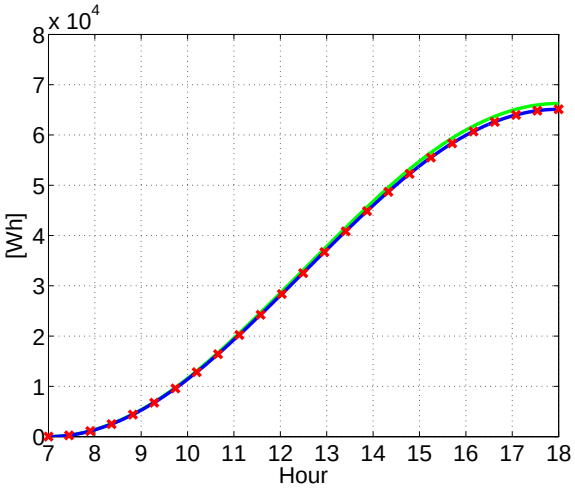

(a)

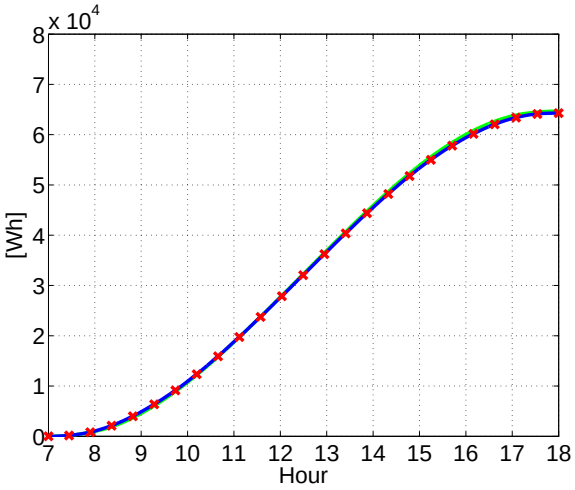

(b)

Figure 4.16: Shadow of a chimney appearing at sunrise and at the sunset. Daily Energy generated by no reconfiguring (green colored line) and by synchronously reconfiguring the PV field every 30 minutes (blue colored line). The reconfiguration instants are indicated by red crosses markers. Shadow strength = 25% (a) and 75% (b)

Sharp shadow covering only one panel row

In this scenario, a shadow moves only on the first string of the PV field. The effect on the maximum power point depends on the shadow strength value.

In Figure 4.17 (a), it is shown that there is no high efficiency in reconfiguring the PV field every 30 minutes. In fact, the generated power trend of the default configuration overlaps with that obtained by synchronously reconfiguring the PV field. Moreover, there is no energy gain, as illustrated in Figure 4.18 (a).

Conversely, it is really interesting the analysis of power and energy trends when the shadow strength increases to 75% (see Figure 4.17 (b)).
In this case, if the default configuration is used, the V_{mpp} voltage decreases under the minimum constraint value for the correct operating conditions of inverter (200V). So, if the MPP voltage assumes this value for a long time, the inverter could turn off.
Instead, a great advantage of the reconfiguration process, by constantly searching for a more performing configuration, maintain the V_{mpp} voltage in the allowed range for the inverter.
So, as shown in Figure 4.18 (b), in this case there is an evident energy gain (13.86%, as reported in Table 4.1).

The synchronous reconfiguration process can increase the generated power but it does not ensure the maximization of the daily energetic production.
As shown in this case, it ensures that the voltage constraints of inverter are respected but it doesn't provide an high sensibility respect to any shadowing change.

For this reason, a more adaptive reconfiguration procedure is discussed in the following section and the results obtained for the same shading scenarios are illustrated.

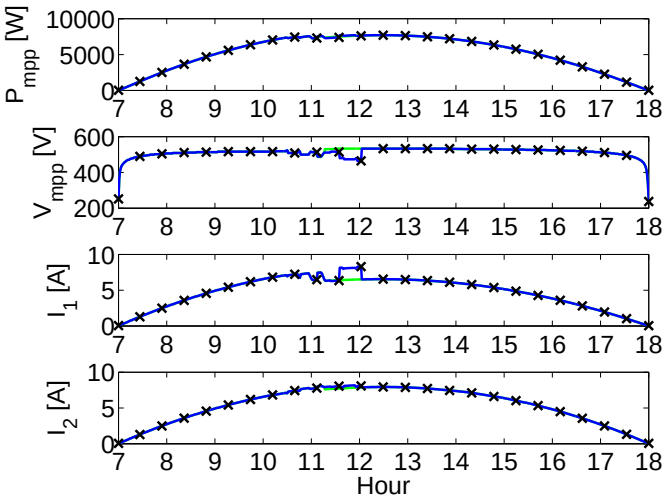

(a)

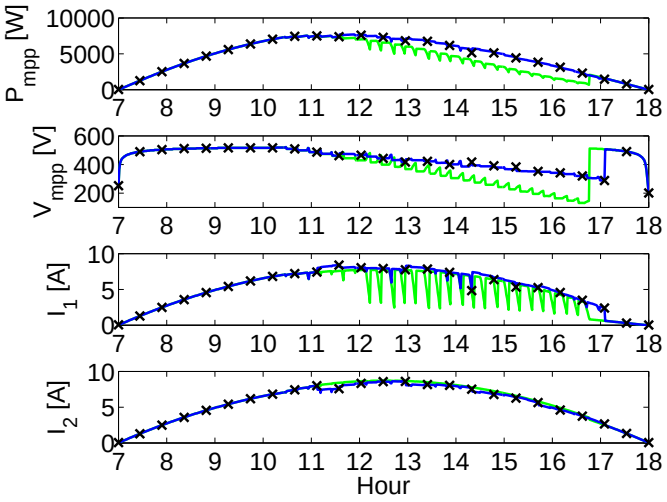

(b)

Figure 4.17: Sharp asymmetrical shadow (building). Trend of generated power, voltage V_{mpp} and string currents I_1 and I_2. Shadow strength = 25% (a) and 75% (b)

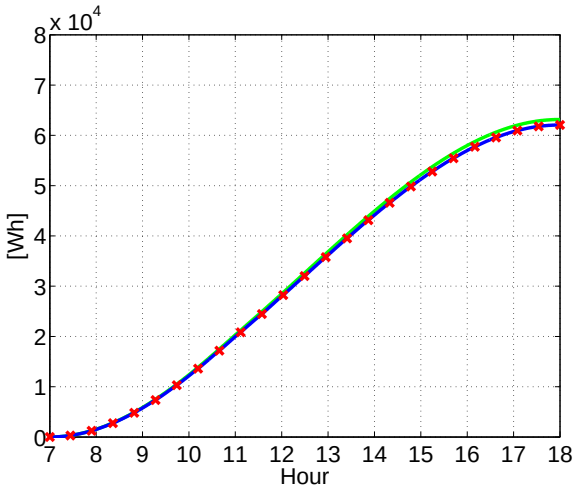

(a)

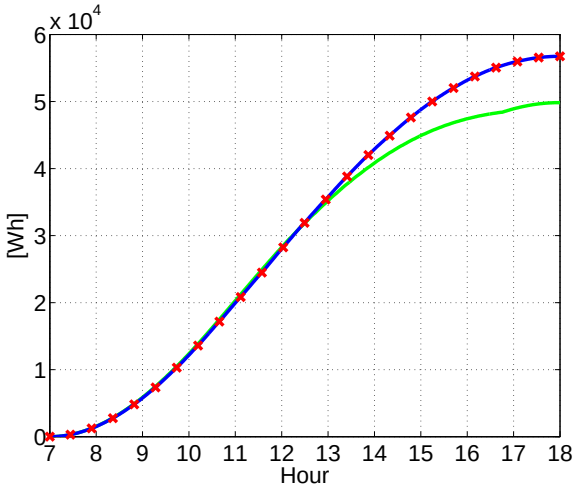

(b)

Figure 4.18: Sharp asymmetrical shadow (building). Daily Energy generated by no reconfiguring (green colored line) and by synchronously reconfiguring the PV field every 30 minutes (blue colored line). The reconfiguration instants are indicated by red crosses markers. Shadow strength = 25% (a) and 75% (b)

4.2 Adaptive Reconfiguration

An *adaptive* reconfiguration procedure has been achieved by triggering its execution if a set of conditions are verified.

This set of conditions has been deducted by observing how the V_{mpp} voltage across the PV field and the currents I_1 and I_2 of each row of the PV field evolve during different simulated shading phenomena.

In a real PV system, the voltage and currents are *continuously* measured by using proper sensors. If the values of voltage and currents achieved after each reconfiguration of the PV generator are used as *reference*, then the variation of at least one of these parameters respect to this reference values could indicate a partial shading is occurring over the PV field [CMPS14].

The voltage and current variations respect to these reference values strongly depend on different factors, such as the shadow strength, the shape and the size of shadow, the speed and motion direction of the shadow respect to the modules orientation in the panels.
At the same time, the maximum irradiance value hitting the PV plant isn't constant but it has a parabolic trend. So, even if no shadowing is occurring, voltage and currents change constantly during the day.
The voltage and current variations respect to the reference values also depend on the used MPPT algorithm and inverter topology. In fact, the voltage and/or the string currents change according to the robustness of the MPPT algorithm respect to the shadow effects on voltage-power curve of the PV field.
In general, if a shading occurs, the MPPT algorithm searches for a new working point having the highest power *in proximity of* the present MPP.
The new working point position depends on the strategy adopted by the algorithm respect to the variations affecting the voltage-

power curve of the field.
For a fixed shading phenomenon, inverter topology and MPPT strategy, the sensibility of the procedure to shading phenomena depends on the chosen working point (MPP).
Each working point of the voltage-power curve has a different sensibility respect to the same shading phenomena occurring over the PV generator. Moreover, even if no significant voltage and/or current variation are observed, a shadow could cover the PV field.
In the simulations, a central inverter topology and a Perturbe&Observe (P&O) MPPT algorithm have been considered.

4.2.1 The Rules Set

The observation of voltage and currents during simulated shading conditions lead to define three classes of set of rules:

- Precautionary Rules (PRs)
- Skipping Rules (SRs)
- Activating Rules (ARs)

These rules are analyzed in the order they are provided. In particular, if a rule is verified, then the remaining rules are ignored.
The Precautionary Rules (PRs) include highest-priority criteria triggering the reconfiguration process independently of all following rules. The term *precautionary* refers to the need to reconfigure the PV plant because no parameters variations have been observed. So, the reconfiguration could lead to choose a different MPP and so to improve the sensibility respect to shadowing.
The Skipping Rules (SRs) include criteria for detecting the conditions that indicate that the actual panels interconnections must not be changed, i.e. the reconfiguration operation is actually not needed. The Activating Rules (ARs) include criteria for detecting the conditions indicating that a reconfiguration of the panels interconnections is mandatory. So, the reconfiguration process is

executed or skipped each time a proper set of conditions is verified.

Precautionary Rule : *If the time period ΔT elapsed from the previous reconfiguration step is greater than a fixed time interval ΔT_{max}, a precautionary reconfiguration step must be executed.*

This rule prevents situations where the maximum power point has a very low sensitivity respect to the solar radiance variations, independently of the causes (global solar radiance change or partial shading of the PV field). Thus it can be considered a precautionary rule.
The maximum time interval between two executions of the reconfiguration process is set to two times the time period of the synchronous reconfiguration process.

Skipping Rule n. 1 : *If a minimum time interval ΔT_{min} hasn't been elapsed from last reconfiguration, a new reconfiguration step doesn't have to be executed.*

If the precautionary rule provides the maximum time interval between two reconfigurations, this rule ensures that the reconfiguration is executed at least after an interval time ΔT_{min} has elapsed from last partial shadow detection.

The reconfiguration process should not be executed also when the solar radiance is globally changing over the PV field.
In these conditions, the variation of the V_{mpp} voltage and that of the string currents depends on the global solar radiance value. In particular, when the PV field is subjected to under high solar radiance values ($G \geq 100 \frac{W}{m^2}$), as occurs for the central hours of the day, a global radiance change leads to a proportional variation of both string currents and a negligent change of voltage V_{mpp}. Instead, when the solar radiance maintains at very low values ($G < 100 \frac{W}{m^2}$), both string currents and voltage change significantly.

So, the reconfiguration process is disabled when the variations of string currents and voltage respect to their reference values have the same sign and they are confined into a given range of values that depend on the global solar radiance value. In particular, since it is not possible to measure this information, as indicator is used the average string current after each reconfiguration. In fact, it is assumed that the MPP chosen by reconfiguration process has the highest value and that it is related to the maximum solar radiance hitting the PV field.
Thus, the two following skipping rules are obtained:

Skipping Rule n. 2 : *A new reconfiguration action is not needed if the string currents measured at the last reconfiguration are on average greater or equal than a value I_{med}, if both the string currents and the V_{mpp} voltage change simultaneously and with the same sign respect to their reference values, if both currents exceed their respective threshold values and the voltage variation is limited to the range [-ΔV_{th_high},0] if a voltage reduction occurs or to the range [0, ΔV_{th_high}] if, instead, a voltage increase occurs.*

Skipping Rule n. 3 : *A new reconfiguration action is not needed if the string currents measured at the last reconfiguration are on average lower than a value I_{med}, if both the string currents and the V_{mpp} voltage change simultaneously and with the same sign respect to their reference values, if both currents exceed their respective threshold values and the voltage variation is limited to the range [-ΔV_{th_low},0] if a voltage reduction occurs or to the range [0, ΔV_{th_low}] if, instead, a voltage increase occurs.*

The activation rules can be divided into a set of three rules valid for high values of global solar radiance, a set of three rules valid for low global radiance values and a couple of rules not depending on the particular solar conditions.

In general, when a module in a panel is shaded, its bypass diode turns on and the voltage across the module assumes a neg-

ative voltage value equal to the forward-biased voltage across the p-n region of the diode.
This voltage variation occurs without a significant current change, so the first AR is obtained:

Activating Rule n. 1 : *A new reconfiguration is needed if the string currents measured at the last reconfiguration are on average greater or equal than a value I_{med}, if both strings currents variation don't exceed their correspondent threshold values but a voltage variation greater than ΔV_{th_high} occurs.*

If the variations of at least one string current and V_{mpp} voltage have an opposite sign, then these variations are *always* caused by a partial shading.
In fact, if at least one of the string currents is reduced and the voltage variation is positive, then the positive voltage change of the MPP depends on the presence of modules generating a current value that is greater than that of the MPP value itself. In this case, the current reduction leads to increase the voltage across the unshaded modules and this effect can be seen on the MPP itself. So, the following AR is obtained:

Activating Rule n. 2 : *A new reconfiguration is needed if the string currents measured at the last reconfiguration are on average greater or equal than a value I_{med}, if at least one of the strings currents reduces under its correspondent threshold value and the voltage variation is greater than zero.*

A similar rule is applied for a positive change of at least one of the strings currents but considering in this case a reduction of the V_{mpp} voltage. In fact, if this occurs, then the MPP change its position from a non-linear region of the voltage-power curve to the another one. This effect is generally observed when the voltage-power curve of the field has different local MPPs.

Activating Rule n. 3 : *A new reconfiguration is needed if the string currents measured at the last reconfiguration are on average greater or equal than a value I_{med}, if at least one of the strings currents increases over its correspondent threshold value and the voltage variation is lower than ΔV_{th_high}.*

At lower solar radiance values (G$< 100\frac{W}{m^2}$), a partial shading is mainly detected by a variation of at least of one between the strings currents over its threshold or an opposite variation of both strings currents or if both currents string don't change significantly but a great voltage change is observed due to the turning on of the bypass diode (as well as for AR1).

Activating Rule n. 4 : *A new reconfiguration is needed if the string currents measured at the last reconfiguration are on average lower than a value I_{med}, if the change of only one of the strings currents exceeds its correspondent threshold value and the voltage variation is greater than ΔV_{th_low}.*

Activating Rule n. 5 : *A new reconfiguration is needed if the string currents measured at the last reconfiguration are on average lower than a value I_{med}, if both the strings currents don't exceed their correspondent threshold value and a voltage variation greater than ΔV_{th_low} is measured.*

Activating Rule n. 6 : *A new reconfiguration is needed if the string currents measured at the last reconfiguration are on average lower than a value I_{med}, if both strings currents exceed their correspondent threshold values, the variations of the currents have an opposite sign and the voltage variation is greater than ΔV_{th_low}.*

In general, at lower irradiance conditions, it is really difficult to detect partial shading phenomena since the voltage change is non-linear respect to the solar irradiance both when partial shading is occurring or not.

Basing on [CMPS14], also two further rules analyzing only the power change, independently of the global solar irradiance value, are considered.

Activating Rule n. 7 : *A new reconfiguration is needed if a power reduction greater than ΔP_{th} occurs.*

Activating Rule n. 8 : *A new reconfiguration is needed if the power variation ΔP is greater than a fixed threshold ΔP_{th}, where $\Delta P_{th} > 0$, and a fixed time period from the previous reconfiguration ΔT_{avg} has been elapsed.*

4.2.2 Thresholds Estimation

The proposed set of rules requires some threshold for the PV power, voltage and current variation. The value of such threshold has been evaluated accounting the PV panels parameters (Axitec AC-250M/156-60S), summarized in Table 4.2 as well as the typical daily irradiance changing rate as defined in the EN 50530 standard [RB09].

Parameter	$G = \mathbf{1000}W/m^2$	$G = \mathbf{300}W/m^2$	$G = \mathbf{100}W/m^2$
V_{oc} [V]	53	49.98	47.95
V_{MPP} [V]	42.9	41.89	40.88
I_{MPP} [A]	8.22	2.47	0.84

Table 4.2: Parameters of a fully sunny PV panel for different values of the irradiance G. The operation temperature has been considered fixed and equal to 320 K.

The irradiance profile during a whole day is assumed to be parabolic. Moreover, the operating current of the PV strings depends approximately linearly on the irradiance level. Thus, the following equation can be used to calculate the thresholds $\Delta I_{n,th}$

for the current in the two strings:

$$\Delta I_{n,th} = a \cdot I_{n,last} + b \qquad n = 1, 2 \tag{4.2}$$

where $I_{n,last}$ is the MPP current at which the n-th string was operating at the last reconfiguration step. The value of a and b is determined by imposing the value of $\Delta I_{n,th}$ when $I_{n,last}$ is equal to $I_{MPP}(G = 100\ W/m^2)$ and $I_{MPP}(G = 1000\ W/m^2)$ respectively:

$$\begin{aligned} \Delta I_{n,th}(I_{n,last} = 0.84A) = 0.1A \\ \Delta I_{n,th}(I_{n,last} = 8.22A) = 0.5A \end{aligned} \tag{4.3}$$

so that equation (4.2) becomes:

$$\Delta I_{n,th} = 0.055 \cdot I_{n,last} + 0.054 \qquad n = 1, 2 \tag{4.4}$$

The equation (4.4) allows to achieve a reconfiguration system whose sensitivity with respect to the irradiance variation is higher at low operation current and lower at high operation current. In the second case, a higher threshold increase the tolerance of the reconfiguration system to variation due to parassitic parameters as well as temperature and irradiance oscillations.

A similar approach has been used to define the threshold ΔP_{th}: by assuming a linear variation of the PV power with respect to the irradiance within the range [300, 1000] W/m^2, it is possible to evaluate the following relation:

$$\frac{dP}{dG} = \frac{1}{A} \cdot \frac{P_{MPP}(G = 1000W/m^2) - P_{MPP}(G = 300W/m^2)}{1000 - 300} \tag{4.5}$$

where $A = 39.2 \quad m^2$ is the area of the PV field, so that $dP/dG = 0.23$. By imposing a irradiance variation $dG = 100W/m^2$, that is the 10% of the maximum irradiance value, the threshold ΔP_{th} can be evaluated as following:

$$\Delta P_{th} = \frac{dP}{dG} \cdot A \cdot dG = 901.6W \tag{4.6}$$

By assuming that, at an almost constant temperature, the PV panel MPP voltage is approximately constant in the range [100,

1000] W/m^2, two values of the threshold ΔV_{th} can be defined as a function of the average value I_{med} of the strings currents:

$$\begin{aligned} \Delta V_{th} &= \frac{2}{N_{mod}} \cdot V_{oc} \qquad if \quad I_{med} < 0.84A \\ \Delta V_{th} &= \frac{1}{N_{mod}} \cdot V_{oc} \qquad if \quad I_{med} \geq 0.84A \end{aligned} \tag{4.7}$$

where $N_{mod} = 3$ is the number of modules in each PV panel and $V_{oc} = 53V$ is the open circuit voltage of the PV panel in Standard Test Conditions (STC).

The values of the thresholds are summarized in Table 4.3.

Threshold	**Value**
ΔV_{th} [V] @ $I_{med} < 0.84$A	35.34
ΔV_{th} [V] @ $I_{med} \geq 0.84$A	17.67
$\Delta I_{n,th}$ [A] $n = 1, 2$	$0.055 \cdot I_{n,last} + 0.054$
ΔP_{th} [W]	901.6
ΔT_{min} [min]	5
ΔT_{avg} [min]	30
ΔT_{max} [min]	60

Table 4.3: Threshold values

So, the threshold values, in order to be estimated, require the knowledge of the features of the photo-voltaic panels composing the PV field and the PV field size to be known.
Thus the calculation of these threshold values is a crucial task for the adaptive procedure but it is not automated yet.
The choice of the threshold values must lead to a very reactive system respect to unexpected shading phenomena but, at the same time, it should guarantee the minimum number of reconfigurations and a low susceptibility to the signal noise. A balance between these two aspects is difficult to achieve, because these values should be optimized for *all* the shading scenarios.

4.2.3 Simulated Results

The adaptive reconfiguration has been tested on the same shading scenarios presented in Section 4.1 in order to compare the proposed technique with the synchronous reconfiguration.

	Shadow strength					
	25%	**75%**	**25%**	**75%**	**25%**	**75%**
	Synchronous		**Adaptive**			
Case	**Energy [kWh]**		**Energy gain (%)**		**Nr**	
No shadow	66.735		0.87		14	
Sharp, symm.	59.478	48.816	1.23	-0.12	28	41
Sharp, vertical	62.193	51.438	0.64	0.61	16	24
Pole	62.123	54.831	0.51	0.54	22	36
Chimney	65.106	64.285	0.23	0.5	21	21
Sharp, asym.	62.058	56.739	0.79	0.56	17	23

Table 4.4: Energy gain (adaptive vs synchronous reconfiguration)

The energy gained and the number of reconfigurations N_r executed by the adaptive reconfiguration, respect to that synchronous, are summarized in Table 4.4.
Respect to the synchronous procedure, that is executed 25 times during the whole day, that adaptive reduces the number of reconfigurations N_r in the majority of cases. In fact, this number exceeds that of the reconfiguration procedure only when the shadow moves along the whole field by interesting each module one by one, as occurs for the shadow strip horizontally translating over the field, or for the pole shadow that covers for many hours both the panels rows of the PV field. In fact, in these cases, a minimal movement or rotation of the shadow could lead the strings currents or the voltage of the field to exceed the given thresholds.
Nevertheless, the most interesting result is that even when the number of executions exceeds that the synchronous procedure, as occurs for a pole shadow rotating over the PV field and having a shadow strength equal to 75%, a positive energy gain is achieved.

The unique case this doesn't occur is when the reconfiguration is executed 41 times, i.e. for a shadow strip moving along the PV field and having a shadow strength of 75%. Nevertheless, in that case, the lost energy is only the 0.12% of that generated by the synchronous reconfiguration.
As expected, the highest energy gain is achieved if no shading phenomenon occur all day.
In effect, the increase of the generated power respect to the synchronous procedure is only about 0.5%–1%, but this percentage is strongly lowered by the high number of reconfigurations triggered during the time a shadow is passing over the PV field.

Unfortunately, even if the performances of the adaptive reconfiguration are in general better than that synchronous, the daily energy generated by the adaptive reconfiguration is instead lower then that produced by the default configuration due to the repeated execution of the reconfiguration processes.
In the Table 4.5, the energy gained and the number of reconfigurations N_r executed by the adaptive reconfiguration, respect to the case the default configuration is used, are summarized.

	Shadow strength					
	25%	**75%**	**25%**	**75%**	**25%**	**75%**
	Default configuration		**Adaptive reconfiguration**			
Case	**Energy [kWh]**		**Energy gain (%)**		**Nr**	
No shadow	67.92		-0.89		14	
Sharp, symm.	57.215	50.476	5.24	-3.41	28	41
Sharp, vertical	63.287	52.492	-1.1	-1.41	16	24
Pole	60.827	56.170	2.65	-1.85	22	36
Chimney	66.254	64.680	-1.5	-0.11	21	21
Sharp, asym.	63.155	49.834	-0.96	14.5	17	23

Table 4.5: Energy gain (adaptive reconfiguration vs no recofiguration)

In effect, the chosen threshold values lead to an adaptive procedure that is very reactive to each partial shading phenomenon and that doesn't minimize the number of reconfigurations.
Moreover, even if the total daily energy could be less than that produced by default configuration, this is not true at every hour of day. So, each shading scenario should be analyzed separately.
For each shading scenario, beyond the power and energy trends, a statistical analysis of the reconfiguration rules is provided in order to discuss about the effective precision of the proposed rules.
It should be stressed that the rules precision depends on the chosen threshold values that are calculated basing on the knowledge of the PV field features.

Full sunny day

In a full sunny day, no reconfiguration is needed. So, as expected the efficiency of the only three applied rules is zero, as illustrated in the Table 4.6.

The trend of the power curve obtained by both synchronous and adaptive reconfiguration overlap.
The adaptive procedure uses only 14 reconfigurations respect to the 25 of that synchronous.
At low power, i.e. at low solar radiance level, the reconfiguration is executed because the power change exceeds its fixed threshold. In fact, at sunrise and at the sunset, the solar radiation changes by a rate grater than during the central hours of the day, when, instead, the reconfiguration is triggered by the precautionary rule (PR1).

So, even if the generated daily energy is lower than that of the default configuration, the energy production is improved respect to the synchronous procedure due to almost halved number of reconfigurations, as shown in Figure 4.21.

Rule	N. of executions	Total number of successes	%
PR1	11	0	0
AR7	1	0	0
AR8	2	0	0
Total	14	0	0

Table 4.6: Full sunny day: efficiency of rules activating the reconfiguration process

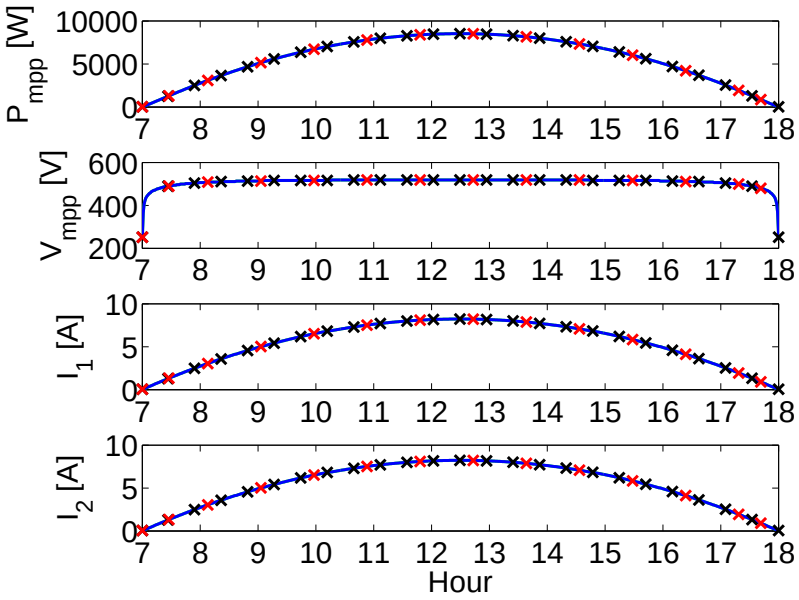

Figure 4.19: Full sunny day. Trend of generated power, voltage V_{mpp} and string currents I_1 and I_2. Synchronous reconfiguration (green line), adaptive reconfiguration (blue line). Reconfiguration instants: (black crosses) synchronous, (red crosses) adaptive.

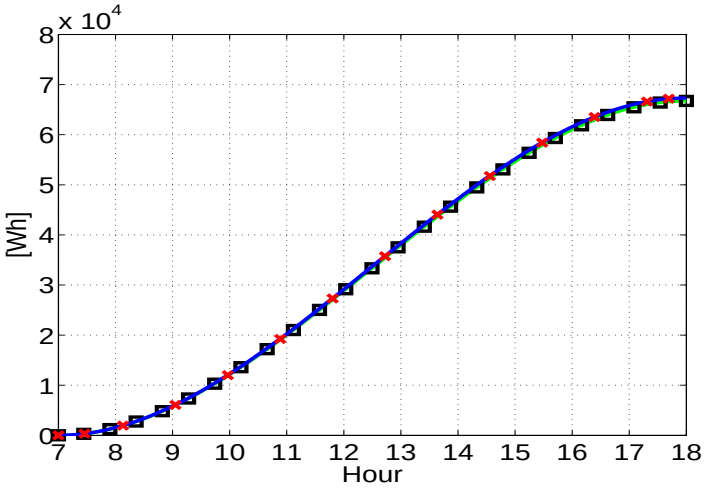

Figure 4.20: Full sunny day. Daily energy. Synchronous reconfiguration (green colored line), adaptive reconfiguration (blue line). Reconfiguration instants: synchronous (black squares) and adaptive (red crosses).

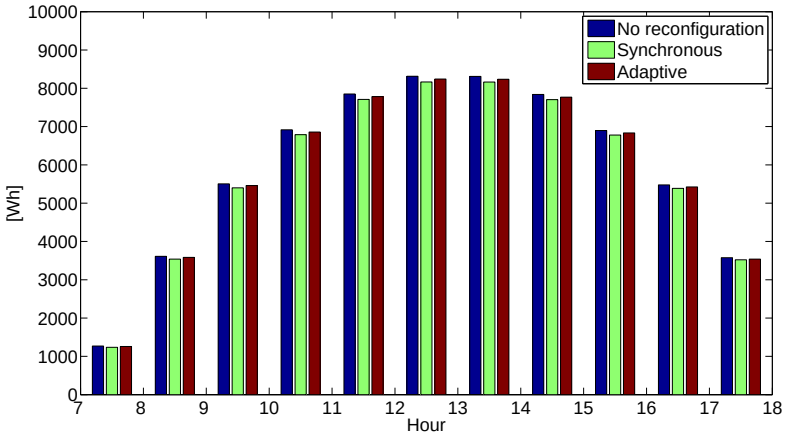

Figure 4.21: Full sunny day. Hourly energy generated by no reconfiguring (blue bar), by synchronous reconfiguration (green bar) and by the adaptive procedure (red bar).

Sharp symmetrical shadow

The efficiency of precautionary and activating rules is shown in Tables 4.7 and 4.8. In these Tables, the efficiency of a rule is equal to the number of times the power generated after a reconfiguration occurs is greater than that obtained if no reconfiguration is triggered at that instant.

Rule	**N. of executions**	**Total number of successes**	**%**
PR1	3	1	33.3
AR1	4	4	100
AR2	11	9	81.82
AR3	6	4	66.67
AR7	2	0	0
AR8	2	0	0
Total	28	18	64.29

Table 4.7: Sharp symmetrical shadow (shadow strength: 25%): efficiency of rules activating the reconfiguration process

Rule	**N. of executions**	**Total number of successes**	**%**
PR1	3	1	33.3
AR1	13	8	61.54
AR2	13	10	76.92
AR3	9	6	66.67
AR7	1	1	100
AR8	2	0	0
Total	26	15	63.415

Table 4.8: Sharp symmetrical shadow (shadow strength: 75%): efficiency of rules activating the reconfiguration process

In the majority of cases, the partial shading is detected as positive voltage change when at least one of the strings current reduces, so that the AR2 is verified. The positive voltage variation, respect to the reference value, increases with the reduction

of at least one of the strings currents. So, this rule is verified especially when the shadow strength assumes a value equal to 75%. In this case, while shading percentage of the PV field is increasing, the maximum power point can reduce its voltage but increase its current, so that the AR3 is verified.
Instead, if no current change is measured, it means that the partial shading is detected due to the turning on of one or more bypass diodes. In this case, the AR1 is verified.
In general, the threshold values chosen for both voltage and current are more strict than that chosen to detect a power increase or decrease. So, it is expected that the last two activation rules are verified fewer times.
Moreover, if a power change occurs, not necessarily it corresponds to a partial shading but it could be due to the a greater change rate of the power daily trend, as happens generally at the sunrise and at the sunset, and, for this reason, the efficiency of these rules can be the lowest one.
The same could occur for the precautionary rule, that is executed independently of the behavior of the electrical parameters.
The rules efficiency, for both shadow strength values, is much greater than 60%. In particular, the verification of these rules increases the energy production for about 5 hours respect to both the default configuration and the synchronous procedure when a 25% of shadow strength is considered, as shown in Figure 4.24 (a).
In fact, this occurs because the unshaded and the shaded panels are properly separated into two series-connected rows so that, for each string, both the generated current and the voltage are boosted. Instead, if the 75% of shadow strength is considered, then the reconfiguration procedure disconnects the shaded panels, so that when the shadow moves away from them, the generated power doesn't rapidly increase, as instead can occur if all panels are connected into the default configuration.
So, the recovery of the disconnected panels should be executed with the smallest possible delay respect to the instant time the shadows leaves one or more panels.

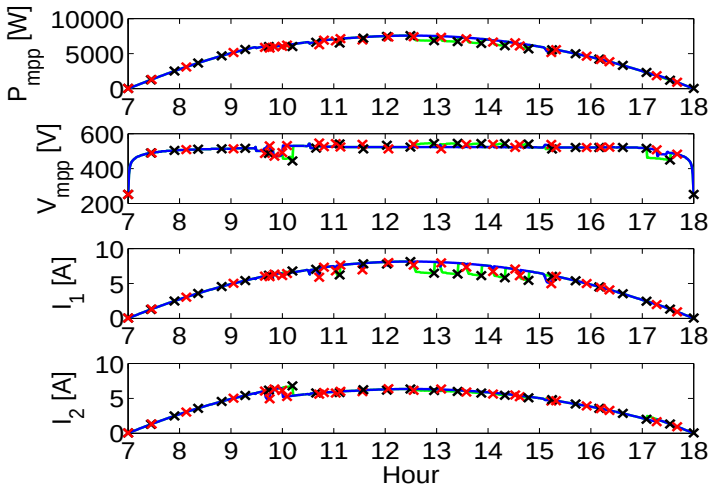

(a)

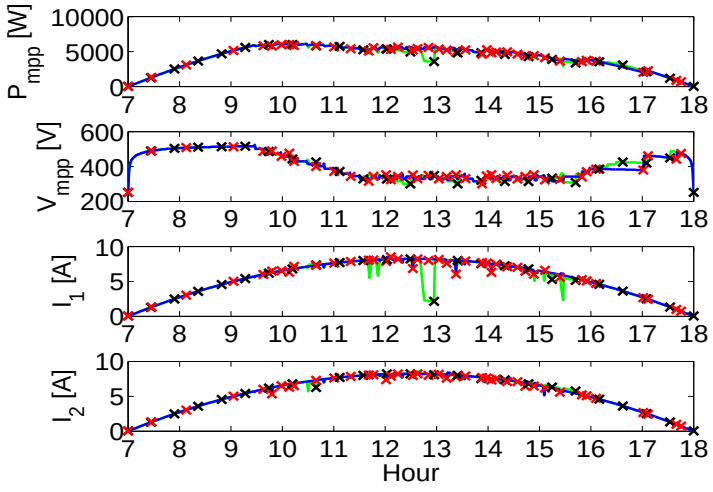

(b)

Figure 4.22: Sharp symmetrical shadow. Trend of generated power, voltage V_{mpp} and string currents I_1 and I_2. Synchronous reconfiguration (green line), adaptive reconfiguration (blue line). Reconfiguration instants: synchronous (black crosses), adaptive (red crosses). Shadow strength = 25% (a) and 75% (b)

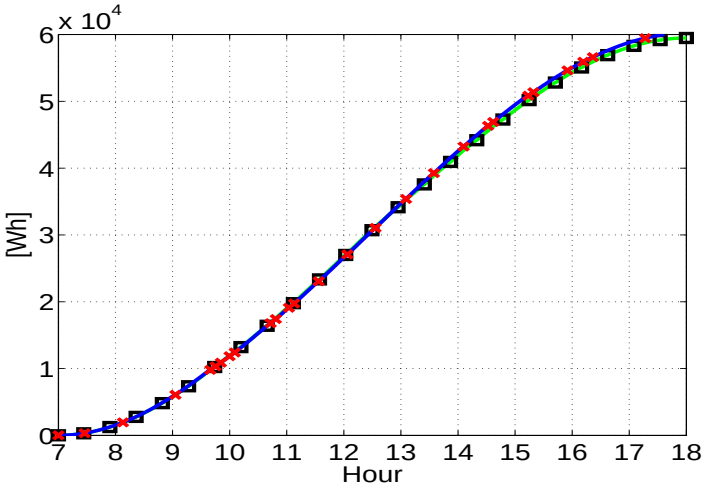

(a)

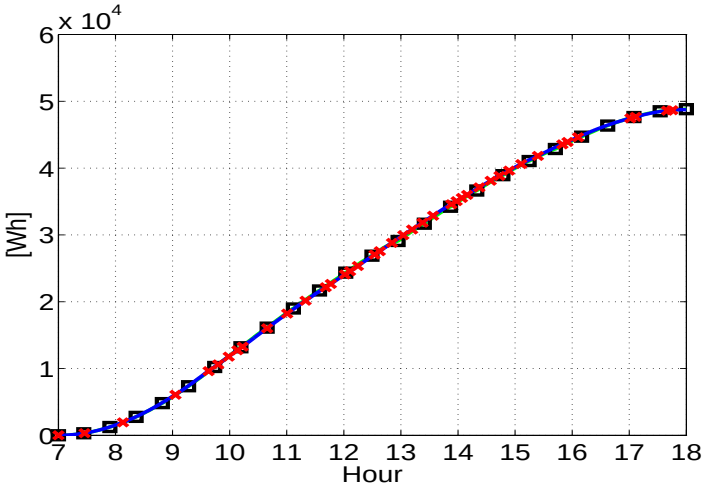

(b)

Figure 4.23: Sharp symmetrical shadow (building). Daily Energy. Synchronous reconfiguration (green line), adaptive reconfiguration (blue line). Reconfiguration instants: synchronous (black crosses), adaptive (red crosses). Shadow strength = 25% (a) and 75% (b)

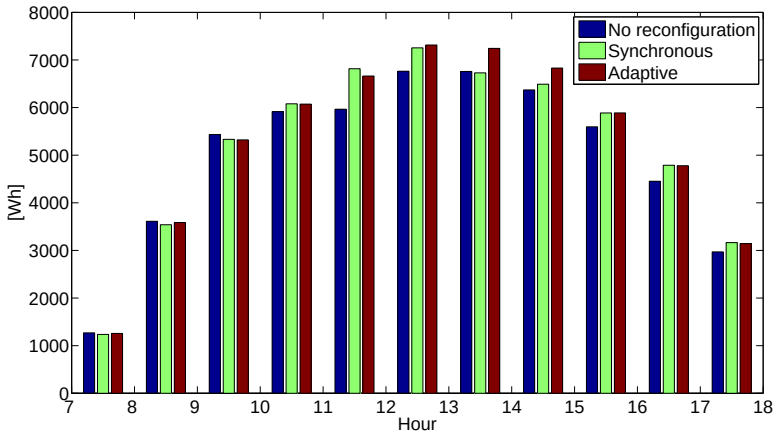

(a)

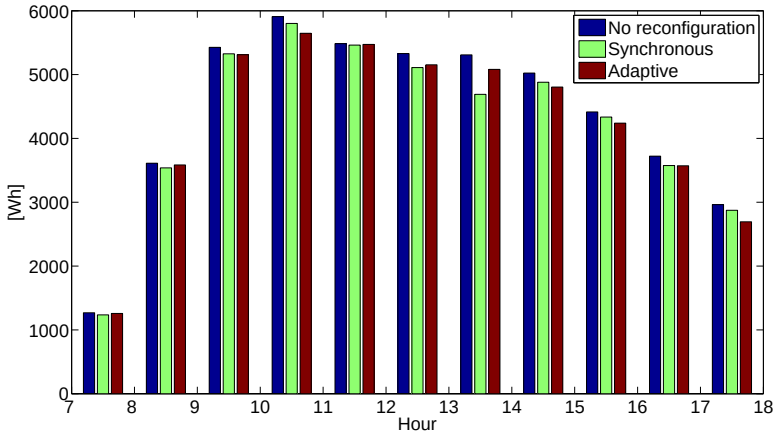

(b)

Figure 4.24: Sharp symmetrical shadow. Hourly energy generated by no reconfiguring (blue bar), by synchronously reconfiguring the PV field every 30 minutes (green bar) and by the adaptive procedure (red bar). Shadow strength = 25% (a) and 75% (b)

Sharp shadow moving from one first to second panels row

In this scenario, the low total efficiency achieved by rules (see Tables 4.9 and 4.10) mainly depends on the precautionary rule and on the activation rule that trigger the reconfiguration procedure when a reduction beyond a given fixed threshold (901W) is verified.

Rule	N. of executions	Total number of successes	%
PR1	8	3	37.5
AR2	3	2	66.67
AR7	3	0	0
AR8	2	2	100
Total	16	7	43.75

Table 4.9: Sharp shadow moving from the first to the second string (shadow strength: 25%): efficiency of rules activating the reconfiguration process

Rule	N. of executions	Total number of successes	%
PR1	6	2	33.3
AR1	2	2	100
AR2	9	4	44.44
AR3	1	1	100
AR7	4	1	25
AR8	2	2	100
Total	24	12	50

Table 4.10: Sharp shadow moving from the first to the second string (shadow strength: 75%): efficiency of rules activating the reconfiguration process

In fact, the precautionary rule is valid many times since, especially when the shadow strength is equal to 25%, there isn't a huge variation of voltage and/or strings currents.
Instead, in this scenario, the MPP value could easily exceed its

threshold once the shadow moves over one or both rows contemporary, above all with a shadow strength of the 75% (see Figure 4.25).
On the contrary, when a huge power increase is detected by rule AR8, the execution of the reconfiguration procedure is always required.

The adaptive procedure is able to detect the moving of the shadow over the whole PV field by sensing a positive voltage change when each or both strings current are reduced (rule AR2). In this case no reconfiguration is required because the default configuration is the best one.
Nevertheless, also in this case, the adaptive system maintains an high level of reactivity respect to environmental conditions.
Both in Figures 4.25 and 4.26, it is shown that an high reconfiguration frequency is mainly achieved during the shading phenomenon.
In Figure 4.27, the comparison among the hourly generated energy for the default configuration, the synchronous and the adaptive procedure shows that the last one performs better then synchronous when no shadowing is present and the shadow is leaving the PV field. In particular, better performance are achieved due to lower reconfiguration frequency when no shadowing occurs.

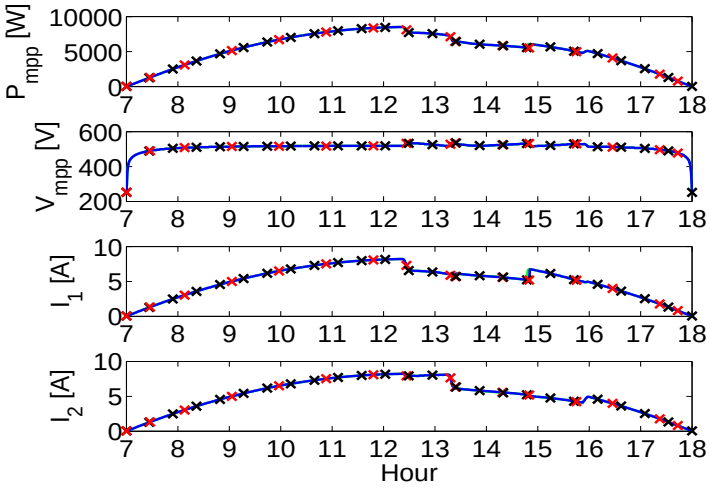

(a)

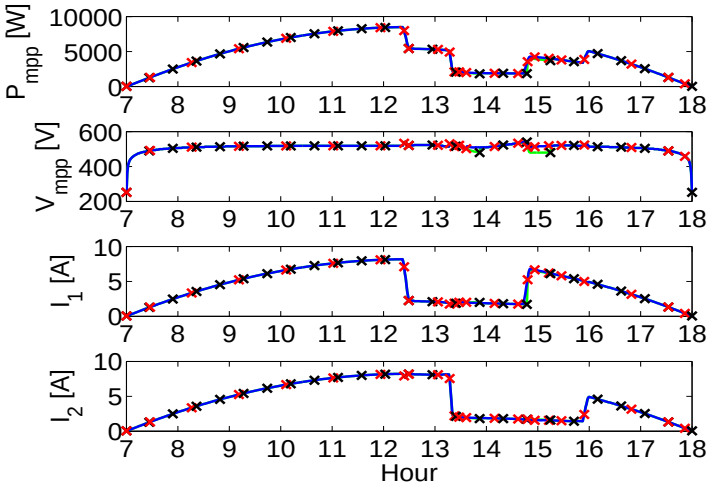

(b)

Figure 4.25: Sharp shadow moving from the first to the second string. Trend of generated power, voltage V_{mpp} and string currents I_1 and I_2. Synchronous reconfiguration (green line), adaptive reconfiguration (blue line). Reconfiguration instants: synchronous (black crosses), adaptive (red crosses). Shadow strength = 25% (a) and 75% (b)

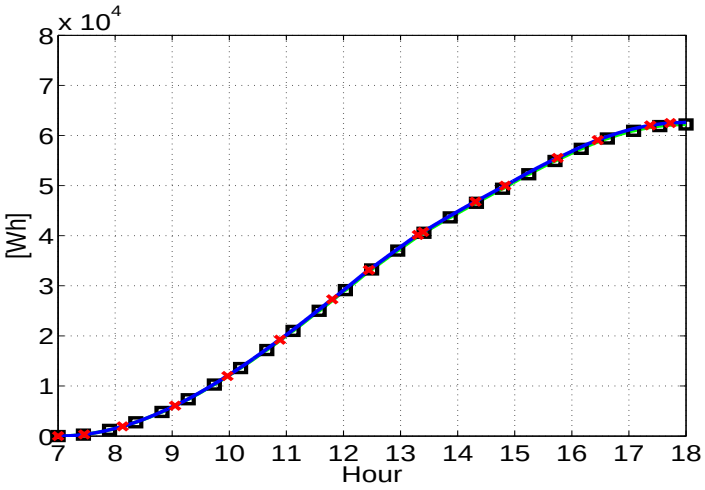

(a)

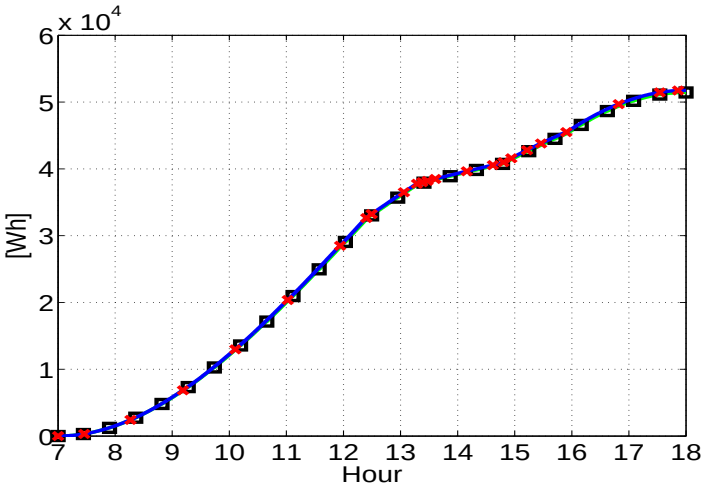

(b)

Figure 4.26: Sharp shadow moving from the first to the second string. Daily Energy:. Synchronous reconfiguration (green line), adaptive reconfiguration (blue line). Reconfiguration instants: synchronous (black crosses), adaptive (red crosses). Shadow strength = 25% (a) and 75% (b)

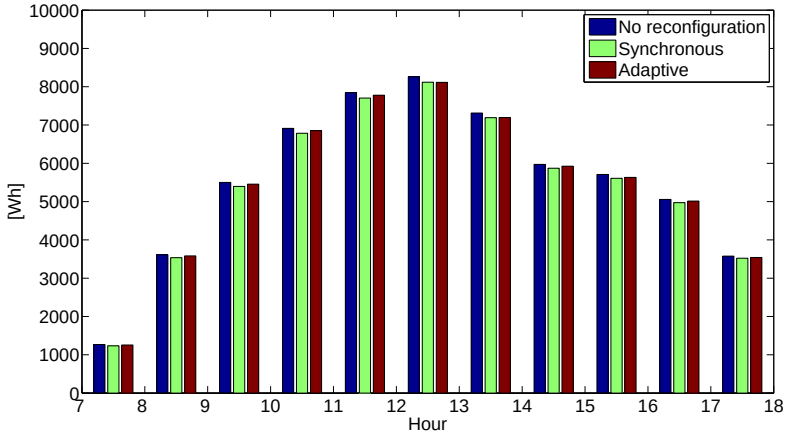

(a)

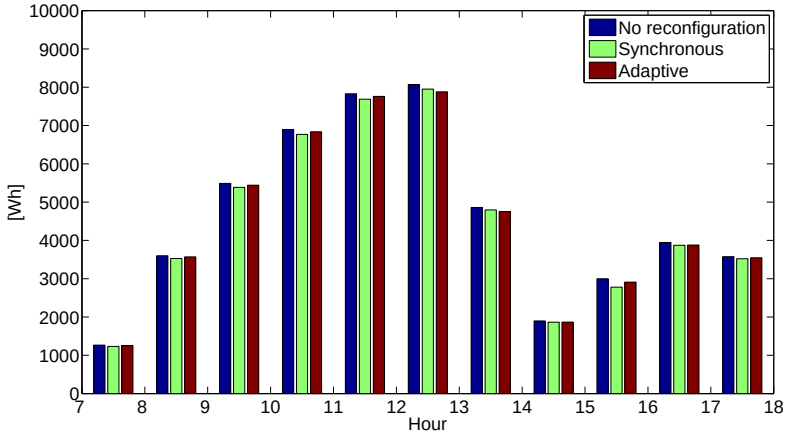

(b)

Figure 4.27: Sharp shadow moving from the first to the second string. Hourly energy generated by no reconfiguring (blue bar), by synchronously reconfiguring the PV field every 30 minutes (green bar) and by the adaptive procedure (red bar). Shadow strength = 25% (a) and 75% (b)

Pole shadow rotating over the PV field

Independently of the shadow strength, the rules efficiency is high (68% and 75% respectively in Tables 4.11 and 4.12). As always occurs, the precautionary rule cannot offer an high efficiency when no shadow is passing over the PV field. So, for that rule, the lowest efficiency is achieved.
Instead, the power obtained by reconfiguring the PV field is always greater than that achieved if not actuated when the activating rule AR2 is verified. Indeed, when the pole shadow is moving, while a set of PV modules becomes unshaded, the shading percentage increases over a new set of panels. So, the parameters, and especially the voltage value, due to also to a length of the shadow greater then the PV itself, change accordingly to the shading percentage of each module.
For this reason, the activating rules detect almost always correctly the instants at which the reconfiguration is more appropriate.

The Figure 4.28 shows that the adaptive procedure, respect to the synchronous one, chooses always the configuration achieving a greater power value. In particular, as shown also in Figure 4.29, the energy generated by the adaptive procedure is maximized respect both that of synchronous procedure and of the default configuration, when the shadow leaves the PV field.

Rule	**N. of executions**	**Total number of successes**	**%**
PR1	6	3	50
AR1	1	1	100
AR2	6	6	100
AR3	5	4	80
AR7	2	1	50
AR8	2	0	0
Total	22	15	68.18

Table 4.11: Pole shadow (shadow strength: 25%): efficiency of rules activating the reconfiguration process

Rule	N. of executions	Total number of successes	%
PR1	5	1	20
AR1	17	16	94.11
AR2	5	5	100
AR3	5	4	80
AR7	2	1	50
AR8	2	0	0
Total	36	27	75

Table 4.12: Pole shadow (shadow strength: 75%): efficiency of rules activating the reconfiguration process

The drawback of the adaptive procedure is the high number of reconfigurations due to the high sensibility of the system, whose performance are unfortunately reduced under that of the default configuration of 1.85% when an high shadow strength (75%) is considered.

The strong energy reduction is evident in Figure 4.30, where the slope of the energy trend reduces for about 2 hours.
The problem is that, in order to reduce the number of reconfigurations, a proper increase of the threshold values doesn't ensure both the minimization of reconfigurations and the energy maximization. In fact, the increase of the thresholds values leads only to delay the triggering of the reconfiguration process, i.e. to be less sensitive to shading phenomena.

A change of at least one parameter, as seen for the previous scenario, doesn't correspond always to the need of reconfiguring the PV field despite a dynamical shading phenomenon has been correctly detected. On the contrary, since the pole shadow is rotating over the PV field, in this scenario, it is effectively convenient to execute the reconfiguration process when decided by activation rules.
So, the real problem is the estimation of the threshold values leading to the highest performance in all studied cases.

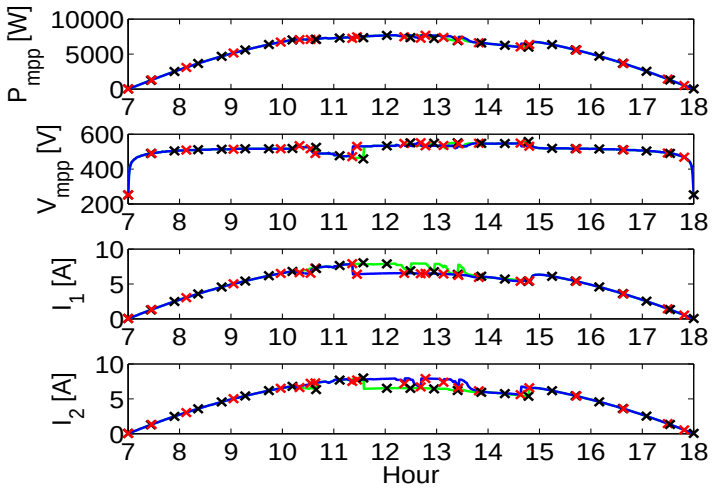

(a)

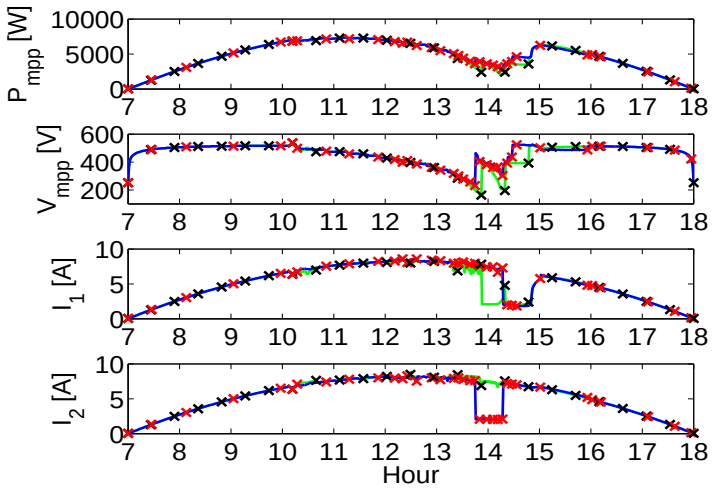

(b)

Figure 4.28: Pole shadow. Trend of generated power, voltage V_{mpp} and string currents I_1 and I_2. Synchronous reconfiguration (green line), adaptive reconfiguration (blue line). Reconfiguration instants: synchronous (black crosses), adaptive (red crosses). Shadow strength = 25% (a) and 75% (b)

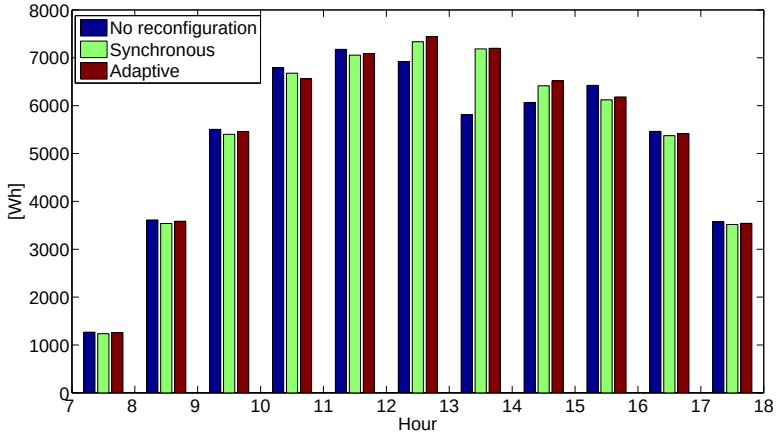

(a)

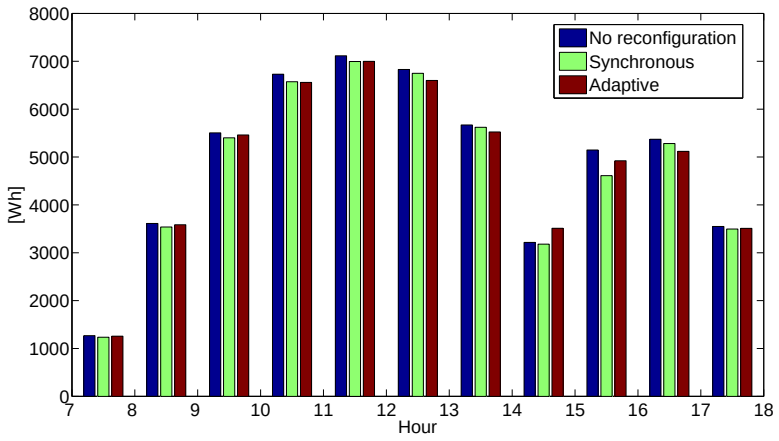

(b)

Figure 4.29: Pole shadow. Hourly energy generated by no reconfiguring (blue bar), by synchronously reconfiguring the PV field every 30 minutes (green bar) and by the adaptive procedure (red bar). Shadow strength = 25% (a) and 75% (b)

Moreover, one limitation of this procedure is that, by the only sensing of the voltage and currents values and detecting when the

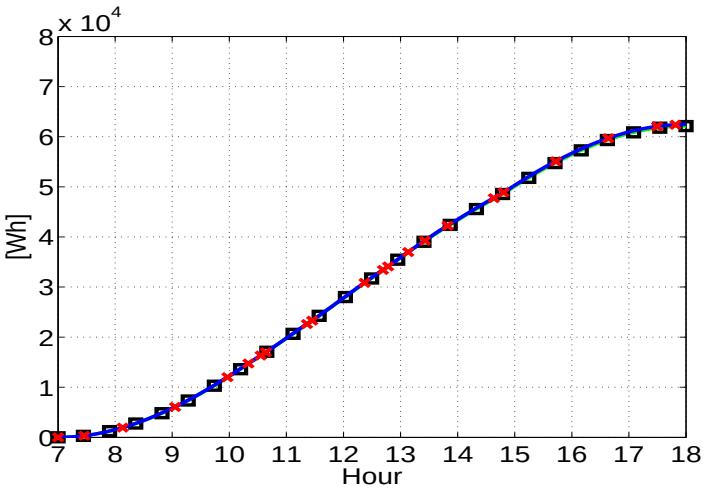

(a)

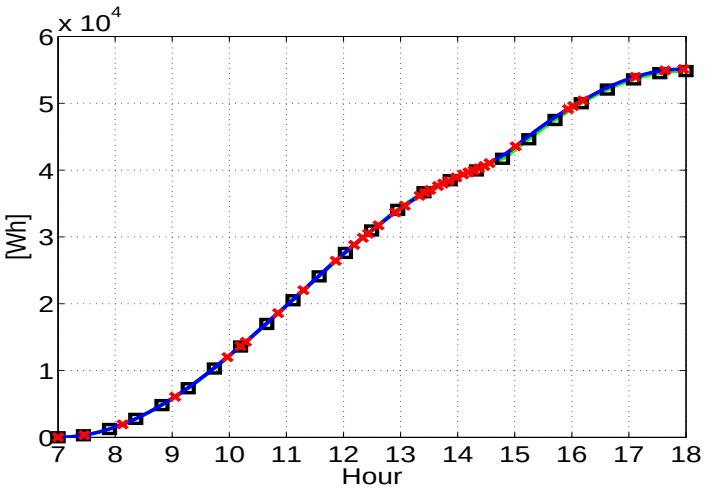

(b)

Figure 4.30: Pole shadow. Daily Energy:. Synchronous reconfiguration (green line), adaptive reconfiguration (blue line). Reconfiguration instants: synchronous (black crosses), adaptive (red crosses). Shadow strength = 25% (a) and 75% (b)

variation of these parameters exceed a given threshold, it is difficult to estimate the mismatching effects occurring into voltage-power curve of the field, and discerning the case all modules have the same short circuit current, as occurs for each string in the previous scenario, from that where all modules have different short circuit current values, as instead occurs for this scenario when, for example, the shadow is leaving the PV field and all modules belonging to a string are differently radiated.

Shadow of a chimney at the sunrise and at the sunset

This scenario considers the shadowing of a single row of the PV generator at the sunrise and at the sunset. In this case, during the first and last hours of the day, the reconfiguration process is triggered by the last three activation rules both by the activating rule AR6, verified if the variation of only one of the strings currents at a lower global irradiance level occurs, and by the activating rules bases on power change (AR7 and AR8). As illustrated in Tables 4.13 and 4.14, these rules achieve an high efficiency in detecting partial shadowing over the PV generator.

Rule	N. of executions	Total number of successes	%
PR1	9	5	50
AR1	1	0	0
AR2	5	2	40
AR3	2	2	100
AR7	2	2	100
AR8	2	2	100
Total	21	13	61.90

Table 4.13: Shadow of a chimney (shadow strength: 25%): efficiency of rules activating the reconfiguration process

During the central part of the day, the adaptive procedure, by halving the number of the executed reconfigurations, increases

Rule	N. of executions	Total number of successes	%
PR1	7	2	28.57
AR1	1	0	0
AR2	3	3	100
AR6	1	1	100
AR7	5	4	80
AR8	4	4	100
Total	21	14	66.67

Table 4.14: Shadow of a chimney (shadow strength: 75%): efficiency of rules activating the reconfiguration process

the energy generated by the PV field respect to that of the synchronous (see Figure 4.33).

In this case, the default configuration at the sunrise and at the sunset isn't the best one, but the energy lost at these periods of the day are gained, respect to the synchronous and the adaptive procedure, during the rest of the day (see Figure 4.33).

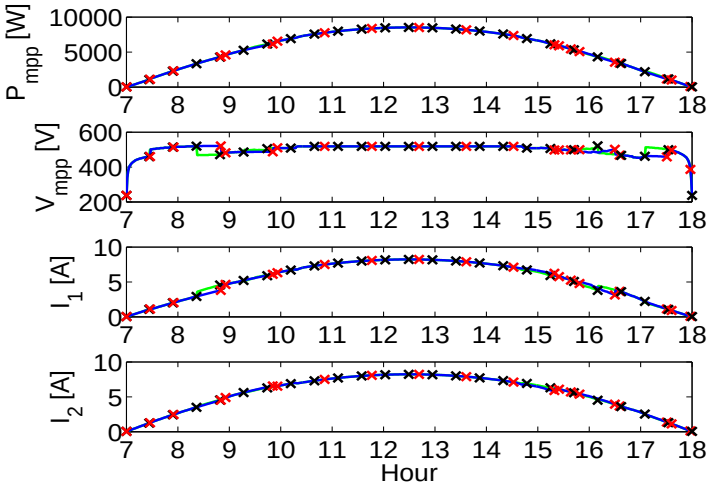

(a)

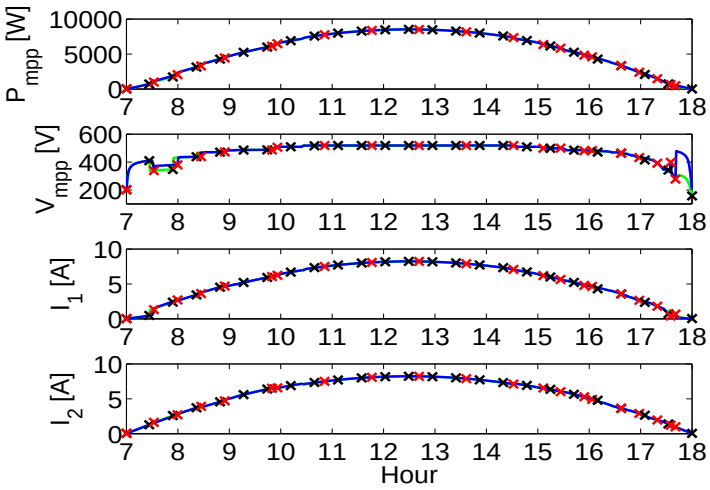

(b)

Figure 4.31: Shadow of a chimney. Trend of generated power, voltage V_{mpp} and string currents I_1 and I_2. Synchronous reconfiguration (green line), adaptive reconfiguration (blue line). Reconfiguration instants: synchronous (black crosses), adaptive (red crosses). Shadow strength = 25% (a) and 75% (b)

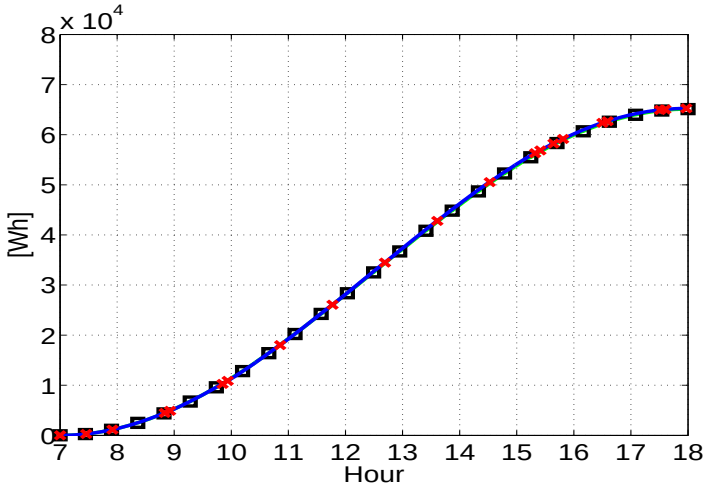

(a)

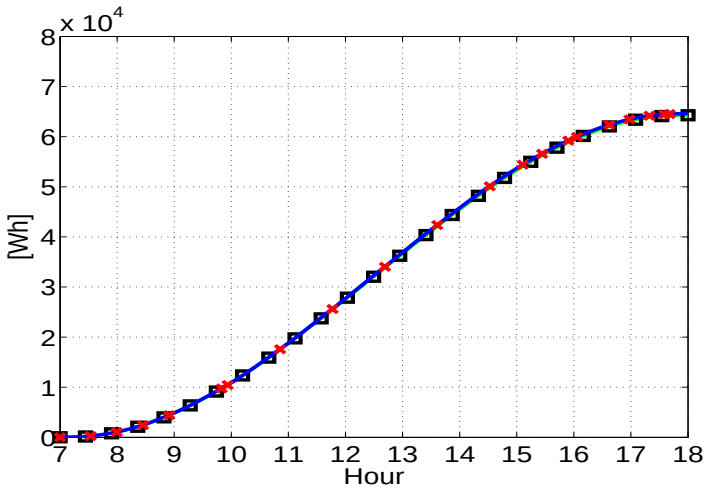

(b)

Figure 4.32: Shadow of a chimney. Daily Energy:. Synchronous reconfiguration (green line), adaptive reconfiguration (blue line). Reconfiguration instants: synchronous (black crosses), adaptive (red crosses). Shadow strength = 25% (a) and 75% (b)

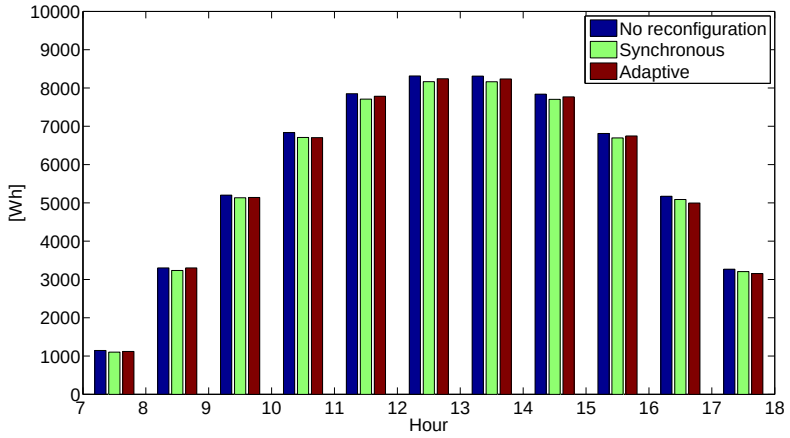

(a)

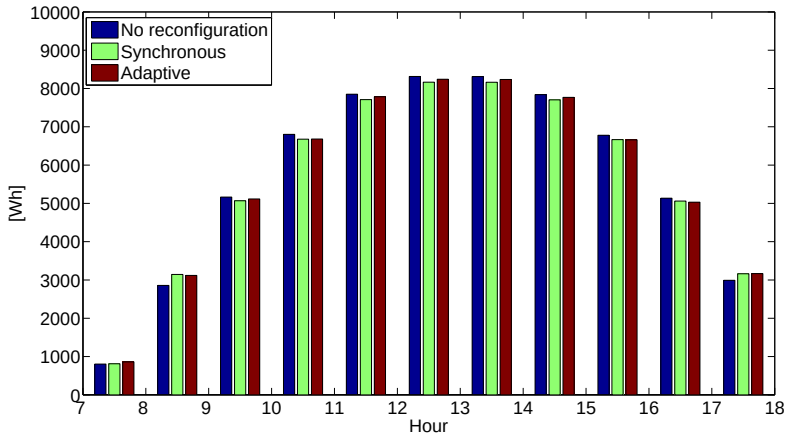

(b)

Figure 4.33: Shadow of a chimney. Hourly energy generated by no reconfiguring (blue bar), by synchronously reconfiguring the PV field every 30 minutes (green bar) and by the adaptive procedure (red bar). Shadow strength = 25% (a) and 75% (b)

Sharp shadow moving on one panels row only

For this scenario, despite the reconfiguration is executed useless in almost 44% of times when the highest shadow strength is considered, the generated energy is maximized both respect to the synchronous procedure and to the default configuration.

Rule	N. of executions	Total number of successes	%
PR1	9	1	11.11
AR2	2	1	50
AR3	2	1	50
AR7	2	0	0
AR8	2	0	0
Total	17	3	17.65

Table 4.15: Sharp asymmetric shadow (shadow strength: 25%): efficiency of rules activating the reconfiguration process

Rule	N. of executions	Total number of successes	%
PR1	6	2	33.33
AR1	2	2	100
AR2	6	4	66.67
AR3	3	1	33.33
AR7	4	4	100
AR8	2	0	0
Total	23	13	56.52

Table 4.16: Sharp asymmetric shadow (shadow strength: 75%): efficiency of rules activating the reconfiguration process

Also in this case, the reconfiguration is executed each time the shadow covers new series-connected modules leading the voltage to exceed its threshold value.

In this case, the adaptive procedure ensures the energy maximization because, for this shading scenario, the current generating

by the shaded string is always inexorable reduced if the default configuration is used.
Instead, by properly changing the electrical connections of panels, the generated energy is increased. Indeed, despite the reconfiguration process is executed 23 times, there is a great energy difference between that generated by the adaptive procedure and that of the default configuration.

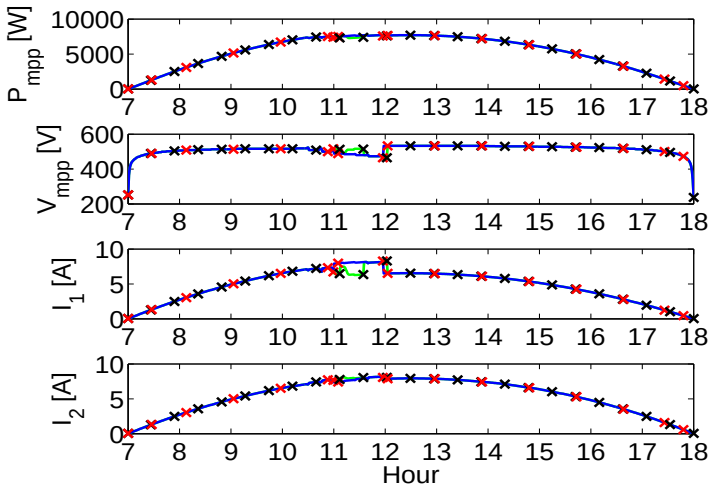

(a)

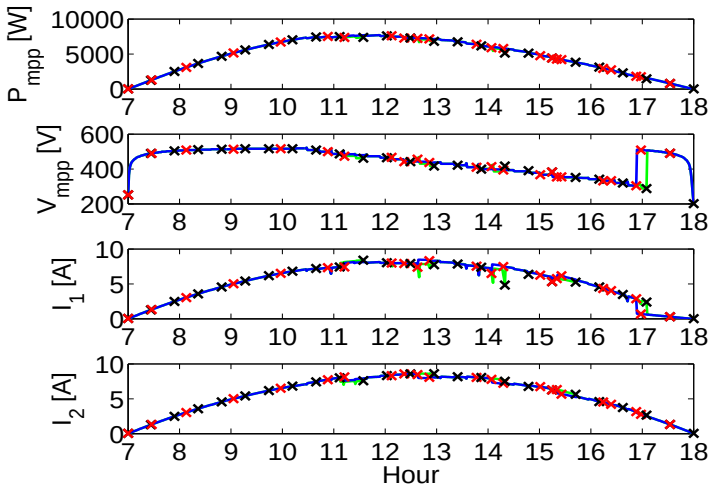

(b)

Figure 4.34: Sharp asymmetric shadow. Trend of generated power, voltage V_{mpp} and string currents I_1 and I_2. Synchronous reconfiguration (green line), adaptive reconfiguration (blue line). Reconfiguration instants: synchronous (black crosses), adaptive (red crosses). Shadow strength = 25% (a) and 75% (b)

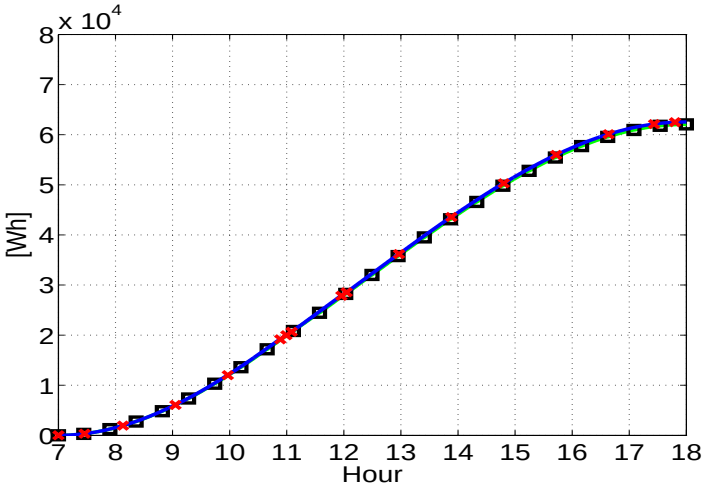

(a)

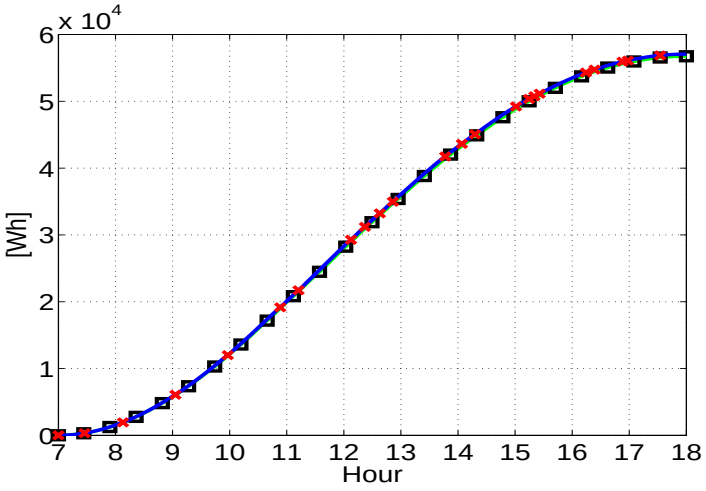

(b)

Figure 4.35: Sharp asymmetric shadow. Daily Energy:. Synchronous reconfiguration (green line), adaptive reconfiguration (blue line). Reconfiguration instants: synchronous (black crosses), adaptive (red crosses). Shadow strength = 25% (a) and 75% (b)

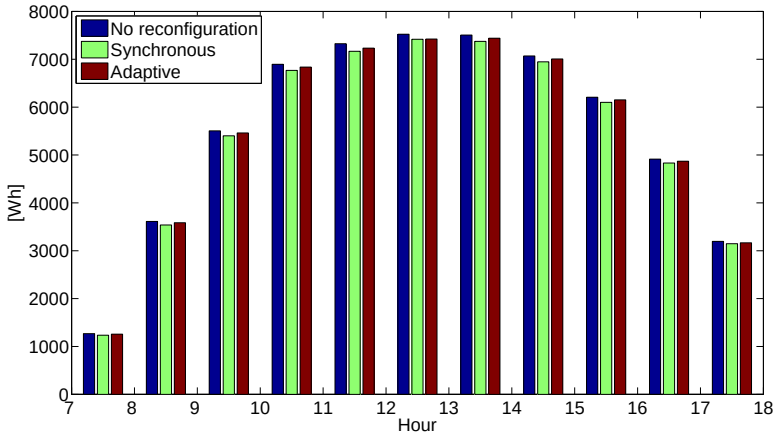

(a)

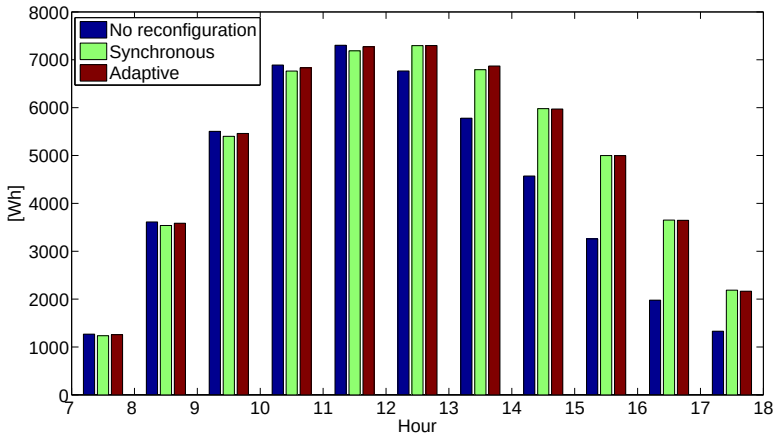

(b)

Figure 4.36: Sharp asymmetric shadow. Hourly energy generated by no reconfiguring (blue bar), by synchronously reconfiguring the PV field every 30 minutes (green bar) and by the adaptive procedure (red bar). Shadow strength = 25% (a) and 75% (b)

4.3 The Motion Tracking of Shadows

The adaptive reconfiguration procedure proposed in the previous Section can detect a partial shading occurring on the PV generator by processing voltage and currents signals.
By this way, it reduces the energy losses of the synchronous reconfiguration by almost halving the number of reconfiguration when no shadowing is present over the PV field.
The real-time shadowing detection and the capability to discern between a shading phenomenon and a full solar radiance variation are the main advantage of this procedure.
Despite this capability, the minimization of the energy losses during a shadowing phenomenon is not ensured because this procedure triggers the reconfiguration process each time an activating rule is verified.

Moreover, this procedure has further disadvantages.
First of all, additional hardware is required to measure voltage and currents values. The greater are the maximum values of voltage and current needed to be measured, the higher are the hardware costs. There are commercial devices that combine and monitor different panels rows by sensing the voltage of the whole PV field and the current of each row and they are, for this reason, called *string combiner* [ABB14].
The analysis of voltage and currents signals is insufficient to the complete understanding of the shading phenomenon occurring at a certain time instant. So, it is not possible to determine the shadow size and angular orientation, its maximum strength, its transit speed, and so the time period required by the shadow to leave definitively the PV generator.
Moreover, the shading effects on the working points depend on the chosen topology of the PV generator as well as on the present actuated electrical configuration of panels. So, the chosen rules set and thresholds must be adapted to the PV plant topology and, respect to the same shading scenario, different rules can be triggered depending on the chosen configuration.

The analysis of voltage and currents variations is insufficient to determine if, under detected partial shading conditions, the present configuration of panels should be changed in different one or not. In effect, in some cases, the reconfiguration procedure doesn't change the present connections among panels, but only the MPP. Furthermore, a great disadvantage of this procedure is that shading effects on voltage-current characteristics of *disconnected panels* are not detected. In fact, in this case, the position of working point is not affected at all by phenomena involving them. In order to verify if the scenario has changed, the reconfiguration should be executed every time a proper timeout event occurs.

For all these limitations, a further algorithm has been developed in order to understand when effectively the reconfiguration should be executed after the partial shading of the PV field has been detected and so to maximize the usage of the already actuated configuration of panels.
By this way, the number of the reconfiguration executions is sure reduced and the gap between the energy values generated by the synchronous and the adaptive procedure further increases.

4.3.1 The Proposed Method

The goal of this new procedure is estimating the motion path and the transit speed of one or multiple shadows passing over a PV field by processing data provided by the under-sampling algorithm at two different reconfiguration instants.

The prediction of the shadow position for any future instant leads to different advantages.
Once a shading phenomenon has been detected by using the rules based technique and the reconfiguration has been executed at least a couple of times, the proposed procedure estimates the motion path and transit speed of the shadow and indicates the time instants at which a new reconfiguration should be executed by max-

imizing, at the same time, the usage of each actuated configuration. So, during the time period the shadows is passing over the PV field, the first technique can be disabled and the reconfiguration efficiency is totally assigned to this new procedure.
The knowledge of the shadow position can further reduce the execution time of a reconfiguration procedure.
In fact, if a decision algorithm is used, the unshaded panels could be pre-allocated properly into strings. After a partial solution has been achieved, by considering as 'frozen' the position of the unshaded panels, a minimal amount of combinations are then required to calculate the final solution. So, a faster reconfiguration procedure is achieved. This approach is illustrated in [PM13], where the reconfiguration procedure calculates the optimal configuration by executing an exhaustive research or a stochastic algorithm depending on the number of unfrozen position of panels.

The proposed method is based on the reconstruction of solar radiance scenario over the PV generator at module level. Instead of sensing solar radiance hitting each module by using an additional hardware, the current value of each MPP provided by the under-sampling algorithm is used as measure of the solar radiance hitting the modules of the considered panel. So, each PV module is used like an irradiance sensor and the current generated by each module depends on the lowest irradiance value hitting its cells.

At each execution of the reconfiguration procedure, the proposed procedure runs three main steps:

1. Detection and indexing of shadows over the PV generator
2. Association between shadows detected at the present and previous executions of the reconfiguration procedure
3. Shadow position and disappearing time estimations

At each execution of reconfiguration procedure, the shadows covering the PV generator are detected and indexed basing on analysis of currents values of MPPs of each PV module.

Sorting of currents values

The first faced problem is that different shading scenarios over a panel could provide the same voltage-current curve. In fact, if the modules in a panels work under mismatched conditions, then three current levels appear in the voltage-current curve of the panel and the voltage measured across the panel strongly depends on the required current. If the irradiance values have been fixed for each module in a panel, the order they are series-connected is irrelevant, i.e. always the same voltage-current curve of the panel is obtained.
So, before analyzing the currents values of MPPs, the correct relationship between a module in a panel and the current value of its MPP on the voltage-current curve of the panel should be found.
In order to achieve this result, different methods can be used taking into account the hypothesis that two modules in a panel or two modules belonging to a couple of nearest panels that are generating the same current level are probably located side by side.
So, for example, a procedure based on a spatial regression method, like the Kriging [ADP09] [P.L15], can be used.

In this Thesis, this step of the procedure is bypassed since the irradiance hitting each module is known.
For all panels of the field, each correct relationship between the current value of an MPP and the module that can generate it is found. So, the current levels of voltage-current curves of panels are automatically sorted in a way that reproduces, even if with a low resolution, the shading scenario over the whole PV generator.

Shadows identification

The analysis of the sorted currents levels allow to identify each shadow covering the PV field.
If the PV field is composed by all equal panels and the sorted current values are stored into a two-dimensional array (in the sequel, the *sorted currents matrix*), then the maximum current value I_{max}

represents that generated by unshaded panels.
Shadows can be identified and indexed by executing the following steps:

1. In each row of the sorted currents matrix, consecutive elements having a value less than 95% of maximum are grouped and marked as shaded modules. By this way, all the consecutive modules covered by the same shadow are grouped as a unique element into *clusters*. A 5% of tolerance to noise has been considered.

2. If at least one shaded module has been detected, then two different rows of the matrix are analyzed in order to search for the sections that are covered by the same shadow. So, the nearest clusters, separated at maximum by a column of modules not marked as shaded, are merged together.

At the end, these elements represent the set of modules covered by same shadow as well as the indexed shadows over the PV plant.

For each detected group of shaded modules, the width (the difference between the maximum and minimum index of shaded modules), the height (the difference between the maximum and minimum index of shaded rows) and the center of mass are calculated. In particular, the coordinates of the center of mass are calculated basing on current values of the shaded modules, as expressed by equations 4.8 and 4.9.

$$x_c = \frac{\sum_{k=r_1}^{r_2} \sum_{j=m_1}^{m_2} j \cdot (I_{max} - I_j)}{\sum_{k=r_1}^{r_2} \sum_{j=m_1}^{m_2} (I_{max} - I_j)} \tag{4.8}$$

$$y_c = \frac{\sum_{k=r_1}^{r_2} \sum_{j=m_1}^{m_2} k \cdot (I_{max} - I_j)}{\sum_{k=r_1}^{r_2} \sum_{j=m_1}^{m_2} (I_{max} - I_j)} \tag{4.9}$$

where x_c and y_c are the coordinates of center of mass representing respectively the modules and rows indexes, r_1 and r_2 are respectively the initial and final indexes of rows covered by the analyzed shadow, m_1 and m_2 are the initial and final indexes of modules belonging to the row having index k covered by the analyzed shadow.

Temporal association between shadows

The second main step of the procedure is represented by temporal association between shadows identified at the present time and those identified at the previous execution of the reconfiguration procedure.
Shadows moving over the PV generator can change their properties between these two time instants.
An optimal association strategy should always recognize if two shadows observed at different times are effectively the same shadow or two different ones.
In this Thesis, since at maximum one shadow is covering the PV field, the choice of the optimal strategy is not an issue.
In any case, a general strategy has been adopted by considering as first hypothesis that all shadows are moving approximately in the same direction and having a similar transit speed. The second hypothesis is that only shadows having a very low transit speed are analyzed, such as those caused by movement of the sun during the day.
Basing on the strategy adopted in this Thesis, two shadows, detected at different times, are recognized as the same if they are at the lowest distance between them.
In fact, if the transit speed is constant for all the shadows, then, during a fixed time interval, they move by the same distance too. Then, a minimum distance-based rule could be used to recognize the same shadow observed at two different times.

Prediction of the new shadow position

For each association between shadows observed at two different times, the prediction of shadow properties related to a future instant can be performed.
Since the analyzed shadows are caused by fixed obstacles, such as building, their speed is comparable respect the speed of sun over the PV generator. For this reason, the uniform motion law can be applied in order to estimate width, height and position variations of the shadow, as expressed by equations 4.10, 4.11, 4.12 and 4.13.

$$x_c(t_2) = x_c(t_1) + \frac{x_c(t_1) - x_c(t_0)}{t_1 - t_0} \cdot (t_2 - t_1) \tag{4.10}$$

$$y_c(t_2) = y_c(t_1) + \frac{y_c(t_1) - y_c(t_0)}{t_1 - t_0} \cdot (t_2 - t_1) \tag{4.11}$$

$$W(t_2) = W(t_1) + \frac{W(t_1) - W(t_0)}{t_1 - t_0} \cdot (t_2 - t_1) \tag{4.12}$$

$$H(t_2) = H(t_1) + \frac{H(t_1) - H(t_0)}{t_1 - t_0} \cdot (t_2 - t_1) \tag{4.13}$$

where t_0 and t_1 are respectively the instants of the previous and present reconfiguration, t_2 is the instant for which prediction is calculated, x_c and y_c are the barycentric coordinates, W and H are respectively the width and the height of the considered shadow.

So, in a first attempt, the temporal association of two observations of the same shadow leads to predict the rectangular portion of the PV generator that is shaded at a generic future instant. The sizes of this portion are W(t_2) and H(t_2). But not all modules included in this rectangle are shaded since it depends on the shape of shadow.
In order to detect which modules belonging to this rectangle are really shaded, the estimation of current variation of shaded modules is needed.

The current variation could be predicted, for each module belonging to the predicted rectangular portion of the field, by using a similar linear law, expressed by equation 4.14.

$$I(x_2, y_2, t_2) = I(x_1, y_1, t_1) + \frac{I(x_1, y_1, t_1) - I(x_0, y_0, t_0)}{t_1 - t_0} \cdot (t_2 - t_1) \tag{4.14}$$

where I is the current value associated to module having indexes x and y. The subscripts of x and y are referred to the considered instant times t_0, t_1 and t_2.

The same relationship is calculated for the maximum current of unshaded module by using the equation 4.15.

$$I_{max}(t_2) = I_{max}(t_1) + \frac{I_{max}(t_1) - I_{max}(t_0)}{t_1 - t_0} \cdot (t_2 - t_1) \tag{4.15}$$

In general, the maximum current value follows a parabolic trend during the day. So, the algorithm approximates the parabolic trend with a linear one and this approximation is more valid as much lower is the time interval $[t_0, t_1]$ but also $[t_1, t_2]$.
The estimation of parabolic trend requires at least the execution of three reconfiguration processes, since at least three points are needed to fitting a parabolic curve.

Nevertheless, this estimation is used only to distinguish among modules having an current lower than 5% of maximum current value $I_{max}(t_2)$. These are the shaded modules belonging to the predicted rectangular portion of the PV field.
The estimated currents values are useless and unreliable, since currents, that depend on the shading strength, don't evolve basing on a deterministic law.

For each association, the relationship among x_0, x_1 and x_2 (y_0, y_1 and y_2) depends on widths (heights) of rectangular portions of the field including the shaded modules.

In fact, these values are calculated by iterating on an index value k_x belonging to the range [0, W(t_2)] and considering the following equations:

$$x_0 = x_c(t_0) + \frac{W(t_0)}{W(t_2)} \cdot k_x - \frac{W(t_0)}{2} \tag{4.16}$$

$$x_1 = x_c(t_1) + \frac{W(t_1)}{W(t_2)} \cdot k_x - \frac{W(t_1)}{2} \tag{4.17}$$

$$x_2 = x_c(t_2) + k_x - \frac{W(t_2)}{2} \tag{4.18}$$

The same operation is performed by iterating on an index value k_y belonging to the range [0, H(t_2)] and considering the following equations:

$$y_0 = y_c(t_0) + \frac{H(t_0)}{H(t_2)} \cdot k_y - \frac{H(t_0)}{2} \tag{4.19}$$

$$y_1 = y_c(t_1) + \frac{H(t_1)}{H(t_2)} \cdot k_y - \frac{H(t_1)}{2} \tag{4.20}$$

$$y_2 = y_c(t_2) + k_y - \frac{H(t_2)}{2} \tag{4.21}$$

Next reconfiguration time estimation

By inverting the uniform motion law, the instant time the shadow moves on a different group of panels or the instant time it leaves the PV field (also referred as *disappearing time*) can be predicted.

The estimation of the x-coordinate of center of mass is provided by equation 4.10.
In general, this equation can be inverted in order to achieve the instant time at which the x-coordinate of the center of mass assumes a given value. So, this instant time can be calculated as follows:

$$t_{x*} = \begin{cases} t_1 - \frac{x_{c*}+x_c(t_1)}{v_{tx}} & v_{tx} < 0 \\ t_1 + \frac{x_{c*}-x_c(t_1)}{v_{tx}} & v_{tx} > 0 \\ \infty & v_{tx} = 0 \end{cases} \tag{4.22}$$

$$v_{tx} = \frac{x_c(t_1) - x_c(t_0)}{t_1 - t_0} \tag{4.23}$$

where t_0 and t_1 are the observation times, x_c is the x-coordinate of the center of mass, x_{c*} is a given x-coordinate and v_{tx} is the x component of the transit speed of the shadow calculated by equation 4.23. The given x-coordinate x_{c*} must be greater than $x_c(t_1)$ if $v_{tx} > 0$ or lower than that value if $v_{tx} < 0$.

Similarly, this relationship can be obtained for the y axis:

$$t_{y*} = \begin{cases} t_1 - \frac{y_{c*}+y_c(t_1)}{v_{ty}} & v_{ty} < 0 \\ t_1 + \frac{y_{c*}-y_c(t_1)}{v_{ty}} & v_{ty} > 0 \\ \infty & v_{ty} = 0 \end{cases} \tag{4.24}$$

$$v_{ty} = \frac{y_c(t_1) - y_c(t_0)}{t_1 - t_0} \tag{4.25}$$

where t_0 and t_1 are the observation times, y_c is the y-coordinate of the center of mass, y_{c*} is a given y-coordinate and v_{ty} is the y component of the transit speed of the shadow calculated by equation 4.25. The given y-coordinate y_{c*} must be greater than $y_c(t_1)$ if $v_{ty} > 0$ or lower than that value if $v_{ty} < 0$.

The equations 4.22 and 4.24 can be used to estimate the *next* reconfiguration instant. In particular, they can be used to estimate when the shading conditions will change respect to the present ones.

The reconfiguration should be executed when the shadow moves on an adjacent panel or on a different groups of panels respect to that shaded at the instant t_1. In the former case, an higher reconfiguration frequency is expected.

Since the resolution of the PV panels height is much lower than their width that depends on the number of modules, the detection of a shadow moving along the vertical axis is more difficult than that a shadow moving along the horizontal axis.

The time required by the shadow to move on a different panels is the minimum between that needed to move of a give number of modules and that needed to move on a different panels row. Since this time can be expressed as an interval time, rather than be identified by a time instant, it is referred also as *reconfiguration delay* because the reconfiguration is disabled during it.

Disappearing time estimation

The equations 4.22 and 4.24 are also used to estimate when a shadow leaves the PV field.
Since the direction of movement is known, then also the index of last module that the considered shadow covers is known.
So, when the shadow leaves the row, composed by M series-connected panels, the x-coordinate of center of mass could be $M + 1 + \frac{W(t_d)}{2}$, where $W(t_d)$ is the width of the shadow at the disappearing time t_d.
On the contrary, if the shadow is moving along the x negative direction, then, when it leaves the PV field, the index of center of mass of the shadow is equal to $-\frac{W(t_d)}{2}$.
However, the estimation of $W(t_d)$ requires the knowledge of t_d itself. So, t_d and $W(t_d)$ should be iteratively evaluated. In order to not increase execution time of the procedure, the maximum width of the shadow estimated at the two observed instants t_0 and t_1 could be considered, since it has been assumed that the consid-

ered shadows don't change their properties during the time period $[t_0, t_1]$.
By substituting one of these values into equation 4.10, the disappearing time is calculated by using one of equations 4.26.

$$t_{dx} = \begin{cases} t_1 - \frac{x_c(t_1) + \frac{max(W(t_0), W(t_1))}{2}}{v_{tx}} & v_{tx} < 0 \\ t_1 + \frac{M + 1 + \frac{max(W(t_0), W(t_1))}{2} - x_c(t_1)}{v_{tx}} & v_{tx} > 0 \\ \infty & v_{tx} = 0 \end{cases} \tag{4.26}$$

$$v_{tx} = \frac{x_c(t_1) - x_c(t_0)}{t_1 - t_0} \tag{4.27}$$

where t_0 and t_1 are the observation times, x_c is the x-coordinate of the center of mass, W is the width of the considered shadow, M is the number of modules in a row of the PV field and v_{tx} is the x component of the transit speed of the shadow calculated by equation 4.27.

Similarly, the transit speed and the disappearing time of a shadow moving only along the y axis can be calculated by using one of equations 4.28, depending on the value of v_{ty}.

$$t_{dy} = \begin{cases} t_1 - \frac{y_c(t_1) + \frac{max(H(t_0), H(t_1))}{2}}{v_{ty}} & v_{ty} < 0 \\ t_1 + \frac{R + 1 + \frac{max(H(t_0), H(t_1))}{2} - y_c(t_1)}{v_{ty}} & v_{ty} > 0 \\ \infty & v_{ty} = 0 \end{cases} \tag{4.28}$$

$$v_{ty} = \frac{y_c(t_1) - y_c(t_0)}{t_1 - t_0} \tag{4.29}$$

where t_0 and t_1 are the observation times, y_c is the y-coordinate of the center of mass, H is the height of the considered shadow, R is the number of modules rows of the PV field and v_{ty} is the y component of the transit speed of the shadow calculated by equation 4.29.

Independently of the direction towards a shadow is moving, both the x and y component of disappearing time are calculated. Then the estimated disappearing time is equal to the minimum value between t_{dx} and t_{dy}.

4.3.2 Simulated Results

The estimation of shadow motion has been tested on four dynamical shadows scenarios: a shadow strip moving horizontally, a shadow strip moving vertically, a diagonal shadow and a pole shadow rotating over the PV field.
For each scenario, the sensibility of this procedure is tested respect to the size of the shadow and its strength. So, shadow having a width equal to 330, 660, 990 and 1980 millimeters respectively have been tested. Moreover, for each size, both a sharp and a smoothed shadow strength has been tested.
For each scenario, the position of the center of mass of the shadow at each instant time, the prediction of the time period during which no reconfiguration process has to be executed (i.e. the reconfiguration delay) and the prediction of the instant time the shadow leaves the PV generator (i.e. the disappearing time) are illustrated.

The voltage-current characteristics of the PV panels are acquired every 15 minutes during the day.
Since this procedure requires at least two data acquisitions, a delay of 15 minutes occurs respect to the time instant when the shadow begins to cover the PV field.
In order to compare the predicted and the real shadow over the PV field, the shadow position is predicted for the next reconfigu-

ration time (after 15 minutes).

In these simulations, the estimated period after that the reconfiguration procedure has to be executed is the minimum time required to cover five further PV modules or to move on a different row of panels. The choice of shading five further modules before reconfiguring depends on the maximum number of modules that can compose a PV panel.

Shadow strip moving horizontally

The motion tracking procedure achieves the best performance for this scenario, since the shadow moves along the direction of the PV field having the greatest resolution. In fact, the number of PV modules belonging to a single row is much more than the number of rows itself.

In Figure 4.37, a typical result of the tracking procedure for this scenario is given. The shadows are identified by a cluster (red rectangle) having the position indicated by its center of mass (black colored X). In this Figure, the predicted cluster position at the desired time t_2 is exactly the same of the real one.

The smoothing of the shadow is obtained by using a 3x3 averaging filter for the solar radiance scenario (see Figure 4.38). In the following Figures, all red colored lines refer to parameters value obtained for smoothed shadows.

The estimated position of center of mass, that depends on the currents values of the shaded modules, is not susceptible to the smoothing of the shadow strength, but mainly on the shadows widths, as shown in Figure 4.39 where the coordinates of the center of mass appear to be located on a line having a constant slope. In this case, the lines having the same width overlap. The lines slope reduces only during starting and final step of the shadowing

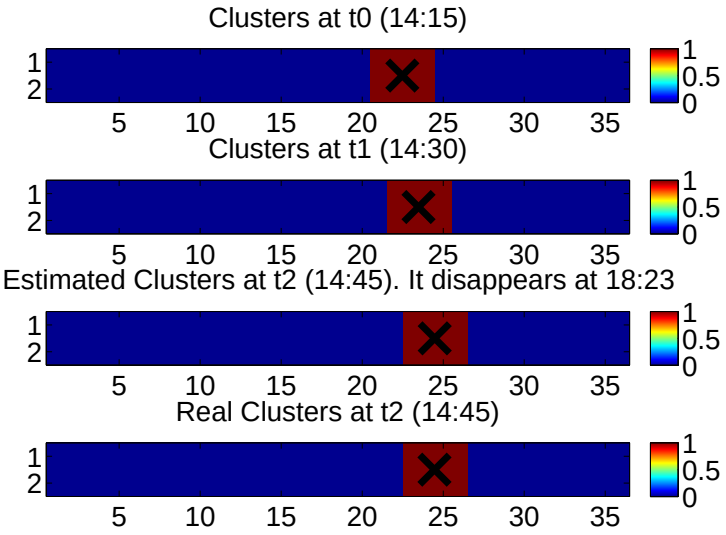

Figure 4.37: Shadow strip moving horizontally (width: 660mm). Clusters (red rectangles) and center of mass (black colored X).

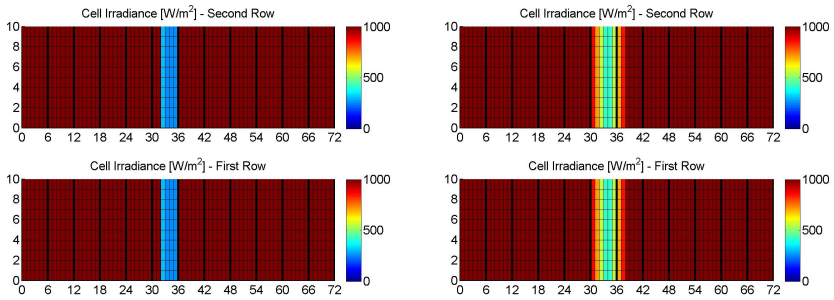

Figure 4.38: Sharp shadow (left) and smoothed shadow (right)

phenomenon, proportionally to the shading percentage of the PV field.
Since the currents of the shaded modules have the same values on both panels rows, then the y-coordinate of the center of mass is constant along time.

In Figure 4.40(a), the maximum time period during which the

reconfiguration could be not executed is shown. A stable time value is obtained only during the central hours of the day, when the solar radiance trend changes with a lower rate and so, between two reconfiguration instants, the current generated by unshaded panels is quite the same.
When the shadow begins to cover the PV field and until the shadow percentage on the PV field doesn't reach its maximum value or, similarly, when the shadow completely leaves the PV field, the transit speed is underrated and then the the predicted time is overrated. This is mainly due to the lack of information about the features of the shadow externally to the PV field. So, the shadow appears to increase its size as it begins to cover the PV field and to decrease its size as it begins to leave the PV field.
In Figure 4.40(b), where the predicted disappearing time is shown, the standard deviation is greater than that achieved for the reconfiguration delay because of the greater distance that has to be covered by the shadow strip.
Furthermore, the shadows width, the parabolic trend of the currents and the lower resolution of modules respect to real shadow shape increase the variability of the predicted time values.
In Figure 4.40, the average value is greater when shadow smoothing is applied because of increased shadows width.
Due to high resolution, both the disappearing time and the reconfiguration delay quickly achieve a stable value. The time required to stabilize depends on shadow strip width.

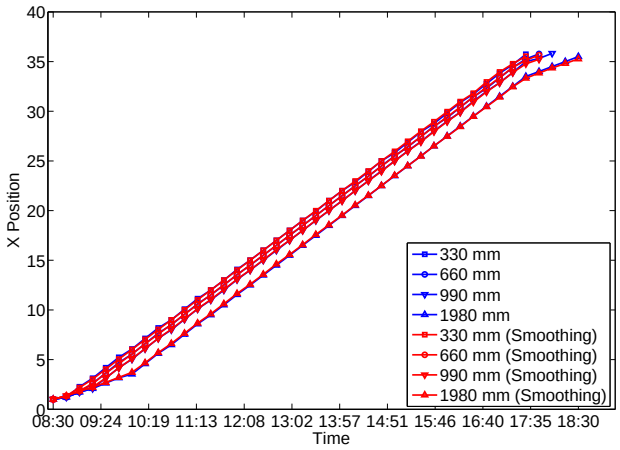

(a)

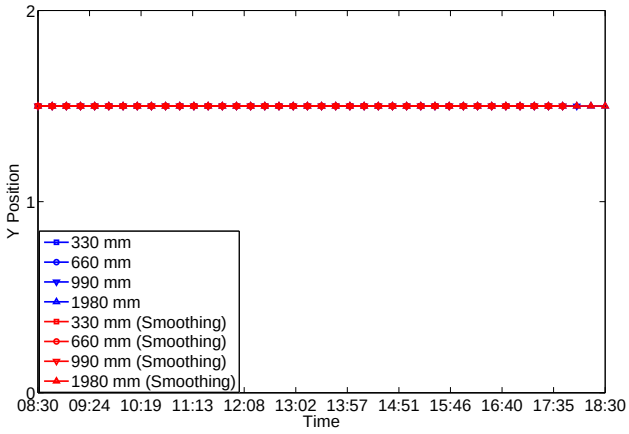

(b)

Figure 4.39: Shadow strip moving horizontally. Center of mass: x-coordinate (a) and y-coordinate (b)

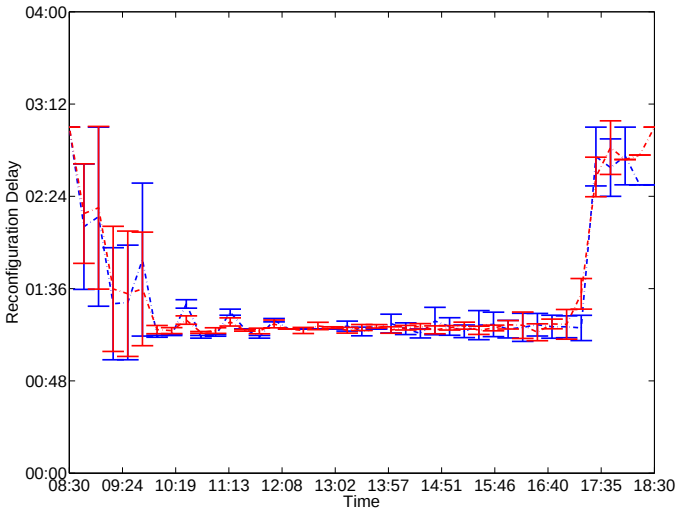

(a)

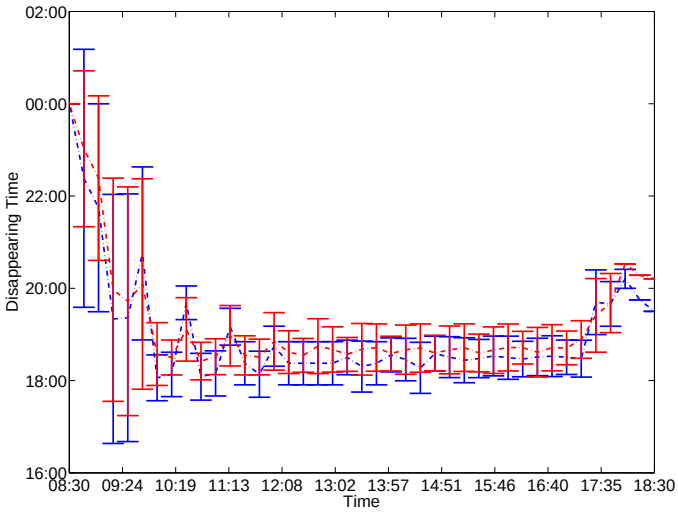

(b)

Figure 4.40: Shadow strip moving horizontally. Sharp shadows (blue line) and smoothed shadows (red line). Error bar graphs of the next reconfiguration delay (a) and disappearing time (b)

Shadow strip moving vertically

The motion tracking procedure is not able to predict correctly reconfiguration delay, and a fortiori the time when the shadow leaves the PV field, in the direction having the minimum resolution. In fact, since the shadow is identified always in the same position over the PV field, then the transit speed is estimated to be zero and so an infinite time is predicted both for the reconfiguration delay and the disappearing time. In this case, sure the reconfiguration cannot be delayed for an infinite time and a lower delay (e.g., 3 hours) could be acceptable.
In Figure 4.41, the disappearing time is limited to 12 hours more respect to the present reconfiguration instant.

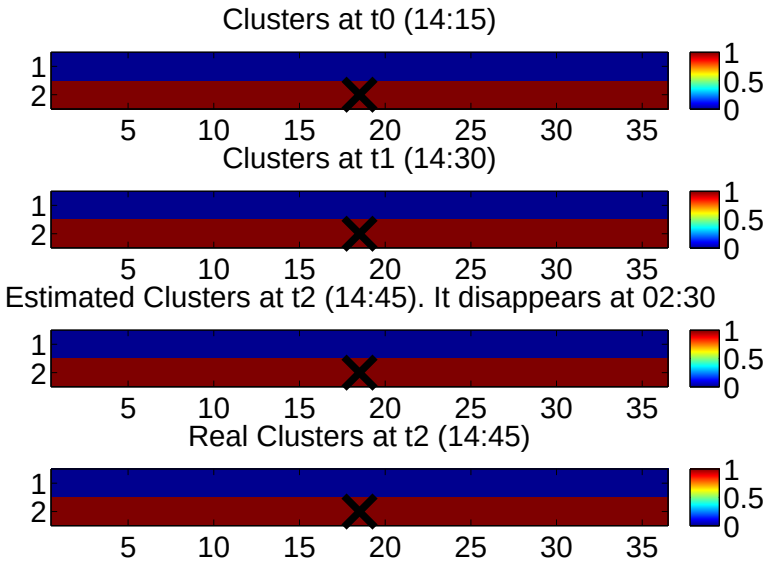

Figure 4.41: Shadow strip moving vertically. Clusters (red rectangles) and center of mass (black colored X).

Shadow strip moving diagonally

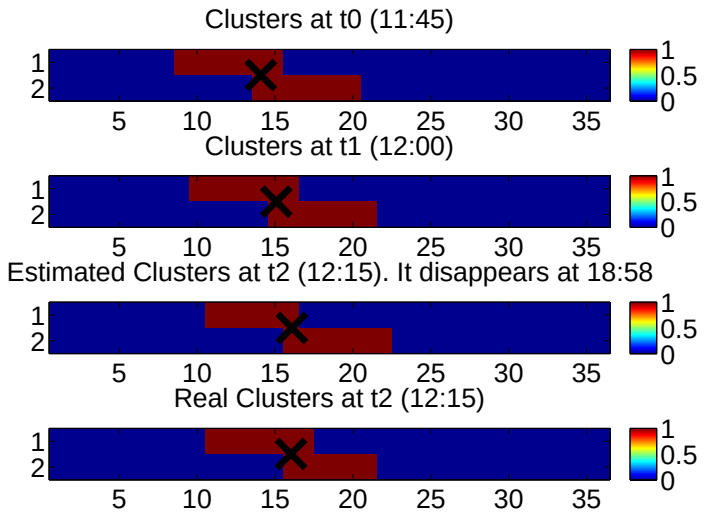

Figure 4.42: Shadow strip moving diagonally. Clusters (red rectangles) and center of mass (black colored X).

This scenario is only partially similar to the first one. In fact, it is really equivalent to an oblique shadow strip that is horizontally moving over the PV field.
Indeed, when the shadow starts or ends to cover the PV field, not only the shading percentage reduces, but the shadow covers only one of the two panels rows.
For this reason, even if a similar plot for the x-coordinate estimation is obtained (see Figure 4.43 (a)), on the contrary the estimated value of the y-coordinate assumes different values during the shadowing. Indeed, it is constant only when the shadow equally covers both panels rows (see Figure 4.43 (b)).

The shadowing of only one single row at the starting and at the ending of the shadowing phenomenon leads the predicted time values to oscillate. Instead, they stabilize and achieve the right value only when the shadow moves away from the borders of the PV field (see Figure 4.44).

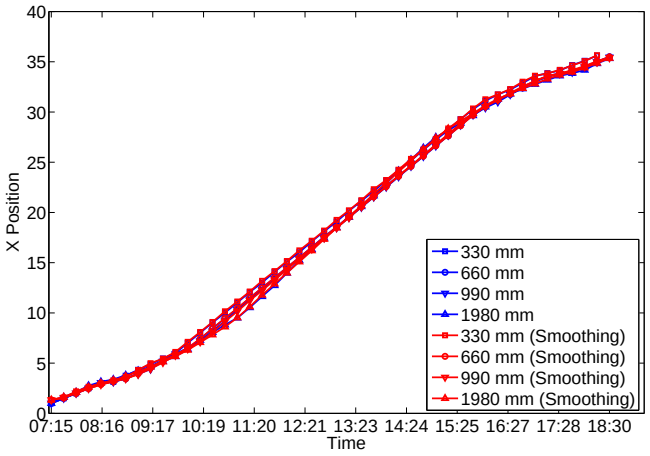

(a)

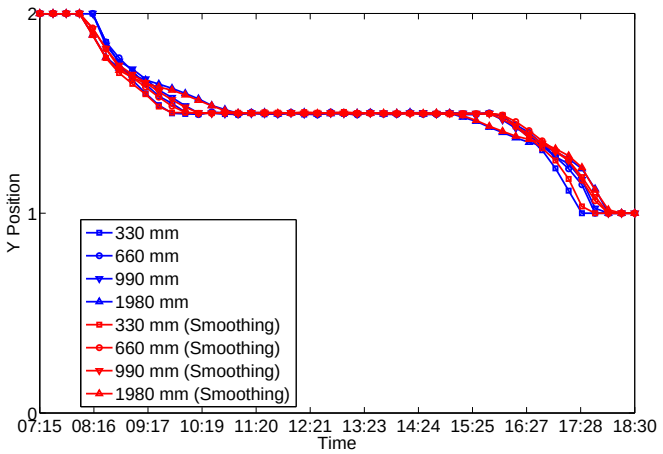

(b)

Figure 4.43: Shadow strip moving diagonally. Center of mass: x-coordinate (a) and y-coordinate (b)

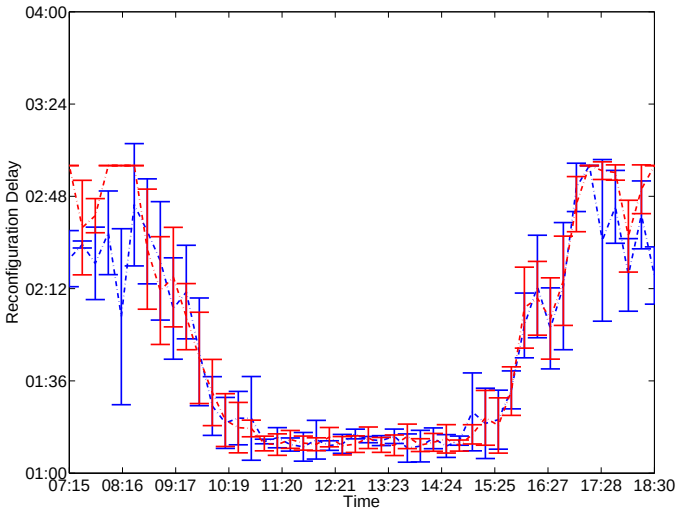

(a)

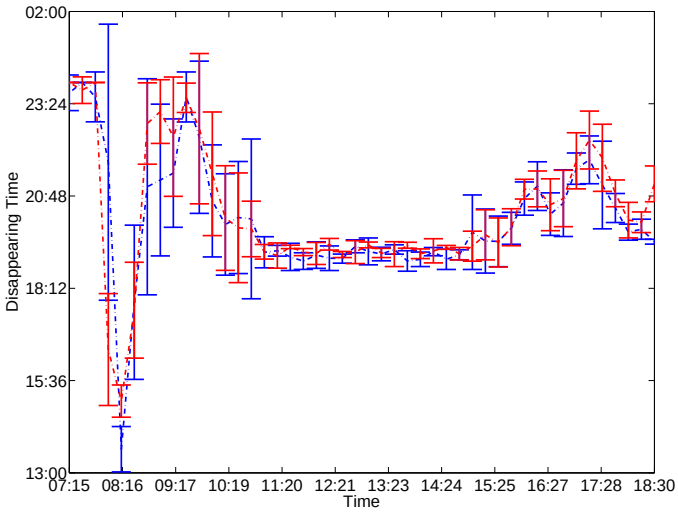

(b)

Figure 4.44: Shadow strip moving diagonally. Sharp shadows (blue line) and smoothed shadows (red line). Error bar graphs of the next reconfiguration delay (a) and disappearing time (b).

Pole shadow rotating over the PV field

Since the shadow is rotating over the PV field, its properties change during all the shading phenomena. In particular, respect to the horizontal axis, the shadow increases its transit speed until it becomes parallel to this axis. For this reason, the x-coordinate of the center of mass has a non-linear trend, as shown in Figure 4.45 (a). Moreover, in Figure 4.45 (b), the y-coordinate of the center of mass has an abrupt variation when the shadow covers first both panels rows and then only the first one.
Since the x-coordinate shows a non-linear trend having an increasing slope during the day, at the beginning of the day, the transit speed of the shadow is underrated while it achieves the maximum value when the shadow becomes parallel to the horizontal axis. So, at the beginning of the shading phenomenon, both the reconfiguration delay and the disappearing time are overrated.

Basing on the estimation of Figure 4.46 (a), the reconfiguration should be delayed for about 3 hours, and thus the next reconfiguration is executed when the shadow is starting to cover both panels rows. Similarly, the disappearing time is overrated too, since no shadow can be yet present after the sun has gone down.

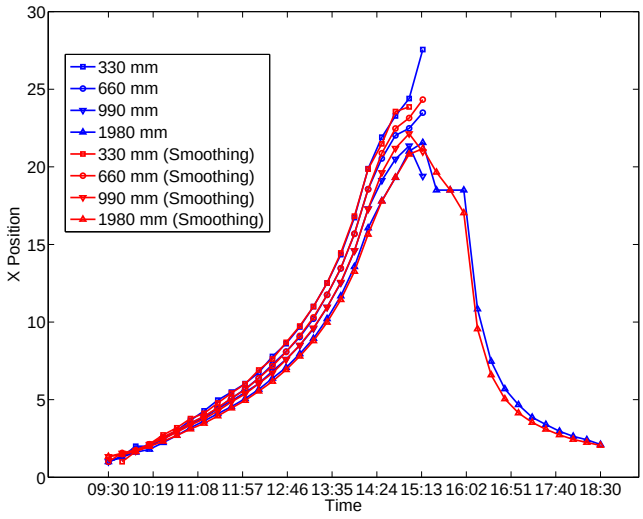

(a)

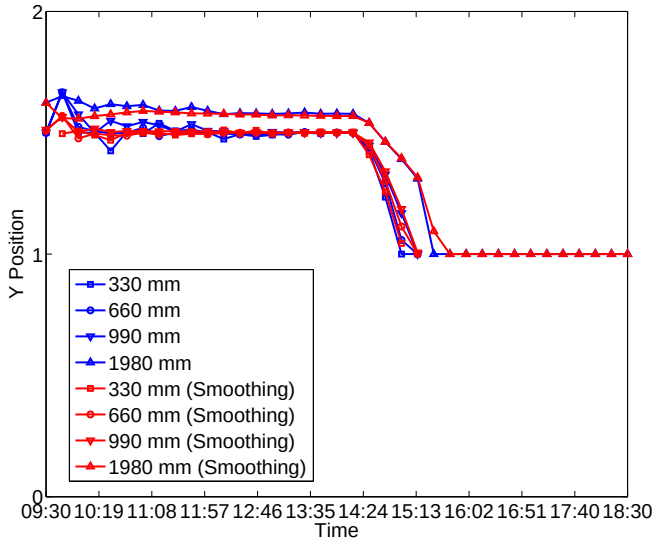

(b)

Figure 4.45: Pole shadow. Center of mass: x-coordinate (a) and y-coordinate (b)

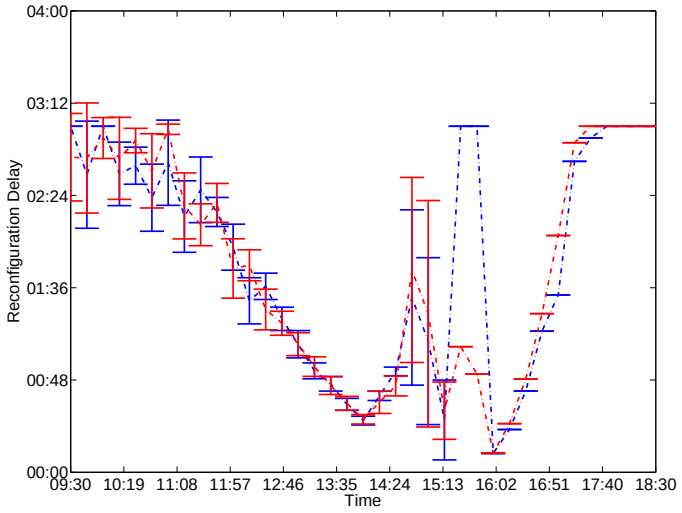

(a)

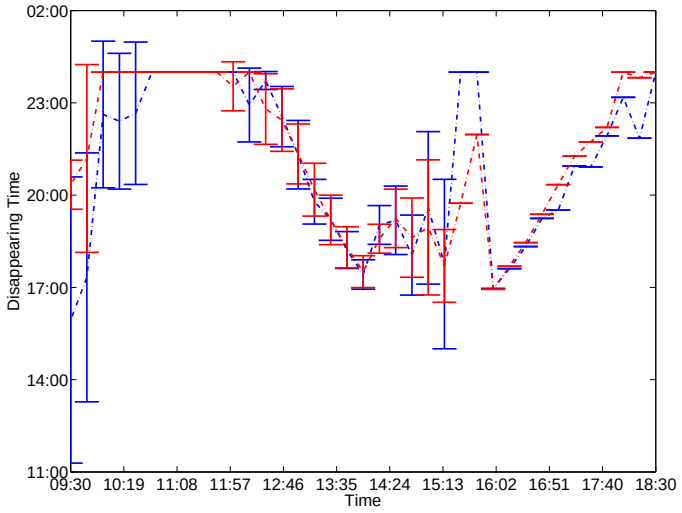

(b)

Figure 4.46: Pole shadow. Sharp shadows (blue line) and smoothed shadows (red line). Error bar graphs of the next reconfiguration delay (a) and disappearing time (b).

Conclusions

In this research work the mismatch losses caused by shadowing phenomenons and the methods used to reduce them are discussed, in particular by focusing on the reconfiguration of photovoltaic systems.
The photovoltaic systems reconfiguration has different advantages. In fact, it not only ensures the maximization of the generated power, but also ensures that both functional and design constraints of the photovoltaic system are properly respected.

A Genetic Algorithm (GA) is proposed to reconfigure a photovoltaic field having a series-parallel topology. In fact, this kind of algorithms is well suited to locate optimal solutions in complex landscapes and in a reduced amount of time. So, they are largely used for design or minimization/maximization goals.
Moreover, depending on the complexity of the objective function, they don't require a huge amount of computational resources, so that these procedures can be implemented on Embedded Systems.

Unfortunately, as regards the reconfiguration problem, the evaluation of the objective function requires too much time respect the dynamic of the shadowing phenomenon. Most of the time is spent to calculate the whole voltage-power curve of the PV field for each given solution.
So, in order to reduce the data analyzed by the objective function, an under-sampling procedure for the V-I curves of photovoltaic panels is presented. This procedure can be used also for the diagnostics of the PV panels.

The use of this procedure can both drastically reduce the execution time of the genetic algorithm and improve the quality of the provided solutions. In fact, the reduction of samples of V-I curves introduces an approximation error respect to the original curves and so of the fitness value of each provided solution. Thus, also the order of the solutions in each population changes respect to that achieved by using the complete V-I curves of panels. So, this sorting difference could also affect the final solution provided by the genetic algorithm. In particular, the difference of fitness between the optimal and the sub-optimal solutions could be increased. Instead, in other cases, depending on the efficiency of the under-sampling procedure, the ranking order between two solutions can be also inverted respect to the real case leading to achieve worst solutions.
The difference between the fitness values obtained by using the complete and the under-sampled curves of panels for a given solution can be nulled by only guaranteeing that, in both cases, the working point of each panel connected to the PV field has the same voltage and current values. If this occurs for each considered solution, then the genetic algorithms using the complete and the under-sampled curves of the panels have an identical evolution. Since it is not possible to predict the working point of each panel before sampling their voltage-current characteristics and before calculating the best electrical configuration, an approximation error is always present unless an higher amount of samples is selected. Thus, the risk of missing the information about the working point conditions even only for a PV panel is reduced but not eliminated.
In fact, since the characteristics of the panels cannot be numerically identical from each other and since the execution of the under-sampling procedure is independent for each curve of the panels, the loss of information about the exact working point condition of some panels is unavoidable.
Moreover, the sampling process of voltage-current characteristics of panels should guarantee that no data missing or excessive redundancies occur to achieve the best performance of the under-

sampling procedure.
In the future, in order to further reduce the approximation error and the execution time, other searching techniques for the samples corresponding to the boundaries of the non-linear regions could be implemented, such as that using gradient descent.
Moreover, the reconstruction of the voltage-current curves of panels could be executed by using non-linear fitting curves, thus requiring that the selected samples meet also well-defined mathematical conditions.

The reconfiguration frequency also plays an important role into maximizing the energy extracted from the PV field. In fact, since the PV panels should be disconnected in order to acquire their voltage-current characteristics before executing the reconfiguration procedure, then the total daily generated energy is inexorably reduced.
In order to execute the reconfiguration mainly when a shadowing occurs, a rules-based algorithm is proposed. This procedure senses voltage and string currents signal and, if one of the rules is verified, then trigger the reconfiguration procedure. These rules are based on the elapsed time respect to the previous reconfiguration and/or the variation of sensed parameters respect to their reference values.
The efficiency of this procedure cannot be very high for many different reasons. First, this procedure depends on the choice of proper thresholds whose optimal values are difficult to define. Furthermore, this procedure is designed for a given PV field topology, without taking into account physical phenomenons like the degradation of the photovoltaic modules or typical differences among them, that is the strongest approximation, thus simplifying the analysis of the MPP variations caused by shadowing phenomenons.
The chosen thresholds values, as well as the chosen rules, lead to a procedure that, when no shading occurs, executes the reconfiguration procedure approximately every hour while, when shading is occurring, is able to detect each shadow movement over the PV field, also depending on shadow size.

To reduce the reconfiguration frequency and further improve the efficiency of the proposed procedure, a motion tracking algorithm is illustrated.
The motion tracking, by analyzing the current values of the maximum power points found by the under-sampling procedure, is able to estimate the transit speed of a shadow moving over the PV field at the reconfiguration instant and to predict its position at a future instant. But this procedure is mainly used to predict the time when the shadow leaves the PV field and when it moves of a given number of modules, that is the instant of the next reconfiguration. The estimation of these informations is influenced by the accuracy of the shadow position at each reconfiguration instant. So, when the shadow is moving along the direction where the accuracy is lower, then also the time of next reconfiguration is not correctly estimated.

In order to improve the performance of the motion tracking procedure for the shadows, different motion laws could be investigated. In particular, both the translational and the rotational motion components of the shadow should be considered.
At the same time, the prediction error achieved when the shadow is located at the borders of the PV field have to be further analyzed in order to be taken into account and corrected.
A future approach could also consider the addition of a minimal number of sensors (e.g., reference PV cells) disposed in a way that the accuracy of shadow position is improved along each possible direction over the PV field. Moreover, new rules could be added to the list taking into account other particular phenomenons affecting the MPP, such as the permanent degradation of PV modules or the temperature effects. At the end, a method to estimate the threshold values for any given PV field has to be developed.

Bibliography

[ABB14] ABB, *Pv junction box - string combiner*, December 2014.

[ada13] *Method to evaluate the need to perform a reconfiguration step of two or more photovoltaic panels*, 9 2013.

[ADP09] Gianpaolo Vitale Annalisa Di Piazza, Maria Carmela Di Piazza, *A kriging-based partial shading analysis in a large photovoltaic field for energy forecast*, International Conference on Renewable Energies and Power Quality (ICREPQ 09) - Valencia (Spain) - 15th to 17th April, 2009, 2009.

[APCO98] Y. Auttawaitkul, B. Pungsiri, K. Chammongthai, and M. Okuda, *A method of appropriate electrical array reconfiguration management for photovoltaic powered car*, Circuits and Systems, 1998. IEEE APCCAS 1998. The 1998 IEEE Asia-Pacific Conference on, Nov 1998, pp. 201–204.

[Bea14] Beagleboard, *Beagleboard xm*, December 2014.

[BIS88] J. W. BISHOP, *Computer simulation of the effects of electrical mismatches in photovoltaic cell interconnection circuits*, Solar Cells **25** (1988), 73–89.

[BMAM+11] R. Baños, F. Manzano-Agugliaro, F.G. Montoya, C. Gil, A. Alcayde, and J. Gómez, *Optimization*

methods applied to renewable and sustainable energy: A review, Renewable and Sustainable Energy Reviews **15** (2011), no. 4, 1753 – 1766.

[BMV14] M. Balato, P. Manganiello, and M. Vitelli, *Fast dynamical reconfiguration algorithm of pv arrays*, Ecological Vehicles and Renewable Energies (EVER), 2014 Ninth International Conference on, March 2014, pp. 1–8.

[BVF+11] M. Balato, M. Vitelli, N. Femia, G. Petrone, and G. Spagnuolo, *Factors limiting the efficiency of dmppt in pv applications*, Clean Electrical Power (ICCEP), 2011 International Conference on, June 2011, pp. 604–608.

[CAN+10] M.A. Chaaban, M. Alahmad, J. Neal, J. Shi, C. Berryman, Y. Cho, S. Lau, H. Li, A. Schwer, Z. Shen, J. Stansbury, and T. Zhang, *Adaptive photovoltaic system*, IECON 2010 - 36th Annual Conference on IEEE Industrial Electronics Society, Nov 2010, pp. 3192–3197.

[CCL13] Kuei-Hsiang Chao, Long-Yi Chang, and Hsueh-Chien Liu, *Maximum power point tracking method based on modified particle swarm optimization for photovoltaic systems*, International Journal of Photoenergy **2013** (2013).

[CDDDN+13] G. Cipriani, V. Di Dio, L.P. Di Noia, F. Genduso, D. La Cascia, R. Miceli, and R. Rizzo, *A pv plant simulator for testing mppt techniques*, Clean Electrical Power (ICCEP), 2013 International Conference on, June 2013, pp. 482–489.

[CDDM+14] G. Cipriani, V. Di Dio, N. Madonia, R. Miceli, F. Pellitteri, and F.R. Galluzzo, *Reconfiguration*

strategies to reduce mismatch effects on pv array: An arduino-based prototype, Power Electronics, Electrical Drives, Automation and Motion (SPEEDAM), 2014 International Symposium on, June 2014, pp. 1003–1008.

[CDDSR07] R. Candela, V. Di Dio, E.R. Sanseverino, and P. Romano, *Reconfiguration techniques of partial shaded pv systems for the maximization of electrical energy production*, Clean Electrical Power, 2007. ICCEP '07. International Conference on, May 2007, pp. 716–719.

[CMPS14] P.L. Carotenuto, P. Manganiello, G. Petrone, and G. Spagnuolo, *About the criteria for triggering the reconfiguration of a photovoltaic array*, Industrial Electronics (ISIE), 2014 IEEE 23rd International Symposium on, June 2014, pp. 2472–2477.

[Dav90] Yuval Davidor, *Epistasis variance: Suitability of a representation to genetic algorithms*, Complex Systems (1990).

[EAS+10] A. Elasser, M. Agamy, J. Sabate, R. Steigerwald, R. Fisher, and M. Harfman-Todorovic, *A comparative study of central and distributed mppt architectures for megawatt utility and large scale commercial photovoltaic plants*, IECON 2010 - 36th Annual Conference on IEEE Industrial Electronics Society, Nov 2010, pp. 2753–2758.

[EC07] T. Esram and P.L. Chapman, *Comparison of photovoltaic array maximum power point tracking techniques*, Energy Conversion, IEEE Transactions on **22** (2007), no. 2, 439 –449.

[EDKS13] M.Z.S. El-Dein, M. Kazerani, and M.M.A. Salama, *Optimal photovoltaic array reconfiguration to reduce partial shading losses*, Sustainable

Energy, IEEE Transactions on **4** (2013), no. 1, 145–153.

[ERC11] V.M.F. Mendes E.M.G. Rodrigues, R. Melï¿½cio and J.P.S. Catalï¿½o, *Simulation of a solar cell considering single-diode equivalent circuit model*, 2011, pp. 1–5.

[FD81] David Freedman and Persi Diaconis, *On the histogram as a density estimator:l 2 theory*, Zeitschrift für Wahrscheinlichkeitstheorie und Verwandte Gebiete **57** (1981), no. 4, 453–476 (English).

[FLP+08] N. Femia, G. Lisi, G. Petrone, G. Spagnuolo, and M. Vitelli, *Distributed maximum power point tracking of photovoltaic arrays: Novel approach and system analysis*, Industrial Electronics, IEEE Transactions on **55** (2008), no. 7, 2610–2621.

[GDdV13] P. Guerriero, S. Daliento, V. d'Alessandro, and G. Vallone, *A simple test-bench to evaluate partial shading effects on the mppt efficiency of a pv inverter*, Clean Electrical Power (ICCEP), 2013 International Conference on, June 2013, pp. 20–23.

[GLTGEE12] Daniel Gómez-Lorente, Isaac Triguero, Consolación Gil, and A Espín Estrella, *Evolutionary algorithms for the design of grid-connected pv-systems*, Expert Systems with Applications **39** (2012), no. 9, 8086–8094.

[Hae05] H Haeberlin, *Optimum dc operating voltage for grid-connected pv plants choice of vmpp for measurement of efficiency and vmpp-stc at pv plants for grid-connected inverters with a wide dc input voltage range*, 20th European Photovoltaic Solar Energy Conference, Barcelona, Spain, June 2005.

[HCW+14] Yihua Hu, Wenping Cao, Jiande Wu, Bing Ji, and D. Holliday, *Thermography-based virtual mppt scheme for improving pv energy efficiency under partial shading conditions*, Power Electronics, IEEE Transactions on **29** (2014), no. 11, 5667–5672.

[HNDM13] D.C. Huynh, T.M. Nguyen, M.W. Dunnigan, and M.A. Mueller, *Global mppt of solar pv modules using a dynamic pso algorithm under partial shading conditions*, Clean Energy and Technology (CEAT), 2013 IEEE Conference on, Nov 2013, pp. 134–139.

[HR00] D.P. Hohm and M.E. Ropp, *Comparative study of maximum power point tracking algorithms using an experimental, programmable, maximum power point tracking test bed*, Photovoltaic Specialists Conference, 2000. Conference Record of the Twenty-Eighth IEEE, 2000, pp. 1699 –1702.

[Ibr11] A. Ibraim, *Analysis of electrical characteristics of photovoltaic single crystal silicon solar cells at outdoor measurements*, vol. 2, 2011, pp. 169–175.

[JM14] Lianlian Jiang and D.L. Maskell, *A simple hybrid mppt technique for photovoltaic systems under rapidly changing partial shading conditions*, Photovoltaic Specialist Conference (PVSC), 2014 IEEE 40th, June 2014, pp. 0782–0787.

[KK13] K. A. Kim and P.T. Krein, *Photovoltaic hot spot analysis for cells with various reverse-bias characteristics through electrical and thermal simulation*, Control and Modeling for Power Electronics (COMPEL), 2013 IEEE 14th Workshop on, June 2013, pp. 1–8.

[KKPK06] Eftichios Koutroulis, Dionissia Kolokotsa, Antonis Potirakis, and Kostas Kalaitzakis, *Methodology for optimal sizing of stand-alone photovoltaic/wind-generator systems using genetic algorithms*, Solar Energy **80** (2006), no. 9, 1072 – 1088.

[KL13] S. Valkealahti K. Lappalainen, A. Mäki, *Effects of the sharpness of shadows on the mismatch losses of pv generators under partial shading conditions caused by moving clouds*, 28th European Photovoltaic Solar Energy Conference and Exhibition, 2013, pp. 4081 – 4086.

[KMAP14] M. Karakose, K. Murat, E. Akin, and K.S. Parlak, *A new efficient reconfiguration approach based on genetic algorithm in pv systems*, Industrial Electronics (ISIE), 2014 IEEE 23rd International Symposium on, June 2014, pp. 23–28.

[Kol97] K. Kolarov, *Landscape ruggedness in evolutionary algorithms*, Evolutionary Computation, 1997., IEEE International Conference on, Apr 1997, pp. 19–24.

[Kor10] Aris Kornelakis, *Multiobjective particle swarm optimization for the optimal design of photovoltaic grid-connected systems*, Solar Energy **84** (2010), no. 12, 2022–2033.

[LPC10] Yanli Liu, Zhichao Pang, and Ze Cheng, *Research on an adaptive solar photovoltaic array using shading degree model-based reconfiguration algorithm*, Control and Decision Conference (CCDC), 2010 Chinese, May 2010, pp. 2356–2360.

[Mey12] M.A. ; Simon M. Meyer, E.L. ; Malape, *Influence of temperature on photovoltaic cells spectral response*, 2012, pp. 254 – 257.

[MJ14] Sener Uysal Moein Jazayeri, *A comparative study on different photovoltaic array topologies under partial shading conditions*, April 2014, pp. 1–5.

[MTF+11] Masafumi Miyatake, Fujii Toriumi, N Fujii, Hideyoshi Ko, et al., *Maximum power point tracking of multiple photovoltaic arrays: a pso approach*, Aerospace and Electronic Systems, IEEE Transactions on **47** (2011), no. 1, 367–380.

[MV14] Anssi Mï¿½ki and Seppo Valkealahti, *Differentiation of multiple maximum power points of partially shaded photovoltaic power generators*, Renewable Energy **71** (2014), no. 0, 89 – 99.

[NFV12] Giovanni Spagnuolo Nicola Femia, Giovanni Petrone and Massimo Vitelli, *Power electronics and control techniques for maximum energy harvesting in photovoltaic systems*, CRC Press 2'12, 2012.

[NL08] Dzung Nguyen and B. Lehman, *An adaptive solar photovoltaic array using model-based reconfiguration algorithm*, Industrial Electronics, IEEE Transactions on **55** (2008), no. 7, 2644–2654.

[NRE14] NREL, *National renewable energy laboratory (nrel)*, December 2014.

[OGRSSRP14] M.L. Orozco-Gutierrez, J.M. Ramirez-Scarpetta, G. Spagnuolo, and C.A. Ramos-Paja, *A method for simulating large {PV} arrays that include reverse biased cells*, Applied Energy **123** (2014), no. 0, 157 – 167.

[PA08] H. Patel and V. Agarwal, *Maximum power point tracking scheme for pv systems operating under*

partially shaded conditions, Industrial Electronics, IEEE Transactions on **55** (2008), no. 4, 1689–1698.

[PGBSA11] Paola Pezzini, Oriol Gomis-Bellmunt, and Antoni SudriÃ -Andreu, *Optimization techniques to improve energy efficiency in power systems*, Renewable and Sustainable Energy Reviews **15** (2011), no. 4, 2028 – 2041.

[P.L15] M.C.Di Piazza M.Luna G.Petrone G.Spagnuolo P.L.Carotenuto, A.Di Piazza, *A geostatistical approach for identifying the shadowing conditions affecting a photovoltaic plant*, 6-18 June 2015, ICCEP Conference, Taormina, Sicily - Italy, 2015.

[PM13] Salvatore Curcio Giovanni Petrone Giovanni Spagnuolo Massimo Vitelli Patrizio Manganiello, Pietro Luigi Carotenuto, *Algorithms and devices for the dynamical reconfiguration of pv arrays*, International Exhibition and Conference on Power Electronics, Intelligent Motion, Renewable Energy and Energy Management (PCIM Europe 2013), ISBN 978-3-8007-3505-1, 2013.

[Ram] R Ramaprabha, *Selection of an optimum configuration of solar pv array under partial shaded condition using particle swarm optimization.*

[Ram72] Urs Ramer, *An iterative procedure for the polygonal approximation of plane curves*, Computer Graphics and Image Processing **1** (1972), no. 3, 244 – 256.

[RB09] H. Häberlin B. Burger A. Bergmann F. Baumgartner R. Bründlinger, N. Henze, *pren 50530 - the new european standard for performance characterisation of pv inverters*, 24th European Pho-

tovoltaic Solar Energy Conference, 21-25 September 2009, Hamburg, Germany, September 2009, pp. 3105 – 3109.

[Ren14] Renesas, *http://am.renesas.com/products/mpumcu/v850/*.

[Say12] A. Sayal, *Mppt techniques for photovoltaic system under uniform insolation and partial shading conditions*, Engineering and Systems (SCES), 2012 Students Conference on, March 2012, pp. 1–6.

[SD90] Z.M. Salameh and F. Dagher, *The effect of electrical array reconfiguration on the performance of a pv-powered volumetric water pump*, Energy Conversion, IEEE Transactions on **5** (1990), no. 4, 653–658.

[She07] David J. Sheskin, *Handbook of parametric and nonparametric statistical procedures*, 4 ed., Chapman & Hall/CRC, 2007.

[SKS12] K. Stefferud, J. Kleissl, and J. Schoene, *Solar forecasting and variability analyses using sky camera cloud detection amp; motion vectors*, Power and Energy Society General Meeting, 2012 IEEE, July 2012, pp. 1–6.

[SM10] Michael Simon and Edson L. Meyer, *Detection and analysis of hot-spot formation in solar cells*, Solar Energy Materials and Solar Cells **94** (2010), no. 2, 106 – 113.

[Sol14] Axitec Solar, *Axitec ac-250m/156-60s*, December 2014.

[SSDG14] N.S. Shiradkar, E. Schneller, N.G. Dhere, and V. Gade, *Predicting thermal runaway in bypass diodes in photovoltaic modules*, Photovoltaic Specialist Conference (PVSC), 2014 IEEE 40th, June 2014, pp. 3585–3588.

[SSS03] Biswajit Sarkar, Lokendra K. Singh, and Debranjan Sarkar, *Approximation of digital curves with line segments and circular arcs using genetic algorithms*, Pattern Recognition Letters **24** (2003), no. 15, 2585 – 2595.

[SWH14] S. Strache, R. Wunderlich, and S. Heinen, *A comprehensive, quantitative comparison of inverter architectures for various pv systems, pv cells, and irradiance profiles*, Sustainable Energy, IEEE Transactions on **5** (2014), no. 3, 813–822.

[TPM08] Francesco Tortorella, Rossella Patraccone, and Mario Molinara, *A dynamic programming approach for segmenting digital planar curves into line segments and circular arcs.*, ICPR, Citeseer, 2008, pp. 1–4.

[TSI+10] H Taheri, Z Salam, K Ishaque, et al., *A novel maximum power point tracking control of photovoltaic system under partial and rapidly fluctuating shadow conditions using differential evolution*, Industrial Electronics & Applications (ISIEA), 2010 IEEE Symposium on, IEEE, 2010, pp. 82–87.

[usa13] *Method to decimate the samples necessary to identify one characteristic curve of at least one power supply module and computer program for associated distributor*, 9 2013.

[VQGGPL+09] G. Velasco-Quesada, F. Guinjoan-Gispert, R. Pique-Lopez, M. Roman-Lumbreras, and A. Conesa-Roca, *Electrical pv array reconfiguration strategy for energy extraction improvement in grid-connected pv systems*, Industrial Electronics, IEEE Transactions on **56** (2009), no. 11, 4319–4331.

[Web14] Website, *http://www.bitronenergy.com/*.

[WLK+14] Yanzhi Wang, Xue Lin, Younghyun Kim, Naehyuck Chang, and M. Pedram, *Architecture and control algorithms for combating partial shading in photovoltaic systems*, Computer-Aided Design of Integrated Circuits and Systems, IEEE Transactions on **33** (2014), no. 6, 917–930.

[Yin06] P.Y. Yin, *Genetic particle swarm optimization for polygonal approximation of digital curves*, Pattern Recognition and Image Analysis **16** (2006), no. 2, 223–233 (English).

[ZMv11] V. Benda Z. Macháček and L. Černá, *Electrical parameters of c?si and cis photovoltaic cells in dependence on temperature and irradiance*, 2011, pp. 492 – 496.

Acknowledgements

I would like to thank all people I met during my Ph.D., in particular my Ph.D. advisor Prof. Giovanni Spagnuolo and all the colleagues that supported me during these past three years.

I had the fortune to be part of the Power Electronics research group, improving but mainly acquiring new skills.

In particular, I'd like to thank Prof. Walter Zamboni that gave to me the possibility to be a co-advisor and work closely with him for an interesting Bachelor's Thesis project.

I want to thank Prof. Giovanni Petrone that, together to Prof. Spagnuolo, involved me into an important European project. The time spent together was the best of all these three years. Giovanni Petrone is a very hard working and a very trusted person.

I had also the fortune to work closely again with Prof. Angelo Marcelli and to meet Prof. Antonio Della Cioppa. I will never forget the long walks with Prof. Antonio Della Cioppa talking about Artificial Intelligence and, above all, some helpful life lessons.

I will never forget the time spent with Martha Lucia Orozco-Gutierrez and Juan David Bastidas-Rodriguez. Martha is a very smiling girl and always available to help others. Martha has become not only a colleague but above all a friend. I hope to meet again Juan David too, a very talented researcher and trusted person. I'd like to thank also Antonio Parziale, Mattia Ricco and Patrizio Manganiello, that I consider friends and very talented researchers.

Finally, I'd like to embrace all people working in the Lab T17, especially Prof. Femia, and my colleagues of Lab 142 for the time spent together.